AMIDOPHOSPHINE COMPLEXES OF RUTHENIUM (II)

by

MICHAEL JOHN PETRELLA

B. Sc. (Hon.), McMaster University, 1997

A thesis submitted in partial fulfillment of

the requirements for the degree of

DOCTOR OF PHILOSOPHY

in

THE FACULTY OF GRADUATE STUDIES

DEPARTMENT OF CHEMISTRY

We accept this thesis as conforming

to the required standard

THE UNIVERSITY OF BRITISH COLUMBIA

April 2003

In presenting this thesis in partial fulfilment of the requirements for an advanced degree at the University of British Columbia, I agree that the Library shall make it freely available for reference and study. I further agree that permission for extensive copying of this thesis for scholarly purposes may be granted by the head of my department or by his or her representatives. It is understood that copying or publication of this thesis for financial gain shall not be allowed without my written permission.

Department of CHEMISTRY

The University of British Columbia
Vancouver, Canada

Date June 27, 2003

ABSTRACT

The preparation and reactivity of ruthenium(II) complexes that incorporate the chelating amidophosphine ligands [NPN] (where [NPN] = $PhP(CH_2SiMe_2NPh)_2$) or [P_2N_2] (where [P_2N_2] = $PhP(CH_2SiMe_2NSiMe_2CH_2)_2PPh$) are presented. The reaction of the dilithium salt [P_2N_2]$Li_2(S)$ (S = 1,4-dioxane) with the ruthenium starting material $[RuCl_2(cod)]_x$ (cod = 1,5-cyclooctadiene, η^2:η^2-C_8H_{12}) generates the diamido complex [P_2N_2]Ru(η^2:η^2-C_8H_{12}) and the reaction with $RuCl_2(PPh_3)_3$ gives the *ortho*-metalated species [P_2NNH]Ru($C_6H_4PPh_2$). The [P_2N_2] cyclooctadiene complex reacts with hydrogen gas (one atmosphere) to give the fluxional dihydrogen-hydride species [P_2NNH]Ru(η^2-H_2)(H). The minimum longitudinal relaxation time (T_1(min)) for the hydride ligands in this complex is 62 ms (at 240 K) and the $^1J_{HD}$ coupling constant in the HD isotopomer is 15 Hz. These data both lead to an estimated H-H distance of 1.2 Å corresponding to an elongated H_2 moiety. The *ortho*-metalated species reacts with H_2 forming the monohydride complex [P_2NNH]RuH(PPh_3). Exposure of this hydride species to an atmosphere of deuterium gas results in the incorporation of deuterium into both the N-H and Ru-H sites. Whereas the dihydrogen complex catalyzes the hydrogenation of olefins under mild conditions the monohydride complex is inactive.

Reaction of [NPN]$Li_2(S)_2$ (S = tetrahydrofuran) with $[RuCl_2(cod)]_x$ generates the ruthenium cyclooctadienyl complex [NPNH]Ru(η^3:η^2-C_8H_{11}) that forms via deprotonation of the cyclooctadiene ligand by one of the amido donors of the tridentate ligand. This product exists in equilibrium as a mixture of two diastereomers; inter-conversion of the two isomers occurs via intramolecular proton transfer between the amido side-arms of the [NPNH] ligand. The solid-state molecular structure of one of the isomers was determined by X-ray crystallography and it shows that the complex adopts a distorted trigonal bipyramidal (a Y-shape in the trigonal plane) coordination geometry. This structure allows for maximal π-overlap of the amido lone pair with the metal LUMO. Exposure of [NPNH]Ru(η^3:η^2-C_8H_{11}) to H_2 gas yields the three ruthenium hydride complexes [NPNH(η^6-C_6H_5)]RuH, [$NPNH_2$]Ru$(H)_2(C_7D_8)$ and [$NPNH_2$(η^6-C_6H_5)]Ru$(H)_2$. Each of these complexes contains an η^6-bound arene group; in two of the complexes this moiety is the amino phenyl group of the chelating ligand set and in the other it is a coordinated solvent molecule. Each of these three hydride products is inactive toward olefin and imine hydrogenation reactions, however, the cyclooctadienyl complex [NPNH]Ru(η^3:η^2-C_8H_{11})

does reduce these substrates. The catalytic hydrogenation studies that have been performed with all of these complexes are also discussed.

The attempted preparation of [NPN] and [P_2N_2] ruthenium alkylidene and vinylidene complexes is reported. The terminal alkynyl complex [NPNH](P^iPr_3)Ru(CCPh) forms from the reaction of the dilithium salt of the [NPN] ligand with $Cl_2(P^iPr_3)_2Ru(=CCHPh)$ via deprotonation of the vinylidene ligand. The addition of hydrogen gas to this complex produces the thermally unstable bis-dihydrogen dihydride complex $[NPNH_2]Ru(\eta^2\text{-}H_2)_2(H)_2$. The T_1(min) value for the metal-bound hydrogen atoms within this complex is 51 ms observed near 220 K. The dilithium salt of the [P_2N_2] ligand reacts with $Cl_2(P^iPr_3)_2Ru\{=CC(SiMe_3)(Ph)\}$ to give the five-coordinate vinylidene complex $[P_2N_2]Ru\{=CC(SiMe_3)(Ph)\}$. Olefin metathesis reactions including the ring opening metathesis polymerization of norbornene and cross metathesis with styrene are unsuccessful with this complex, however, it does react with H_2 (4 atm) to generate the previously described dihydrogen-hydride complex $[P_2NNH]Ru(\eta^2\text{-}H_2)(H)$.

TABLE OF CONTENTS

LIST OF TABLES

LIST OF FIGURES

GLOSSARY OF TERMS

The following abbreviations, most of which are commonly found in the literature, are used in this thesis.

Å	Angström
Anal	analysis
atm	atmosphere
Ar	aryl (or argon)
binap	2,2′-bis(diphenylphosphino)-1,1′binaphthyl
br	broad
^{n}Bu	*n*-butyl group, $-CH_2CH_2CH_2CH_3$
^{t}Bu	tertiary butyl group, $-C(CH_3)_3$
Bz	benzyl
^{13}C	carbon-13
C_α	carbon atom in the α position
C_β	carbon atom in the β position
cal	calories
Calcd	calculated
CCD	charge coupled device
cod	1,5-cyclooctadiene, C_8H_{12}
COSY	correlated spectroscopy (NMR experiment)
cm	centimetres
cm^{-1}	wave number
Cp	cyclopentadienyl, C_5H_5
Cp^*	pentamethylcyclopentadienyl group, C_5Me_5
cryst	crystal
Cy	cyclohexyl
d	doublet
dd	doublet of doublets
deg (or °)	degrees
dppe	1,2-bisdiphenylphosphino)ethane
dppm	bis(diphenylphosphino)methane

D or ^{2}H	deuterium
1-D	one dimensional
2-D	two dimensional
d^n	numbers of *d*-electrons
d_n	n-deuterated
E_a	energy of activation
eu	entropy units (cal mol^{-1} K^{-1})
Et	ethyl group, $-CH_2CH_3$
^{1}H	proton
$\{^1H\}$	proton decoupled
$\Delta H^{\ddagger}$	enthalpy of activation
$\Delta H°$	standard enthalpy
HOMO	highest occupied molecular orbital
Hz	Hertz, $seconds^{-1}$
I	nuclear spin
IPR	isotopic perturbation of resonance
IR	infrared
$^nJ_{AB}$	n-bond scalar coupling constant between nuclei A and B
K	Kelvin
k	Boltzmann constant
kcal	kilocalories
^{6}Li	lithium-6
^{7}Li	lithium-7
L	neutral two-electron donor
LUMO	lowest unoccupied molecular orbital
M	central metal atom (or molar, when referring to concentration)
M^+	parent ion
m	meta
m	multiplet (NMR spectroscopy)
mm	millimetres
Me	methyl group, $-CH_3$
MHz	megahertz
mL	milliliter

mmol	millimole
MO	molecular orbital
mol	mole
NBD	2,5-norbornadiene
NMR	nuclear magnetic resonance
[NPN]	diamidophosphine ligand $PhP(CH_2SiMe_2NPh)_2$
o	ortho
OTf	triflate anion, $^-OSO_2CF_3$
ORTEP	Oakridge Thermal Ellipsoid Plotting Program
p	para
^{31}P	phosphorus-31
Ph	phenyl group, $-C_6H_5$
PHIP	para hydrogen induced polarization
[PNP]	amidodiphosphine ligand, $N(SiMe_2CH_2PPh_2)_2$
$[P_2N_2]$	diamidodiphosphine ligand, $PhP(CH_2SiMe_2NSiMe_2CH_2)_2PPh$
ppb	parts per billion
ppm	parts per million
^iPr	isopropyl group, $-CH(CH_3)_2$
q	quartet
R	hydrocarbyl substituent
R^2	coefficient of determination for a linear regression
ROMP	ring opening metathesis polymerization
reflns	reflections (X-ray crystallography)
$\Delta S^{\ddagger}$	entropy of activation
$\Delta S°$	standard entropy
s	singlet
$SiMe_3$	trimethylsilyl group, $Si(CH_3)_3$
t	triplet
T	temperature in Kelvin or °C
THF	tetrahydrofuran (C_4H_8O)
tmen	tetramethylethylenediamine, $Me_2NCH_2CH_2NMe_2$
TON	turnover number (mol products per mol catalyst)
V	unit cell volume

VSEPR	valence-shell electron pair repulsion
VT	variable temperature
$w_{1/2}$	width at half height
w	weak
X	halide substituent
η^n	n-hapto
μ	bridging or absorption coefficient (X-ray crystallography)
ρ	density
ρ_{calc}	calculated density
τ	excited state lifetime (NMR)
ν	spectrometer frequency
ν_{xx}	vibrational band for bond xx
λ	wavelength
δ	chemical shift in ppm
μ-X	bridging X-ligand
°C	degrees Celsius

ACKNOWLEDGEMENTS

Over the last five years I have been granted the opportunity to study, learn and experience many of the joys and frustrations that chemical research has to offer. For this I am grateful to my research supervisor Professor Mike Fryzuk who did his best to insure that the joys outweighed the frustrations. His insights into the art of setting up a Schlenk line have remained with me since day one. For the excitement and many good times that have unfolded each and every day in the lab I would like to thank my lab mates both past and present. To Bruce MacKay, Michael Shaver, James Corkin, Lara Morello, Chris Carmichael, Erin Baker and Drs. Chris Kozak, Sam Johnson, Fran Kerton, Laleh Jafarpour, Volker Schmitz, Peihua Yu and Wolfram Seidel, your many helpful suggestions over the years are greatly appreciated. I am especially grateful to Dr. Sam Johnson who taught me to face a challenge from all directions and to answer questions, not with answers, but with more questions.

The UBC support staff are also thanked for their expertise and assistance: Dr. Nick Burlinson, Marietta Austria and Liane Darge (NMR), Mr. P. Borda and Mr. M. Lakha (elemental analysis), Steve Rak and Brian Ditchburn (glassblowing), as well as the personnel of the Mechanical Engineering and Electronics shop. I am especially indebted to Dr. Brian Patrick for solving every crystal structure presented in this thesis. Without his help, much of this work would have been merely speculative.

To my good friends Barry and Rosaleen, Dave and Kelly, Udo, Tanja, Lynsey, Chris and Rob, you have all made my experience in Vancouver one of the most memorable in my life. I would also like to thank the Bricklayers, the greatest basketball team that the chemistry department has produced, and with whom I have shared great times both on and off of the court. I would not be known as "clutch" if not for you guys.

Finally, and most importantly, I am grateful to my family whose support and faith have truly been my pillar of strength.

Michael John Petrella

To my Parents

with love and respect

Chapter 1

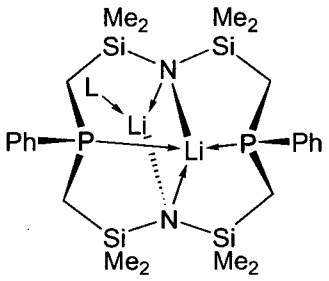

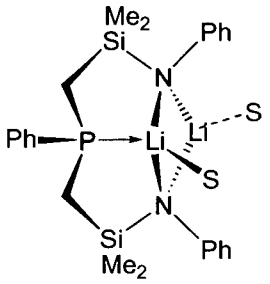

Amido and Phosphine Ligands in Transition Metal Chemistry

1.1 An introduction to amide and phosphine ligands

The structure, stabilization and reactivity patterns of a transition metal complex are governed in large part by the ligands that surround the metal center.[1] A suitable choice of ligands can allow for the production of well-defined reaction centers within a transition metal complex, and the chemistry exhibited by these species can often be "fine-tuned" by simple modification of the ligand sphere; to this end, much effort has been devoted to the development of new ancillary ligands. In the Fryzuk research group, this goal has entailed the design and synthesis of chelating (or macrocyclic) ligand sets comprised of neutral phosphine donors and mono-anionic amide donors. Before discussing the various mixed-donor ligands that have been developed in our lab, a brief discussion concerning these two individual donor types will be given.

References begin on page 23

(i) Phosphine ligands in transition metal chemistry

Phosphine ligands are one of the most important classes of ligands in transition metal chemistry.[2,3] Phosphines are neutral, two electron donors and have the general formula PR_3 (where R = H, alkyl, aryl or halide). A phosphine ligand binds to a metal center through σ-donation of its lone pair to an empty metal orbital. They also possess π-accepting capabilities allowing for back-donation from a filled metal orbital to an empty orbital on the phosphine ligand. This orbital has been described as being either a *d*-orbital[3] or an antibonding sigma orbital (σ^*)[4]; current consensus favours the latter given the relatively high energy of a phosphorus *d*-orbital. A representation of this synergistic bonding scheme is given in Figure 1.1. The π-accepting ability of phosphine ligands renders them as useful donors for electron-rich late transition metals (i.e. metals in low oxidation states).

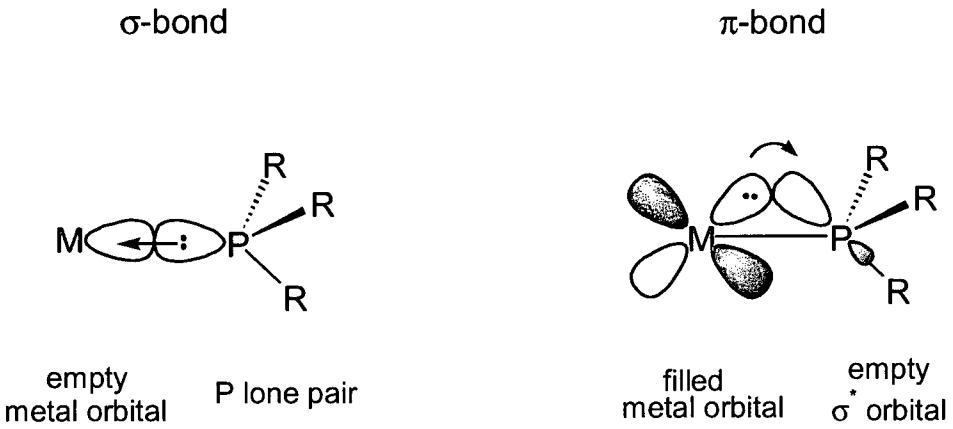

Figure 1.1. Orbital representation of the σ and π-bonding interactions between a phosphine ligand and a metal center.

Phosphine ligands can exhibit a range of σ-donor and π-accepting capabilities depending on the nature of the R-groups bound to the phosphorus atom.[5] As electron-donating groups are placed on the phosphorus atom, for instance, the σ-donating ability will

References begin on page 23

increase whereas the π-accepting ability will decrease. The electron-rich phosphine P^tBu_3 is a stronger σ-donor than PPh_3, which in turn is a stronger σ-donor than PF_3 (which contains electron withdrawing fluorine atoms). On the other hand, the metal-phosphorus π-interaction for these same ligands would be strongest for PF_3 and weakest for P^tBu_3. The electronic properties of a metal center can therefore be fine tuned by substitution of electronically different phosphine ligands.

Modification of the phosphine substituents will also have an effect on the steric attributes of the ligand. An evaluation of the steric demands of a ligand can be deduced by measurement of its cone angle.[2] This entails measuring the "cone" swept out by the ligand at the metal center; in its simplest form, the cone angle is defined as the angle (ϕ) of a cylindrical cone centered 2.28 Å from the phosphorus and touches the outermost atoms of the substituent R groups (Figure 1.2). The triphenylphosphine ligand (PPh_3) has a cone angle of 145°.[3] Replacement of the phenyl groups with cyclohexyl substituents yields the bulkier PCy_3 ligand, which has a cone angle of 170°.[3] The reactivity of a metal complex can also be tuned by modifying the bulk of the ligands in its coordination sphere. For example, whereas the complex $RhCl(PPh_3)_3$ (Wilkinson's catalyst)[6] is effective in olefin hydrogenation processes, the species $RhCl(PMe_3)_3$ does not hydrogenate olefins even under extreme conditions.[7] An important step in the catalytic cycle for Wilkinson's catalyst is dissociation of a phosphine ligand in order to access the active species and the use of the bulkier PPh_3 ligands facilitates this important step (as opposed to PMe_3).

References begin on page 23

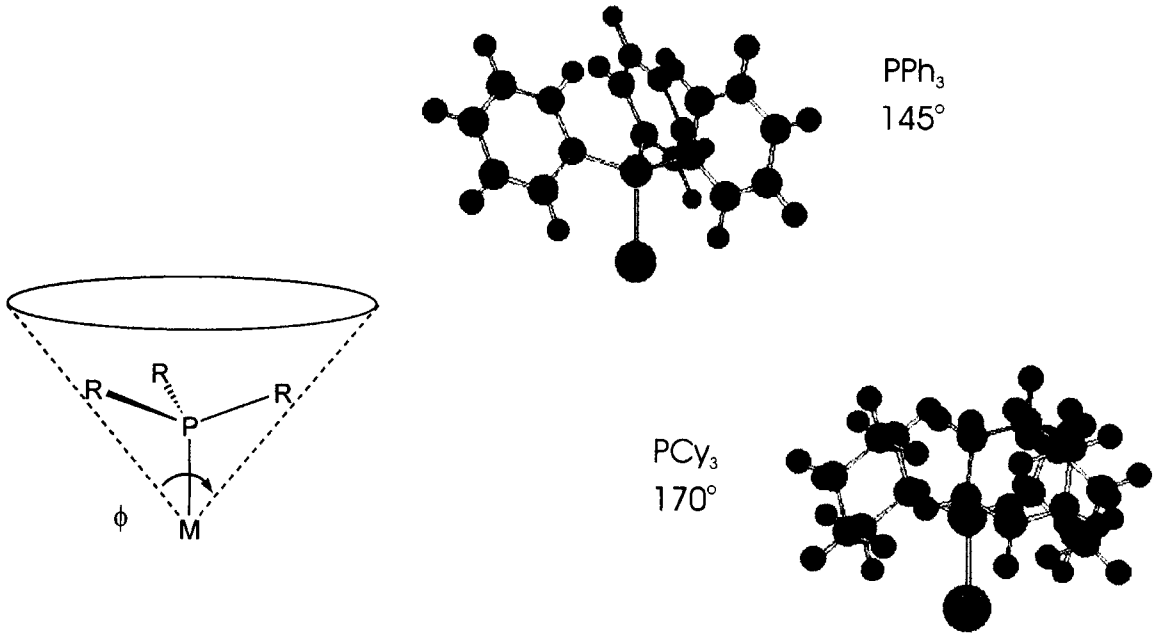

Figure 1.2. Measurement of the cone angle (ϕ) for a phosphine donor (PR_3) with ball-and-stick representations of the PPh_3 ($\phi = 145°$) and PCy_3 ligands ($\phi = 170°$).

In addition to the numerous monodentate phosphine ligands that exist there are many examples of polydentate phosphines[2] including bidentate ligands such as $R_2PCH_2CH_2PR_2$ or $R_2PCH_2PR_2$, and tridentate chelates such as $HC(CH_2PR_2)_3$ or $N(CH_2CH_2PPh_2)_3$. Furthermore, a variety of chiral phosphine ligands (mono- and polydentate) have been synthesized allowing for the preparation of chiral metal complexes; these species are useful in facilitating enantioselective transformations and are employed in asymmetric synthesis and catalytic processes.[8,9]

An additional advantage of using phosphine donors in metal complexes is that the phosphorus-31 (^{31}P) nucleus has a nuclear spin of ½ and is 100 % abundant making it readily observable by nuclear magnetic resonance (NMR) techniques.[10] It is a relatively sensitive nucleus (relative sensitivity = 0.07 with respect to ^{1}H) so that ^{31}P NMR acquisition times and sample concentrations are usually low. The chemical shift window for ^{31}P NMR is rather

References begin on page 23

large and therefore allows for phosphine ligands in different chemical environments to be easily distinguished. Coupling of the phosphorus-31 nucleus to other spin-active nuclei (e.g. ^{1}H, ^{13}C, ^{7}Li) can provide significant details into the solution structure of a complex and the number of peaks present in a ^{31}P NMR spectrum can allow for the symmetry of a complex to be deduced. Monitoring the progress of a reaction by ^{31}P NMR spectroscopy is also a valuable tool.

(ii) Amido ligands in transition metal chemistry

An amide ligand (or amido ligand) is a negatively charged donor, $^{-}NRR'$ (where R, R′ = hydrogen, alkyl, aryl or silyl groups) that results from the deprotonation of an amine HNRR′. In valence bond terms, an amido ligand has two lone pairs of electrons and thus is capable of three types of bonding modes as shown in Figure 1.3.[11] In structure **A** the amide is bound to the metal via a σ-bond leaving one electron pair localized on the nitrogen atom; this requires that the nitrogen centre is sp^3 hybridized and has a pyramidal geometry. An amide ligand can also act as a π-base in which donation of the remaining lone pair of electrons to a suitable vacant orbital on the metal occurs. This results in a planar sp^2 hybridized nitrogen atom (structure **B**). The ability to partake in π-bonding interactions with amide substituents (e.g. aryl or silyl groups) can also yield a planar nitrogen atom.[12] In **C**, both lone pairs are involved in σ-bonding to two separate metal centers such that the amide acts as a bridging ligand; in this coordination mode, the amido ligand is sp^3 hybridized. This bonding mode is often favoured for smaller amide ligands such as the parent amido moiety $^{-}NH_2$.

References begin on page 23

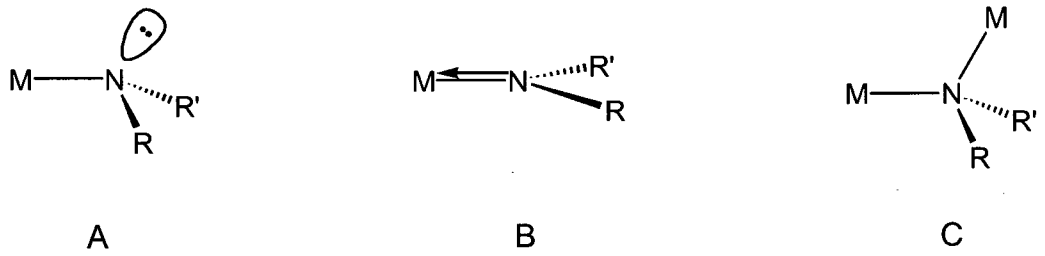

Figure 1.3. Various bonding modes of an amido ligand to a transition metal.

(iii) Metal-amide (M-N) bonding considerations

Amide ligands have been used as anionic donors for both the early[13] and late transition metals[11,12,14] as well as for the lanthanides.[13] The reactivity patterns of the amide linkage when coordinated to a late transition metal, however, are distinctively different from those of early metal complexes. Whereas early transition metal amide bonds are generally thermodynamically and kinetically stable,[13] late transition metal amide complexes have been shown to be much more reactive.[11,14-16] This difference has commonly been explained in terms of the hard-soft acid-base theory.[17] According to this premise an amido ligand (a hard donor) is better suited with the early transition metals (hard acceptors) due to the compatible donor-acceptor properties, whereas M-N linkages are characteristically weak with late metals due to a mismatch of these hard, basic ligands with soft late metals.

Another rationalization that has been given for the observed difference in reactivity of the M-N bond between early and late transition metals involves the interaction of the amido lone pair of electrons with the metal *d*-orbitals.[18] As illustrated in Figure 1.4 (a), complexes that have low valence electron counts (e.g. $\leq d^4$) can be stabilized via π-bonding between the nitrogen lone pair and an empty metal *d*-orbital of correct symmetry. Early transition metals in high oxidation states commonly have d^0 electron counts, and are therefore well suited for amido ligands since they can allow for delocalization of π-electron density from the donor onto the metal. In contrast, the presence of d_π electrons on a metal centre in close proximity to a ligand heteroatom lone pair results in π-electron conflict that increases the reactivity of

References begin on page 23

the heteroatom moiety. As shown in Figure 1.4 (b), this interaction keeps the full population of two electrons on the amide nitrogen atom (and thus keeps the Brønsted basicity and nucleophilicity high). It also raises the energy of the metal d_π-electrons, thus enhancing the oxidizability of the metal center. For late transition metal complexes in low oxidation states the *d*-orbitals will most likely be occupied (e.g. ruthenium(II) has a d^6 valence electron count) thereby destabilizing the metal-amide bond. According to this qualitative bonding scheme amido donors should be well suited for the preparation of high-valent late transition metal complexes. The oxidation of ruthenium(II) amine complexes, for example, results in the formation of stable ruthenium (IV) amido complexes $[Ru(bpy)\{H_2NCMe_2CMe_2NH\}_2]^{2+}$ (where bpy = 2,2′-bipyridine) and $[Ru(L)\{H_2NCMe_2CMe_2NH\}_2]^{2+}$ (where L = 2,3-diamino-2,3-dimethylbutane).[19]

References begin on page 23

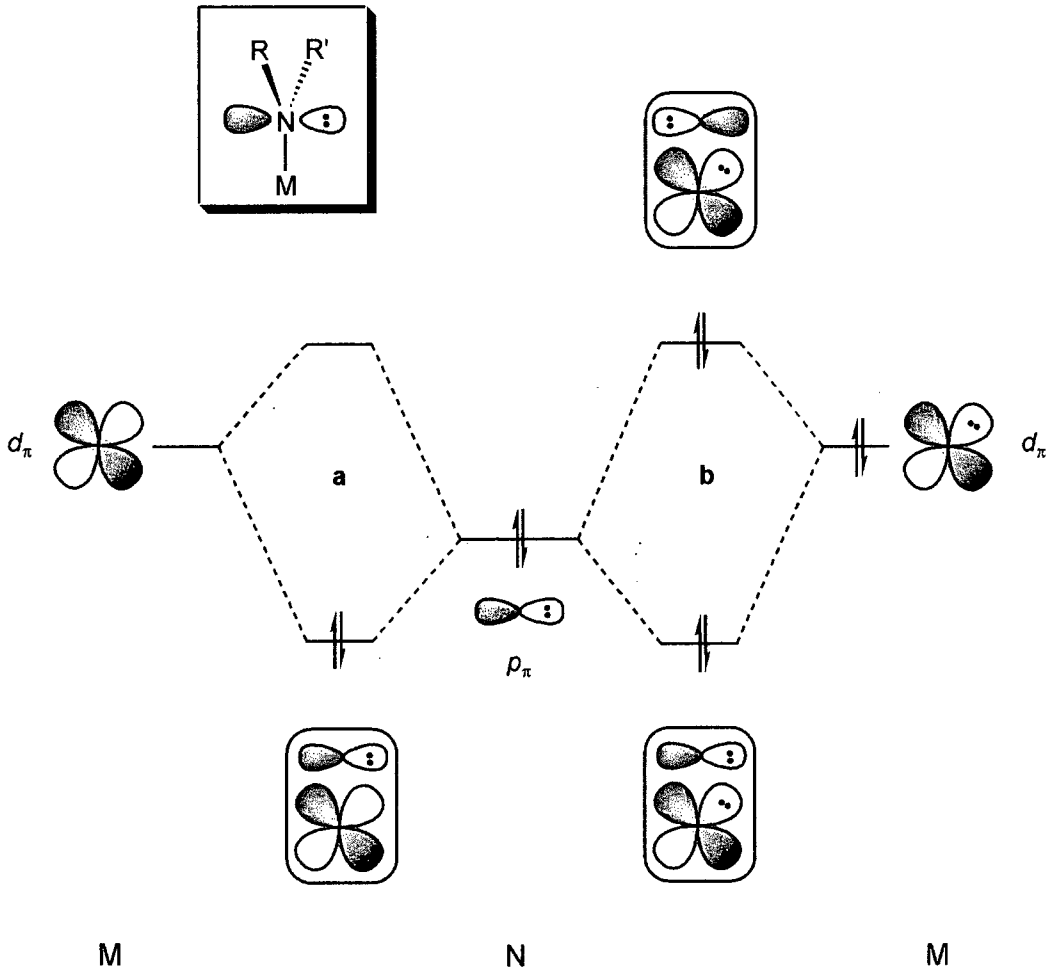

Figure 1.4. A qualitative molecular orbital diagram illustrating the interaction between a π-symmetry amide lone pair of electrons (p_π) and the (**a**) empty and (**b**) filled d_π-orbitals of a transition metal.

The electrostatic-covalent (*E-C*) theory of bonding[20,21] has also been used to describe the interaction between a transition metal and an anionic donor such as an amide ligand.[22,23] This theory states that every bond has both an electrostatic and a covalent component; in the case of a metal amide bond (M-N) it was shown that the electrostatic component has a greater contribution to the bond strength than does the covalent component. In other words, a transition metal has a greater inclination to bind electrostatically than covalently to an amide ligand. Since the electronegativity of the transition series increases from the early to

References begin on page 23

the late metals, the electrostatic interaction between an amido ligand and a transition metal decreases from left to right across this series. Accordingly, electropositive early transition metals will have a stronger electrostatic metal-amide interaction and consequently a stronger M-N bond.

(iv) Preparation of late transition metal amide complexes

A variety of synthetic strategies are available for the incorporation of an amide unit onto a late transition metal.[11,14] One of the most convenient procedures involves the metathesis of a transition metal halide or triflate complex with an alkali metal amide. Care must be taken in this transmetalation process since reduction in lieu of metathesis is a common side reaction and in many cases the choice of cation and solvent system is crucial to the success of these reactions.[11] The ruthenium(II) diphenyl amido complex $Cp^*(PMe_3)_2Ru(NPh_2)$ has been prepared via salt metathesis as depicted in Scheme 1.1.[24]

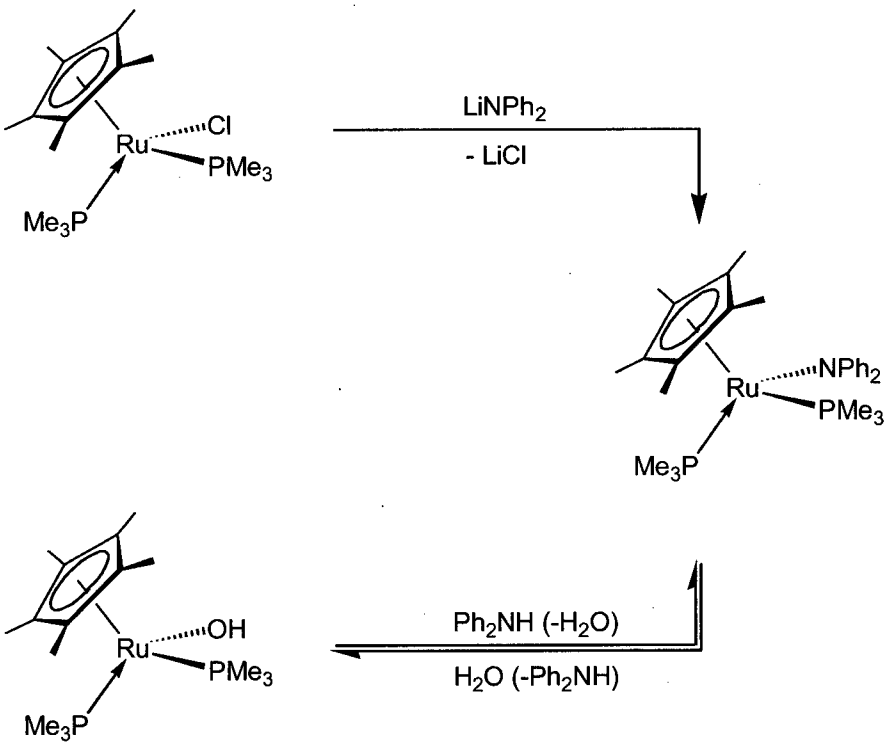

Scheme 1.1

References begin on page 23

The protonation of basic ligands such as alkoxides or alkyls by amine ligands (σ-ligand metathesis) is another route that has been employed for the preparation of late transition metal amido complexes. The addition of diphenyl amine (Ph_2NH) to the hydroxy complex $Cp^*(PMe_3)_2Ru(OH)$, for example, affords $Cp^*(PMe_3)_2Ru(NPh_2)$; the amido and hydroxy complexes exists as an equilibrium mixture (Scheme 1.1).[24] This methodology is also applicable in the rhenium-amide system shown in equation 1.1. In this system the equilibrium can be driven towards the rhenium anilido complex by the use of 4 Å molecular sieves, which sequester the methanol that is generated.[15]

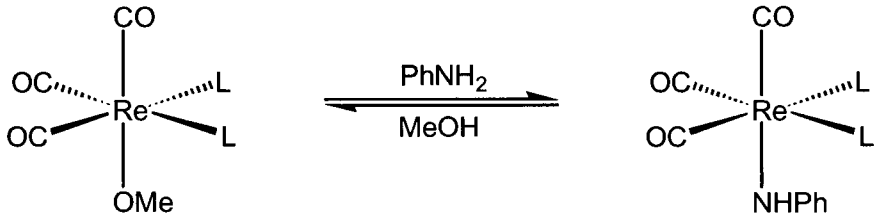

[1.1]

Other methods that have been employed for the preparation of late transition metal amide complexes include the deprotonation of a coordinated amine ligand (equation 1.2)[11] and nucleophilic attack of a coordinated imine ligand (equation 1.3).[25,26]

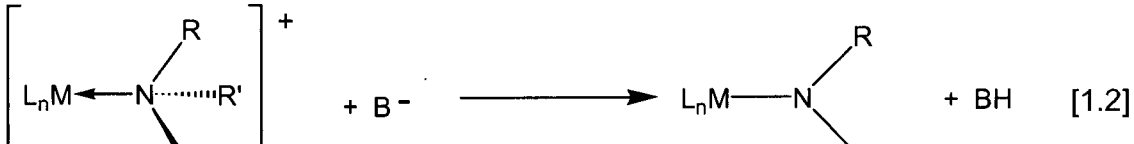

[1.2]

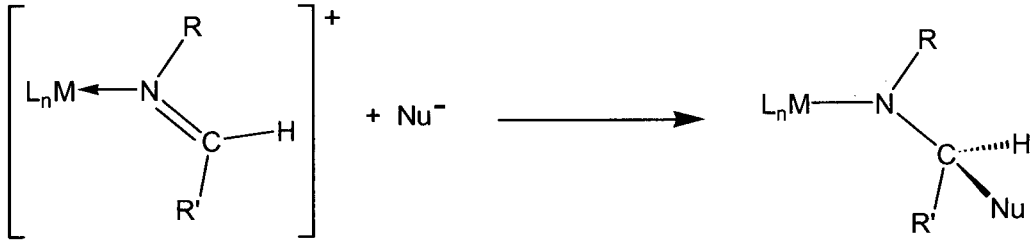

[1.3]

References begin on page 23

(v) Reactivity of the late transition metal-amide bond

(a) Protonation reactions of late metal amides

The majority of late transition metal amide complexes display reactivity at the M-N bond that is more closely related to the chemistry that might be expected of an alkali metal amide rather than the reactivity of a charge-neutral organic amine.[15] Late metal amides have been shown to act as Brønsted bases and undergo protonation reactions with a variety of acids.[16] In the example shown in equation 1.4 protonation of the aryl amide ligand by water generates a dinuclear nickel species containing two hydroxy bridges along with an equivalent of aryl amine.[27]

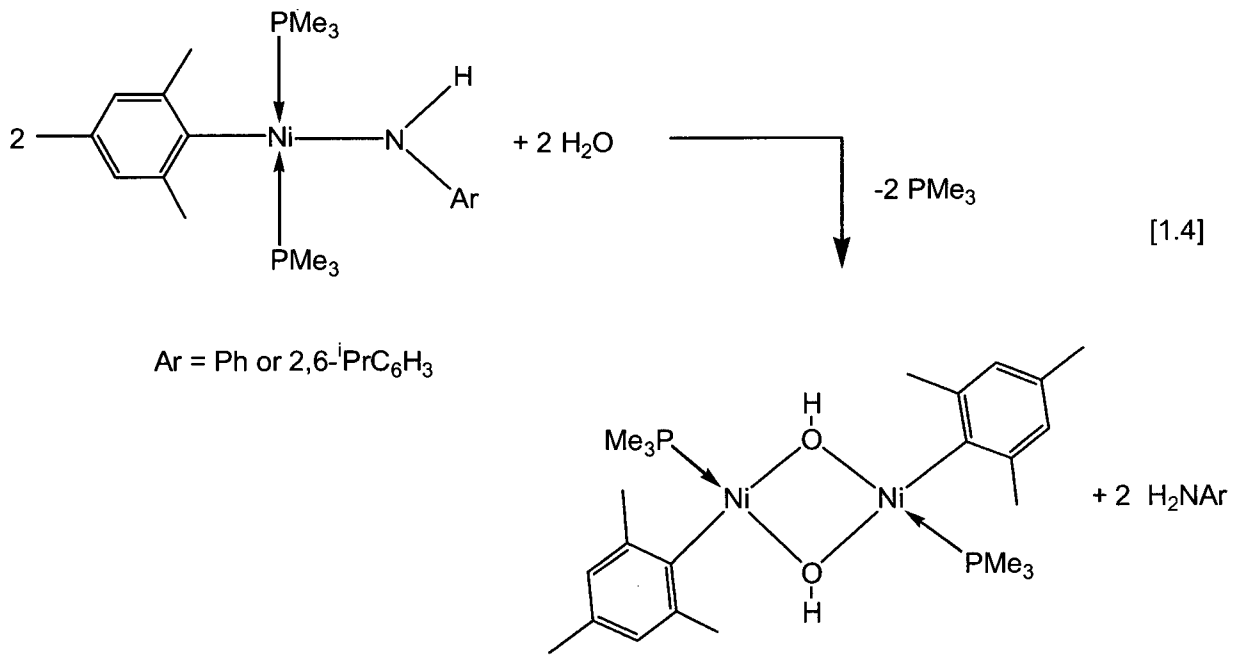

The substituents at the amido nitrogen position have been shown to play a key role in the observed basicity of the amido ligand in late metal systems. The parent amido complex $TpRu(CO)(PPh_3)(NH_2)$ (Tp = tris{pyrazolylborate}), for instance, can deprotonate weak acids including phenylacetylene ($pK_a \approx 23$) at room temperature.[28] The related complex $TpRu(CO)(PPh_3)(NHPh)$ bearing a phenyl-substituted amido ligand on the other hand was

References begin on page 23

unreactive towards weak acids even at elevated temperatures for prolonged periods (72 h at 70 °C).[28] It was suggested that the presence of the amido phenyl ring mitigated the amido basicity via delocalization of the nitrogen lone electron pair.

(b) Late metal amides as nucleophiles and migratory insertion reactions

Related to the protonation reactions discussed above are the reactions of late metal amides with electrophiles and Lewis acids. Nucleophilic chemistry has been reported for the platinum (II) complex (dppe)(Me)Pt{N(Me)(Ph)} (dppe = $Ph_2PCH_2CH_2PPh_2$) with acetyl chloride and CD_3I as shown in Scheme 1.2.[29]

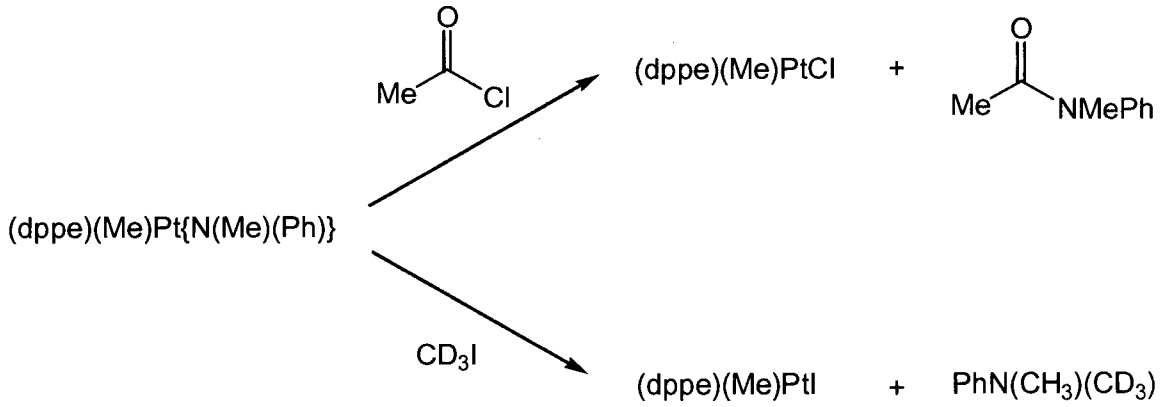

Scheme 1.2

Heterocumulenes (e.g. CO_2, CS_2, RNCO) have commonly been used to probe the nucleophilicity of metal alkoxide and amide complexes. The amido complex $Cp^*(PPh_3)(H)Ir(NHPh)$ undergoes nucleophilic insertion chemistry with carbon disulfide to form the metalloxanthate complex $Cp^*(PPh_3)(H)Ir(SC(S)NHPh)$ as shown in equation 1.5.[15] The product of this reaction is a result of net nucleophilic attack by the amido nitrogen atom at the electrophilic carbon of the CS_2 molecule.

References begin on page 23

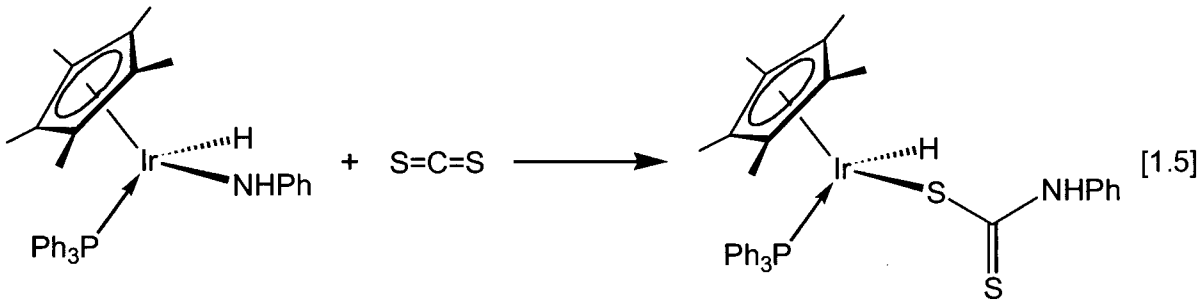

[1.5]

The reaction of CO_2 with ruthenium(II) anilido complexes of the type (η^6-arene)(PMe_3)(R)Ru(NR'Ph) is related to the iridium system discussed above, and also provides evidence for nucleophilic behaviour of the amido nitrogen atom.[30] This chemistry is summarized in equation 1.6. The addition of carbon dioxide to the ruthenium complexes results in the net insertion of CO_2 into the Ru-N bond to give a metal carbamate complex. Given the electronic saturation at the metal centre a likely reaction pathway involves direct attack of the nitrogen lone pair on CO_2 followed by Ru-O bond formation. While the reaction with complex **A** proceeded to only 70 % conversion, the quantitative formation of the carbamate complexes was observed with **B** and **C**. It was postulated that the increased electron richness of the *para*-toluamide ligand in **C** and the better electron donating ability of the methyl ligand in **B** (versus the phenyl group in **A**) makes the amido nitrogen atom more nucleophilic; this difference in reactivity supports a nucleophilic insertion process.

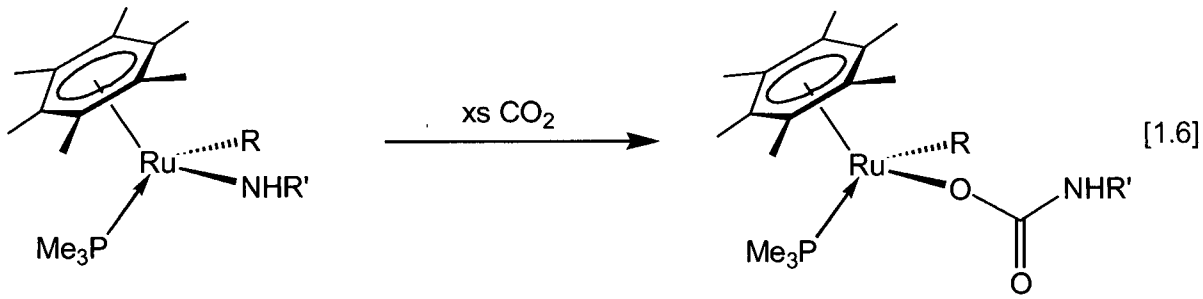

[1.6]

A: R = Ph, R' = Ph
B: R = Me, R' = Ph
C: R = Ph, R' = *p*-tol

The migratory insertion of unsaturated molecules into the M-N bond of late transition metal amido complexes has also been reported.[11,14,31-35] Whereas the insertion of CO into

References begin on page 23

metal-carbon bonds is a widely observed phenomenon in organometallic chemistry[3] relatively fewer examples with metal amides are known.[15,36,37] In one report the facile insertion of carbon monoxide in an iridium anilido complex was shown to take place (equation 1.7).[34] The platinum amide complex (dppe)(CH_3)Pt($NHCH_2Ph$) preferentially inserts carbon monoxide into the Pt-N bond to generate (dppe)(CH_3)Pt{$CONH(CH_2Ph)$}.[33] However, in many cases the addition of carbon monoxide to a late transition metal amide complex does not result in its insertion into the M-N bond. For example, the complex (η^5-C_5Me_5)(PMe_3)$_2$Ru(NPh_2) reacts with CO by displacement of PMe_3 to give the carbonyl complex (η^5-C_5Me_5)(PMe_3)(CO)Ru(NPh_2),[24] and the platinum (0) species (PEt_2)$_2$(CO)$_2$Pt is generated upon addition of CO to the complex *trans*-(PEt_2)$_2$(H)Pt(NHPh) with the concomitant formation of aniline.[33]

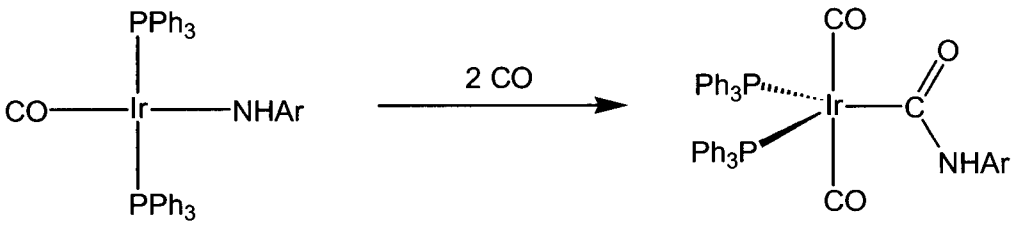

[1.7]

(c) β-hydride elimination

A viable decomposition route for late transition metal amide complexes is β-hydride elimination (Scheme 1.3); given that the amide ligand $^-NR_2$ is isoelectronic with an alkyl moiety $^-CR_3$ it is not surprising that β-hydride elimination occurs since this is also a common decomposition pathway for metal alkyls.[11,38-40]

References begin on page 23

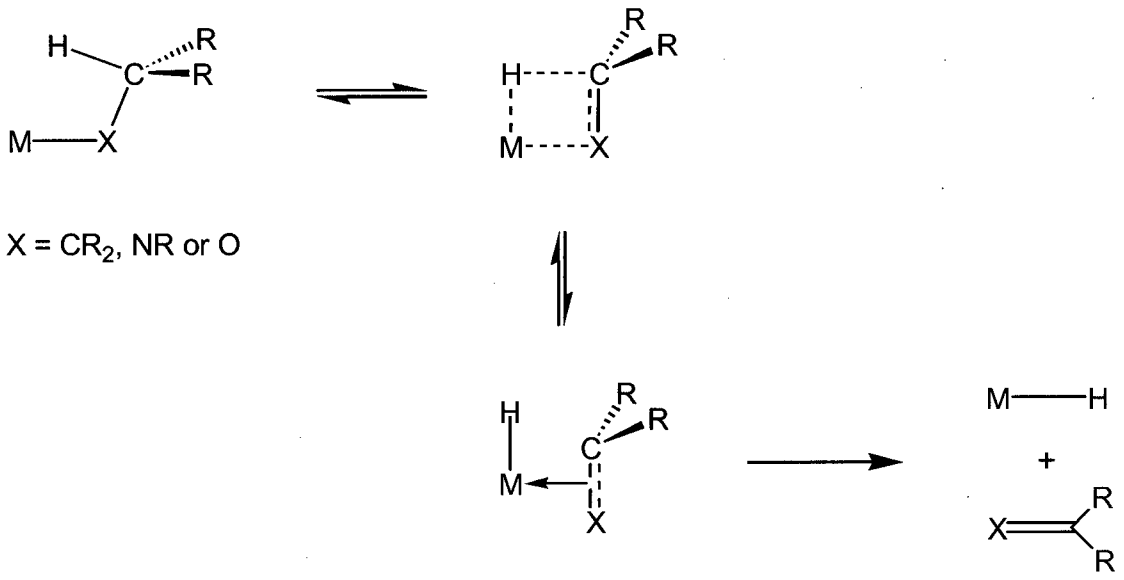

Scheme 1.3

This process can be a useful preparative reaction for the synthesis of late transition metal hydride complexes as shown in Scheme 1.4 for the reaction of lithium dimethyl amide ($LiNMe_2$) with $RuCl_2(PPh_3)_4$.[41] The use of $LiN(CD_3)Me$ in the reaction with $RhCl(PPh_3)_3$ generated both $RhH(PPh_3)_3$ and $RhD(PPh_3)_3$ isotopomers in a ratio of 6:1 (thus giving a deuterium isotope effect, k_H/k_D of 6), indicating that cleavage of the C-H bond is the rate-determining step.[41] One way to circumvent this decomposition pathway is to utilize amido substituents that do not contain β-hydrogen atoms such as the trimethylsilyl moiety or the phenyl group; the complexes $RuH\{N(SiMe_3)_2\}(PPh_3)_2$ and $Pt(PEt_2)(NPh_2)$, for example, have successfully been prepared.[11]

References begin on page 23

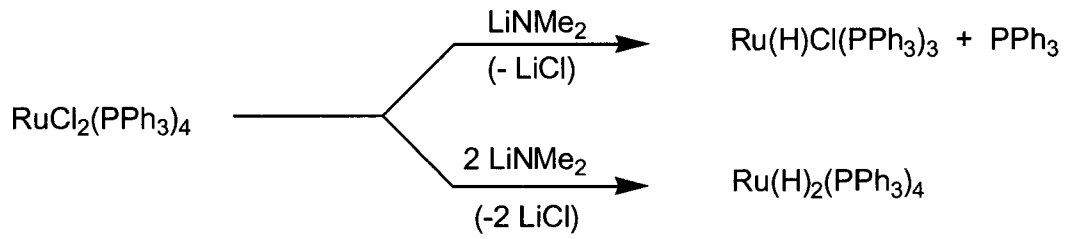

Scheme 1.4

(d) Hydrogenolysis of metal amides

Of particular importance to this thesis is the ability of a late transition metal-amide bond to effect the heterolytic cleavage of dihydrogen.[11] Recent experimental studies have shown the metal-amide linkage in late transition metal complexes to be highly polarized and possess significant ionic character.[15,23] This feature is well suited for the deprotonation of a coordinated H_2 ligand as depicted in equation 1.8. In this heterolytic cleavage process a metal hydride and an amine ligand are formed.

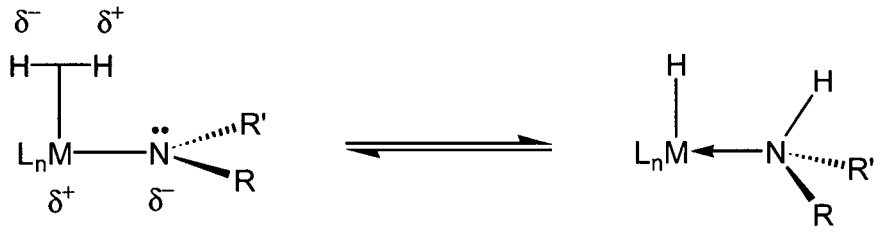

[1.8]

The first example of the activation of dihydrogen by a late metal amide complex was reported in the Fryzuk research group and involved an iridium (I) [PNP] system (equation 1.9).[42] Since the amine ligand is anchored within the chelating ligand set it does not dissociate from the metal centre. [PNP] complexes of rhodium(I)[43,44] and ruthenium(II)[45] were also shown to be capable of splitting H_2 in a heterolytic fashion. The cleavage of H_2 by ruthenium amido moieties has been proposed as a key step in catalytic hydrogenation of ketones and imines by ruthenium(II) complexes that operate by the bifunctional mechanism.[46-49]

References begin on page 23

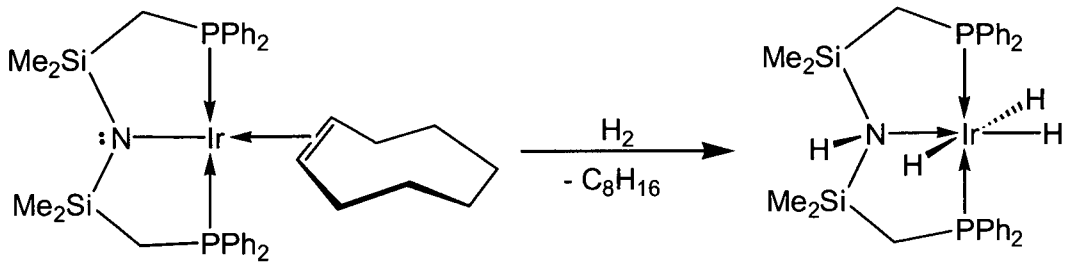

[1.9]

1.2 The mixed-donor amidophosphine ligands [PNP], [P_2N_2] and [NPN]

In the Fryzuk research group, hybrid ligands that contain phosphine and amide donors in a chelating array have been developed. It was envisioned that by combining these "hard" and "soft" donor types within a single ligand scaffold, these ligands would be suitable for coordination to a variety of metals in various oxidation states. The first such ligand utilizing this combination of donor types was the tridentate amidodiphosphine ligand $N(SiMe_2CH_2PR_2)_2$, abbreviated ^{R}[PNP] (where R = Me, ^{i}Pr, ^{t}Bu or Ph).[50] This mono-anionic ligand contains an amido donor flanked by two phosphines; it is an extremely versatile ligand that has been successfully applied to both early and late transition metals.[51] The pendant phosphine donors are well suited for coordination to low oxidation state late transition metals whereas the central amide binds strongly to high oxidation state early transition metals.[12,13] The chelating nature of the ^{R}[PNP] ligand assists stabilization of the apparent mismatch in donor types, and thus aids in securing the ligand to a variety of metals. Although an overview of the chemistry of the ^{R}[PNP] ligand will not be given in this thesis, a summary of ^{R}[PNP] complexes of ruthenium(II) will be given in a later section. The preparation of the lithiated ligand precursor ^{R}[PNP]Li is shown in equation 1.10. For alkyl phosphines, a single step procedure is possible, which involves the addition of the commercially available disilazane $HN(SiMe_2CH_2Cl)_2$ with three equivalents of $LiPR_2$; two equivalents functionalize the chloromethyl side-arms and the third equivalent deprotonates the amine generating a lithium amide. Metal complexes of ^{R}[PNP] are easily prepared by reaction of the lithiated ligand precursor with metal halide via salt metathesis.

References begin on page 23

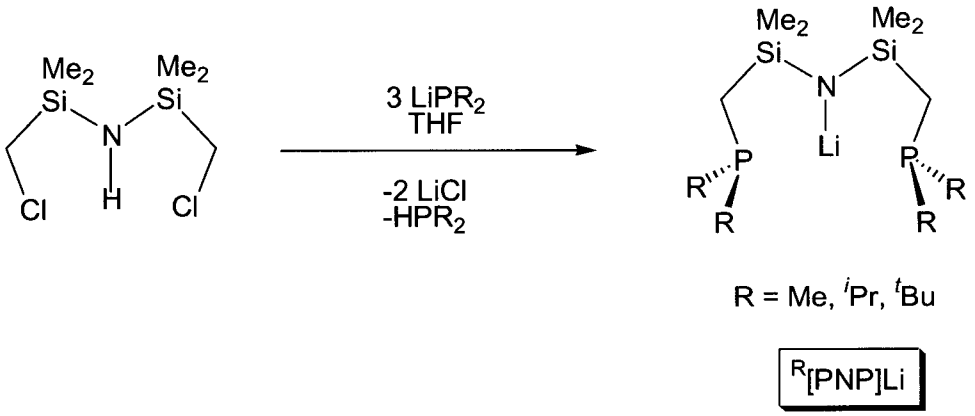

[1.10]

The $[P_2N_2]$ macrocycle is another mixed-donor ligand that has been developed in the Fryzuk research group.[52] It is a four-coordinate, dianionic ligand that can be considered an extension of the tridentate ^{R}[PNP] set in which the two phosphine donors have been linked with an additional disilazane moiety. The preparation of the dilithium salt $[P_2N_2]Li_2{\bullet}(C_4H_8O_2)$ (where, $[P_2N_2]$ = $PhP(CH_2SiMe_2NSiMe_2CH_2)_2PPh$ and $C_4H_8O_2$ is 1,4-dioxane) is outlined in Scheme 1.5. The dilithium salt of the macrocycle is a useful precursor to $[P_2N_2]$ metal complexes and both early and late transition metal species have been prepared via salt metathesis reactions with metal halide starting materials.[53-60] The relative ease at which this ligand is prepared is quite remarkable. Macrocyclic ligand synthesis is often achieved by employing very high dilution techniques or by utilizing metal templates to enforce ring-closure.[61,62] It is possible that the Li_2N_2 core within this ligand facilitates ring-closure via phosphine coordination. Since the phosphine atoms within the $[P_2N_2]$ ligand are able to exhibit different stereochemistries[63,64] that can result in two isomeric forms of this ligand, it also impressive that the *syn*-$[P_2N_2]$ isomer (shown in Scheme 1.5 with the phosphine phenyl groups oriented in the same direction) can be exclusively prepared by the appropriate choice of solvent and temperature. Only the *syn* isomer is utilized in the work discussed throughout this thesis, and as such this prefix will be omitted. An advantage of the $[P_2N_2]$ macrocycle is that the steric and electronic properties of this ligand can be modified by varying the substituent of the phosphine donor.

References begin on page 23

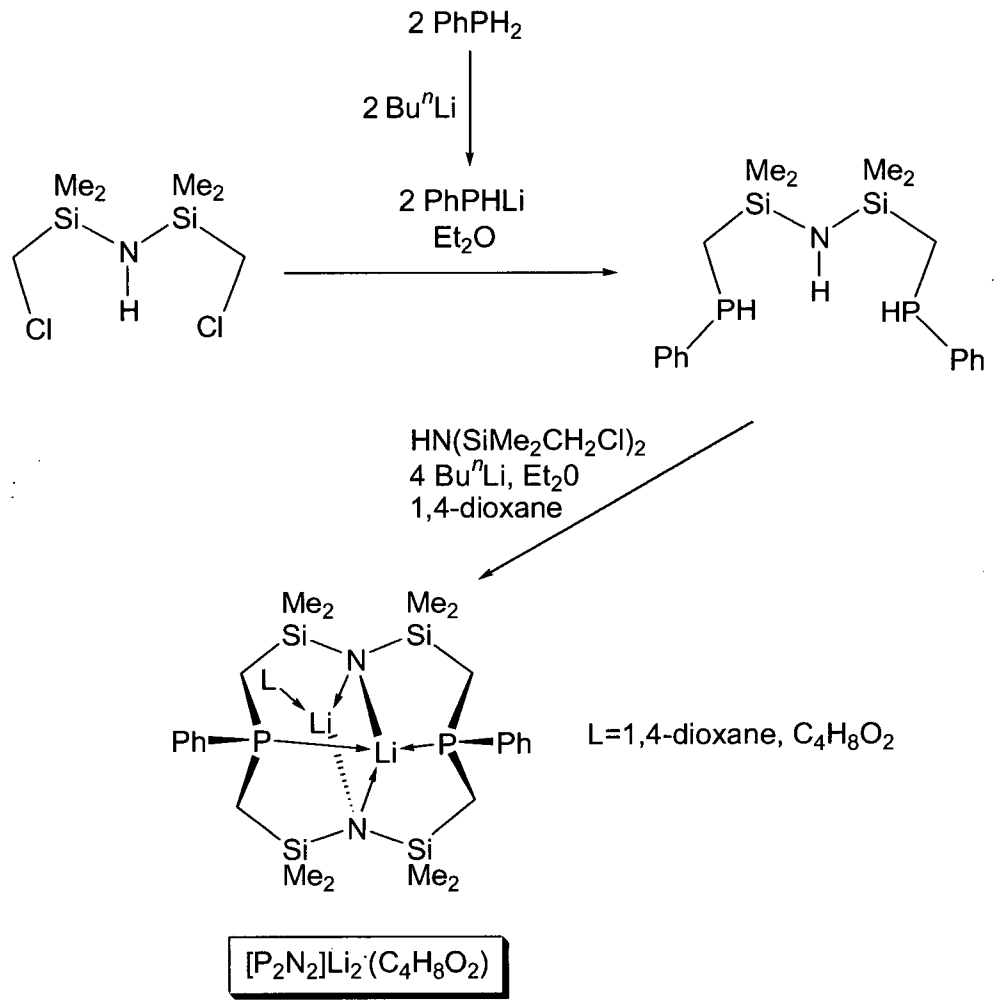

Scheme 1.5

A drawback of some metal complexes that contain the $[P_2N_2]$ macrocycle is that they are often coordinatively and electronically saturated, and this can result in the formation of very stable species with unreactive metal centers. One way to alleviate this problem is to allow for more coordinative unsaturation at the metal centre; this has been achieved by the development of the diamidophosphine ligand $PhP(CH_2SiMe_2NPh)_2$ (abbreviated as [NPN]). The synthesis of the dilithium salt of the [NPN] ligand is given in Scheme 1.6.[65] Similar to the $[P_2N_2]$ ligand the [NPN] donor set is dianionic, however, it is a tridentate chelating ligand. It can be considered as a variant of the $[P_2N_2]$ ligand with one of the phosphine ligands removed. Also, whereas in the $[P_2N_2]$ macrocycle only the phosphine groups could

References begin on page 23

be changed, the [NPN] chelate allows for modification of both the phosphorus and nitrogen donors.

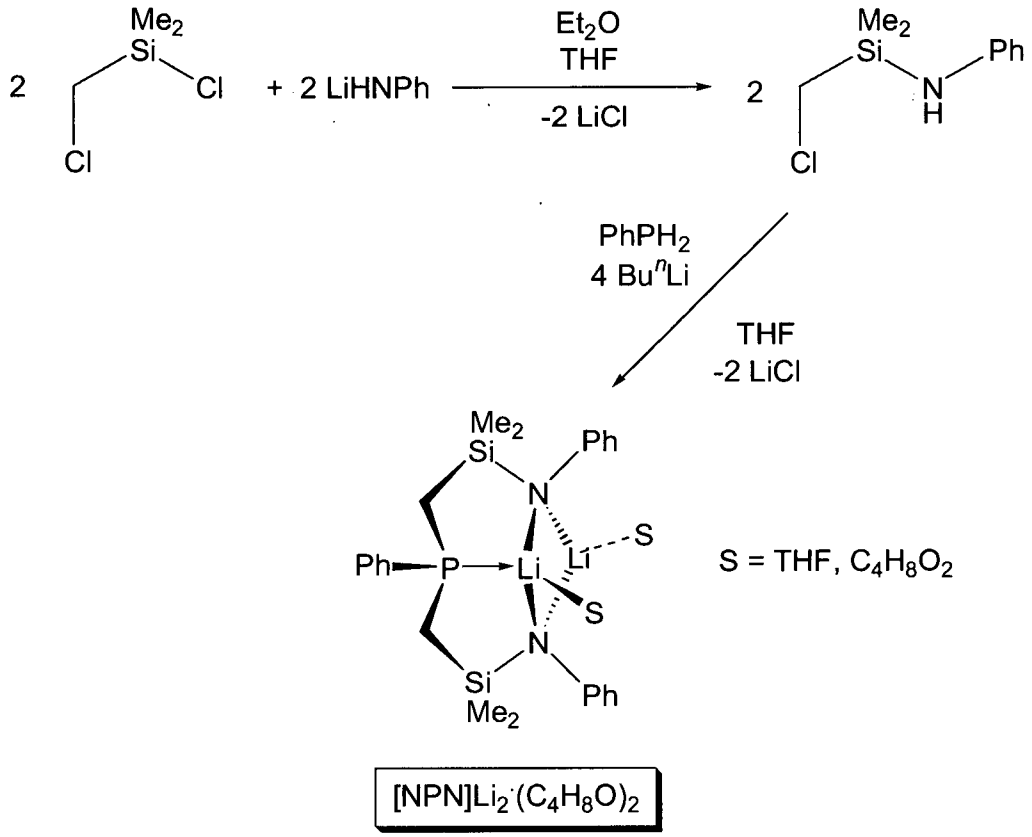

Scheme 1.6

1.3 [PNP] ruthenium(II) chemistry

A summary of the chemistry of ruthenium(II) complexes that incorporate the tridentate [PNP] ligand set is shown in Scheme 1.7.[45] The reaction of the lithium salt [PNP]Li with $RuCl_2(PPh_3)_3$ generates the amide complex [PNP]RuCl(PPh_3) (**A**). The presence of the soft phosphine donors and the chelating nature of the [PNP] array help to stabilize the hard amido donor towards the soft ruthenium(II) centre. In addition, the lack of

References begin on page 23

β-hydrogen atoms on the amido donor eliminates the possibility of β-hydride elimination as a decomposition pathway. Treatment of complex **A** with one atmosphere of hydrogen gas generates the hydrido-amide complex [PNHP]RuHCl(PPh_3) (**B**); the coordinated amide ligand in **A** acts as a base and cleaves the H_2 molecule heterolytically. This reaction is the first reported example of the heterolytic activation of H_2 by a ruthenium-amide species. The hydrogenation product actually exists as a pair of isomers (**B** and **B′**) and both contain an intramolecular hydrogen bond between the amino proton and the chloride ligand. In an attempt to prepare ruthenium alkyl complexes the reaction of complex **A** with lithium alkyl and Grignard reagents was performed. In all of these cases the product that formed was the *ortho*-metalated complex [PNP]Ru($C_6H_4PPh_2$) (**C**). Upon exposure of complex **C** to an atmosphere of hydrogen gas it is converted to the monohydride amide [PNP]RuH(PPh_3) (**D**). Interestingly, no further reaction is observed with excess H_2. The addition of triethylphosphine to complex **A** also results in *ortho*-metalation of the triphenylphosphine ligand and generates the complex [PNHP]RuCl($C_6H_4PPh_2$) (**E**). It was proposed that coordination of PEt_3 to the open site of the square pyramidal geometry of **A** forced the PPh_3 ligand in closer proximity to the amide nitrogen, thus assisting removal of the phenyl *ortho* hydrogen atom. Complex **E** reacts with dihydrogen to give the previously identified hydrido amine complex **B′**.

References begin on page 23

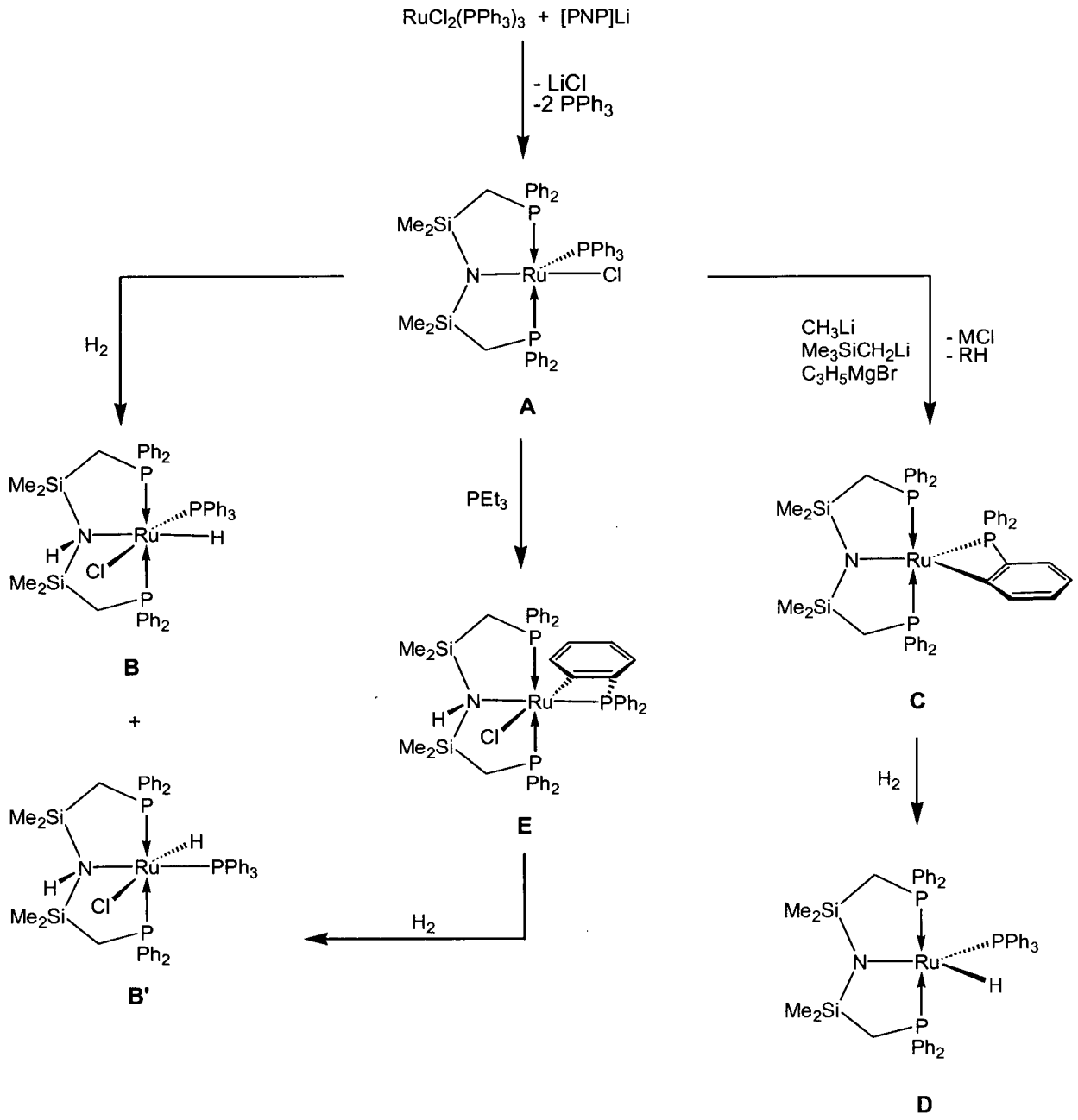

Scheme 1.7

References begin on page 23

1.4 Scope of this thesis

In this thesis an investigation into the chemistry of ruthenium(II) complexes that incorporate the mixed-donor [NPN] and [P_2N_2] ligands is undertaken. Two different roles for these ligand sets were envisioned. In one capacity the reactive nature of the ruthenium-amido moiety was exploited to effect the heterolytic cleavage of molecular hydrogen in an attempt to prepare ruthenium complexes with *cis*-coordinated hydride and amine ligands. Coordinatively saturated ruthenium(II) complexes that contain *cis*-located hydride and amine ligands have been reported to be among the most active species for catalytic ketone and imine hydrogenation reactions.[46-49,66] Chapter 2 presents the synthesis and characterization of various ruthenium(II) amido complexes of the [P_2N_2] and [NPN] ligands. Whereas X-ray diffraction proved to be of fundamental importance in the characterization of these new species, the utility of NMR spectroscopy including variable-temperature and isotopic labeling studies to elucidate structure and solution behaviour is also described. The reactivity of these complexes with hydrogen gas is discussed in Chapter 3 along with catalytic hydrogenation studies of olefin and imine substrates. The second role that was anticipated for the [P_2N_2] and [NPN] ligands was for these ligand sets to act as stabilizing ancillary donors and to examine their influence in known catalytic processes involving ruthenium(II) systems. In particular, modification of ruthenium alkylidene and vinylidene complexes that have been used in olefin metathesis processes has been investigated. In Chapter 4 the reaction of the [P_2N_2] and [NPN] ligand sets with alkylidene and vinylidene precursors is described together with structural characterization of the new complexes and their reactivity towards H_2 and olefin substrates.

1.5 References

(1) McAuliffe, C. A. *Comprehensive Coordination Chemistry*; Wilkinson, G., Gillard, R. D. and McCleverty, J. A., Eds; Pergamon Press: London, 1987; Vol. 2.

References begin on page 23

(2) Cotton, F. A.; Wilkinson, G.; Murillo, C. A.; Bochmann, M. *Advanced Inorganic Chemistry: A Comprehensive Text*; 6th ed.; John Wiley and Sons, Inc.: Toronto, 1999.

(3) Collman, J. P.; Hegedus, L. S. *Principles and Applications of Organotransition Metal Chemistry*; University Science Books: Mill Valley, 1980.

(4) Marynick, D. S. *J. Am. Chem. Soc.* **1984**, *106*, 4064.

(5) Greenwood, N. N.; Earnshaw, A. *Chemistry of the Elements*; 2nd ed.; Butterworth-Heinemann: Oxford, 1997.

(6) Osborn, J. A.; Jardine, F. H.; Young, J. F.; Wilkinson, G. *J. Chem. Soc. A.* **1966**, 1711.

(7) Jones, R. A.; Real, F. M.; Wilkinson, G.; Galas, A. M. R.; Hursthouse, M. B.; Malik, K. M. A. *J. Chem. Soc., Chem. Commun.* **1979**, 489.

(8) Comarov, I. V.; Borner, A. *Angew. Chem. Int. Ed.* **2001**, *40*, 1197.

(9) Knowles, W. S. *Acc. Chem. Res.* **1983**, *16*, 206.

(10) Pregosin, P. S.; Kunz, R. W. *NMR Basic Principles and Progress*; Springer-Verlag: Heidelberg, 1979; Vol. 16.

(11) Fryzuk, M. D.; Montgomery, C. D. *Coord. Chem. Rev.* **1989**, *95*, 1.

(12) Lappert, M. F.; Power, P. P.; Sanger, A. R.; Srivastava, R. C. *Metal and Metalloid Amides*; John Wiley and Sons Canada Limited: Toronto, 1980.

(13) Kempe, R. *Angew. Chem. Int. Ed.* **2000**, *39*, 468.

References begin on page 23

(14) Bryndza, H. E.; Tam, W. *Chem. Rev.* **1988**, *88*, 1163.

(15) Fulton, J. R.; Holland, A. W.; Fox, D. J.; Bergman, R. H. *Acc. Chem. Res.* **2002**, *35*, 44.

(16) Fulton, J. R.; Bouwkamp, M. W.; Bergman, R. G. *J. Am. Chem. Soc.* **2000**, *122*, 8799.

(17) Pearson, R. G. *J. Chem. Educ.* **1968**, *45*, 581.

(18) Caulton, K. G. *New. J. Chem.* **1994**, *18*, 25.

(19) Chiu, W. H.; Peng, S. M.; Che, C. M. *Inorg. Chem.* **1996**, *35*, 3369.

(20) Drago, R. S.; Wong, N. M.; Ferris, D. C. *J. Am. Chem. Soc.* **1992**, *114*, 91.

(21) Drago, R. S. *Applications of Electrostatic-Covalent Models in Chemistry*; Surfside: Gainesville, Fl., 1994.

(22) Holland, P. L.; Andersen, R. A.; Bergman, R. G. *Comments Inorg. Chem.* **1999**, *21*, 115.

(23) Holland, P. L.; Andersen, R. A.; Bergman, R. G.; Huang, J.; Nolan, S. P. *J. Am. Chem. Soc.* **1997**, *119*, 12800.

(24) Bryndza, H. E.; Fong, L. K.; Paciello, R. A.; Tam, W.; Bercaw, J. E. *J. Am. Chem. Soc.* **1987**, *109*, 1444.

(25) Martin, G. C.; Boncella, J. M. *Organometallics* **1989**, *8*, 2968.

(26) Martin, G. C.; Boncella, J. M.; Wucherer, E. J. *Organometallics* **1991**, *10*, 2804.

References begin on page 23

(27) VanderLende, D. D.; Abboud, K. A.; Boncella, J. M. *Inorg. Chem.* **1995**, *34*, 5319.

(28) Jayaprakash, K. N.; Gunnoe, T. B.; Boyle, P. D. *Inorg. Chem.* **2001**, *40*, 6481.

(29) Bryndza, H. E.; Fultz, W. C.; Tam, W. *Organometallics* **1985**, *4*, 939.

(30) Boncella, J. M.; Eve, T. M.; Rickman, B.; Abboud, K. A. *Polyhedron* **1998**, *17*, 725.

(31) Cabeza, J. A.; del Rio, I.; Grepioni, F.; Moreno, M.; Riera, V.; Suarez, M. *Organometallics* **2001**, *20*, 4190.

(32) Cabeza, J. A.; del Rio, I.; Moreno, M.; Riera, V. *Organometallics* **1998**, *17*, 3027.

(33) Cowan, R. L.; Trogler, W. C. *Organometallics* **1987**, *6*, 2451.

(34) Rahim, M.; Ahmed, K. J. *Organometallics* **1994**, *13*, 1751.

(35) Rahim, M.; Bushweller, H.; Ahmed, K. J. *Organometallics* **1994**, *13*, 4952.

(36) Hauger, B. E.; Huffman, J. C.; Caulton, K. G. *Organometallics* **1996**, *15*, 1856.

(37) Li, J. J.; Li, W.; James, A. J.; Holbert, T.; Sharp, T. P.; Sharp, P. R. *Inorg. Chem.* **1999**, *38*, 1563.

(38) Driver, M. S.; Hartwig, J. F. *J. Am. Chem. Soc.* **1995**, *117*, 4708.

(39) Cetinkaya, B.; Lappert, M. F.; Torroni, S. *Chem. Commun.* **1979**, 599.

(40) Hartwig, J. F. *J. Am. Chem. Soc.* **1996**, *118*, 7010.

(41) Diamond, S. E.; Mares, F. *J. Organomet. Chem.* **1977**, *142*, C55-C57.

References begin on page 23

(42) Fryzuk, M. D.; MacNeil, P. A. *Organometallics* **1983**, *2*, 682.

(43) Fryzuk, M. D.; MacNeil, P. A.; Rettig, S. J. *Organometallics* **1985**, *4*, 1145.

(44) Fryzuk, M. D.; MacNeil, P. A.; Rettig, S. J. *J. Am. Chem. Soc.* **1987**, *109*, 2803.

(45) Fryzuk, M. D.; Montgomery, C. D.; Rettig, S. J. *Organometallics* **1991**, *10*, 467.

(46) Noyori, R.; Yamakawa, M.; Hashiguchi, S. *J. Org. Chem.* **2001**, *66*, 7931.

(47) Noyori, R.; Ohkuma, T. *Angew. Chem. Int. Ed.* **2001**, *40*, 40.

(48) Abdur-Rashid, K.; Faatz, M.; Lough, A. J.; Morris, R. H. *J. Am. Chem. Soc.* **2001**, *123*, 7473.

(49) Abdur-Rashid, K.; Lough, A. J.; Morris, R. H. *Organometallics* **2001**, *20*, 1047.

(50) Fryzuk, M. D.; MacNeil, P. A.; Rettig, S. J.; Secco, A. S.; Trotter, J. *Organometallics* **1982**, *1*, 918.

(51) Fryzuk, M. D. *Can. J. Chem.* **1992**, *70*, 2839.

(52) Fryzuk, M. D.; Love, J. B.; Rettig, S. J. *Chem. Commun.* **1996**, 2783.

(53) Fryzuk, M. D.; Love, J. B.; Rettig, S. J. *Organometallics* **1998**, *17*, 846.

(54) Fryzuk, M. D.; Johnson, S. A.; Rettig, S. J. *J. Am. Chem. Soc.* **2001**, *123*, 1602.

(55) Fryzuk, M. D.; Kozak, C. K.; Patrick, B. O. *Inorg. Chim. Acta* **2002**, *345*, 53.

References begin on page 23

(56) Fryzuk, M. D.; Kozak, C. K.; Bowdridge, M. R.; Patrick, B. O.; Rettig, S. J. *J. Am. Chem. Soc.* **2002**, *124*, 8389.

(57) Fryzuk, M. D.; Kozak, C. K.; Mehrkhodavandi, P.; Morello, L.; Patrick, B. O.; Rettig, S. J. *J. Am. Chem. Soc.* **2002**, *124*, 516.

(58) Johnson, S. A. *Ligand Design and The Synthesis of Reactive Organometallic Complexes of Tantalum for Dinitrogen Activation*; University of British Columbia: Vancouver, 2000.

(59) Kozak, C. M. *Activation of Small Molecules by Low Valent Niobium Complexes Stabilized by a Bis(Amidophosphine) Macrocycle*; University of British Columbia: Vancouver, 2002.

(60) Leznoff, D. B. *Paramagnetic Organometallic Complexes*; University of British Columbia: Vancouver, 1997.

(61) Lindoy, L. F. *The Chemistry of Macrocyclic Ligand Complexes*; Cambridge University Press: 1989.

(62) Kyba, E. P.; Davis, R. E.; Hudson, C. W.; John, A. M.; Brown, S. B.; McPhaul, M. J.; Liu, L. K.; Glover, A. C. *J. Am. Chem. Soc.* **1981**, *103*, 3868.

(63) Ansell, C. W. G.; Cooper, M. K.; Dancey, K. P.; Duckworth, P. A.; Henrick, K.; McPartlin, M.; Tasker, P. A. *J. Chem. Soc., Chem. Commun.* **1985**, 439.

(64) Caminade, A. M.; Majoral, J. P. *Chem. Rev.* **1994**, *94*, 1183.

(65) Fryzuk, M. D.; Johnson, S. A.; Patrick, B. O.; Albinati, A.; Mason, S. A.; Koetzle, T. K. *J. Am. Chem. Soc.* **2001**, *123*, 3960.

References begin on page 23

(66) Abdur-Rashid, K.; Lough, A. J.; Morris, R. H. *Organometallics* **2000**, *19*, 2655.

References begin on page 23

Chapter 2

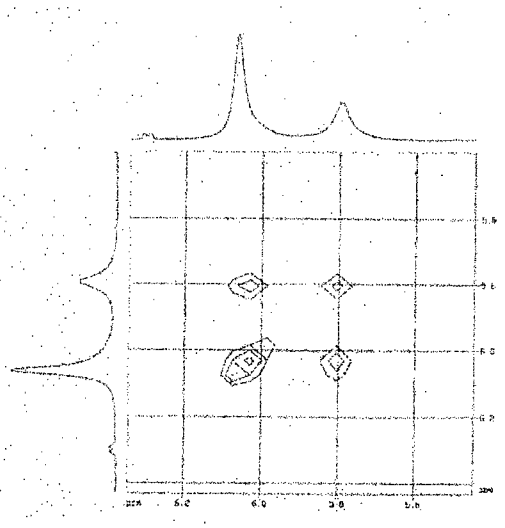

Synthesis, Solution Dynamics and Reactivity of Ruthenium(II) Complexes Incorporating the [NPN] and [P_2N_2] Ligand Sets

2.1 Introduction

In recent years 18-electron ruthenium(II) complexes bearing *cis*-coordinated primary or secondary amine and hydride ligands have been employed as precursors for the catalytic asymmetric reduction of prochiral ketone and imine substrates.[1-10] Complexes of this type are among the most active species for the hydrogenation of polar substrates, and in addition, these compounds display remarkable chemoselectivity in that preferential reduction of polar C=O or C=N functionalities over non-polar C=C groups is observed.[11] This important process supplies chiral alcohol and amine products in high yields and excellent enantiomeric purities. The desire for such compounds is significant in the pharmaceutical and agricultural chemical industries as well as in the field of synthetic organic chemistry.[12-28] Some examples of ruthenium(II) complexes that catalyze the hydrogenation of imines and ketones are shown in Figure 2.1. For his many accomplishments in the area of asymmetric hydrogenation, including the development of chiral ruthenium(II) systems capable of effecting the rapid asymmetric reduction of prochiral

References begin on page 98

imine and ketone substrates, Professor Ryoji Noyori of Nagoya University in Japan was awarded the Nobel Prize in Chemistry for the year 2001.[29] He shared this award with Dr. William S. Knowles[30] and Professor K. Barry Sharpless[31] who were also recognized for their contributions in asymmetric synthesis.

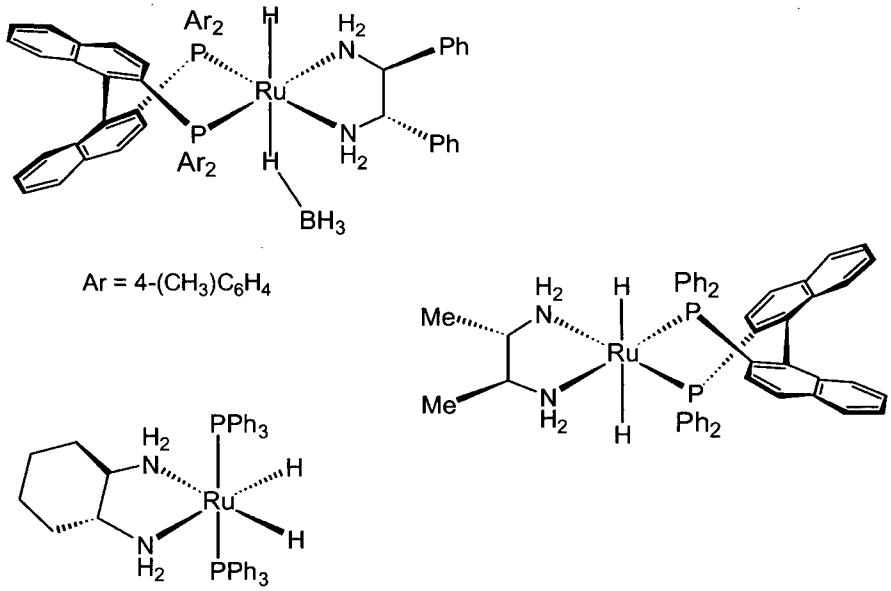

Figure 2.1. Ruthenium(II) complexes that act as precursors for the catalytic reduction of ketone and imine substrates. Both chiral and achiral complexes are shown.

An intriguing proposal to rationalize the observed chemoselectivity and the very high turnover rates has been developed.[1,2,32-35] This process, illustrated in Scheme 2.1, has been coined the "metal-ligand bifunctional mechanism" since it involves a cooperative effort between the transition metal hydride and the coordinated amine ligand. This is an intriguing hydrogenation mechanism since the substrate never binds to the metal centre at any point during the catalytic cycle. Rather, acting in an outersphere process, both the Ru-*H* hydride and N-*H* proton are simultaneously delivered to the ketone or imine functionality. A key companion step in this scheme includes the formation of an intermediate ruthenium amide complex that heterolytically cleaves a molecule of H_2 regenerating the catalytically active species, and thereby completing the cycle.

References begin on page 98

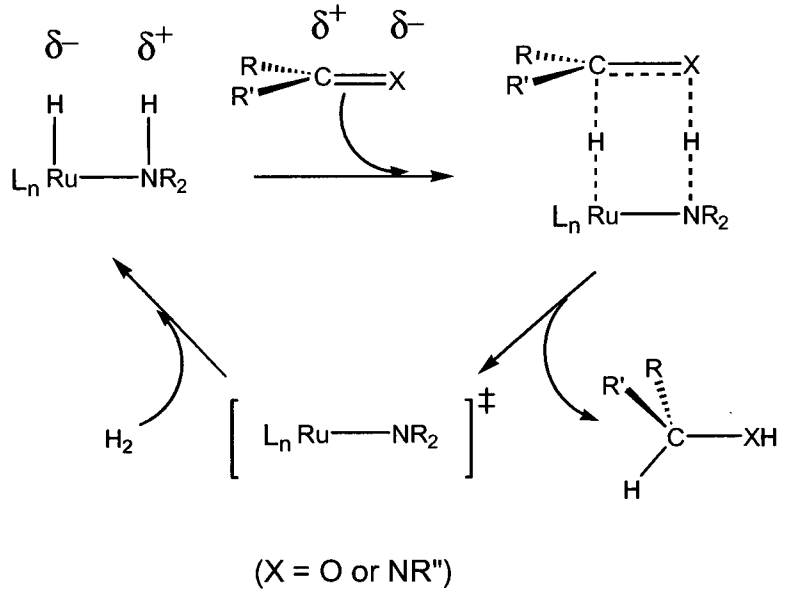

Scheme 2.1

The ability of the ruthenium amide (Ru-N) unit to heterolytically activate molecular hydrogen was first reported in the Fryzuk group utilizing the mixed-donor [PNP] (where [PNP] = $N(SiMe_2CH_2PPh)_2$) ligand set.[36] The details of this process are discussed in Chapter 1. Since the coordinated amine moiety and hydride ligand in the product of this reaction are not *cis*-disposed (a feature necessary for catalysis) its catalytic potential has not been investigated.

In an attempt to generate complexes containing *cis*-coordinated hydride and amine ligands we examined the incorporation of the amidophosphine ligands, $[NPN]Li_2{\cdot}(C_4H_8O)_2$ ([NPN] = $PhP(CH_2SiMe_2NPh)_2$), and $[P_2N_2]Li_2{\cdot}(C_4H_8O_2)$ ([P_2N_2] = $PhP(CH_2SiMe_2NSiMe_2CH_2)_2PPh$) onto ruthenium(II). A general outline summarizing the intended goal of this project is shown in Scheme 2.2. Rather than preparing new catalysts for the hydrogenation of ketones and imines, our focus was aimed at examining the individual steps involved in the metal-ligand bifunctional mechanism. We sought a stable and isolable ruthenium amido species (**A**) that could react with H_2 to generate a stable and isolable ruthenium complex with *cis*-coordinated amine and hydride ligands (**B**). The stoichiometric addition of an imine (or ketone) substrate could then possibly regenerate an unsaturated ruthenium amide species (**C**). In this fashion, a step-by-step examination of the catalytic hydrogenation of ketones or imines would be possible.

References begin on page 98

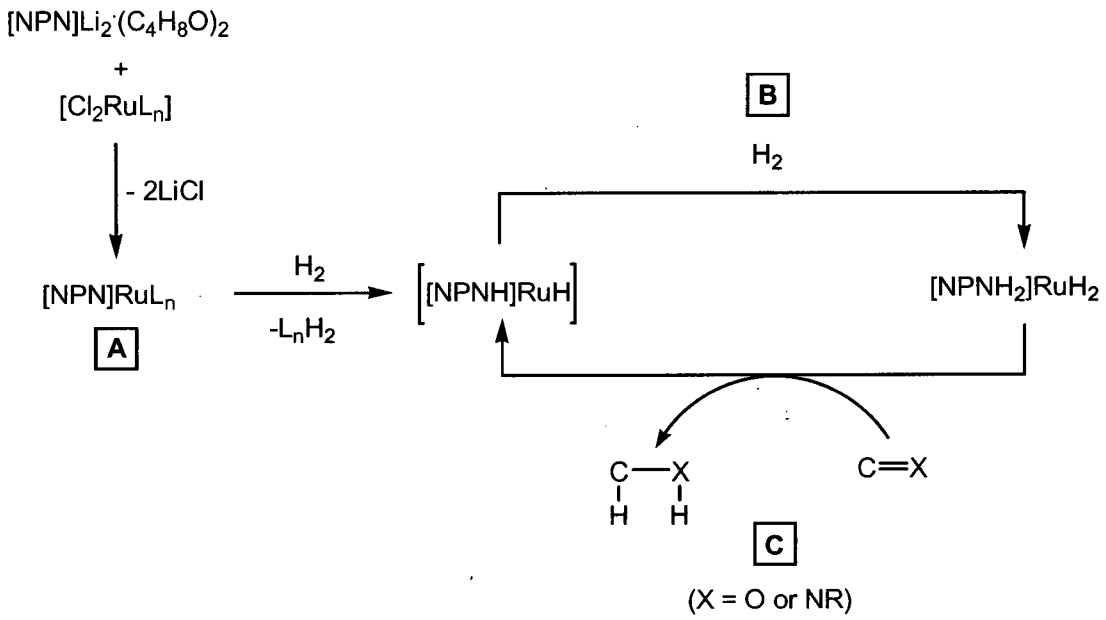

Scheme 2.2

In order to study the reactivity of ruthenium(II) complexes bearing the tridentate [NPN] and macrocyclic [P_2N_2] ligands, a means of introducing these ligands to the metal centre was required. One procedure that has been successfully employed for the preparation of late transition metal amide complexes is the metathetical reaction of alkali metal amides with metal halide precursors. This method was used for coordination of the [PNP] ligand set to iridium (I), rhodium (I) and ruthenium(II).[36,37] Due to the convenient synthesis and ease of isolation of the [NPN][38] and [P_2N_2][39] ligands as the dilithium salts, metathesis seemed a viable route for the preparation of their ruthenium(II) complexes.

The compounds $[RuCl_2(cod)]_x$ (where cod = 1,5-cyclooctadiene, η^2:η^2-C_8H_{12}) and $RuCl_2(PPh_3)_3$ were utilized as the ruthenium(II) precursors. Both compounds are readily prepared, and because they contain two chloride ligands it was anticipated that metathesis with the lithium salts of the [NPN] and [P_2N_2] ligands would provide the corresponding diamido-ruthenium(II) complexes, [NPN]RuL_2 and [P_2N_2]RuL_2 (where L_2 = η^2:η^2-C_8H_{12} or L = PPh_3). Moreover, it was suspected that reaction of the resulting complexes with hydrogen gas would result in the elimination of either cyclooctane (C_8H_{16}) or triphenylphosphine (PPh_3) allowing for the facile preparation of hydrido-amine ruthenium(II) complexes. The remaining sections of this chapter

References begin on page 98

describe the synthesis, characterization and reactivity of various ruthenium(II) complexes that incorporate the [NPN] and [P_2N_2] ligand sets. Chapter 3 will focus on the hydrogenation reactivity of these compounds including catalytic studies.

2.2 Synthesis and Characterization of [P_2N_2]Ru(η^2:η^2-C_8H_{12}) (1)

(i) Synthesis and Structure of [P_2N_2]Ru(η^2:η^2-C_8H_{12}) (1)

The reaction of the colourless ligand salt [P_2N_2]Li_2·$C_4H_8O_2$ with the brown starting material [$RuCl_2$(cod)]$_x$ generates a dark yellow-brown solution from which [P_2N_2]Ru(η^2:η^2-C_8H_{12}), (**1**), can be isolated in 73 % yield (equation 2.1). Compound **1** is the first ruthenium complex of the [P_2N_2] ligand that has been prepared; [P_2N_2] complexes of other transition metals have previously been investigated.[40-45] Because the yellow diamido species **1** is only moderately soluble in hexanes, it can be separated from the more soluble dark coloured impurities by rinsing the crude product mixture with hexanes. The slow evaporation of the hexanes rinsings gives yellow crystals of **1**.

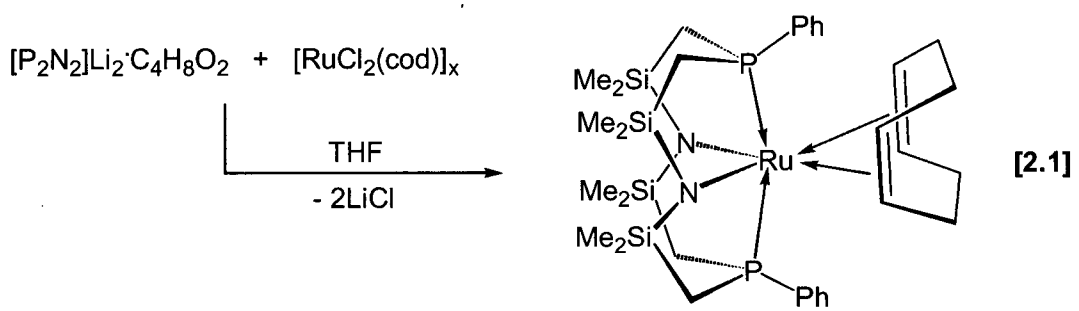

[2.1]

1

The solid-state molecular structure of **1** as determined by a single crystal X-ray diffraction study is shown in Figure 2.2, with selected bond lengths and angles highlighted in Table 2.1. The complex adopts a distorted octahedral geometry in which the amido donors of the [P_2N_2] ligand set and the olefin donors of the cyclooctadiene ligand lie in the equatorial plane. The phosphine ligands occupy the axial positions with a P(1)-Ru(1)-P(1)* angle of 152.18(4)°. The compound

References begin on page 98

exhibits C_2 symmetry in the solid-state; a C_2 axis of rotation runs through the cyclooctadiene ligand and bisects the N-Ru-N angle. A comparison of the P-M-N-Si dihedral angles in [P_2N_2] metal complexes has previously been used to measure the degree of twist present in the ligand backbone.[44] A substantial difference between dihedral angles indicates a high degree of twist in the [P_2N_2] ligand and this feature reduces the symmetry of the complex. In complex **1**, the P(1)-Ru(1)-N(1)-Si(1) and the P(1)*-Ru(1)-N(1)*-Si(1)* dihedral angles are identical (145.33(14)°) further demonstrating the symmetrical nature of the complex.

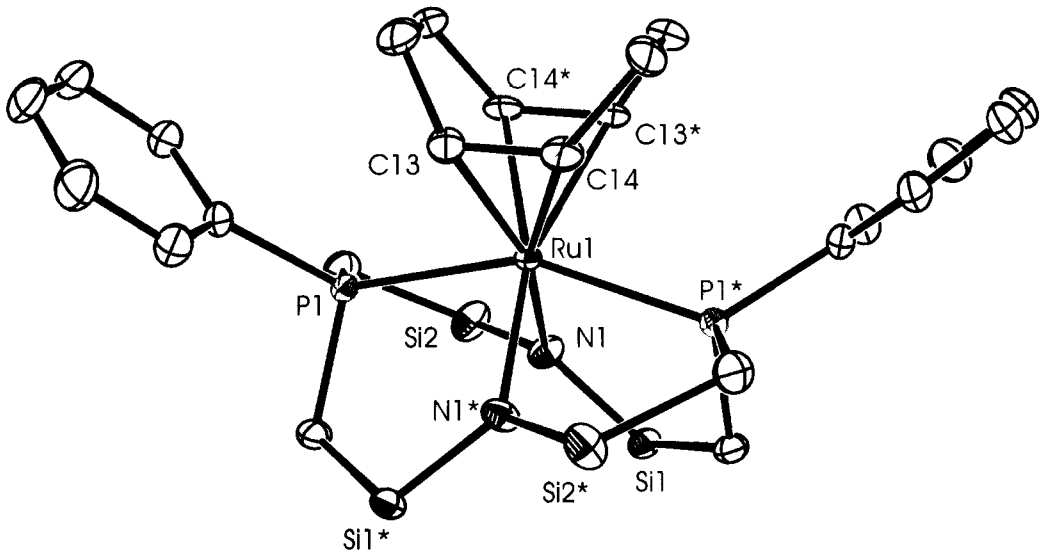

Figure 2.2. ORTEP representation (thermal ellipsoids shown at 50 % probability) of the solid-state molecular structure of [P_2N_2]Ru(η^2:η^2-C_8H_{12}) (**1**). The silyl methyl groups of the [P_2N_2] ligand have been omitted for clarity.

Table 2.1. Selected bond lengths, angles and dihedral angles in [P_2N_2]Ru(η^2:η^2-C_8H_{12}) (**1**).

Atom	Atom	Distance (Å)
Ru(1)	N(1)/N(1)*	2.223(2)
Ru(1)	P(1)/P(1)*	2.3908(7)
Ru(1)	C(13)/C(13)*	2.200(3)
Ru(1)	C(14)/C(14)*	2.202(3)
C(13)	C(14)	1.386(4)

References begin on page 98

Atom	Atom	Atom	Angle (°)	Atom	Atom	Atom	Angle (°)
P(1)	Ru(1)	P(1)*	152.18(4)	N(1)	Ru(1)	C(14)*	90.59(10)
N(1)	Ru(1)	N(1)*	92.91(12)	P(1)	Ru(1)	C(13)	83.98(8)
P(1)	Ru(1)	N(1)	75.88(6)	P(1)	Ru(1)	C(13)*	116.39(8)
P(1)	Ru(1)	N(1)*	84.99(6)	P(1)	Ru(1)	C(14)	120.34(8)
N(1)	Ru(1)	C(13)	158.62(10)	P(1)	Ru(1)	C(14)*	80.40(8)
N(1)	Ru(1)	C(13)*	92.40(10)	C(13)	Ru(1)	C(13)*	90.15(16)
N(1)	Ru(1)	C(14)	163.67(9)	C(14)	Ru(1)	C(14)*	90.51(17)

Atom	Atom	Atom	Atom	Dihedral Angle (°)
P(1)	Ru(1)	N(1)	Si(1)	-145.33(14)
P(1)	Ru(1)	N(1)*	Si(2)*	-158.50(13)
P(1)*	Ru(1)	N(1)	Si(2)	-158.50(13)
P(1)*	Ru(1)	N(1)*	Si(1)*	-145.33(14)

The smaller N-Ru-N bite angle of 92.91(12)° compared to the larger P-Ru-P bite angle of 152.18(4)° is consistent with the previously observed binding of the [P_2N_2] ligand in which the amide donors are typically *cis* while the phosphines are located approximately *trans* to one another. Similar to [P_2N_2] complexes of the early transition metals, the ruthenium centre in **1** is perched on, rather than nested in, the macrocycle.

(ii) Variable-Temperature NMR Spectroscopy of [P_2N_2]Ru(η^2:η^2-C_8H_{12}) (1)

The room temperature ^{1}H NMR spectrum of complex **1** in toluene-d_8 is indicative of a C_{2v} symmetric solution structure. For instance, the [P_2N_2] ligand in **1** gives rise to two resonances for the silyl methyl protons at δ 0.4 and δ 0.5. These correspond to the silyl methyl groups directed to the "top" and "bottom" of the ligand (where top refers to the side of the ligand to which the metal is bound). If the C_2 symmetry evident in the solid-state molecular structure of **1** was maintained in solution, four silyl methyl proton resonances would be expected. In addition, there is a single peak present for the four methylene protons of the cyclooctadiene ligand and a broad signal for the eight methyl protons. The $^{13}C\{^1H\}$ NMR spectrum at this same temperature is also consistent with complex **1** exhibiting C_{2v} symmetry in solution. Two resonances for the silyl methyl carbon nuclei are observed and only one peak for the [P_2N_2] methylene carbon nuclei is present; no

References begin on page 98

coupling to the ^{31}P nucleus could be resolved. The cyclooctadiene ligand has a single methylene carbon resonance at δ 70.0 and a single methyl carbon resonance at δ 25.0.

The higher symmetry of complex **1** in solution as evidenced by the ^{1}H and $^{13}C\{^{1}H\}$ NMR data is due to the conformationally flexible nature of the [P_2N_2] ligand. It has previously been suggested that a locked conformation of the [P_2N_2] ligand may arise from electronic effects due to a π-interaction of the amide lone pairs with metal-based orbitals.[44] In the case of complex **1**, the metal orbitals of correct symmetry available for such a π-bonding interaction (d_{xy}, d_{xz} or d_{yz}) are filled. Consequently, ligand to metal π-donation is eliminated allowing for greater flexibility within the [P_2N_2] ligand framework. A geometry of C_{2v} symmetry can be rationalized via a twisting motion of the [P_2N_2] ligand about the amido nitrogen atoms of the macrocycle, as shown in Figure 2.3. At room temperature this fluxional process occurs rapidly such that two apparent mirror planes of symmetry exist in complex **1**. One of these is contained within the N-Ru-N plane while the other is contained within the P-Ru-P plane. In the solid-state the [P_2N_2] ligand is conformationally rigid allowing only for a C_2 axis of rotation.

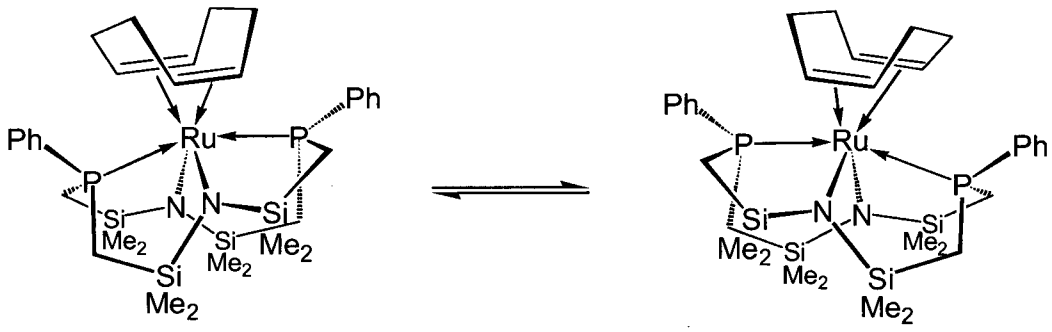

Figure 2.3. Depiction of the fluxional behaviour of complex **1** in solution via twisting of the [P_2N_2] framework about the amido nitrogen atoms.

A variable-temperature ^{1}H NMR study of complex **1** was undertaken and the effect of temperature on the olefinic proton resonances of the cyclooctadiene ligand in **1** is shown in Figure 2.4. As the temperature is lowered, the singlet that is observed at room temperature begins to broaden until decoalescence occurs at 234 K. At the low-temperature limit (198 K) two signals are present at δ 2.6 and δ 3.0, each integrating to two methylene protons. Also at 198 K four

References begin on page 98

signals are present for the silyl methyl groups of the [P_2N_2] ligand between δ 0.3 and δ 0.8. The broad peak for the cyclooctadiene methyl protons collapses to four singlets and the [P_2N_2] methylene protons remain as two peaks. Although the resolution at this temperature was not adequate to distinguish the anticipated couplings, the features present in the low-temperature limiting spectrum are consistent with C_2 symmetry, as observed in the solid state.

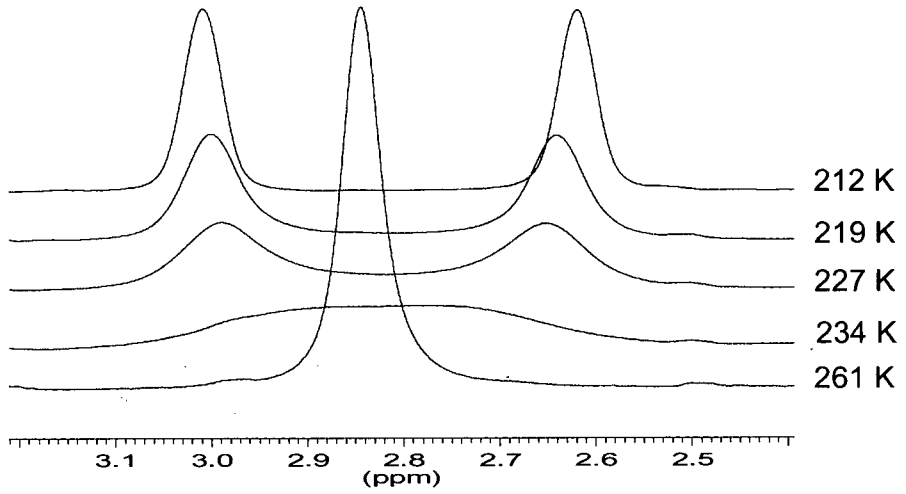

Figure 2.4. The effect of temperature on the methylene resonance of the cyclooctadiene ligand in the 500 MHz ^{1}H NMR spectrum of [P_2N_2]Ru(η^2:η^2-C_8H_{12}) (**1**).

A line-shape analysis of the methylene protons of the cyclooctadiene ligand from 212 K to 243 K combined with an Arrhenius plot of the resulting rate constants provided an activation barrier of 18.6 ± 1.6 kcal mol^{-1} for the twisting motion of the [P_2N_2] framework within complex **1**. The Arrhenius plot is shown in Figure 2.5 and the rate constants are given in Table 2.2.

References begin on page 98

Table 2.2. Calculated rate constants (k) for the fluxionality of the [P_2N_2] ligand in the complex [P_2N_2]Ru(η^2:η^2-C_8H_{12}) (**1**).

Rate Constant, k (s^{-1})	Temperature, T (K)
5 304 ± 265	243 ± 1
865 ± 43	234 ± 1
560 ± 28	230 ± 1
433 ± 22	227 ± 1
66 ± 3	219 ± 1
18 ± 1	212 ± 1

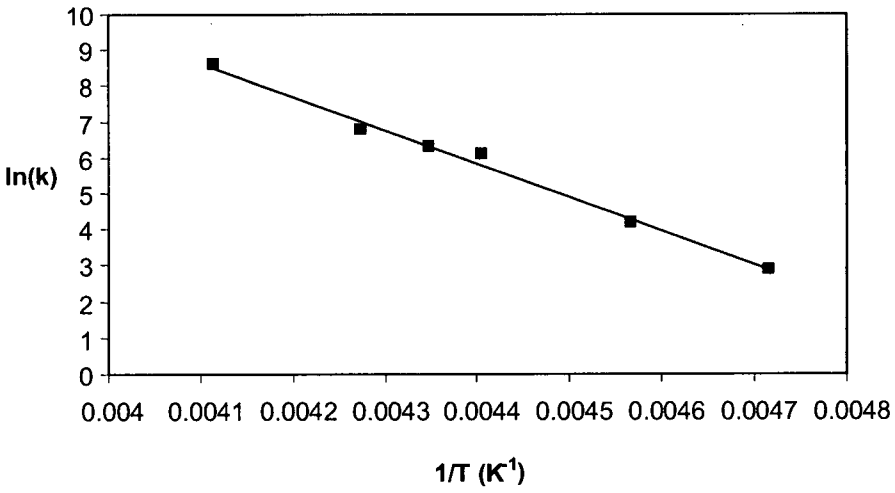

Figure 2.5. Arrhenius plot for the fluxionality of the [P_2N_2] ligand framework in the complex [P_2N_2]Ru(η^2:η^2-C_8H_{12}) (**1**) (R^2 = 0.9920 and E_a = 18.6 ± 1.6 kcal mol^{-1}).

References begin on page 98

2.3 Synthesis and Characterization of [P_2NNH]Ru($C_6H_4PPh_2$) (2)

(i) Synthesis and NMR Spectroscopic Characterization of [P_2NNH]Ru($C_6H_4PPh_2$) (2)

The reaction of $RuCl_2(PPh_3)_3$ with the [P_2N_2] ligand did not afford the expected diamidodiphosphine ruthenium(II) complex [P_2N_2]$RuPPh_3$. Rather, the compound isolated was the product of *ortho*-metalation of the triphenylphosphine ligand, [P_2NNH]Ru($C_6H_4PPh_2$) (**2**), as shown in equation 2.2. The propensity for the PPh_3 ligand to *ortho*-metalate is well known not only for complexes of ruthenium(II)[36,46] but for other metals as well.[47,48] Previous studies in the Fryzuk laboratory have shown that the related species [PNP]$RuCl(PPh_3)$ suffers a similar fate upon addition of triethylphosphine, resulting in the formation of [PNHP]Ru($C_6H_4PPh_2$).[36]

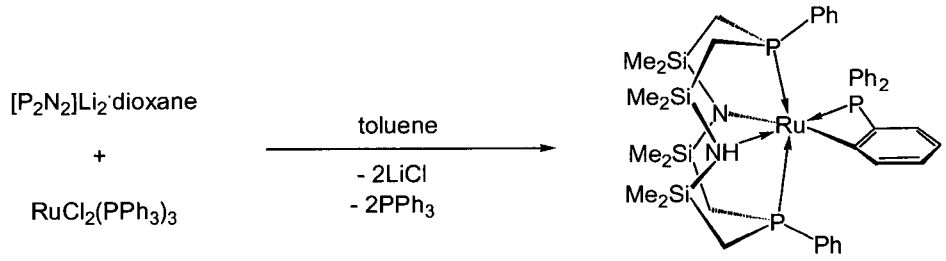

[2.2]

2

Stirring a solution containing an equimolar mixture of [P_2N_2]$Li_2{\cdot}C_4H_8O_2$ and $RuCl_2(PPh_3)_3$ in toluene results in the formation of an orange-brown coloured solution within three hours. Removal of LiCl is accomplished by filtration, however, separation of **2** from free triphenylphosphine proved more difficult due to the similar solubilities of these two compounds in hydrocarbon solvents. Isolation of **2** was successfully accomplished by the addition of two equivalents of anhydrous CuCl; this generates an insoluble "$CuCl{\cdot}PPh_3$" oligomeric complex[49] that is more easily removed by filtration.

Diagnostic of complex **2** is the $^{31}P\{^1H\}$ NMR spectrum, which shows a doublet (at δ 25.8) and a triplet (at δ -11.8) for the ancillary phosphine donors of the [P_2NNH] ligand set and the P($C_6H_4Ph_2$) ligand, respectively ($^2J_{PP}$ = 31 Hz). These signals integrate in the ratio 2:1. An

References begin on page 98

upfield shift for the ^{31}P nucleus of the P($C_6H_4Ph_2$) ligand has been observed in other complexes that incorporate an *ortho*-metalated triphenylphosphine ligand.[50] The equivalency of the phosphorus centres in the [P_2NNH] ligand is consistent with the proposed structure, which has C_s symmetry.

The room-temperature 500 MHz ^1H NMR data is also consistent with the proposed structure of complex **2** shown in equation 2.2. Four resonances for the silyl methyl groups of the [P_2NNH] ligand set are observed between δ 0.40 and δ 0.60 in accordance with a mirror plane of symmetry contained within the equatorial plane of the octahedral coordination geometry of **2**. The ligand methylene protons give rise to two sets of overlapping resonances consisting of a second-order AA'BX pattern. A singlet at δ 2.8 has been ascribed to the amino proton (N-*H*). The aromatic protons of the triphenylphosphine and [P_2N_2] phosphorus phenyl substituents occur as overlapping resonances between δ 6.5 and δ 8.2.

(ii) X-ray diffraction study of [P_2NNH]Ru($C_6H_4PPh_2$) (2)

Single crystals of [P_2NNH]RuP($C_6H_4PPh_2$) (**2**) suitable for an X-ray diffraction study were grown by the slow evaporation of a saturated pentane solution. The solid-state molecular structure of **2** as determined by X-ray crystallography is shown in Figure 2.6 with selected bond lengths and bond angles detailed in Table 2.3. Complex **2** crystallizes with two crystallographically distinct but structurally related molecules in the asymmetric unit, in addition to one molecule of *n*-pentane. The following structural discussion will be concerned with only one of the molecules for the sake of brevity.

References begin on page 98

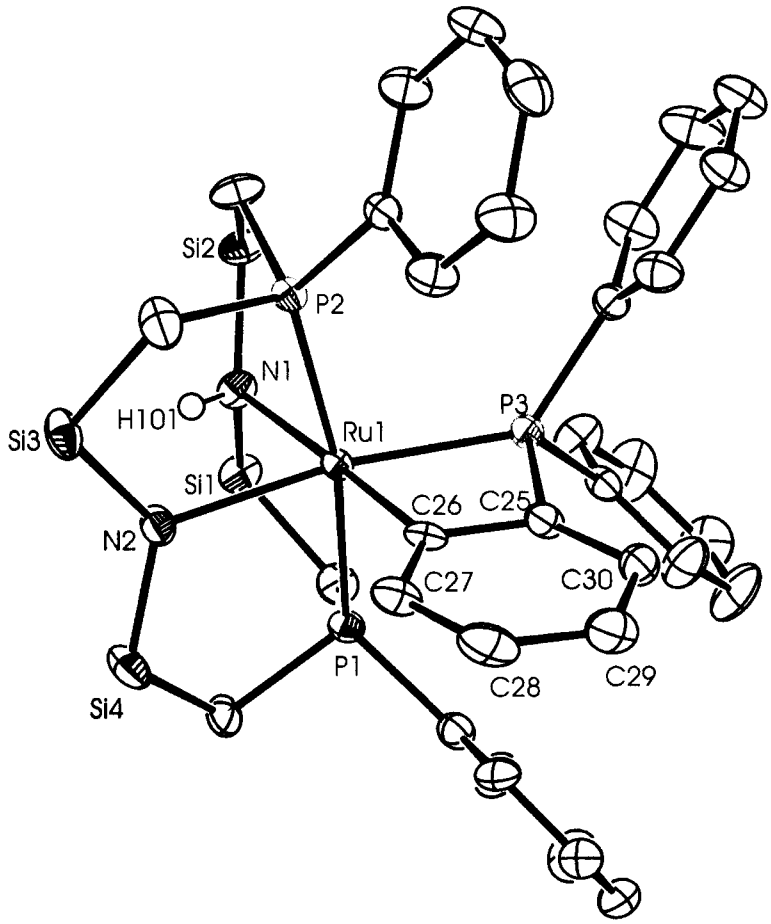

Figure 2.6. The solid-state molecular structure (ORTEP representation, 50 % thermal ellipsoid probability) of [P_2NNH]Ru($C_6H_4PPh_2$) (**2**) as determined by X-ray crystallography. The silyl methyl groups of the [P_2NNH] ligand have been omitted for clarity.

References begin on page 98

Table 2.3. Selected bond lengths, bond angles and dihedral angles in the complex [P_2NNH]Ru($C_6H_4PPh_2$) (**2**).

Atom	Atom	Distance (Å)	Atom	Atom	Distance (Å)
Ru(1)	C(26)	2.034(5)	Ru(1)	P(1)	2.3565(13)
Ru(1)	N(2)	2.260(4)	Ru(1)	N(1)	2.414(4)
Ru(1)	P(3)	2.2989(13)	N(1)	H(101)	0.73(6)
Ru(1)	P(2)	2.3248(13)	N(2)	H(101)	2.404

Atom	Atom	Atom	Angle (°)	Atom	Atom	Atom	Angle (°)
C(26)	Ru(1)	N(2)	99.66(18)	P(3)	Ru(1)	P(1)	93.02(5)
C(26)	Ru(1)	P(3)	68.39(14)	P(2)	Ru(1)	P(1)	168.67(5)
N(2)	Ru(1)	P(3)	167.65(12)	C(26)	Ru(1)	N(1)	178.48(18)
C(26)	Ru(1)	P(2)	93.96(14)	N(2)	Ru(1)	N(1)	79.33(17)
N(2)	Ru(1)	P(2)	86.15(11)	P(3)	Ru(1)	N(1)	112.55(13)
P(3)	Ru(1)	P(2)	97.51(5)	P(2)	Ru(1)	N(1)	87.12(11)
C(26)	Ru(1)	P(1)	93.80(14)	P(1)	Ru(1)	N(1)	84.99(11)
N(2)	Ru(1)	P(1)	84.41(11)	N(1)	H(101)	N(2)	137.72

Atom	Atom	Atom	Atom	Angle (°)
P(1)	Ru(1)	C(26)	C(25)	86.4(3)
P(2)	Ru(1)	C(26)	C(25)	-101.9(3)
Ru(1)	N(1)	H(101)	N(2)	-15.1
P(3)	Ru(1)	N(1)	H(101)	-172.7

The geometry of complex **2** was found to be distorted octahedral with the two phosphine donors of the [P_2NNH] ligand occupying the axial positions; these are pinched back from an ideal *trans* disposition giving a P(1)-Ru(1)-P(2) angle of 168.67(5)°. The *ortho*-metalated triphenylphosphine ligand as well as the amide and amine ligands all lie in the plane of the octahedron with a combined equatorial angle of 359.93°. The orientation of the σ-bound phenyl group lies nearly orthogonal to the P-Ru-P axis as indicated by the P(1)-Ru(1)-C(26)-C(25) torsion angle of 86.4(3)°. As a consequence, a mirror plane of symmetry exists within the equatorial plane of the complex rendering the phosphine donors of the macrocycle magnetically

References begin on page 98

equivalent. This is in accordance with the solution structure of **2**, which shows only one resonance for these phosphine ligands in the $^{31}P\{^1H\}$ NMR spectrum. The N(1)-Ru(1)-N(2) bond angle of 79.33(17)° is quite low in comparison to complex **1**, which has a N-Ru-N bond angle of approximately 92°. We speculate that the smaller bond angle is a consequence of an intramolecular hydrogen bonding interaction between the amino proton and the amido nitrogen atom (to be discussed in greater detail later).

The Ru-P bond distances (2.3248(13) and 2.3565(13) Å) for the [P_2NNH] ligand of complex **2** are slightly elongated compared to P(3) of the coordinated triphenylphosphine (2.2989(13) Å). Presumably this structural feature is due to the high *trans* influence of phosphines relative to that of amides. This difference, however, is not as significant as that which is observed in the isoelectronic species [PNHP]RuCl($C_6H_4PPh_2$).[51] In this complex, the phosphine donors of the tridentate ligand are displaced 2.3945 Å on average from the metal centre, whereas the Ru-P distance for the triphenylphosphine ligand is 2.2545 Å. These distances are comparable to those found in $RuCl_2(PPh_3)_3$,[52,53] in which the two mutually *trans* triphenylphosphine ligands exhibit Ru-P distances of 2.374(6) and 2.388(7) Å, while the remaining phosphine (*trans* to an open site) is located 2.230(8) Å from the metal. The shorter Ru-P distances for the phosphine donors of the [P_2NNH] ligand in **2** may be the result of a "macrocyclic effect" in which an *n*-dentate macrocyclic ligand gives more stable complexes than the most similar *n*-dentate open chain ligand or *n*-unidentate ligands of similar type. [54] The longer Ru(1)-P(3) distance in complex **2**, on the other hand, may be a consequence of minimizing steric interactions with the [P_2NNH] ligand set.

Structural features of the four-membered ring of the metalacycle are typical of other such rings found in the literature. For instance, the C-Ru-P angle of 68.39(14)° measured in **2** is similar to that found in the ruthenate complex K[$RuH_2(C_6H_4PPh_2)(PPh_3)_2$] [55] (67.6(3)°), as well as the related species [PNHP]RuCl($C_6H_4PPh_2$) (68.24(8)°). [51] In the ruthenate complex, the Ru-C distance is 2.098(11) Å whereas in the tridentate [PNHP] complex it is observed to be 2.054(3) Å. In **2**, a slightly shorter Ru-C distance of 2.034(5) Å was found. This trend in bond distances is in accordance with the *trans*-influence differences between PPh_3, Cl and amine donors[56] in the respective complexes. The ruthenium-amine bond length in complex **2** is likewise lengthened (2.414(4) Å) by the high *trans* influence of the *ortho*-metalated aryl group.

References begin on page 98

An interesting feature evident in the solid-state molecular structure of complex **2** is the presence of a hydrogen bond between the amino proton (H(101)) and the amido nitrogen (N(2)). A similar bonding interaction was also evident between the amine and chloride ligands in the complex [PNHP]RuCl($C_6H_4PPh_2$), as well as in other complexes of rhodium and iridium that also incorporate this tridentate ligand system.[57] The NH···N distance of 2.404 Å in complex **2** is shorter than the expected van der Waals contact distance of 2.7 Å between these two nuclei.[58] Also indicative of the presence of a bonding interaction between the hydrogen and amido nitrogen atom is the fact that the amine hydrogen lies nearly in the plane of N(1), N(2) and Ru(1) illustrated by the Ru(1)-N(1)-H(101)-N(2) torsion angle of –15.1°, thus, minimizing the NH···N separation.

(iii) Mechanism for the formation of complex 2

The structure of complex **2** in solution is consistent with the solid-state structure in which the *ortho*-metalated triphenylphosphine ligand as well as the amide and amine donors occupy the equatorial positions of an octahedron. The axial phosphine ligands are related by a mirror plane of symmetry that is contained in the equatorial plane. The position of the donor ligands within the equatorial plane, however, cannot be ascertained in solution by the ^1H and $^{31}P\{^1H\}$ NMR data. Since removal of the *ortho* hydrogen atom occurs by an amido donor it may be expected that the resulting amine and σ-aryl ligands would be arranged *cis* to one another in the product. In fact, the solid-state data shows that the amine ligand is located *trans* to the *ortho*-metalated carbon atom. One rationalization for this may be that the reaction of the [P_2N_2] ligand with $RuCl_2(PPh_3)_3$ is not kinetically controlled and that the formation of complex **2** proceeds under thermodynamic control. The position of the donors in the equatorial plane may be governed by electronics and arranged according to the relative *trans* influences of phosphine, amine, aryl and amide ligands. The known *trans* influence decreases in the order $PPh_3 > C_6H_5 >$ amine[56] suggesting that the amido ligand in **2** may exhibit the weakest *trans* influence. This rearrangement deserves a further comment. Figure 2.7 depicts a plausible reaction pathway for the formation of the isolated species **2**. For simplicity, only the donor atoms contained in the equatorial plane are shown. It is speculated that the amine donor in the kinetic product dissociates, undergoes inversion, and re-coordinates allowing for an intramolecular hydrogen bonding interaction with the coordinated amido ligand. A similar transformation was found to occur upon *ortho*-metalation in the complex

References begin on page 98

[PNHP]RuCl($C_6H_4PPh_2$). Consequent transfer of the amino proton to the amide nitrogen atom generates the observed complex **2**.

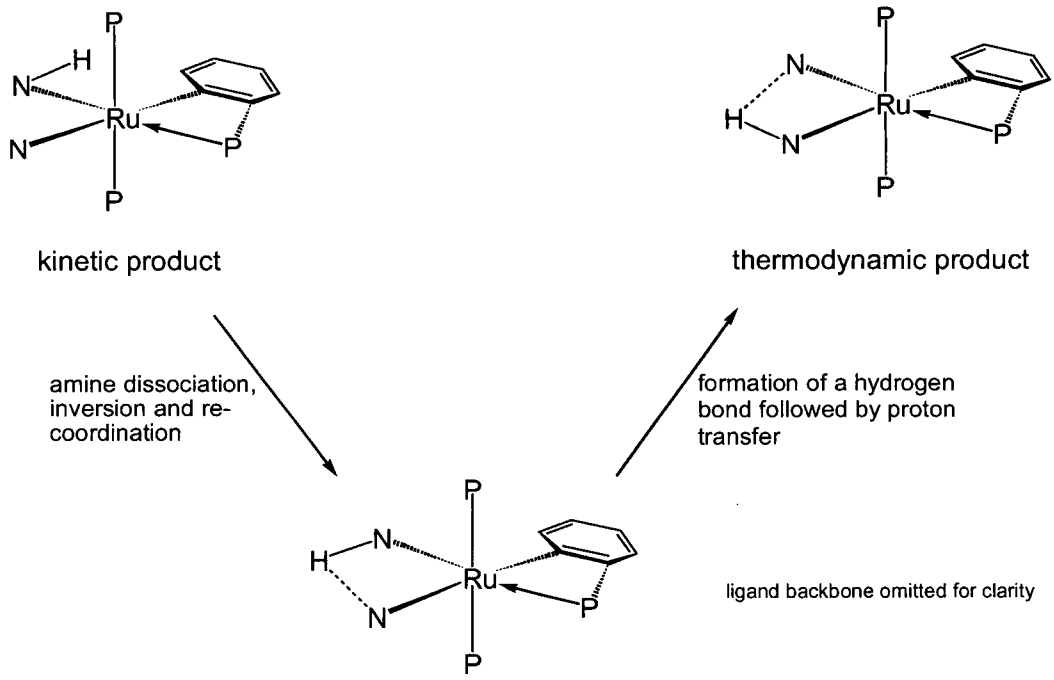

Figure 2.7. Proposed mechanism for the formation of the observed species **2**.

2.4 Synthesis, Characterization and Solution Dynamics of *exo*- and *endo*-[NPNH]Ru(1-3:η^3-5,6:η^2-C_8H_{11}) (*exo*-3 and *endo*-3)

(i) Reaction of [NPN]Li_2·$(C_4H_8O)_2$ with $[RuCl_2(cod)]_x$

As discussed earlier, the reaction of the macrocyclic [P_2N_2] ligand with $[RuCl_2(cod)]_x$ generates the species [P_2N_2]Ru(η^2:η^2-C_8H_{12}) (**1**) via metathetical exchange of the two chloride ligands with the amide ligands. In a similar fashion, we anticipated that the outcome of the reaction between the tridentate [NPN] ligand with $[RuCl_2(cod)]_x$ would be the formation of the diamidophosphine complex [NPN]Ru(η^2:η^2-C_8H_{12}). That this was not the isolated product from this reaction was immediately apparent upon inspection of the room-temperature ^{1}H NMR spectrum. The number of peaks present implied the existence of two species (of low symmetry) in

References begin on page 98

solution, and furthermore, the broadened resonances were indicative of a fluxional process occurring in solution. The ^{1}H NMR spectra at 298 K and 245 K are shown in Figure 2.8. Combustion analysis of the red crystalline solid that was isolated from this reaction was consistent with the formulation of the expected product, [NPN]Ru(η^2:η^2-C_8H_{12}), suggesting that the isolated products were structurally related isomers of this species.

As portrayed in Scheme 2.3, the products that are formed in the reaction between the [NPN] ligand and $[RuCl_2(cod)]_x$ are a pair of diastereomers. Transfer of an allylic C-H atom of the cyclooctadiene ligand to one of the amido donors of the [NPN] ligand occurs generating a mixture of the two species *exo*- and *endo*-[NPNH]Ru(1-3-η^3:5,6-η^2-C_8H_{11}) (*exo*-**3** and *endo*-**3**, respectively). Deprotonation of the cyclooctadiene ligand generates a 1-3-η^3-allyl, 5,6-η^2-olefin coordinated cyclooctadienyl ligand and a [NPNH] ligand array. The activation of an allylic C-H bond of a coordinated cyclooctadiene moiety resulting in the formation of a cyclooctadienyl ruthenium(II) complex has previously been reported.[59-61] The terms "*exo*" and "*endo*" are used to distinguish the two diastereomers, and they refer to the orientation of the amino side-arm of the [NPNH] ligand set with respect to the methylene unit bridging the olefin and allyl donor groups of the cyclooctadienyl ligand. In the *endo* diastereomer the pendant amino ligand and the bridging methylene unit are oriented towards the same "side" of the metal, whereas in the *exo* isomer, the amino ligand is positioned to the opposite face of the metal and points away from the bridging methylene unit.

References begin on page 98

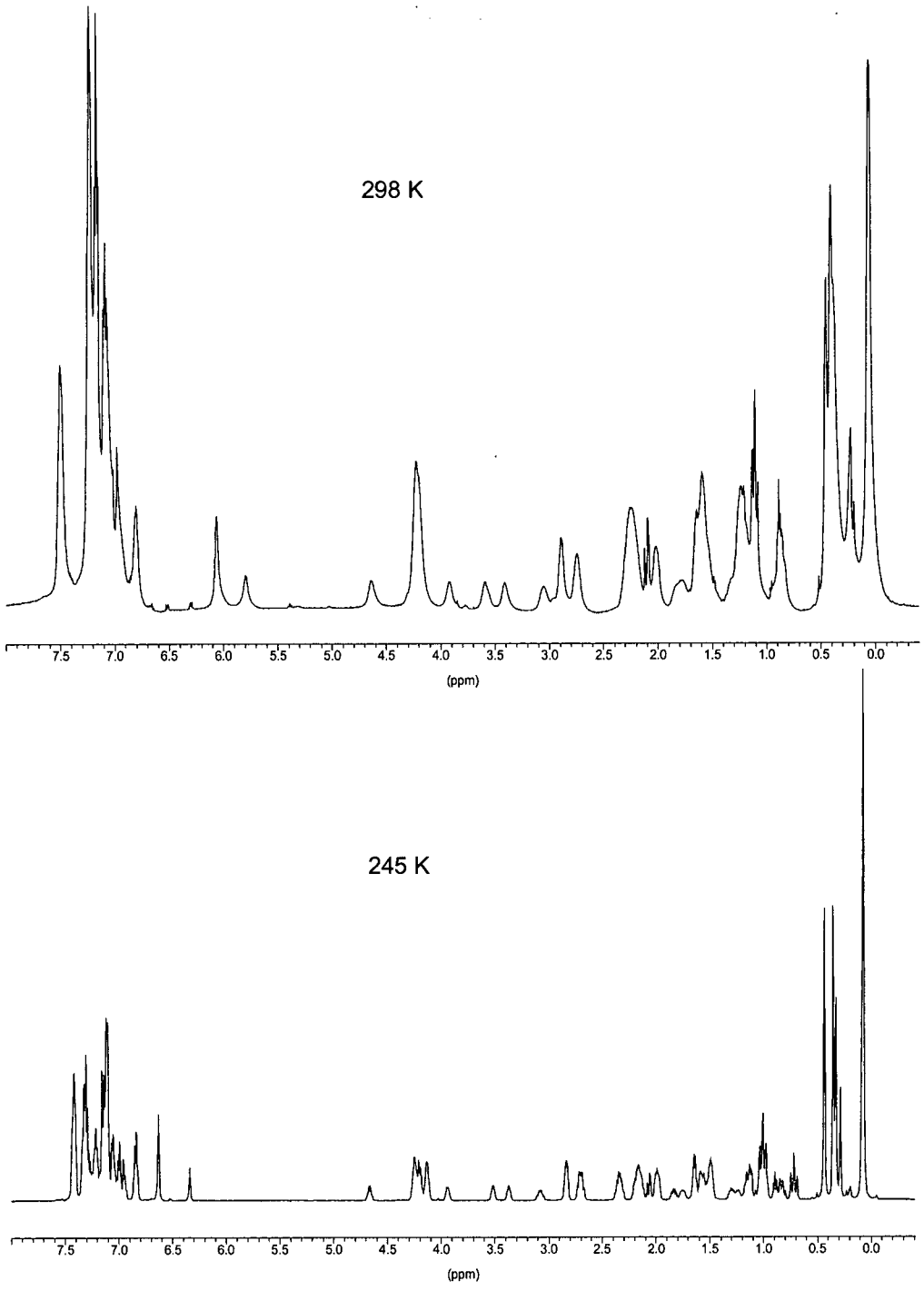

Figure 2.8. The 500 MHz ^{1}H NMR spectrum of complex **3** in toluene-d_8 at 298 K (upper spectrum) and 245 K (lower spectrum).

References begin on page 98

The identification and characterization of the diastereomers *exo*-**3** and *endo*-**3**, as well as an understanding of the dynamic behaviour of these two species in solution proved to be a formidable task. Techniques including X-ray crystallography, variable-temperature one- and two-dimensional NMR spectroscopy (^{1}H, ^{13}C{^{1}H} and ^{31}P{^{1}H}) in addition to performing labelling and reactivity studies all provided valuable insights into this system. The following sections outline, in chronological order, the steps that were taken in order to gain a complete understanding of the process shown in Scheme 2.3.

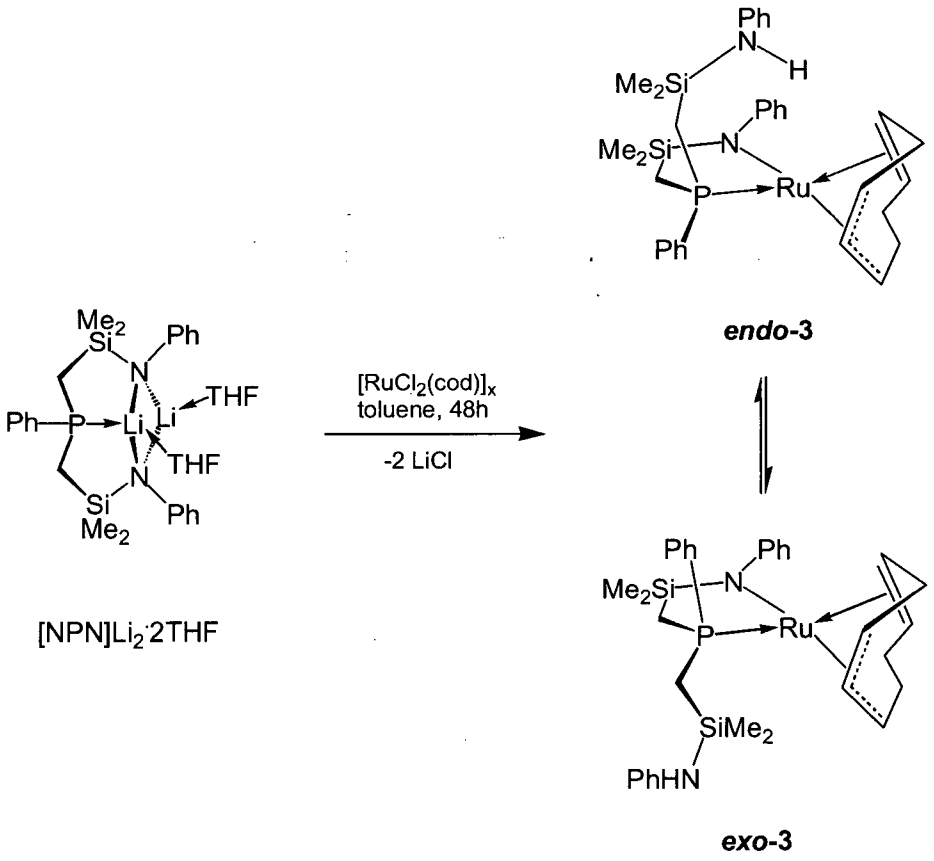

Scheme 2.3

References begin on page 98

(ii) Solid-state molecular structure of diastereomer *endo*-3

The solid-state structural identification of the diastereomer *endo*-**3** provided the first insight into the details of the reaction of the [NPN] ligand with $[RuCl_2(cod)]_x$. Single crystals of the isomer *endo*-**3** suitable for an X-ray diffraction study were isolated by the slow evaporation of a concentrated hexanes solution. The solid-state molecular structure is shown in Figure 2.9; pertinent bond lengths and angles can be found in Table 2.4. Transfer of an allylic C-H atom of the cyclooctadiene ligand to an amido nitrogen atom is clearly evident from the solid-state molecular structure, which shows the η^3-allyl, η^2-olefin coordination mode adopted by the cyclooctadienyl ligand. The protonated side arm of the [NPNH] ligand is also apparent and it does not coordinate to the metal centre. The amino proton (H43) was located and refined isotropically. The complex exhibits a five-coordinate, distorted trigonal bipyramidal geometry at ruthenium (with the allyl donor occupying two coordination sites and the olefin donor one coordination site). The amide and the allyl moieties are contained within the trigonal plane, while the phosphine and olefin ligands occupy the axial positions. The P(1)-Ru(1)-C(25) and P(1)-Ru(1)-C(26) bond angles are 163.35(7)° and 162.61(7)° respectively, indicating a nearly *trans* disposition between the phosphine and olefin donor groups. The allyl moiety of the cyclooctadienyl ligand is symmetrically bound to ruthenium with an average Ru-C_{allyl} bond distance of 2.184 Å. The complex [Ru(1-3-η^3:5,6-η^2-C_8H_{11})(η^6-$C_6H_5BF_3$)] [59] also exhibits a symmetrically coordinated allyl function.

References begin on page 98

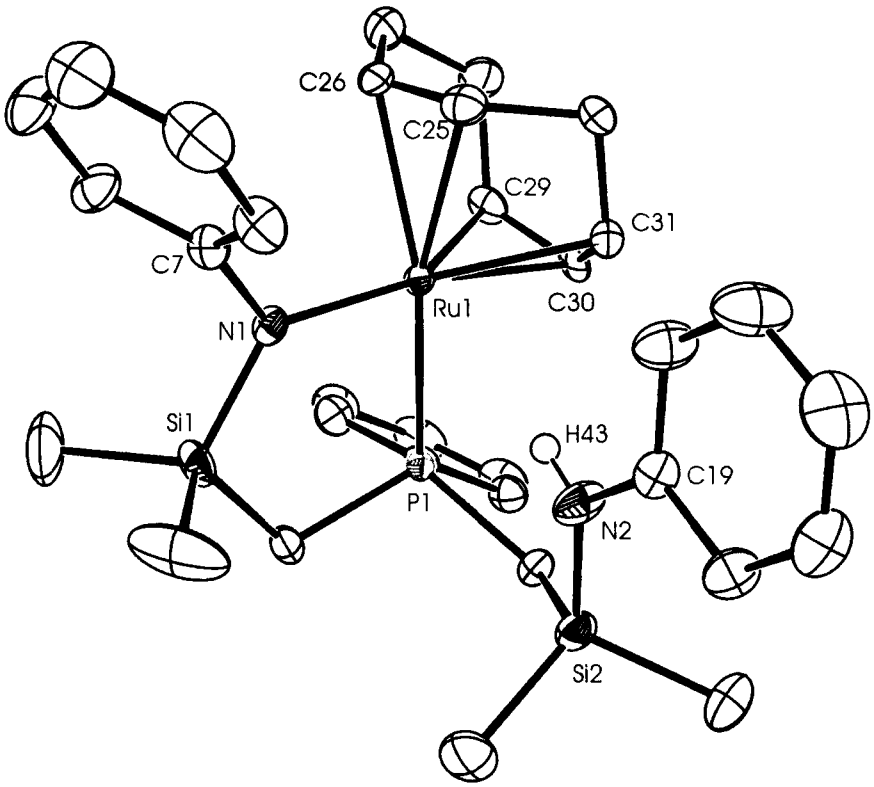

Figure 2.9. The solid-state molecular structure (ORTEP depiction shown at 50 % thermal ellipsoid probability) of *endo*-[NPNH]Ru(1-3-η^3:5,6-η^2-C_8H_{11}) (*endo*-**3**) as determined by X-ray diffraction. The amino proton (H43) was refined isotropically.

Table 2.4. Selected bond lengths, angles and dihedral angles in *endo*-[NPNH]Ru(1-3-η^3:5,6-η^2-C_8H_{11}) (*endo*-**3**).

Atom	Atom	Distance (Å)	Atom	Atom	Distance (Å)
Ru(1)	N(1)	2.019(2)	C(29)	C(30)	1.408(4)
Ru(1)	P(1)	2.3024(6)	C(30)	C(31)	1.411(4)
Ru(1)	C(25)	2.300(3)	N(1)	C(7)	1.430(3)
Ru(1)	C(26)	2.332(2)	N(2)	C(19)	1.392(3)
Ru(1)	C(29)	2.187(2)	N(1)	Si(1)	1.734(2)
Ru(1)	C(30)	2.169(2)	N(2)	Si(2)	1.727(2)
Ru(1)	C(31)	2.195(2)	N(1)	H(43)	3.419
C(25)	C(26)	1.354(4)			

References begin on page 98

Atom	Atom	Atom	Angle (°)	Atom	Atom	Atom	Angle (°)
P(1)	Ru(1)	N(1)	87.32(6)	N(1)	Ru(1)	C(29)	147.35(9)
P(1)	Ru(1)	C(25)	163.35(7)	N(1)	Ru(1)	C(30)	170.65(9)
P(1)	Ru(1)	C(26)	162.61(7)	N(1)	Ru(1)	C(31)	142.72(9)
P(1)	Ru(1)	C(29)	95.22(7)	Ru(1)	N(1)	Si(1)	124.3(1)
P(1)	Ru(1)	C(30)	83.98(7)	Ru(1)	N(1)	C(7)	123.6(2)
P(1)	Ru(1)	C(31)	103.09(7)	Si(1)	N(1)	C(7)	112.2(2)
N(1)	Ru(1)	C(25)	97.09(9)	C(29)	Ru(1)	C(31)	68.2(1)
N(1)	Ru(1)	C(26)	90.06(9)				

Atom	Atom	Atom	Atom	Dihedral Angle (°)
C(25)	C(26)	C(29)	C(30)	10.7
C(26)	C(25)	C(31)	C(30)	1.7
N(1)	Ru(1)	C(29)	C(31)	164.8
P(1)	Ru(1)	C(25)	C(26)	176.2
P(1)	Ru(1)	N(1)	C(7)	172.2(2)
P(1)	Ru(1)	N(1)	Si(1)	-5.8(1)

Although **3** may be considered an unsaturated, 16-electron species, the presence of the π-donating amido ligand can also result in a formal 18-electron configuration at the metal centre. An indication of a π-bonding interaction can be portrayed structurally by a short metal-nitrogen bond distance as well as a trigonal planar coordination geometry at the amido nitrogen atom.[62,63] In the case of *endo*-**3** the ruthenium amide (Ru(1)-N(1)) bond length is 2.019(2) Å. In contrast, the coordinatively saturated species $[P_2N_2]Ru(\eta^2{:}\eta^2\text{-}C_8H_{12})$ (**1**) has a Ru-N bond length of 2.223(2) Å. The six-coordinate complexes *cis*-$Ru(H)(PMe_3)_4(NHPh)$[64] and $Ru(\eta^6\text{-}C_6Me_6)(PMe_3)(Ph)(NHPh)$[65] bearing the anilido ligand have ruthenium to nitrogen distances of 2.160(6) Å and 2.121(3) Å, respectively. The shorter Ru-N bond length in the five-coordinate *endo*-**3** can be attributed to delocalization of the amido nitrogen lone pair to a vacant metal *d*-orbital. Also consistent with the existence of a π-bonding interaction is the planar, sp^2-hydridized geometry displayed by the amido nitrogen atom (sum of angles = 360°); planarity of the amido unit necessarily occurs to maximize π-bonding with the metal centre. This planarity, however, could also arise from similar π-interactions existing between the amide nitrogen atom and the neighbouring silicon atom or phenyl ring. The N(1)-Si(1) bond length (1.734(2) Å) exists in a range commonly found for planar silyl amine and silyl amide compounds[62] implying π-delocalization between these two nuclei. The bond distance (1.430(3) Å) from the amido nitrogen (N(1)) to the phenyl ipso carbon (C(7)) of the amido moiety is longer than that of aniline (1.398

References begin on page 98

Å) suggesting minimal π-delocalization into the amido aromatic ring in complex *endo*-**3**. In an earlier report, an inverse correlation between Ru-N and N-C_{ipso} bond distances in ruthenium(II) phenyl amido systems had been noted.[66]

Theoretical calculations have shown that a diamagnetic d^6 ML_5 complex distorts away from the Jahn-Teller active trigonal bipyramidal structure.[67,68] Two more stable structures are possible: a square pyramid and a distorted trigonal bipyramid. Figure 2.10 gives a qualitative representation of these two types of distortions. Only the x^2-y^2 and xy set of *d*-orbitals are shown since the geometrical preference is governed by these two orbitals. Increasing the angle θ to 180° (giving a square pyramid) stabilizes the xy orbital while the x^2-y^2 orbital is raised in energy. Conversely, decreasing the angle θ below 120° (giving a distorted trigonal bipyramid, namely a Y-shape in the trigonal plane of the five-coordinate structure) increases the energy of the xy orbital and stabilizes x^2-y^2.

References begin on page 98

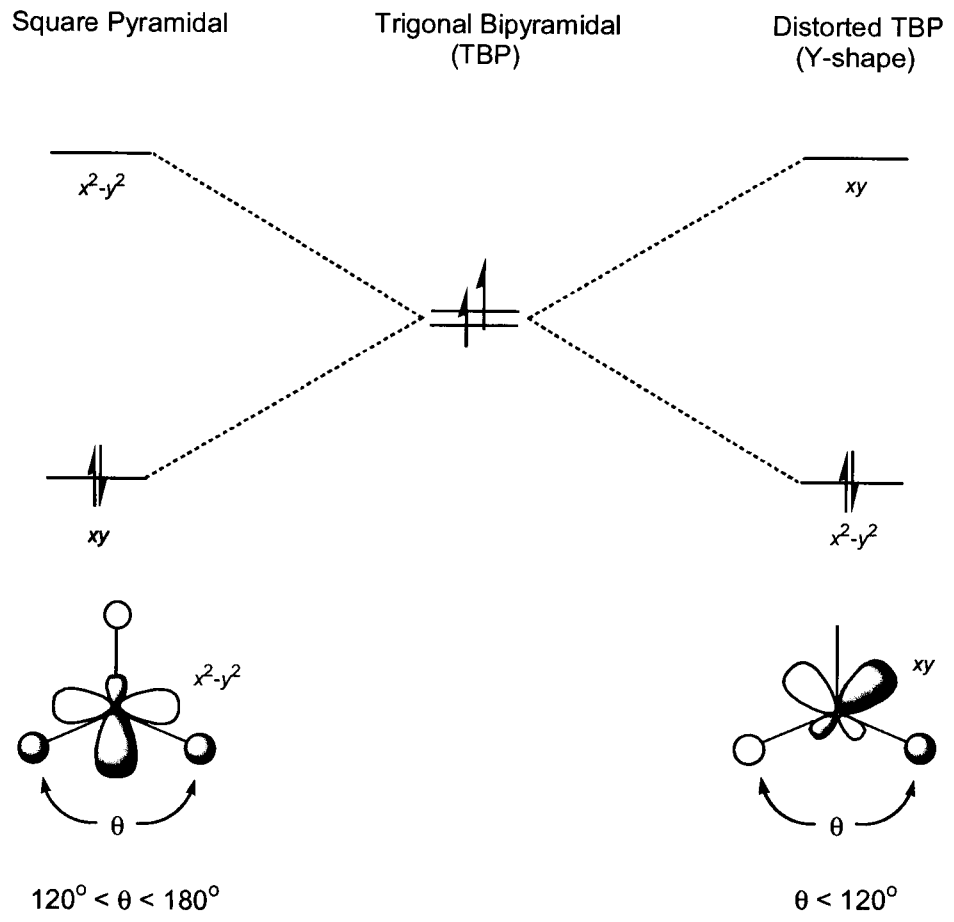

Figure 2.10. A qualitative representation of the two possible Jahn-Teller distortions in a diamagnetic trigonal bipyramidal structure of an d^6 ML_5 complex. The ligand and metal antibonding combinations are shown.

These two extreme geometries were found to be very close in energy and the preference for one over the other comes from a subtle balance of the σ and π properties of the ligands. The presence of π-acceptors, for instance, favours the square pyramidal structure. When one of the ligands is a π-donor, a distorted trigonal bipyramidal geometry is observed with this ligand located opposite to the acute angle in the equatorial plane of the molecule. This finding has also been observed experimentally.[69-72] This geometry permits the formation of a partial double bond between the empty metal *d*-orbital (*xy*) and the lone pair of the π-donor. This manifests as a shortening in the M-X bond and in the case of a single-face π-donor, a preferred orientation to

References begin on page 98

maximize orbital overlap. No such π-interaction is present in the square pyramidal structure since all of the symmetry adapted *d*-orbitals are filled.

The observed geometry of *endo*-**3** in the solid-state coincides well with the theoretical predictions, and on the basis of orbital symmetry allows for amide-to-ruthenium multiple bonding to take place. The P(1)-Ru(1)-N(1)-Si(1) dihedral angle of -5.8(1)° indicates that the plane of the amide donor is perpendicular to the equatorial plane of the molecule, and this allows for maximal overlap of the filled amido lone pair orbital (p_y) with the empty d_{xy} metal orbital. A qualitative depiction of this overlap is shown in Figure 2.11. Complex **3** can therefore be regarded as a "π-stabilized" unsaturated complex.

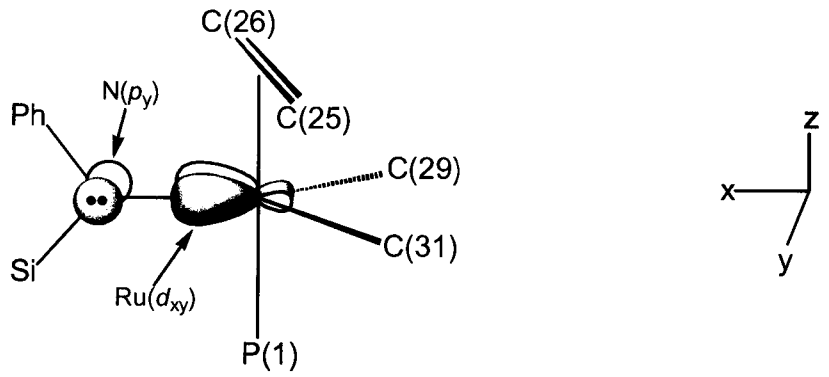

3

Figure 2.11. A schematic representation of the amide lone pair orbital (p_y) and empty ruthenium orbital (d_{xy}) overlap in complex *endo*-**3**.

Reactivity studies with complex **3** are also suggestive of "π-stabilized unsaturation" at the metal centre. For example, no reactivity was observed (as monitored by ^1H and $^{31}P\{^1H\}$ NMR spectroscopy) upon addition of neutral donor ligands including pyridine, THF and various phosphines (PPh_3, P^iPr_3 and PCy_3). Steric considerations should not be neglected, however, as they may also play a role in the observed lack of reactivity. The reaction of complex **3** with carbon monoxide will be discussed in the Future Work section of this chapter. Delocalization of the amido lone pair onto ruthenium may also account for the fact that the amino side-arm of the [NPNH] ligand does not coordinate to the metal centre. A decrease in the electrophilicity of late

References begin on page 98

transition metal complexes containing π-donating ligands such as amide and alkoxide ligands has been reviewed.[73]

(iii) Considerations into the identity of the second species and possible fluxional processes

It was stated earlier that the room-temperature ^{1}H NMR spectrum of **3** indicated the presence of two species in solution, and furthermore, the number of resonances observed suggested that these complexes were of low symmetry. The characterization of *endo*-**3** in the solid state showed that it is chiral, exhibiting C_1 symmetry. The structure of this complex allowed for considerations to be made regarding the identity of the second species as well as related fluxional processes in solution.

In a previous report, it was demonstrated that upon substitution of the cyclooctatriene ligand by phosphorus donor ligands in the complex [Ru(1-3-η^3-5,6-η^2-C_8H_{11})(η^6-C_8H_{10})][PF_6], the cyclooctadienyl fragment undergoes isomerization to yield the η^5-bound cyclooctadienyl ligand.[60] The driving force for this isomerization process was postulated to arise from steric effects. In the presence of bulky phosphine ligands, the 1-5-η^5-coordination mode is favoured since it occupies a smaller portion of the metal's coordination sphere, thus minimizing steric interactions.

The ability of the cyclooctadienyl ligand to isomerize, as demonstrated in the above example, led us to speculate that the second product isolated from the reaction of the [NPN] ligand with $[RuCl_2(cod)]_x$ could be a related species in which the cyclooctadienyl ligand had undergone a rearrangement. Scheme 2.4 portrays two possibilities. As depicted in **A** the η^3-allyl, η^2-olefin bound cyclooctadienyl ligand may isomerize to the η^5-allyl coordination mode. Alternatively, as shown in **B**, the η^3, η^2-coordination mode may remain intact although effectively rotated by 180° such that the phosphine and olefin donors are now *cis* to one another.

The highlighted section of Scheme 2.4 illustrates possible mechanistic pathways for the conversion of *endo*-**3** into the two speculative isomers **A** or **B**. For simplicity, the complexes are shown as viewed through the cyclooctadienyl ligand and bisecting the P-Ru-N angle. Only the

References begin on page 98

phosphorus and amido nitrogen atoms of the [NPNH] ligand set have been shown for clarity. Abstraction of one of the bridging allyl protons (H_h or $H_{h'}$) of the complex *endo*-**3** generates a ruthenium-hydrido species; isomerization to either **A** or **B** evolves through this common intermediate. Migration of the hydride occurs at the same position, then complex *endo*-**3** is regenerated. Migration of the hydride into the carbon bearing H_e, however, would result in the formation of complex **A**, whereas migration into the carbon with H_g generates complex **B**. If either of these pathways were reversible an equilibrium would be established and this could account for the broadened resonances that were observed in the room temperature ^1H NMR spectrum. As will be shown this process is unlikely based on ^1H and $^{13}C\{^1H\}$ NMR spectroscopy as well as reactivity studies.

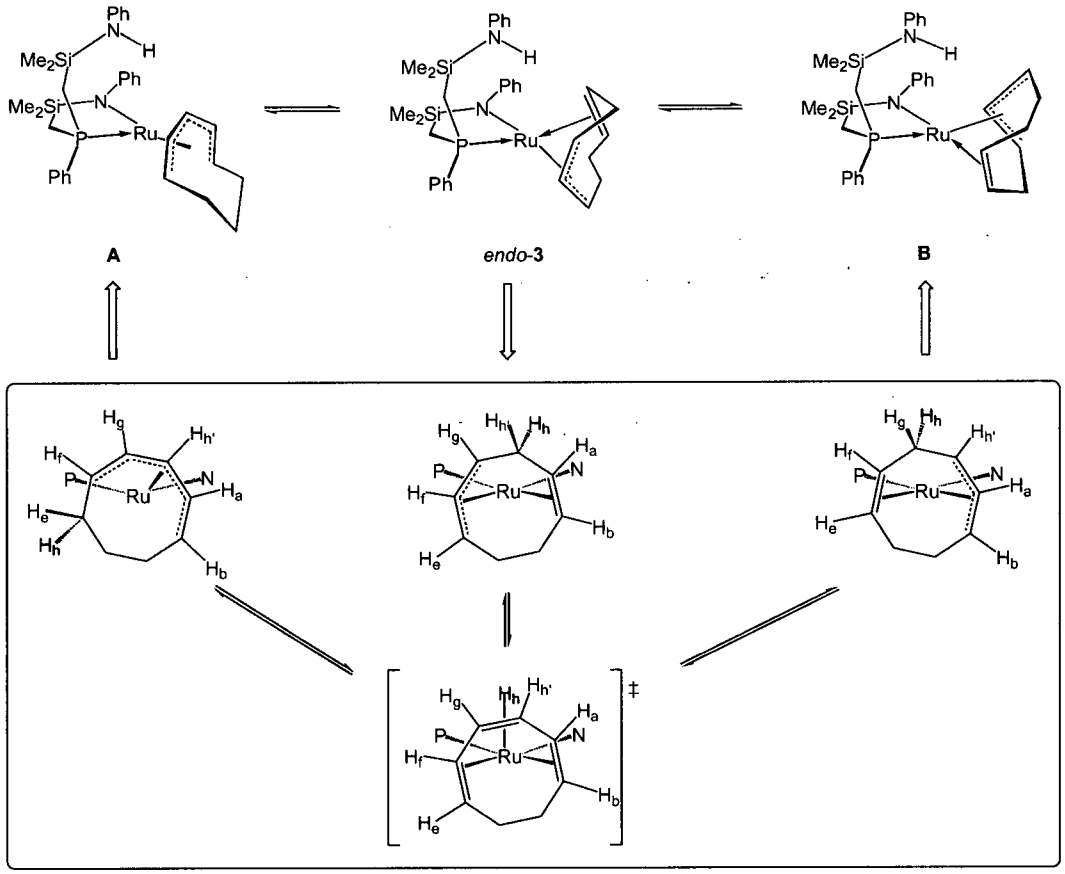

Scheme 2.4

References begin on page 98

Additional fluxionality may arise from epimerization equilibria in **3**. Examination of the solid-state structure of *endo*-**3** shows that the ruthenium and the phosphorus nuclei are both chiral centres. Complex **3** is an example of a chiral-at-metal complex that also contains an additional stereocentre; complexes of this type are known to undergo configurational processes.[74] Epimerization in complex **3** can result in the formation of four diastereomers; these are shown in Figure 2.12. The complexes *endo*-**3** and *exo*-**3** differ in the chirality displayed at the phosphorus centre (similarly for *endo*-**3'** and *exo*-**3'**). Inter-conversion of these complexes involves transfer of the amino proton from one arm of the [NPNH] ligand to the other. The isomers *endo*-**3** and *exo*-**3'** (or *exo*-**3** and *endo*-**3'**), on the other hand, have inverted chirality at the metal centre. The complexes *exo*-**3** (in Figure 2.12) and complex **B** (in Scheme 2.4) are the same species. Inversion at ruthenium involves fluxional behaviour associated with the cyclooctadienyl ligand.

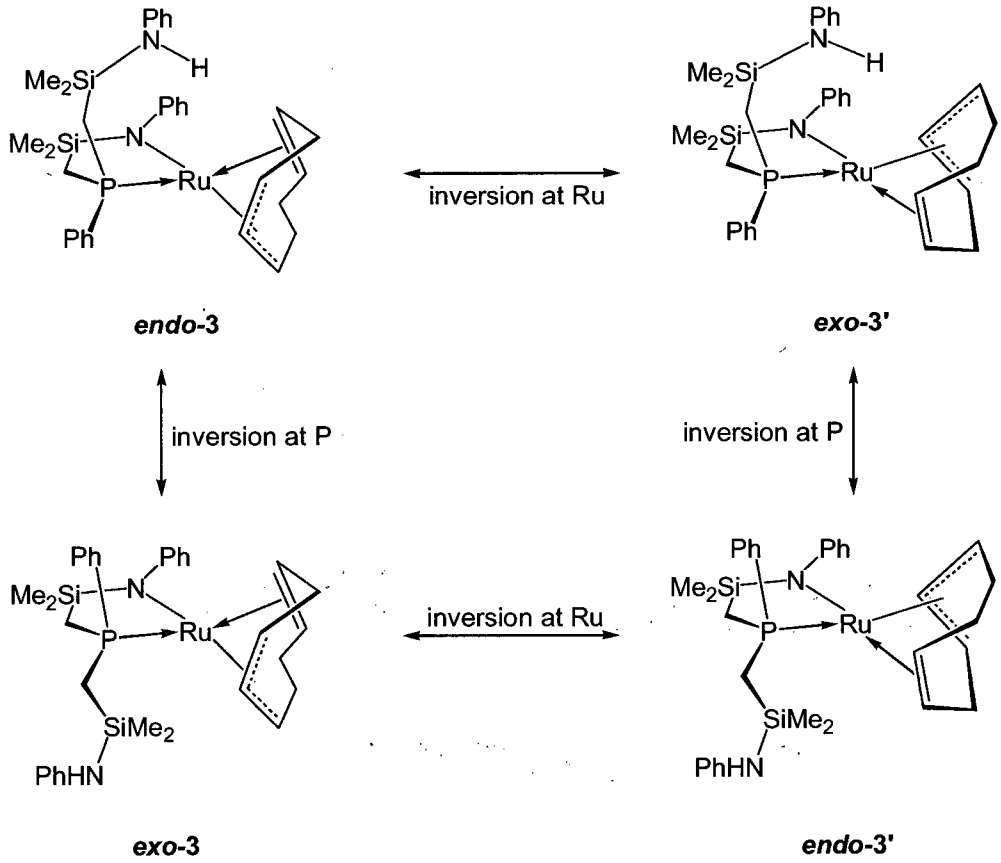

Figure 2.12. The four possible diastereomers of [NPNH]Ru(1-3-η^3:5,6-η^2-C_8H_{11}) (**3**).

References begin on page 98

It is apparent that complex **3** is capable of displaying a variety of fluxional processes related to both the cyclooctadienyl as well as the [NPNH] ligands. In order to determine the nature of the two species in solution variable-temperature NMR studies were required.

(iv) Variable-Temperature NMR Studies of *endo*- and *exo*-[NPNH]Ru(1-3-η^3- 5,6-η^2-C_8H_{11}) (*endo*-3 and *exo*-3)

The room-temperature ^{1}H NMR spectrum of a bulk sample of **3** consists of many broadened resonances, which hampered peak assignments (see Figure 2.8). The $^{31}P\{^1H\}$ NMR spectrum at the same temperature contains one peak at δ 33.0. Cooling the sample, however, results in two singlets in the $^{31}P\{^1H\}$ NMR spectrum in the ratio 2:1 establishing the presence of two species (one major and one minor) in solution. We have not been able to determine which diastereomer is the major or minor species, therefore, in the following discussion concerning the variable temperature NMR studies we assume that *endo*-**3** is the major isomer in solution.

Interestingly, identical spectra (^{1}H and $^{31}P\{^1H\}$) are obtained whether a single crystal of **3** is employed for the NMR investigations or a bulk powdered sample. This suggests that a dynamic equilibrium exists between the two species in solution. At 245 K the fluxional process responsible for the inter-conversion of the two species is slow enough to allow for the identification of *endo*-**3** and *exo*-**3** as the two complexes in solution. Full characterization of these two isomers was based on low-temperature ^{1}H, $^{31}P\{^1H\}$ and $^{13}C\{^1H\}$ NMR data. In addition, two-dimensional homo- and heteronuclear correlation experiments allowed for the complete assignment of the resonances attributed to both of the diastereomers. A collection of the ^{1}H and ^{13}C assignments for the cyclooctadienyl ligand of isomers *endo*-**3** and *exo*-**3** is given in Table 2.5 and Table 2.6 respectively, together with data for other complexes containing this ligand. The labelling convention used for assignment of NMR peaks corresponding to the cyclooctadienyl ligand that will be used in the following discussion is shown below in Figure 2.13.

References begin on page 98

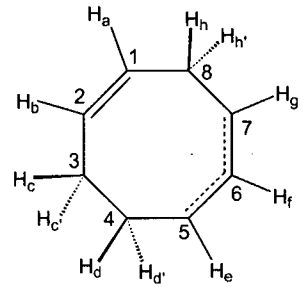

Figure 2.13. The labelling convention used for ^{1}H and ^{13}C NMR assignments of the cyclooctadienyl ligand in complexes containing this ligand.

The *J*-modulated $^{13}C\{^{1}H\}$ NMR spectrum obtained at 245 K (shown in Figure 2.14) identifies the presence of ten CH and six CH_2 resonances for the cyclooctadienyl ligand, consistent with an η^3-allyl, η^2-olefin coordination mode for each isomer. Complex *endo*-**3** contains two doublets at δ 108.1 ($^{2}J_{PC}$ = 10.5 Hz) and δ 61.4 ($^{2}J_{PC}$ = 6.5 Hz) in the $^{13}C\{^{1}H\}$ NMR spectrum that have been ascribed as the olefinic bound carbon atoms C_2 and C_1 respectively; these show a two bond coupling with the *trans* located phosphine donor. The allyl carbon resonances occur at δ 71.6 (C_6), δ 61.6 (C_5) and δ 35.6 (C_7). For these latter peaks no scalar coupling to the ^{31}P nucleus could be resolved; a much smaller coupling would be expected due to the *cis* orientation between these two donor groups. These data agree with the solid-state structure, which shows that the olefin and phosphine donors are *trans*-disposed to one another.

References begin on page 98

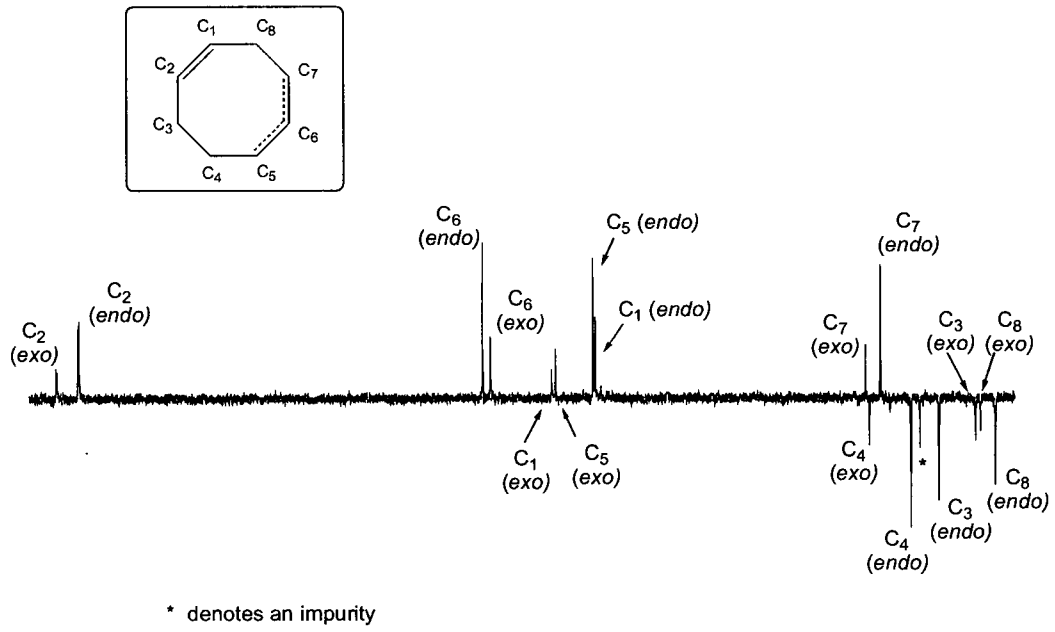

Figure 2.14. The *J*-modulated $^{13}C\{^1H\}$ NMR spectrum for *endo*-**3** and *exo*-**3** obtained at 245 K in toluene-d_8 highlighting the cyclooctadienyl carbon resonances. The *C*H resonances point up and the *C*H_2 resonances point down.

The 500 MHz ^1H NMR spectrum of *endo*-**3** shows four silyl methyl and four methylene proton resonances of the [NPNH] ligand indicating that the asymmetry of the complex is maintained in solution. In addition, there are 11 inequivalent cyclooctadienyl proton resonances. The olefinic protons are shifted furthest downfield at δ 4.25 (H_b) and δ 4.23 (H_a) respectively. The terminal allyl proton resonances are found at δ 4.20 (H_e) and δ 2.85 (H_g), whereas the central allyl proton (H_f) is significantly upfield shifted at δ 1.64. The protons of the methylene unit bridging the olefin and allyl groups (H_h and $H_{h'}$) are observed as multiplets at δ 2.70 and δ 2.00. The remaining methylene proton environments of the cyclooctadienyl ligand are located at δ 2.63 (H_c), δ 1.58 ($H_{c'}$), δ 2.18 (H_d) and δ 1.50 ($H_{d'}$). The two-dimensional ^1H-^1H COSY and ^1H-^{13}C HMQC data aided in the assignment of the cyclooctadienyl proton environments. The amino proton of the dissociated side-arm of the [NPNH] ligand occurs as a singlet at δ 6.63.

References begin on page 98

Table 2.5. ^{1}H resonances of the cyclooctadienyl ligand for complexes **3-6** including J_{HH} coupling constants for complex *exo*-**3** (determined from simulation data).

	endo-**3**	*exo*-**3**	**4**	**5**	*endo*-**6**	*exo*-**6**
H_a	4.23	4.68	2.20	2.17	4.25	4.50
H_b	4.25	3.92	2.45	2.29	4.00	3.87
H_c	2.36	1.83	1.60	1.18	2.10	2.08
$H_{c'}$	1.58	1.30	1.10	1.07	1.47	1.45
H_d	2.18	2.20	1.70	1.76	2.25	2.12
$H_{d'}$	1.50	1.75	1.40	1.33	1.85	1.75
H_e	4.20	3.50	3.40	3.10	4.16	3.60
H_f	1.64	1.50	3.42	3.45	1.52	1.43
H_g	2.85	3.37	4.30	4.35	2.90	3.27
H_h	2.70	3.09	3.40	3.45	2.77	2.95
$H_{h'}$	2.00	2.15	2.50	2.50	2.05	2.20

exo-**3**: $^3J_{ab}$ = 7.80 Hz, $^3J_{ah}$ = 7.70 Hz, $^3J_{ah'}$ = 7.30 Hz, $^3J_{bc}$ = 6.20 Hz, $^3J_{bc'}$ = 6.10 Hz, $^2J_{cc'}$ = 14.60 Hz, $^3J_{cd}$ = 7.60 Hz, $^3J_{cd'}$ = 6.00 Hz, $^3J_{c'd}$ = 7.20 Hz, $^3J_{c'd'}$ = 8.60 Hz, $^2J_{dd'}$ = 17.0 Hz, $^3J_{de}$ = 5.60 Hz, $^3J_{d'e}$ = 5.80 Hz, $^3J_{ef}$ = 8.00 Hz, $^3J_{fg}$ = 9.90 Hz, $^3J_{gh}$ = 7.90 Hz, $^3J_{gh'}$ = 4.20 Hz, $^2J_{hh'}$ = 19.30 Hz. (Determined using the simulation software in the NMR program Mestrix)

Table 2.6. ^{13}C resonances of the cyclooctadienyl ligand for complexes **3-6**. $^2J_{PC}$ values (Hz) are given in parenthesis.

	endo-**3**	*exo*-**3**	**4**	**5**	*endo*-**6**	*exo*-**6**
C_1	61.4 (6.5)	65.3 (5.8)	32.6 (6.5)	33.2 (6.4)	61.6 (6.3)	62.9 (5.9)
C_2	108.1 (10.5)	110.0 (11.3)	67.8 (5.5)	68.2 (5.8)	107.6 (10.6)	108.1 (11.6)
C_3	30.3	27.0	29.8	27.9	28.5	26.9
C_4	32.8	36.3	30.4	27.7	35.0	36.9
C_5	61.6	64.9	46.2 (2.2)	46.0 (2.1)	61.8	63.7
C_6	71.6	70.8	100.5	100.5	70.1	69.9
C_7	35.6	36.5	44.3 (18.9)	45.0 (19.2)	35.6	36.2
C_8	25.2	26.6	22.3	22.7	25.5	26.5

Inspection of the ^{13}C resonances (Table 2.6) for the cyclooctadienyl carbon nuclei of the minor isomer show that they are only slightly shifted with respect to *endo*-**3** suggesting a very similar coordination mode adopted by this ligand. Furthermore, two doublets at δ 110.0 ($^2J_{PC}$ = 11.3 Hz) and δ 65.3 ($^2J_{PC}$ = 5.8 Hz) indicate that the phosphine donor is located *trans* to the olefin

References begin on page 98

moiety, a feature that was also evident in the $^{13}C\{^1H\}$ NMR spectrum of *endo*-**3**. These data implicate *exo*-**3** as the second species in solution (and not *endo*-**3'** nor *exo*-**3'** as shown in Figure 2.12).

The ^1H NMR data also supports the formulation of the second species in solution as the diastereomer *exo*-**3**. Figure 2.15 shows a region of the 500 MHz $^1H\{^{31}P\}$ NMR spectrum highlighting the downfield shifted cyclooctadienyl resonances. In addition to exhibiting a similar trend in the chemical shift of the proton environments (refer to Table 2.5 as well), it can also be seen that they display similar coupling patterns. Once again this suggests that the coordination mode adopted by the cyclooctadienyl ligand is the same in both species. The olefinic protons exist furthest downfield at δ 4.68 (H_a) and δ 3.92 (H_b) with the two terminal allyl protons at δ 3.50 (H_e) and δ 3.37 (H_g). Although the central allyl proton (H_f) is obscured by neighbouring peaks its presence at δ 1.50 was confirmed by ^1H-^1H and ^1H-^{13}C correlation experiments. The significant upfield shift of this proton also occurs for isomer *endo*-**3**. The remaining cyclooctadienyl proton resonances are tabulated in Table 2.5. To further assist in the characterization of isomer *exo*-**3** a calculation of the spin system of the cyclooctadienyl proton environments was performed. The calculated coupling constants, found in Table 2.5, are similar to those obtained for other complexes known to contain a η^3, η^2-cyclooctadienyl ligand bound to ruthenium(II).[60] An asymmetric solution structure is also apparent from the four silyl methyl and four methylene proton environments of the [NPNH] ligand set. The amino proton occurs at δ 6.35, shifted 0.28 ppm upfield from the amino proton of *endo*-**3**.

References begin on page 98

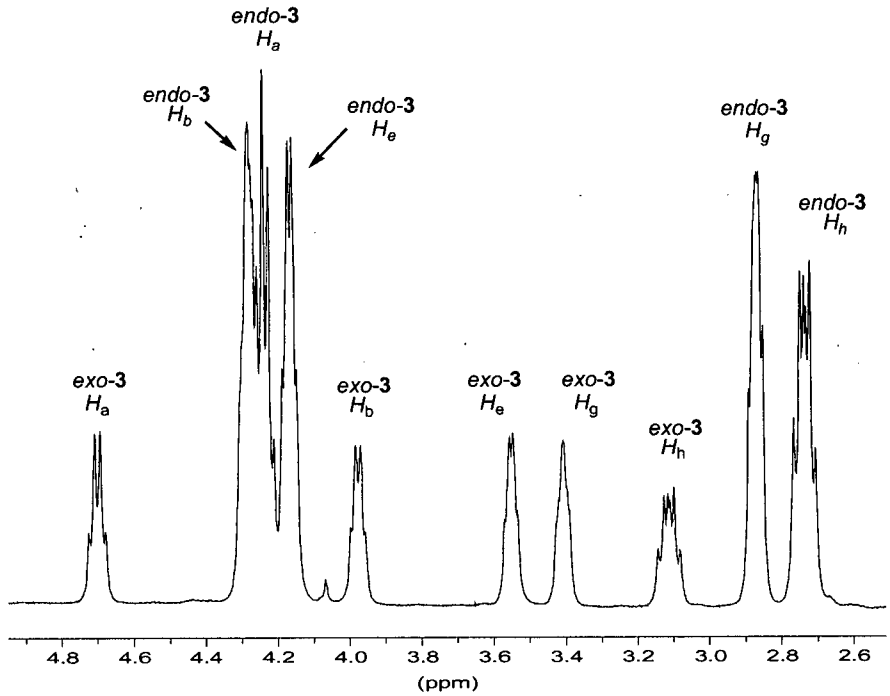

Figure 2.15. A region of the 500 MHz $^1H\{^{31}P\}$ NMR spectrum of isomers *endo*-**3** and *exo*-**3** highlighting the downfield shifted cyclooctadienyl proton resonances at 245 K in toluene-d_8.

The presence of a complex containing a η^5-ligated cyclooctadienyl ligand can be dismissed from the ^1H NMR data. Previous reports on complexes that contain a η^5-cyclooctadienyl moiety indicate that the central allyl proton occurs downfield between δ 6.0 and δ 7.2 as a (expected) triplet.[60] In this system, no such resonance is observed in the temperature range employed for the ^1H NMR studies. In addition, there was no hydride resonance apparent throughout this temperature range suggesting that the cyclooctadienyl ligand does not exhibit any fluxional behaviour; reactivity studies (section 2.5 (v)) confirmed this speculation.

Analysis of the variable-temperature ^1H NMR data confirmed the existence of an equilibrium mixture of the species *endo*-**3** and *exo*-**3** in solution. Integration of the amino proton resonance for each of the diastereomers at various temperatures gave relative concentrations of the two isomers and allowed for the evaluation of the equilibrium constants according to the expression in equation 2.3. A van't Hoff plot (shown in Figure 2.16) permitted the determination

References begin on page 98

of the following thermodynamic parameters for the equilibrium process: $\Delta H^{\circ} = 0.93 \pm 0.10$ kcal mol^{-1} and $\Delta S^{\circ} = 1.62 \pm 0.20$ eu.

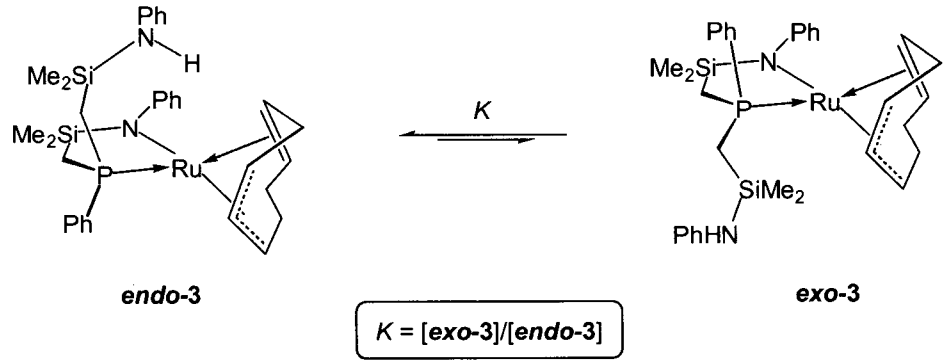

[2.3]

Table 2.7. Calculated equilibrium constants (K) for the equilibrium between diastereomers *endo*-**3** and *exo*-**3** in toluene-d_8.

Equilibrium Constant, K	Temperature, T (K)
0.46 ± 0.04	293 ± 1
0.43 ± 0.04	285 ± 1
0.39 ± 0.04	265 ± 1
0.34 ± 0.04	245 ± 1
0.28 ± 0.03	225 ± 1

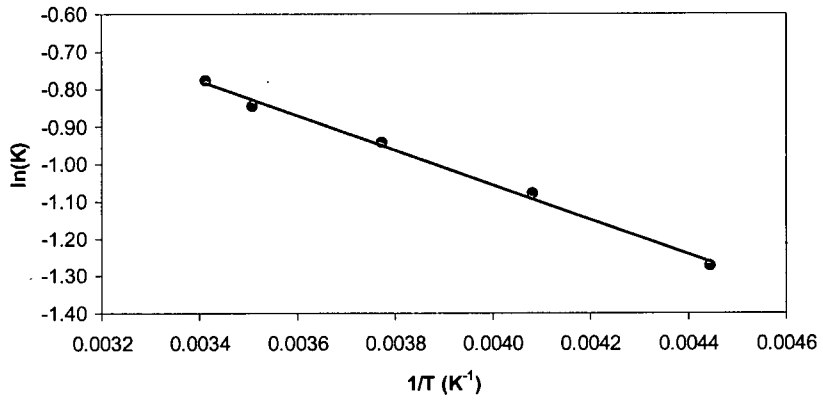

Figure 2.16. Van't Hoff plot for the equilibrium between diastereomers *endo*-**3** and *exo*-**3** (R^2 = 0.9954).

References begin on page 98

Figure 2.17 highlights the N-*H* region of the two-dimensional EXSY[75,76] spectrum obtained at room temperature (500 MHz, t_{mix} = 400 ms) for the mixture of *endo*-**3** and *exo*-**3** in toluene-d_8. A positively phased cross-peak between sites in a 2D-EXSY spectrum indicates that these nuclei are in chemical exchange (just as a cross-peak in a COSY spectrum indicates scalar coupling between the sites). The cross-peak between the two amino protons illustrates that these two nuclei are in chemical exchange, providing further evidence for the dynamic equilibrium that exists in solution. No cross peaks were observed between the amino protons and any of the cyclooctadienyl proton resonances indicating that the N-*H* proton does not get incorporated into the cyclooctadienyl ligand. Cross peaks were also observed for the cyclooctadienyl ligand, however, due to the broadened and overlapping resonances at 298 K, they could not be assigned to specific proton environments. The [NPNH] silyl methyl and methylene resonances between isomers also gave rise to positively phased cross-peaks as would be expected.

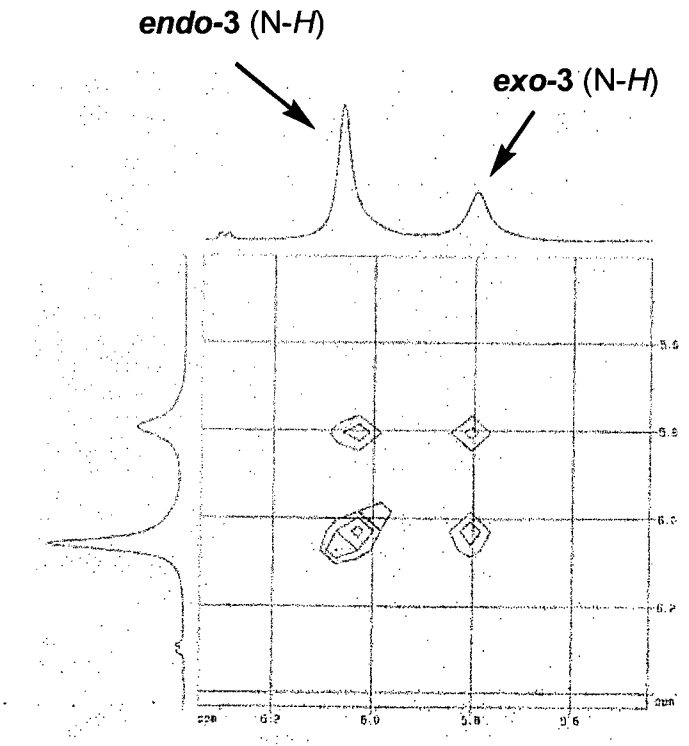

Figure 2.17. The N-*H* region of the 2-D EXSY spectrum for the mixture of *endo*-**3** and *exo*-**3**. Obtained at 298 K in toluene-d_8, 500 MHz and a mixing time of 0.4 s.

References begin on page 98

(v) Postulated mechanism for the inter-conversion of *endo*-3 and *exo*-3

The inter-conversion of the two diastereomers *endo*-**3** and *exo*-**3** requires inversion of chirality at the phosphorus atom. We propose that the mechanism for this process involves the direct transfer of the N-*H* proton from one arm of the [NPNH] ligand to the other via the transition state that is illustrated in Scheme 2.5. Shifting of the phosphine ligand to the "bottom" of the metal and the close approach of the amine side-arm to the ruthenium centre allows for the N-*H* proton to reside in a bridging position between both nitrogen atoms. Transfer of this proton from one arm to the other followed by dissociation of the resulting amine ligand and finally coordination of the phosphine back to the site *trans* of the olefin donor acts to invert the chirality of the phosphorus atom. The proposed six-coordinate transition state resembles the structure of the stable and isolable ruthenate complexes **4** and **5**. The solid-state molecular structure of **4** is shown in Figure 2.19. In the case of complex **4**, a lithium cation (rather than a proton) bridges the two nitrogen atoms. A related transition state has been postulated for aryloxide/phenol proton exchange in a pentamethylcyclopentadienyl nickel (II) system.[77]

References begin on page 98

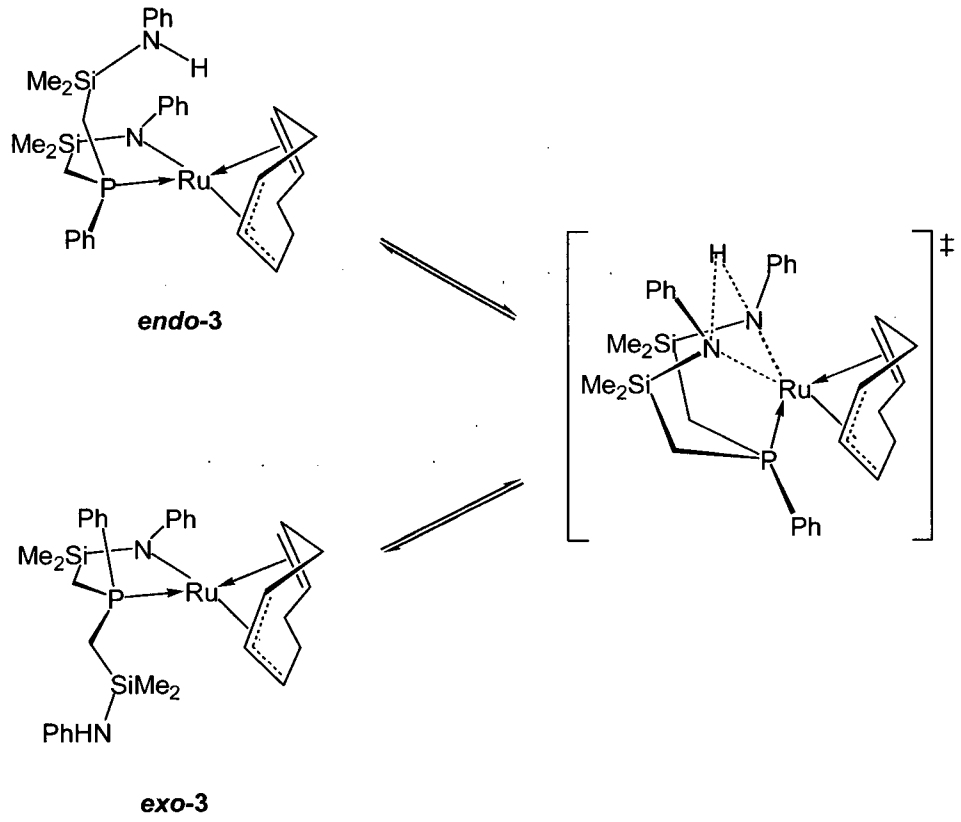

Scheme 2.5

The solid-state molecular structure of complex *endo*-**3** shows that the amino hydrogen atom is positioned towards the amido nitrogen atom. Although the distance between these two nuclei (3.419 Å) is too long to be considered a hydrogen bond, the observed orientation may be the result of an electrostatic attraction between these two nuclei. A hydrogen bonding interaction was evident in the solid-state structure of the complex [P_2NNH]Ru($PC_6H_4Ph_2$), (**2**), with a NH···N distance of 2.404 Å. This species forms as the sole product by the *irreversible* intramolecular protonation of one of the amido ligands of the [P_2NNH] ligand set, as shown in Figure 2.7. The equilibrium process depicted in Scheme 2.5 is similar, although it involves a *reversible* intramolecular protonation of a ruthenium amido ligand that is fast on the NMR timescale at room temperature.

The variable temperature ^{1}H NMR data also permitted a kinetic investigation into the mechanistic details for the process that inter converts isomers *endo*-**3** and *exo*-**3**. Line-shape

References begin on page 98

analysis of the N-*H* resonances allowed for the rate constants to be determined at several temperatures and used in an Eyring plot to calculate the activation parameters of $\Delta H^{\ddagger} = 16 \pm 1$ kcal mol^{-1} and $\Delta S^{\ddagger} = 4 \pm 4$ eu for this process. The calculated rate constants are tabulated in Table 2.8 and the Eyring plot is shown in Figure 2.18.

Table 2.8. Calculated rate constants for the reversible intramolecular proton transfer responsible for the inter-conversion of diastereomers *endo*-**3** and *exo*-**3**.

Rate Constant, k (s^{-1})	Temperature, T (K)
648 ± 32	320 ± 1
308 ± 15	308 ± 1
61 ± 3	293 ± 1
30 ± 2	285 ± 1

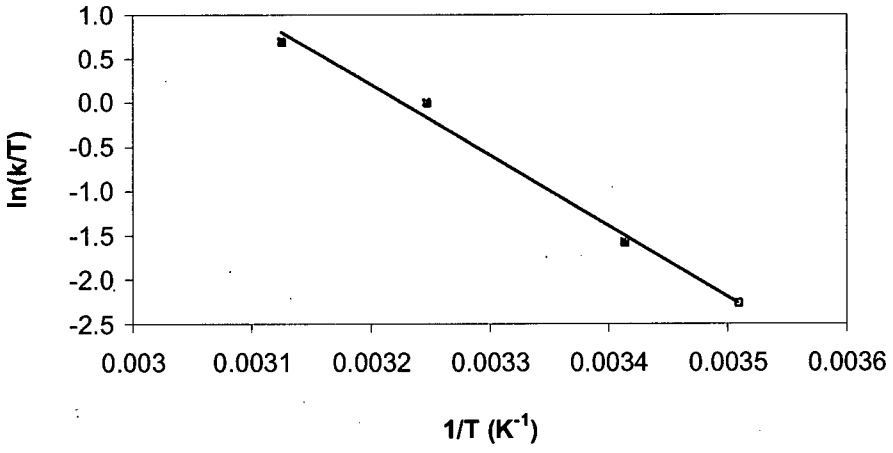

Figure 2.18. Eyring plot for the inter-conversion of diastereomers *endo*-**3** and *exo*-**3** (R^2 = 0.9922). $\Delta H^{\ddagger} = 16 \pm 1$ kcal mol^{-1} and $\Delta S^{\ddagger} = 4 \pm 4$ eu.

References begin on page 98

2.5 Synthesis, characterization and reactivity of the ruthenate complexes {[NPN]Ru(1-3-η^3-5,6-η^2-C_8H_{11})}{M·THF} (4) (M = Li) and (5) (M = Na)

(i) Synthesis of the ruthenate complexes {[NPN]Ru(1-3-η^3-5,6-η^2-C_8H_{11})}{M·THF} (4) (M = Li) and (5) (M = Na)

The addition of one equivalent of $LiN(SiMe_3)_2$ to an equilibrium mixture of *endo*-**3** and *exo*-**3** in toluene generates the ruthenate complex {[NPN]Ru(1-3-η^3:5,6-η^2-C_8H_{11})}{Li·THF} (**4**), as portrayed in Scheme 2.6. The insolubility of the initially formed orange solid in hydrocarbon solvents (hexanes, benzene and toluene) suggests that it has an oligomeric structure, {[NPN]Ru(1-3-η^3:5,6-η^2-C_8H_{11})Li}$_n$.[62] Addition of THF to the reaction mixture dissolves the solid giving the monomeric species **4** as an orange crystalline material in 92 % yield. The synthesis of complex **5** is analogous to that of **4** but employs $NaN(SiMe_3)_2$ as the base.

The addition of an external base to an equilibrium mixture of *endo*-**3** and *exo*-**3** generates a single, non-fluxional ruthenate complex. We propose that the stable ruthenate species (**4** or **5**) may be regarded as structurally related analogue of the proposed transition state for the inter-conversion of the two diastereomers of complex **3** as shown in Scheme 2.5.

References begin on page 98

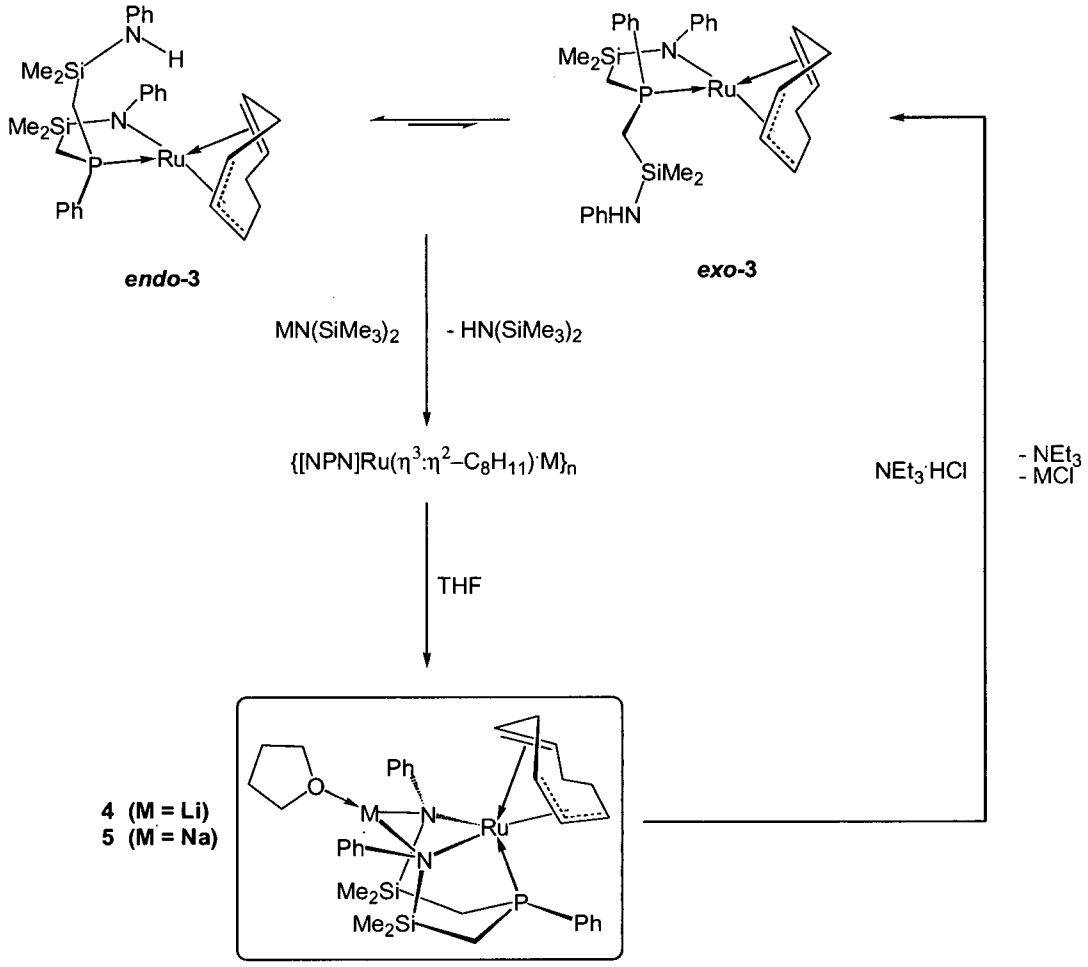

Scheme 2.6

(ii) X-ray diffraction study of compounds 4 and 5

Figure 2.19 shows the solid-state molecular structure of complex **4** as determined by a single crystal X-ray diffraction study. The solid-state structure of complex **5** can be found in the Appendix section of this thesis. Selected bond lengths and angles for both compounds are given in Table 2.9.

References begin on page 98

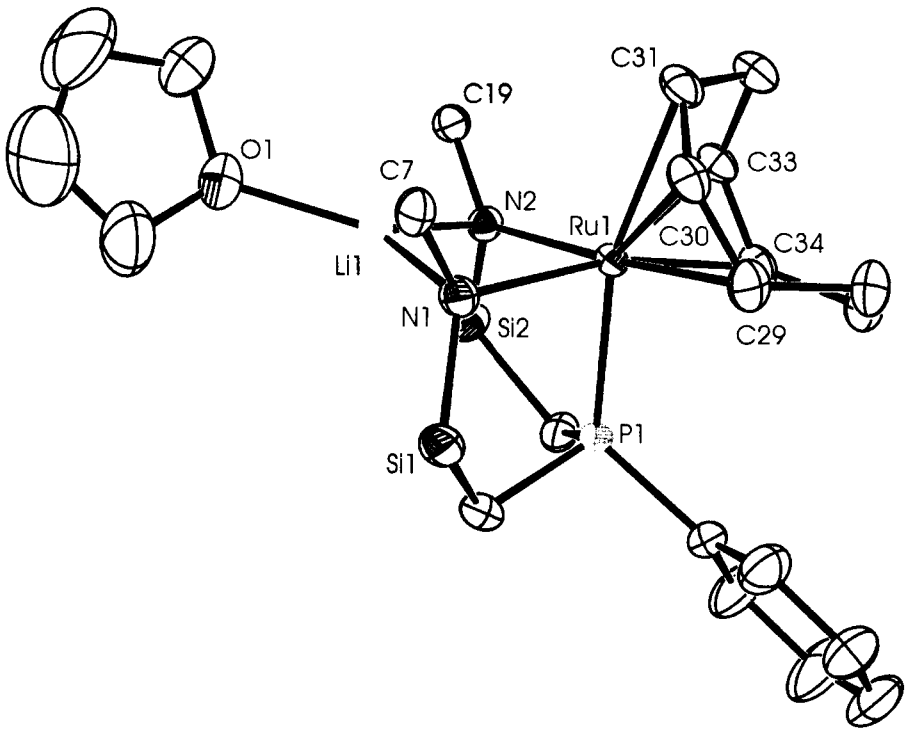

Figure 2.19. ORTEP representation (50 % thermal ellipsoid probability) of the solid-state molecular structure of {[NPN]Ru(1-3-η^3:5,6-η^2-C_8H_{11})}{Li·THF} (**4**) as determined by X-ray diffraction. The [NPN] ligand silyl methyl groups have been omitted for clarity and only the *ipso* carbon atoms of the amido phenyl rings are shown.

Table 2.9. Selected bond lengths and angles in the complexes {[NPN]Ru(1-3-η^3:5,6-η^2-C_8H_{11})}{M·THF}, M = Li (**4**) and M = Na (**5**).

Atom	Atom	Distance (Å)		Atom	Atom	Distance (Å)	
		4	**5**			**4**	**5**
Ru(1)	N(1)	2.275(2)	2.251(2)	N(2)	M(1)	2.010(5)	2.425(2)
Ru(1)	N(2)	2.364(2)	2.347(2)	O(1)	M(1)	1.956(5)	2.246(2)
Ru(1)	P(1)	2.2944(6)	2.2799(6)	N(1)	C(7)	1.410(3)	1.404(3)
Ru(1)	C(29)	2.179(2)	2.162(2)	N(2)	C(19)	1.414(3)	1.405(3)
Ru(1)	C(30)	2.176(2)	2.182(2)	N(1)	Si(1)	1.745(2)	1.724(2)
Ru(1)	C(31)	2.364(2)	2.380(2)	N(2)	Si(2)	1.729(2)	1.723(2)
Ru(1)	C(33)	2.180(2)	2.187(2)	C(29)	C(30)	1.424(4)	1.420(4)
Ru(1)	C(34)	2.224(2)	2.225(2)	C(30)	C(31)	1.396(4)	1.394(4)
N(1)	M(1)	2.004(5)	2.429(2)	C(33)	C(34)	1.384(4)	1.385(4)

References begin on page 98

Atom-Atom-Atom	Angle (°)		Atom-Atom-Atom	Angle (°)	
	4	**5**		**4**	**5**
N(1)-Ru(1)-N(2)	86.49(7)	89.11(7)	P(1)-Ru(1)-C(31)	163.77(7)	163.38(6)
N(1)-Ru(1)-P(1)	87.12(5)	86.66(5)	P(1)-Ru(1)-C(33)	113.17(7)	112.56(7)
N(2)-Ru(1)-P(1)	84.28(5)	85.15(5)	P(1)-Ru(1)-C(34)	81.44(8)	80.94(7)
N(1)-Ru(1)-C(29)	97.13(9)	93.60(8)	C(31)-Ru(1)-C(29)	66.6(1)	66.80(9)
N(1)-Ru(1)-C(31)	100.97(8)	101.50(8)	C(31)-Ru(1)-C(33)	62.87(9)	62.58(9)
N(1)-Ru(1)-C(33)	156.22(8)	158.64(8)	C(31)-Ru(1)-C(34)	88.8(1)	88.40(9)
N(1)-Ru(1)-C(34)	167.14(9)	164.62(8)	C(29)-Ru(1)-C(33)	92.1(1)	92.63(9)
N(2)-Ru(1)-C(29)	175.46(9)	175.56(8)	C(29)-Ru(1)-C(34)	78.9(1)	79.39(9)
N(2)-Ru(1)-C(31)	110.04(8)	109.21(8)	N(1)-M(1)-N(2)	104.8(2)	83.33(7)
N(2)-Ru(1)-C(33)	83.52(8)	83.62(8)	M(1)-N(1)-Ru(1)	84.5(2)	94.33(7)
N(2)-Ru(1)-C(34)	98.12(9)	98.81(8)	M(1)-N(2)-Ru(1)	82.0(2)	92.05(7)
P(1)-Ru(1)-C(29)	98.60(7)	98.52(7)			

Inspection of the solid-state molecular structure of complex **4** shows that the η^3-allyl, η^2-olefin coordination mode of the cyclooctadienyl ligand has been maintained, and that the [NPN] ligand is bound to the ruthenium in a facial manner. The amido donors bridge the lithium and ruthenium centres forming a "LiN_2Ru" core. Complex **4** is six-coordinate at ruthenium and exhibits C_1 symmetry in the solid state. The π-allyl function occupies two sites and the olefin the third site of one face of a distorted octahedron; the amido and phosphine donors of the tridentate [NPN] ligand fill the remaining coordination sites. Deviations from an ideal octahedral coordination geometry arise due to constraints imposed by the chelating [NPN] ligand as well as the cyclooctadienyl ligand. For example, the P(1)-Ru(1)-C(31) and N(2)-Ru(1)-C(31) bond angles (163.77(7)° and 110.04(8)° respectively) show that the terminal allyl carbon atom, C(31), is bent away from its ideal apical position. In addition, atom C(31) is approximately 0.18 Å further displaced from the metal centre than are C(29) and C(30) of the allyl donor. An unsymmetrical coordination mode for the cyclooctadienyl ligand in related ruthenium(II) systems has previously been reported.[60] One rationalization for this structural feature may be the minimization of steric interactions between the methylene unit of the cyclooctadienyl ligand with the aromatic rings of the amido donors. Alternatively, the longer Ru(1)-C(31) bond length may be a consequence of the high *trans* influence of the phosphine ligand. The *bis*-amide bridged "LiN_2Ru" core is asymmetric containing one shorter (2.275(2) Å) and one longer (2.364(2) Å) ruthenium to nitrogen distance; the amido to lithium distances are equivalent within experimental error. The Ru-N bond lengths in **4** are longer than that found in *endo*-**3** (2.019(2) Å). Coordinative saturation at the ruthenium center does not allow for π-donation from the amido lone

References begin on page 98

pair of electrons and consequently both the amide donors exhibit a pseudo-tetrahedral coordination geometry. The lithium atom in complex **4** adopts a planar, three-coordinate geometry with a molecule of THF completing its coordination sphere.

The molecular structure of complex **5** was found to be similar to **4** in the solid-state. An asymmetrically bound cyclooctadienyl ligand is also evident in the solid-state structure of **5** displaying similar bond lengths and angles to those observed in **4** (see Table 2.9). Significant variations arise in the "NaN_2Ru" core of the complex and these are a consequence of the larger ionic radius of sodium as compared to lithium; this results in an elongated distortion of the bimetallic core. For instance, the average M-N distance of 2.008 Å in **4** increases to 2.427 Å in complex **5** and the N(1)-M(1)-N(2) bond angle of 104.8(2)° in **4** decreases to 83.33(7)° in **5**.

(iii) Solution structure of compounds 4 and 5

Complexes **4** and **5** were fully characterized in solution at room temperature by ^1H, $^{31}P\{^1H\}$ and $^{13}C\{^1H\}$ NMR spectroscopy; the labelling convention for the cyclooctadienyl ligand portrayed in Figure 2.13 will be used in the following discussion. Analysis of the crude product indicates the formation of only one species in the reaction of *endo*-**3** and *exo*-**3** with external base. The asymmetry of **4** and **5** evident in the solid-state is maintained in solution denoting a rigid solution structure. To support this, the $^{13}C\{^1H\}$ NMR spectra (for both **4** and **5**) contain four resonances for the silyl methyl carbon atoms and eight resonances for the inequivalent cyclooctadienyl carbon nuclei. Once again, the *J*-modulated $^{13}C\{^1H\}$ spectra confirmed the η^3:η^2-coordination mode of the cyclooctadienyl ligand, as in complex **3**. Differences in the coordination of the cyclooctadienyl ligand arising in the six-coordinate "ate" complexes, however, are apparent by inspection of the ^{13}C resonances for these complexes (see Table 2.6). The greatest variation in peak positions occur for the ruthenium bound carbon nuclei. The central allyl carbon (C_6) for instance, is shifted downfield from *ca.* δ 71.0 in *endo*-**3** and *exo*-**3** to *ca.* δ 100.0 in complexes **4** and **5**. The olefin carbon atom, C_2, experiences an upfield shift of similar magnitude from *ca.* δ 110.0 (in *endo*-**3** and *exo*-**3**) to *ca.* δ 68.0 (in **4** and **5**). Differences are also manifested in the scalar coupling of the cyclooctadienyl carbon nuclei to the ^{31}P nucleus. Whereas coupling to the ^{31}P nucleus could only be distinguished for the *trans* disposed olefin nuclei (C_1 and C_2) in *endo*-**3** and *exo*-**3**, it is also present for the terminal π-allyl carbon atoms C_5 and C_7 in complexes **4** and **5**.

References begin on page 98

No coupling to the central allyl carbon nucleus could be measured in either **4** or **5**. As anticipated from the solid state structures, C_7 of the cyclooctadienyl ligand experiences the greatest coupling ($^2J_{PC}$ = 19 Hz) due to its near *trans* disposition with the phosphine donor.

The ^{1}H NMR spectra of complexes **4** and **5** are each comprised of four silyl methyl resonances, four ligand methylene resonances, 11 inequivalent cyclooctadienyl proton resonances, and three sets of *ortho*, *meta* and *para* phenyl proton resonances for the [NPN] phenyl groups. This number of peaks is consistent with a C_1 symmetric structure in solution. The changes in chemical shift locations of the cyclooctadienyl protons (as compared to *endo*-**3** and *exo*-**3**) mirror those of the carbon nuclei to which they are attached (see Table 2.5). The complete assignment of the proton environments in complexes **4** and **5** was accomplished with the aid of two-dimensional correlation (^{1}H-^{1}H and ^{1}H-^{13}C) experiments. The ^{31}P{^{1}H} NMR spectrum of **4** consists of a singlet at δ 44.3, which indicates that in solution the phosphine ligand remains bound to ruthenium and does not coordinate to the lithium centre; in such a case, one would expect a 1:1:1:1 quartet due to coupling to ^{7}Li (I = 3/2, 92.6% abundance). Likewise, the ^{7}Li{^{1}H} NMR spectrum of **4** contains a singlet at δ -2.50. For complex **5**, a singlet at δ 46.8 is observed in the ^{31}P{^{1}H} NMR spectrum.

(iv) Regeneration of the equilibrium mixture of *endo*-3 and *exo*-3 by addition of acid to 4 or 5

As shown in Scheme 2.6, the equilibrium mixture of *endo*-**3** and *exo*-**3** can be regenerated by the stoichiometric addition of NEt_3·HCl to the ruthenate complex **4** (or **5**). Utilizing the deuterium-labelled acid in the above reaction allows for selective deuteration at the amine nitrogen atom. The assignment of the N-*H* resonance in the ^{1}H NMR spectrum of the diastereomers of complex **3** were verified by synthesis of the amino-deuterio derivatives *endo*-**3**-d_1 and *exo*-**3**-d_1. Allowing an equilibrium mixture of the deuterium labelled derivatives to sit for extended periods did not result in the incorporation of deuterium into the cyclooctadienyl ring as monitored by ^{1}H NMR spectroscopy. This result is consistent with the two-dimensional EXSY data, which do not show a cross peak between the amino protons and cyclooctadienyl hydrogen atom sites. Unfortunately, the broadness in the variable-temperature ^{2}H spectrum and the absence of a low-

References begin on page 98

temperature limiting $^{31}P\{^1H\}$ spectrum did not permit an evaluation of the isotope influence on the kinetics of the equilibrium process.

(v) Reaction of compounds 4 and 5 with Me_3SiCl: formation of the two independent diastereomers *endo*- and *exo*-[NPN($SiMe_3$)]Ru(1-3-η^3- 5,6-η^2-C_8H_{11}) (*endo*-6 and *exo*-6)

The above example illustrates the basic behaviour of the ruthenate complexes towards acidic compounds such as NEt_3·HCl regenerating the equilibrium mixture of *endo*-**3** and *exo*-**3**. This reactivity prompted us to investigate the ability of compounds **4** and **5** to act as nucleophilic reagents. Nitrogen-silicon bonds can be made conveniently by the addition of alkali metal amides with silyl chloride precursors.[62] Formation of the N-Si linkage is facilitated by the formation of MCl (M = alkali metal), which provides a thermodynamic driving force. In fact, formation of the N-Si linkages in the backbone of the [NPN] and [P_2N_2] ligands proceeds via this route. In an earlier report, the tungstenate complex, $[Cp^*WMe_3(NLi)]_x$, was shown to react with Me_3SiCl resulting in the formation of $Cp^*WMe_3NSiMe_3$.[78] If the equilibrium that is established between the two diastereomers *endo*-**3** and *exo*-**3** occurs by the reversible intramolecular protonation of a ruthenium amide ligand, as postulated, then it can be assumed that replacement of the N-H proton by the bulkier trimethylsilyl group (giving N-$SiMe_3$) may slow down or hinder this exchange process all together.

Addition of an excess of chlorotrimethylsilane (Me_3SiCl) to a solution of **4** or **5** in toluene results in a change in colour from orange to red over a period of 24 hours. Removal of the volatile components under vacuum followed by rinsing of the resulting red solid with pentane allows for the isolation of the two independent diastereomers *endo*- and *exo*-[NPN($SiMe_3$)]Ru(1-3-η^3-5,6-η^2-C_8H_{11}) (*endo*-**6** and *exo*-**6**, respectively), as shown in equation 2.4. The two isomers are formed in approximately 50% yield each. Attempts to separate the two complexes via crystallization have failed thus far.

References begin on page 98

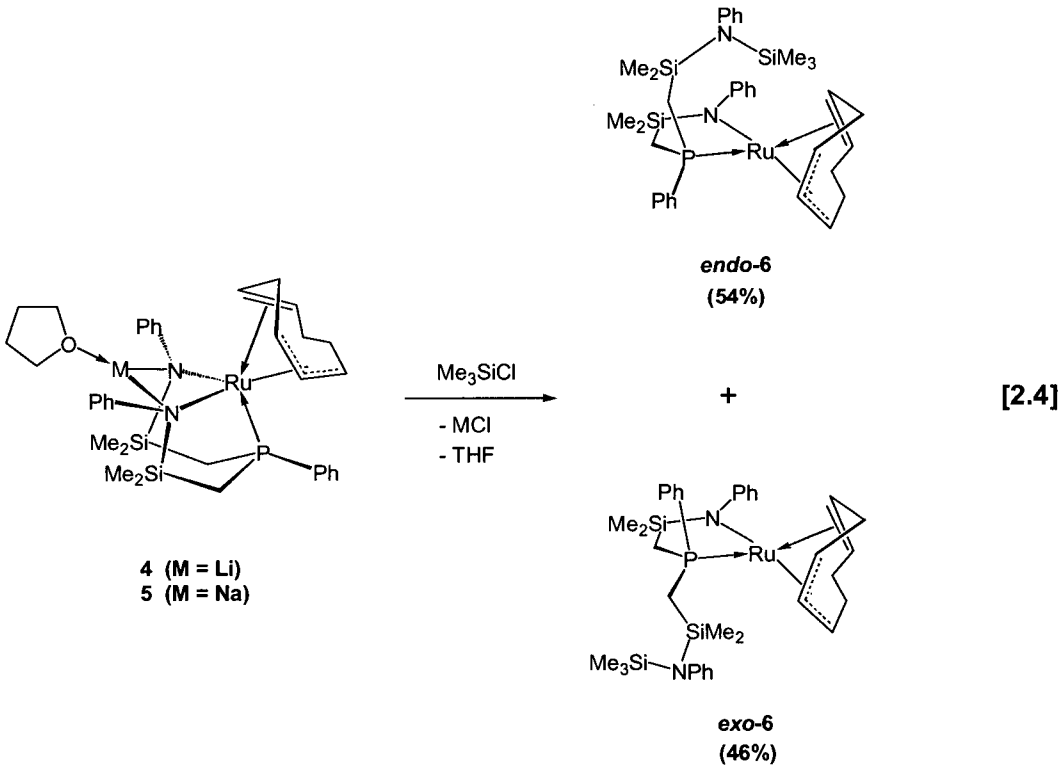

Unlike the room-temperature ^{1}H NMR spectrum for *endo*-**3** and *exo*-**3**, which is comprised of broadened peaks, the ^{1}H NMR spectrum (at 298 K) for complexes *endo*-**6** and *exo*-**6** contains well resolved resonances for all proton environments implying that the two species do not exhibit any fluxionality. In fact, examination of the ^{1}H and ^{31}P{^{1}H} NMR spectra as a function of temperature (from 200 to 360 K) show that the two species are not in equilibrium since no change in product ratios could be discerned. These results provide further evidence for the mechanism depicted in Scheme 2.5 for the inter-conversion of the diastereomers of species **3**. As was expected, the bulky trimethylsilyl group is not exchanged between the two isomers, and consequently, they remain independent of one another. In addition, these results show that the cyclooctadienyl ligand in these two complexes (and by extension in *endo*-**3** and *exo*-**3**) remains conformationally rigid; it does not isomerize, for instance, to an η^5-coordinated cyclooctadienyl ligand.

The characterization of *endo*-**6** and *exo*-**6** was based on solution NMR studies. The ^{13}C{^{1}H} and ^{1}H NMR data were diagnostic for these two isomers. A *trans* disposition between the phosphine and olefin donors in these complexes is indicated by the coupling of the ^{31}P nucleus

References begin on page 98

to the olefinic carbon atoms. In *endo*-**6**, for example, C_1 occurs as a doublet at δ 61.6 ($^2J_{PC}$ = 6.3 Hz) and likewise C_2 appears as a doublet at δ 107.6 ($^2J_{PC}$ = 10.6 Hz). Complex *endo*-**3** shows very similar resonances for these two nuclei, as is detailed in Table 2.6, with nearly identical coupling constants (6.5 Hz and 10.5 Hz respectively). A similar trend is observed for *exo*-**6** and *exo*-**3**. The ^{13}C chemical shifts of the remaining cyclooctadienyl carbon nuclei are only slightly shifted, suggesting that a very similar coordination mode is adopted by this ligand for the related *endo* and *exo* isomers of complexes **3** and **6**.

The room-temperature ^1H NMR spectrum for a mixture of *endo*-**6** and *exo*-**6** resembles the low-temperature spectrum (245 K) for an equilibrium mixture of *endo*-**3** and *exo*-**3**. A survey of Table 2.5 shows that the respective isomers of complexes **6** and **3** display similar chemical shifts for the cyclooctadienyl proton environments. The central allyl proton (H_f) in all four species experiences the greatest amount of shielding and is shifted furthest upfield between δ 1.40 to δ 1.65. The olefinic protons (H_a and H_b), on the other hand, are downfield shifted between δ 3.85 and δ 4.70 in all of the complexes. Both the *endo* and *exo* isomers of complex **6** have four ligand silyl methyl proton resonances; the ligand methylene resonances for both isomers overlap with the cyclooctadienyl resonances and occur between *ca.* δ 1.0 and δ 1.5. The terminal amino silyl methyl (N-Si*Me*$_3$) signal for *endo*-**6** occurs as a singlet at δ 0.15 and integrates for nine protons. The presence of a singlet for this group implies that there is free rotation of the trimethylsilyl group about the N-Si bond. For the isomer *exo*-**6** this resonance appears as a singlet at δ 0.12. The remaining phosphine, amine and amido phenyl resonances occur at expected positions between δ 6.8 and δ 7.7. The $^{31}P\{^1H\}$ NMR spectrum contains two singlets at δ 32.9 and δ 32.3 for complexes *endo*-**6** and *exo*-**6**, respectively.

2.6 Attempted Synthesis of [NPN]Ru(PPh_3)$_2$

(i) Reaction of [NPN]Li_2·(C_4H_8O)$_2$ with $RuCl_2(PPh_3)_3$

Reactions of $RuCl_2(PPh_3)_3$ with the tetrahydrofuran adduct of the lithiated ligand precursor, [NPN]Li_2·(C_4H_8O)$_2$, were performed under a variety of conditions but in all cases a mixture of products was formed as indicated by ^1H and $^{31}P\{^1H\}$ NMR spectroscopy. Solvents

References begin on page 98

such as toluene, benzene and diethyl ether were all utilized giving similar results in each case. The $^{31}P\{^1H\}$ NMR spectrum of the crude product mixture shows free triphenylphosphine indicating that the [NPN] ligand does coordinate to the metal centre; formation of the anticipated five-coordinate species [NPN]Ru(PPh_3)$_2$, however, can be dismissed. A five-coordinate complex could adopt either a square pyramidal or a distorted trigonal bipyramidal coordination geometry. A square pyramidal complex would be expected to give rise to a triplet and a doublet for the ^{31}P nucleus of the [NPN] and triphenylphosphine ligands, respectively. A trigonal bipyramidal complex on the other hand would be expected to exhibit a doublet of doublet coupling pattern for each of the inequivalent ^{31}P nuclei. Neither of these diagnostic coupling patterns was observed. There are many resonances that exist as simple doublets suggesting that there is one equivalent of the chelating [NPN] ligand and one equivalent of coordinated triphenylphosphine per metal centre, giving species of the general formula "[NPN]RuPPh_3". Inspection of the ^1H NMR spectrum allows for speculations to be made regarding the identity of some of the products that formed in this reaction. A broad singlet at δ 2.9 appears in a location very close to the amino proton of complex **2** (N-*H* at δ 2.8) in which *ortho*-metalation of the triphenylphosphine ligand occurs. This suggests that the species [NPNH]Ru($C_6H_4PPh_2$) containing an *ortho*-metalated PPh_3 ligand may have formed. Also evident in the ^1H NMR spectrum are multiplets in the region δ 4.0 to δ 5.2, reminiscent of a coordinated arene moiety. Similar features are present in hydride complexes of ruthenium containing the [NPNH] ligand set. In these systems, the phenyl substituent of the amine donor as well as aromatic solvent molecules (toluene or benzene) were shown to coordinate to the metal centre in an η^6 fashion (Chapter 3). It is possible that similar products are being formed in this case.

2.7 Summary and Conclusions

The synthesis of ruthenium(II) complexes that incorporate the mixed-donor macrocyclic [P_2N_2] and tridentate [NPN] ligand sets is described, with the purpose of utilizing these compounds as precursors for the catalytic hydrogenation of imine substrates. The reaction of [P_2N_2]Li$_2$·$C_4H_8O_2$ with [$RuCl_2$(cod)]$_x$ generates the diamidodiphosphine complex [P_2N_2]Ru(η^2:η^2-C_8H_{12}) (**1**) as a yellow crystalline solid in excellent yield. Complex **1** was characterized in solution and in the solid-state. At room temperature **1** displays C_{2v} symmetry in solution,

References begin on page 98

however, cooling the solution results in a C_2 symmetric complex consistent with the solid-state molecular structure. The reaction between the dilithium salt of the [P_2N_2] ligand with $RuCl_2(PPh_3)_3$ yields the species [P_2NNH]Ru($C_6H_4PPh_2$) (**2**) in which *ortho*-metalation of the triphenylphosphine ligand occurs. The solid-state molecular structure of **2** shows that there is an intramolecular hydrogen bonding interaction involving the amine proton and amide nitrogen atom of the [P_2NNH] ligand. The ligand [NPN]Li_2·(C_4H_8O)$_2$ reacts with [$RuCl_2$(cod)]$_x$ to give an equilibrium mixture of *endo*-**3** and *exo*-**3**. The diastereomers of **3** are formed via deprotonation of the cyclooctadiene moiety by the [NPN] ligand; transfer of the resulting amino proton between the [NPNH] side-arms establishes the observed equilibrium. Deprotonation of co-ligands is a common occurrence in related ruthenium(II) systems containing the [NPN] and [P_2N_2] ligand sets. Formation of the ruthenate complexes {[NPN]Ru(1-3-η^3:5,6-η^2-C_8H_{11})}{M·THF} (**4**, M = Li or **5** M = Na) is accomplished by the addition of $MN(SiMe_3)_2$ (M = Li or Na) to a mixture of *endo*-**3** and *exo*-**3**. These ruthenate species are non-fluxional in solution as evidenced by the NMR data. Complexes **4** and **5** react with acidic compounds to regenerate an equilibrium mixture of *endo*-**3** and *exo*-**3**, or with chlorotrimethylsilane to give the two independent diastereomers *endo*- and *exo*-[NPN($SiMe_3$)]Ru(1-3-η^3-5,6-η^2-C_8H_{11}) (*endo*-**6** and *exo*-**6**, respectively). Although reaction of the [P_2N_2] and [NPN] ligands with the ruthenium(II) precursors did not yield the expected products in all cases, the complexes that were obtained contain a ruthenium amide unit necessary for the heterolytic activation of molecular hydrogen. This reactivity will be discussed in the following chapter.

2.8 Future Work

(i) Reaction of 3 with carbon monoxide

We envisioned that the stoichiometric addition of a neutral donor ligand to an equilibrium mixture of the diastereomers *exo*-**3** and *endo*-**3** would eliminate the inter-conversion process and possibly allow for the separation of two coordinatively saturated analogues of these two species. As was previously described, complex **3** was found to be unreactive towards neutral donors such as pyridine, THF and various phosphines. The addition of one equivalent of CO gas to a red solution of **3**, however, resulted in an immediate change in colour to orange. The reaction was

References begin on page 98

performed in an NMR tube and the ^1H and $^{31}P\{^1H\}$ NMR spectra both indicated the formation of only one product, [NPNH]Ru(1-3-η^3:5,6-η^2-C_8H_{11})(CO) (**7**), as shown in equation 2.5.

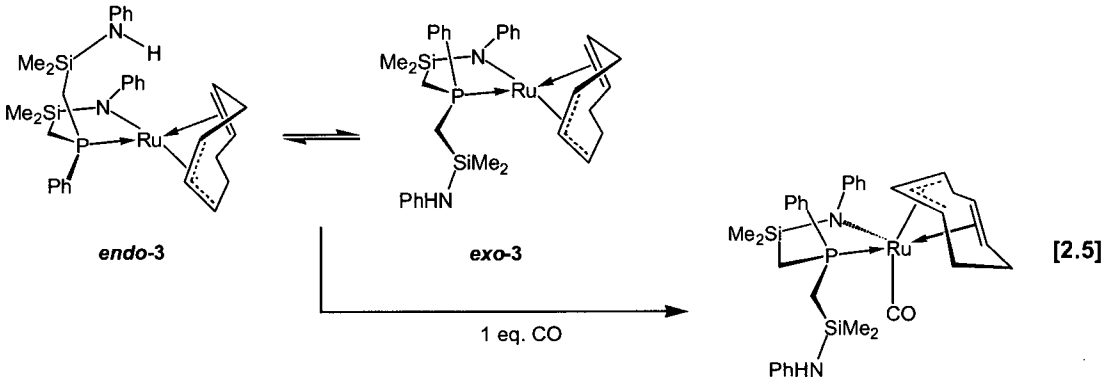

[2.5]

The slow evaporation of the NMR solution (toluene-d_8) allowed for the isolation of single crystals of complex **7** suitable for an X-ray diffraction study. The solid-state molecular structure of **7** is shown in Figure 2.20 and selected bond lengths and angles are given in Table 2.10. The geometry of **7** is best described as distorted octahedral with the olefin and phosphine ligands occupying the axial positions, and the amide, CO and allyl donors contained within the equatorial plane. We have previously described **3** as a π-stabilized unsaturated complex involving a bonding interaction between the amido lone pair of electrons with the metal LUMO (d_{xy} orbital). The addition of CO to **3** generating the coordinatively saturated complex **7** would render the amido ligand a σ-donor with minimal π-bonding interactions. The longer Ru(1)-N(1) bond distance of 2.212(2) Å in **7** compared to 2.019(2) Å in **3** supports this notion. The bond angles about the amide nitrogen atom (N(1)) indicate a planar geometry; this is most likely due to π-interactions with the neighbouring silicon atom or phenyl ring. Interestingly, the plane of the amide donor is tilted away from the equatorial plane of the molecule (P(1)-Ru(1)-N(1)-C(7) = 138.8(2)°). This may be due to a stabilizing effect on the nitrogen lone pair by decreasing the orbital overlap of these electrons with the filled d_π orbitals of the metal.

References begin on page 98

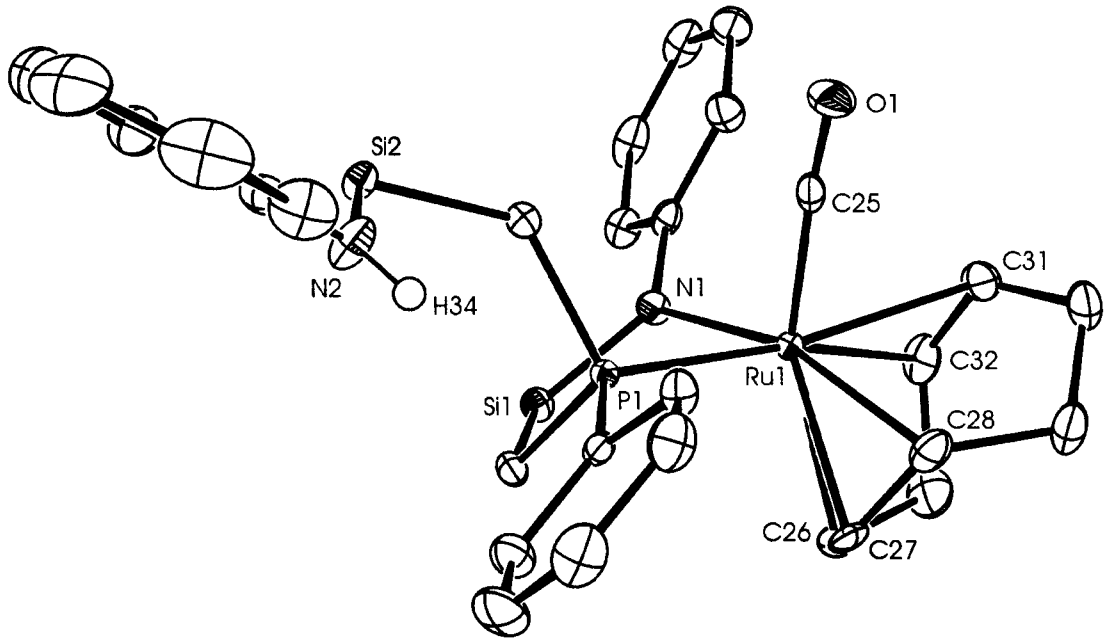

Figure 2.20. ORTEP representation (thermal ellipsoids shown at 50 % probability) of the solid-state molecular structure of the complex [NPNH]Ru(1-3-η^3:5,6-η^2-C_8H_{11})(CO) (**7**) as determined from X-ray diffraction. The silyl methyl groups of the [NPNH] ligand have been omitted for clarity. The amino hydrogen atom H(34) was located and refined isotropically.

Table 2.10. Selected bond lengths and angles [NPNH]Ru(1-3-η^3:5,6-η^2-C_8H_{11})(CO) (**7**).

Atom	Atom	Distance (Å)	Atom	Atom	Distance (Å)
Ru(1)	N(1)	2.212(2)	C(26)	C(27)	1.385(4)
Ru(1)	P(1)	2.2853(6)	C(27)	C(28)	1.424(3)
Ru(1)	C(26)	2.356(2)	C(31)	C(32)	1.355(4)
Ru(1)	C(27)	2.202(2)	N(1)	Si(1)	1.720(2)
Ru(1)	C(28)	2.200(2)	N(2)	Si(2)	1.729(2)
Ru(1)	C(31)	2.407(2)	N(1)	H(34)	0.75(3)
Ru(1)	C(32)	2.334(2)			

References begin on page 98

Atom	Atom	Atom	Angle (°)	Atom	Atom	Atom	Angle (°)
P(1)	Ru(1)	N(1)	78.78(5)	N(1)	Ru(1)	C(31)	105.24(8)
P(1)	Ru(1)	C(25)	88.11(7)	N(1)	Ru(1)	C(32)	84.71(8)
P(1)	Ru(1)	C(26)	104.18(6)	C(25)	Ru(1)	C(26)	158.74(9)
P(1)	Ru(1)	C(28)	101.85(6)	C(25)	Ru(1)	C(28)	94.77(9)
P(1)	Ru(1)	C(31)	168.31(6)	C(25)	Ru(1)	C(31)	80.26(9)
P(1)	Ru(1)	C(32)	157.73(7)	C(25)	Ru(1)	C(32)	110.65(9)
N(1)	Ru(1)	C(25)	104.70(8)	Ru(1)	N(1)	Si(1)	116.04(9)
N(1)	Ru(1)	C(26)	94.80(8)	Ru(1)	N(1)	C(7)	123.2(1)
N(1)	Ru(1)	C(28)	160.53(8)	Si(1)	N(1)	C(7)	120.7(1)

The room temperature ^{1}H, $^{31}P\{^{1}H\}$ and $^{13}C\{^{1}H\}$ NMR spectra all show features characteristic of complex **7**. The $^{31}P\{^{1}H\}$ NMR spectrum consists of a singlet at δ 46.0 and the $^{13}C\{^{1}H\}$ NMR spectrum shows eight resonances for the inequivalent cyclooctadienyl carbon centres. Two of these resonances at δ 69.9 ($^{2}J_{PC}$ = 6.72 Hz) and δ 105.1 ($^{2}J_{PC}$ = 7.63 Hz) are observed as doublets due to coupling with the *trans* phosphine ligand, a finding consistent with the solid state structure. The ^{1}H NMR spectrum is diagnostic of an asymmetric complex; four silyl methyl proton, four methylene proton and 11 cyclooctadienyl proton resonances are all observed. The amino proton in **7** is located as a singlet at δ 2.40.

The fact that only one product is formed in this reaction suggests that the addition of CO may occur preferentially with one isomer of **3**. In the molecular structure of **7** it can be seen that the dissociated amine arm of the [NPNH] ligand set is oriented to the opposite face of the metal as the methylene unit that bridges the olefin and allyl donors of the cyclooctadienyl ligand. The amine arm and the CO ligand are positioned to the same face of the metal. This implies that a molecule of CO reacts with the diastereomer *exo*-**3** by displacing the pendant amine arm away from the metal centre. A decrease in the concentration of *exo*-**3** would cause a shift in the equilibrium between these two isomers producing more *exo*-**3**. If the equilibrium shift occurs faster than the reaction of CO with *endo*-**3** then only complex **7** would be generated.

We speculate that the metal centre may be more accessible in *exo*-**3** thereby increasing its reactivity with CO. In the solid-state molecular structure of **7** it can be seen that the dissociated amino side-arm bends away from the ruthenium centre in order to minimize steric interactions with the bound CO ligand. In a similar fashion, the ethylene unit of the cyclooctadienyl ligand (bridging C(28) and C(31)) is oriented away from the metal centre. This is reflected in the longer

References begin on page 98

ruthenium bond distance for C(31) of the olefin donor as compared to atom C(32) (2.407(2) Å vs. 2.334(2) Å). The longer Ru-C distances observed for C(26) and C(27) of the allyl donor are most likely a consequence of their approximately *trans* disposition with the CO ligand, which has a strong *trans* influence. It appears as though the amine side-arm and the ethylene unit "spread-out", thereby opening an otherwise hindered coordination site at the metal centre. If the analogous complex with *endo*-**3** is envisioned, the amine side-arm and the methylene fragment of the cyclooctadienyl ligand would be required to be displaced away from the metal centre. It is possible that the methylene bridge cannot effectively bend away from the metal centre and this causes enough shielding of the metal, not allowing for coordination of a molecule of CO.

Given the distorted trigonal bipyramidal structure of *exo*-**3** one would also expect that its reaction with CO would generate two products since there are two possible sites for attack, namely in the two wide angles of the trigonal plane. Yet, only one species is formed. The stereospecific addition of CO to distorted trigonal bipyramidal d^6 metal complexes, when there are different ligands occupying the equatorial positions, is a common observation.[67] One rationalization that has been given for this behaviour is that the metal LUMO is not equally developed in both wide angles due to the lack of symmetry in the complex.[67] An example of this is illustrated in Figure 2.21 for the complex $Ir(PR_3)_2(H)(Cl)(\eta^1\text{-}C_6H_5)$, in which the addition of CO occurs *trans* to the hydride ligand. By hybridizing away from the weaker donor the LUMO is stabilized by higher empty orbitals.

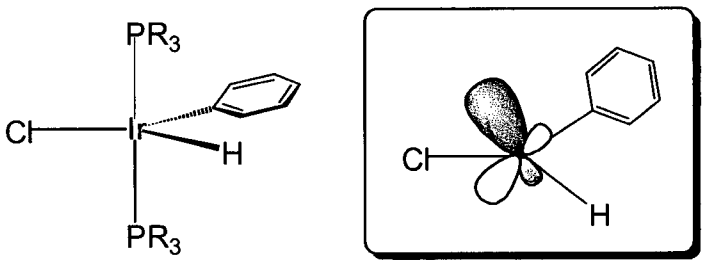

Figure 2.21. A depiction of how the metal LUMO (d_{xy} orbital) in the complex $Ir(PR_3)_2(H)(Cl)(\eta^1\text{-}C_6H_5)$ extends away from the hydride ligand.[67]

References begin on page 98

In *exo*-**3** the allyl moiety occupies the positions subtending the acute angle in the equatorial plane. According to the above explanation the observed stereospecific addition of CO to *exo*-**3** suggests that the two "ends" of the allyl function could have different donor properties so that the metal LUMO is extended preferentially in one direction. The allyl ligand, for instance, may more appropriately be envisioned as an η^2-η^1 donor with localized electron density rather than a symmetrical η^3 function with delocalized electron density when coordinated to the ruthenium centre in **3**. Figure 2.22 shows the bonding combination for the allyl ligand with the metal d_{xy} orbital (the metal orbital with which it has the greatest overlap), which indicates that a nodal plane is present at the central carbon atom, not permitting electron delocalization over all three positions of the allyl ligand. The asymmetry of the allyl ligand could account for the observed stereospecific addition of CO to *exo*-**3**. Theoretical calculations should be performed in order to gain more insights into the electronic structure of **3** in order to verify or discount this hypothesis.

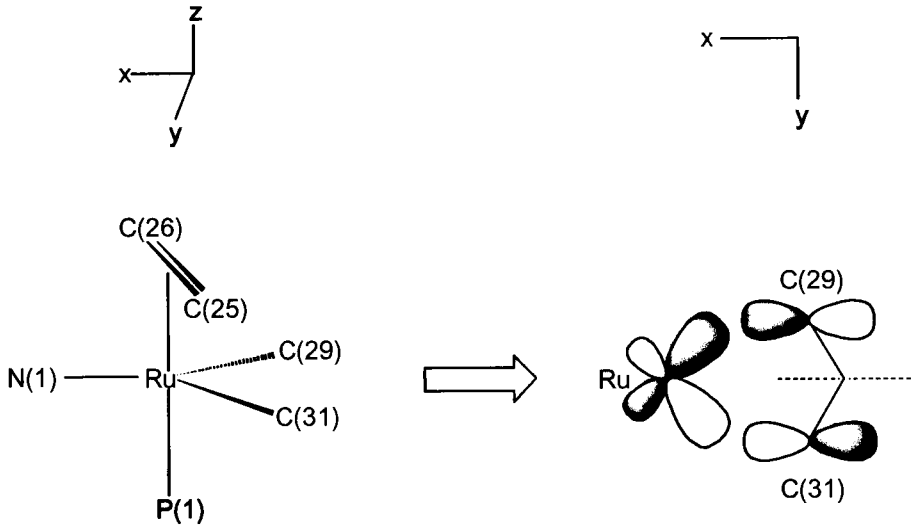

3

Figure 2.22. A schematic representation of the bonding combination between the allyl moiety and the metal d_{xy} orbital in *exo*-**3**.

It would be interesting to scale-up the reaction between complex **3** with one equivalent of CO to examine if similar reactivity occurs on a larger scale. Due to the small surface area of the

References begin on page 98

solution in an NMR tube the observed reactivity may be governed by the rate at which CO can dissolve into the solution.

As shown in Scheme 2.7, the reaction of complex **3** with an excess of CO results in the formation of a ruthenium (0) tetracarbonyl species (**8**) over a period of several hours. Monitoring the reaction by ^{1}H and $^{31}P\{^{1}H\}$ NMR spectroscopy reveals the initial formation of **7**, which reacts slowly with CO to yield **8**. After 30 minutes a solution of the reaction mixture contains complex **7** in *ca.* 90 % yield and complex **8** in *ca.* 10 % yield, as assayed by integration of their ^{31}P NMR signals. After 12 hours complex **8** is the only species remaining in solution. Minor peaks (comprising less than 1 % of the reaction mixture) present during this conversion are most likely due to short-lived intermediates suggesting that initial migratory insertion is the rate limiting step in this process.

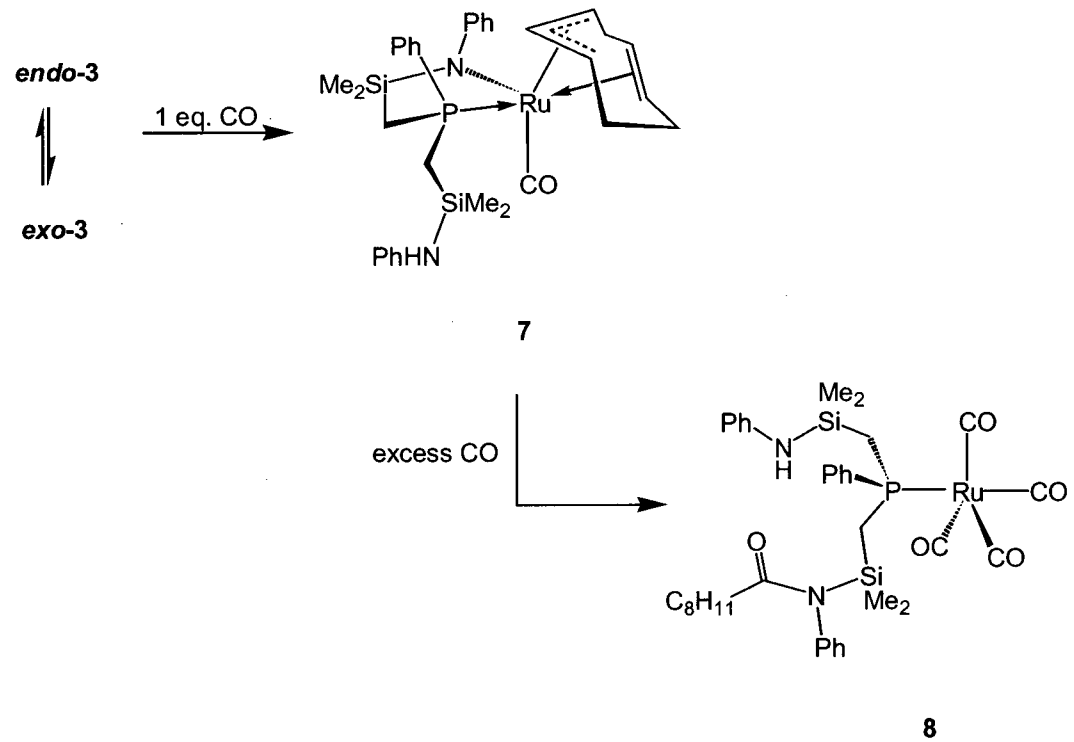

Scheme 2.7

The solid-state molecular structure of **8** as determined by X-ray diffraction is shown in Figure 2.23. Selected bond lengths and angles are highlighted in Table 2.11. The five-coordinate

References begin on page 98

species contains three CO ligands in the plane of a trigonal bipyramidal structure with a fourth CO ligand and the bulky phosphine donor located at the axial coordination sites. Complexes of this type are known, although their preparation usually entails the addition of a phosphine ligand to $[Ru(CO)_5]$.[79] The X-ray structural analysis of the related species $[Ru(CO)_4\{P(OMe)_3\}]$[80] indicates that the ruthenium centre adopts a trigonal bipyramidal geometry with an axial phosphine ligand, similar to that observed in **8**. The bond distances and angles in complex **8** coincide well with those determined in $[Ru(CO)_4\{P(OMe)_3\}]$. The most significant difference between the two complexes is the longer ruthenium-to-phosphorus distance in **8** of 2.3856(7) Å compared to 2.309(2) Å, which can be attributed to the steric bulk of the phosphine ligand in **8**.

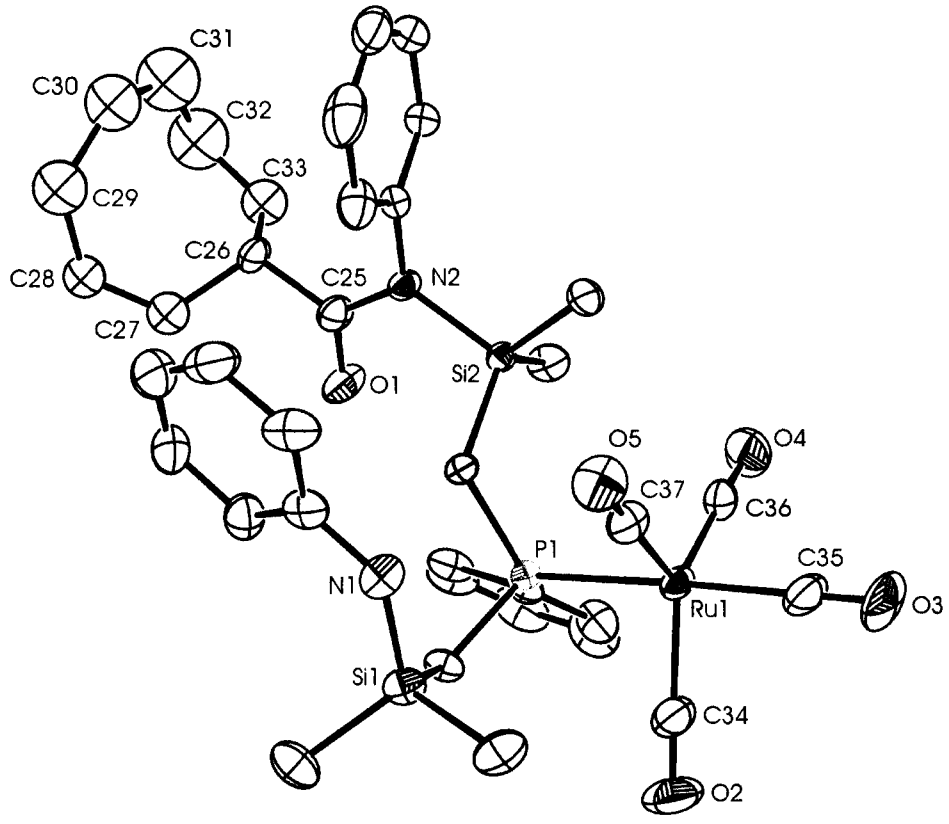

Figure 2.23. ORTEP depiction of the solid-state molecular structure of complex **8** as determined by X-ray diffraction. Thermal ellipsoids are shown at the 50 % probability level.

References begin on page 98

Table 2.11. Selected bond lengths and angles in complex **8**.

Atom	Atom	Distance (Å)	Atom	Atom	Distance (Å)
Ru(1)	P(1)	2.3856(7)	Ru(1)	C(36)	1.929(4)
Ru(1)	C(34)	1.934(3)	Ru(1)	C(37)	1.928(3)
Ru(1)	C(35)	1.917(4)			

Atom	Atom	Atom	Angle (°)	Atom	Atom	Atom	Angle (°)
P(1)	Ru(1)	C(34)	88.67(9)	C(34)	Ru(1)	C(36)	123.35(4)
P(1)	Ru(1)	C(35)	177.78(11)	C(34)	Ru(1)	C(37)	115.47(13)
P(1)	Ru(1)	C(36)	87.49(10)	C(35)	Ru(1)	C(36)	90.34(14)
P(1)	Ru(1)	C(37)	90.45(9)	C(35)	Ru(1)	C(37)	91.09(15)
C(34)	Ru(1)	C(35)	92.12(14)	C(36)	Ru(1)	C(37)	121.07(14)

The room temperature NMR data for complex **8** are indicative of dynamic behaviour for this species in solution. The $^{31}P\{^1H\}$ NMR spectrum, for example, contains a broad resonance at δ 20.7. The ^1H NMR spectrum also consists of broadened resonances. No structural information can be gleaned from this data, although resonances for the silyl methyl, cyclooctadiene, and aromatic environments are all observed. Peaks located between δ 5.2 and δ 5.8 are consistent with a dissociated cyclooctadiene fragment. Five-coordinate, d^8 transition metal complexes are known to exhibit fluxional behaviour.[81] Inter-conversion between square pyramidal and trigonal bipyramidal coordination geometries is possible. As well, the rearrangement of ligands between axial and equatorial positions within a trigonal bipyramidal ground state structure can occur; this can proceed via the Berry mechanism or the "turnstile rotation" mechanism. Further studies are required to unequivocally characterize complex **8**. Low temperature ^1H, $^{31}P\{^1H\}$ and $^{13}C\{^1H\}$ NMR spectroscopy, as well as solution and solid-state infra-red spectroscopy will provide new details into this system. The use of ^{13}C-labelled carbon monoxide will assist in these investigations.

A possible mechanism for the formation of complex **8** could involve initial insertion of CO into the ruthenium-carbon bond of the allyl moiety in complex **7** resulting in a ruthenium-acyl species. In regards to the molecular structure of **7** (Figure 2.20) this insertion step would occur at C(28) (rather than C(26)) due to its nearly *cis*-disposition with the CO ligand. The addition of four equivalents of CO could then displace the olefin donors of the cyclooctadienyl ligand and

References begin on page 98

induce the reductive elimination of the acyl group to the amide nitrogen. This mechanism would yield a 1,4-cyclooctadiene moiety. The cyclooctadiene fragment in the crystal structure was disordered but was successfully modelled as containing both 1,4- and 1,5-cyclooctadiene groups. This suggests that an alternative route for the formation of **8** is also possible. The amido donor in **7** is located *cis* to the CO ligand and so it is likely that initial insertion of CO into the Ru-N bond also takes place. Reductive elimination from C(26) of the allyl function would generate a 1,5-cyclooctadiene fragment. Obviously, more studies are necessary to provide further evidence for either of these postulated pathways. The addition of an equivalent of CO to complex **7** could be a very informative reaction. The use of ^{13}C-enriched carbon monoxide in these studies and homo- and heteronuclear NMR investigations could also be potentially very informative. Similar reactivity was observed in nickel (II) complexes containing the [PNP] ligand set. [82,83]

2.9 Experimental

(i) General Procedures

Unless otherwise stated, all manipulations were performed under a dry, oxygen-free atmosphere of dinitrogen or argon by means of standard Schlenk or glove box techniques (Vacuum Atmospheres HE-553-2 glove box equipped with a MO-40-2H purification system and a -40°C freezer). Toluene and hexanes were purchased in anhydrous form from Aldrich and deoxygenated by passage through a tower containing Q-5 catalyst and further dried by passage through a tower containing alumina under a positive pressure of dinitrogen. Anhydrous THF was pre-dried by refluxing over CaH_2 and then distilled under argon from sodium benzophenone ketyl. Anhydrous diethyl ether was stored over sieves and distilled from sodium benzophenone ketyl under argon. Deuterated benzene, tetrahydrofuran and toluene were dried by refluxing over sodium and potassium alloy in a sealed vessel under partial pressure, then trap-to-trap distilled and degassed by three freeze-pump-thaw cycles prior to use. Nitrogen and argon were dried and deoxygenated by passage through a column containing activated molecular sieves and MnO. Unless otherwise stated, ^1H, $^1H\{^{31}P\}$, ^2H, $^{31}P\{^1H\}$, $^{13}C\{^1H\}$, $^7Li\{^1H\}$ and variable-temperature NMR spectra were recorded on a Bruker AMX-500 instrument operating at 500.1 MHz for ^1H spectra, a Bruker AV-300 instrument (300.1 MHz), or a Bruker AC-200 instrument (200.1 MHz).

References begin on page 98

^1H NMR spectra were referenced to internal C_6D_5H (7.15 ppm) or C_7D_7H (2.09 ppm), $^{31}P\{^1H\}$ NMR spectra to external $P(OMe)_3$ (141.0 ppm with respect to 85% H_3PO_4 at 0.0 ppm), and $^{13}C\{^1H\}$ NMR spectra to $^{13}CC_5D_6$ (128.4 ppm). All δ values are given in ppm units. Infra-red spectra were recorded on an ATI Matton Genesis Series FTIR Spectrometer as KBr pellets. Elemental analyses were performed in the Department of Chemistry at the University of British Columbia by Mr. P. Borda or Mr. M. Lakha. Complexes for which elemental data is not reported were not yet submitted for analysis at the time this thesis was completed.

(ii) Materials

The compounds $[NPN]Li_2{\cdot}(C_4H_8O)_2$,[38] $[P_2N_2]Li_2{\cdot}C_4H_8O_2$,[39] $[RuCl_2(cod)]_x$[84] and $RuCl_2(PPh_3)_3$[85] were prepared according to reported literature procedures. $NEt_3{\cdot}DCl$ was prepared by the dropwise addition of aqueous deuterium chloride to a solution of triethylamine in diethyl ether. The solid was collected by filtration and dried under vacuum. Triphenylphosphine, triisopropylphosphine and tricyclohexylphosphine (Strem Chemicals), $LiN(SiMe_3)_2$, $NaN(SiMe_3)_2$, $NEt_3{\cdot}HCl$, pyridine, CuCl and chlorotrimethylsilane (Aldrich) were used without further purification. $RuCl_3{\cdot}3H_2O$ was obtained on loan from Johnson-Matthey, as well as purchased from Precious Metals Online.

(iii) Synthesis and Reactivity of Complexes

$[P_2N_2]Ru(\eta^2{:}\eta^2\text{-}C_8H_{12})$ (1)

A solution of $[P_2N_2]Li_2{\cdot}C_4H_8O_2$ (0.734 g, 1.16 mmol) in 10 mL of THF was added to a slurry of $[RuCl_2(cod)]_x$ (0.324 g, 1.16 mmol) in 10 mL of THF. The mixture was stirred at room temperature for three hours yielding a yellow-brown solution. The mixture was evaporated to dryness *in vacuo* and the resulting solid was extracted into 20 mL of toluene and filtered through Celite. The solvent was removed until a thick oily residue remained. Addition of hexanes (10 mL) caused a yellow solid to precipitate from the solution. The solid was collected on a frit and washed with hexanes until the dark impurities were removed. The remaining solid was dried under vacuum to yield $[P_2N_2]Ru(\eta^2{:}\eta^2\text{-}C_8H_{12})$ (**1**) (0.628 g, 73 %). X-ray quality crystals were obtained by the slow evaporation of the hexanes rinsings and contained one equivalent of co-

References begin on page 98

crystallized hexane. ^{1}H NMR (C_6D_6, 298 K, 500 MHz): δ 0.40 and 0.50 (s, SiC*H*$_3$, 24H total), δ 0.95 and 1.42 (m (br), P-C*H*$_2$, 8H total), δ 1.82 (m, cyclooctadiene -C*H*$_2$, 8H), δ 2.91 (s (br), cyclooctadiene –C*H*, 4H), δ 7.12 (m, overlapping, PPh-*para*, 1H), δ 7.20 (m, PPh-*meta*, 4H), δ (m, PPh-*ortho*, 4H). ^{31}P{^{1}H} NMR (C_6D_6, 298 K, 202.5 MHz): δ 44.5 (s). ^{13}C{^{1}H} NMR (C_6D_6, 298 K, 125.8 MHz): δ 7.0 and 9.0 (s, Si*C*H$_3$), δ 25.0 (s (br), cyclooctadiene –*C*H$_2$), δ 28.0 (s (br), P-*C*H$_2$), δ 70.0 (s, cyclooctadiene –*C*H), δ 127.5 (s, overlapping, PPh-*para*), δ 128.5 (s, PPh-*meta*), δ 131.0 (s, PPh-*ortho*), δ 143.0 (s (br), PPh-*ipso*). ^{1}H NMR (C_6D_6, 198 K, 500 MHz): δ 0.30 to 0.60 (s, overlapping, SiC*H*$_3$, 24H total), δ 0.90 (s (br), P-C*H*$_2$, 2H), δ 1.30 (s (br), overlapping, P-C*H*$_2$ 2H), δ 1.30 (s (br), overlapping, cyclooctadiene –C*H*$_2$, 2H), δ 1.90 (s, cyclooctadiene –C*H*$_2$, 2H), δ 2.09 (s, cyclooctadiene –C*H*$_2$, 2H), δ 2.20 (s, cyclooctadiene –C*H*$_2$, 2H), δ 2.60 (s (br), cyclooctadiene –C*H*, 2H), δ 3.00 (s (br), cyclooctadiene –C*H*, 2H), δ 6.80 to 7.15 (m, overlapping, PPh-*meta* and *para*, 6H total), δ 7.80 (s (br), PPh-*ortho*, 4H).

[P_2NNH]Ru($C_6H_4PPh_2$) (2)

Toluene (30 mL) was added to a mixture of [P_2N_2]Li_2·$C_4H_8O_2$ (0.170 g, 0.268 mmol) and $RuCl_2(PPh_3)_3$ (0.256 g, 0.267 mmol). The initial slurry was stirred for three hours at room temperature resulting in the formation of an orange-brown coloured solution, which was filtered to remove insoluble LiCl. Anhydrous CuCl (0.054 g, 0.536 mmol) was subsequently added to the solution and the contents stirred for 12 h. The mixture was filtered and the filtrate was evaporated until approximately 2 mL of toluene remained. Addition of pentane (10 mL) caused the deposition of [P_2NNH]Ru($PC_6H_4Ph_2$) (**2**) as an orange solid. The solid was collected by filtration, rinsed with a minimum amount of pentane and dried *in vacuo* to yield 0.207 g of **2** (86 %). Single crystals suitable for an X-ray diffraction study were grown by the slow evaporation of the pentane soluble rinsings. There were two independent molecules in the asymmetric unit as well as a molecule of co-crystallized pentane. NMR (C_6D_6, 298 K, 500 MHz): δ 0.39, 0.41, 0.58 and 0.60 (s, SiC*H*$_3$, 24H total), δ 1.40 (m, overlapping, P-C*H*$_2$, 4H), δ 1.53 (m, overlapping, P-C*H*$_2$, 4H), δ 2.80 (s, N-*H*), δ 6.52 – 8.12 (m, P-*Ph*, [P_2NNH] and $PC_6H_4Ph_2$, 24 H total). ^{31}P{^{1}H} NMR (C_6D_6, 298 K, 202.5 MHz): δ 25.8 (d, $^2J_{PP}$ = 31 Hz, [P_2NNH], 2P), δ -11.8 (t, $^2J_{PP}$ = 31 Hz,

References begin on page 98

$PC_6H_5Ph_2$, 1P). Anal. Calcd. for $C_{42}H_{57}N_2P_3Si_4Ru$: C, 56.28; H, 6.41; N 3.13. Found: C, 56.11; H, 6.58; N, 3.29.

*For complexes **3** through **6** the following labelling convention is employed for assignment of the ^1H and ^{13}C nuclei of the cyclooctadienyl moiety:*

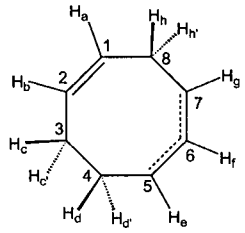

endo- and *exo*-[NPNH]Ru(1-3-η^3-5,6-η^2-C_8H_{11}) (*endo*-**3** and *exo*-**3**)

Toluene (30 mL) was added to a mixture of [NPN]Li_2·$(C_4H_8O)_2$ (1.06 g, 1.78 mmol) and $[RuCl_2(cod)]_x$ (0.50 g, 1.78 mmol) and the mixture was stirred for two days at room temperature. During this time the initial brown slurry turned red and a colourless solid formed. The mixture was then filtered through Celite and the solvent removed under reduced pressure leaving an oily solid. A small amount of hexanes (*ca.* 5 mL) was added to dissolve the solid and the mixture was allowed to stand in a closed vessel for 48 hours during which time complex **3** crystallizes from solution. The supernatant was decanted and the red crystals were washed with hexanes. Yield: 0.90 g, 78 %. A further crop of crystals was obtained by the slow evaporation of the supernatant. Isomer *endo*-**3**: ^1H NMR (C_7D_8, 245 K, 500 MHz): δ 0.08 (s, br, SiCH_3, 6H), δ 0.34 (s, SiCH_3, 3H), δ 0.43 (s, SiCH_3, 3H), δ 0.76 (m, AA'BX, PCHH, 1H), δ 1.0 (m, AA'BX, PCH_2, 2H), δ 1.17 (m, AA'BX, PCHH, 1H), δ 1.50 (m, $CH_dH_{d'}$, 1H), δ 1.58 (m, $CH_cH_{c'}$, 1H), δ 1.64 (m, CH_f, 1H), δ 2.00 (m, C$H H_{h'}$, 1H), δ 2.18 (m, $CH_dH_{d'}$, 1H), δ 2.36 (m, $CH_cH_{c'}$, 1H), δ 2.70 (m, $CH_hH_{h'}$, 1H), δ 2.85 (m, CH_g, 1H), δ 4.20 (m, CH_e, 1H), δ 4.23 (m, CH_a, 1H), δ 4.25 (m, CH_b, 1H), δ 6.63 (s, NH, 1H), δ 6.82 – 7.42 (m, overlapping, NPh, NHPh and PPh,). $^{31}P\{^1H\}$ NMR (C_7D_8, 245 K, 202.5 MHz): δ 33.4 (s). $^{13}C\{^1H\}$ NMR (C_7D_8, 245 K, 125.8 MHz) selected peaks: δ 25.2 (s, C_8,), δ 30.3 (s, C_3), δ 32.8 (s, C_4), δ 35.6 (s, C_7), δ 61.4 (d, C_1, $^2J_{PC}$ = 6.5 Hz), δ 61.6 (s, C_5), δ 71.6 (s, C_6), δ 108.1 (d, C_2, $^2J_{PC}$ = 10.5 Hz). Isomer *exo*-**3**: ^1H NMR (C_7D_8, 245 K, 500 MHz): δ 0.09 (s,

References begin on page 98

overlapping, SiCH_3, 3H), δ 0.28 (s, SiCH_3, 3H), δ 0.32 (s, overlapping, SiCH_3, 6H), δ 0.85 (m, overlapping, AA'BX, PCH_2, 2H), δ 1.0 (m, overlapping, AA'BX, PCH_2, 2H), δ 1.30 (m, $CH_cH_{c'}$, 1H), δ 1.50 (m, overlapping, CH_f, 1H), δ 1.75 (m, $CH_dH_{d'}$, 1H), δ 1.83 (m, $CH_cH_{c'}$, 1H), δ 2.15 (m, overlapping, $CH_hH_{h'}$, 1H), δ 2.20 (m, $CH_dH_{d'}$, 1H), δ 3.09 (m, $CH_hH_{h'}$, 1H), δ 3.37 (m, CH_g, 1H), δ 3.50 (m, CH_e, 1H), δ 3.92 (m, CH_b, 1H), δ 4.68 (m, CH_a, 1H), δ 6.35 (s, NH, 1H), δ 6.82 – 7.42 (m, overlapping, NPh, NHPh and PPh). $^3J_{ab}$ = 7.80 Hz, $^3J_{ah}$ = 7.70 Hz, $^3J_{ah'}$ = 7.30 Hz, $^3J_{bc}$ = 6.20 Hz, $^3J_{bc'}$ = 6.10 Hz, $^2J_{cc'}$ = 14.60 Hz, $^3J_{cd}$ = 7.60 Hz, $^3J_{cd'}$ = 6.00 Hz, $^3J_{c'd}$ = 7.20 Hz, $^3J_{c'd'}$ = 8.60 Hz, $^2J_{dd'}$ = 17.0 Hz, $^3J_{de}$ = 5.60 Hz, $^3J_{d'e}$ = 5.80 Hz, $^3J_{ef}$ = 8.00 Hz, $^3J_{fg}$ = 9.90 Hz, $^3J_{gh}$ = 7.90 Hz, $^3J_{gh'}$ = 4.20 Hz, $^2J_{hh'}$ = 19.30 Hz. $^{31}P\{^1H\}$ NMR (C_7D_8, 245 K, 202.5 MHz): δ 32.9 (s). $^{13}C\{^1H\}$ NMR (C_7D_8, 245 K, 125.8 MHz) selected peaks: δ 26.6 (s, C_8,), δ 27.0 (s, C_3), δ 36.3 (s, C_4), δ 36.5 (s, C_7), δ 64.9 (s, C_5), δ 65.3 (d, C_1, $^2J_{PC}$ = 5.8 Hz), δ 70.8 (s, C_6), δ 110.0 (d, C_2, $^2J_{PC}$ = 11.3 Hz). Infra-red (KBr): ν(NH) at 2945 cm^{-1} and 2906 cm^{-1}. Anal. Calcd. for $C_{32}H_{43}N_2PRuSi_2$: C, 59.69; H, 6.73; N, 4.35. Found: C, 59.68; H, 7.09; N, 4.35.

Addition of neutral donor ligands to a mixture of *endo*-3 and *exo*-3

In an NMR tube complex **3** (0.040 g, 0.062 mmol) was dissolved in benzene-d_6 (~ 1 mL). To the resulting red solution a ten-fold excess of triphenylphosphine (0.163 g, 0.621 mmol) was added. Monitoring the reaction mixture by ^1H and $^{31}P\{^1H\}$ NMR spectroscopy over a time period of 24 hours revealed the presence of unreacted **3** and free PPh_3. A similar procedure was employed for the following donor ligands: THF (0.045 g, 0.621 mmol), pyridine (0.049 g, 0.621 mmol), tricyclohexylphosphine (0.174 g, 0.621 mmol) and triisopropylphosphine (0.107 g, 0.621 mmol). In all cases the NMR data indicated that no reaction had taken place.

{[NPN]Ru(1-3-η^3-5,6-η^2-C_8H_{11})}{Li·THF} (4)

A solution of $LiN(SiMe_3)_2$ (0.064 g, 0.384 mmol) in toluene (10 mL) was added dropwise to a toluene solution of **3** (0.247 g, 0.384 mmol) (20 mL) and the mixture was stirred at room temperature for three hours during which time an orange solid precipitated from the solution. The solvent was removed under reduced pressure until half volume and hexanes (20 mL) was added to

References begin on page 98

ensure complete precipitation. The orange solid is insoluble in aromatic solvents. THF was added to a mixture of the orange solid in toluene until it completely dissolved. Removal of the volatiles *in vacuo* and addition of hexanes caused the deposition of **3** as an orange micro-crystalline solid. The solid was filtered, washed with hexanes and dried under vacuum. Yield: 0.255 g, 92 %. X-ray quality crystals were grown by the slow evaporation of a saturated toluene solution. ^{1}H NMR (C_6D_6, 298 K, 500 MHz): δ 0.10, 0.20, 0.35 and 0.50 (s, SiC*H*$_3$, 12 total), δ 1.00 (m, AA'BX, PC*H*H, 1H), 1.07 (m, CH$_c$*H*$_{c'}$, 1H), δ 1.14 (m, overlapping, OCH$_2$C*H*$_2$, 2H), δ 1.18 (m, overlapping, C*H*$_c$H$_{c'}$, 1H), δ 1.33 (m, CH$_d$*H*$_{d'}$, 1H), δ 1.44 (m, AA'BX, PCH*H*, 1H), δ 1.65 (m, AA'BX, PC*H*H, 1H), δ 1.73 (m, overlapping, AA'BX, PCH*H*, 1H), δ 1.76 (m, C*H*$_d$H$_{d'}$, 1H), δ 2.17 (m, C*H*$_a$, 1H), δ 2.29 (m, C*H*$_b$, 1H), δ 2.50 (m, CH*H*$_{h'}$, 1H), δ 3.06 (m, overlapping, OC*H*$_2$CH$_2$, 2H), δ 3.10 (m, overlapping, C*H*$_e$, 1H), δ 3.45 (m, overlapping, C*H*$_h$H$_{h'}$, 1H), δ 3.45 (m, overlapping, C*H*$_f$, 1H), δ 4.35 (m, C*H*$_g$, 1H), δ 6.58 (t, NPh-*para*, 1H), δ 6.78 (t, N'Ph-*para*, 1H), δ 7.70 (m, NPh-*meta*, 2H), δ 7.20 (m, overlapping, NPh-*ortho*, 2H), δ 7.20 (m, overlapping, PPh-*para*, 1H), δ 7.39 (m, N'Ph-*meta*, 2H), δ 8.05 (m, AX, PPh-*ortho*, 2H), δ 8.30 (d, N'Ph-*ortho*, 2H). ^{31}P{^{1}H} NMR (C_6D_6, 298 K, 202.5 MHz): δ 46.8 (s). ^{13}C{^{1}H} NMR (C_7D_8, 298 K, 125.8 MHz) selected data: δ 22.7 (s, C_8), δ 27.7 (s, C_4), δ 27.9 (s, C_3), δ 33.2 (d, C_1, $^2J_{PC}$ = 6.4 Hz), δ 45.0 (d, C_7, $^2J_{PC}$ = 19.2 Hz), δ 46.0 (d, C_5, $^2J_{PC}$ = 2.1 Hz), δ 68.2 (d, C_2, $^2J_{PC}$ = 5.8 Hz), δ 100.5 (s, C_6).

{[NPN]Ru(1-3-η^3-5,6-η^2-C_8H_{11})}{Na·THF} (5)

Complex **5** is prepared in a similar fashion as **4**. (0.054 g, 0.294 mmol) of NaN(SiMe$_3$)$_2$ and (0.189 g, 0.294 mmol) of **3** were employed. Yield: 0.193 g, 89 %. X-ray quality crystals were grown from a saturated toluene solution at –40 °C. ^{1}H NMR (C_6D_6, 298 K, 500 MHz): δ 0.10, 0.20, 0.35 and 0.50 (s, SiC*H*$_3$, 12 total), δ 1.00 (m, AA'BX, PC*H*H, 1H), 1.07 (m, CH$_c$*H*$_{c'}$, 1H), δ 1.14 (m, overlapping, OCH$_2$C*H*$_2$, 2H), δ 1.18 (m, overlapping, C*H*$_c$H$_{c'}$, 1H), δ 1.33 (m, CH$_d$*H*$_{d'}$, 1H), δ 1.44 (m, AA'BX, PCH*H*, 1H), δ 1.65 (m, AA'BX, PC*H*H, 1H), δ 1.73 (m, overlapping, AA'BX, PCH*H*, 1H), δ 1.76 (m, C*H*$_d$H$_{d'}$, 1H), δ 2.17 (m, C*H*$_a$, 1H), δ 2.29 (m, C*H*$_b$, 1H), δ 2.50 (m, CH*H*$_{h'}$, 1H), δ 3.06 (m, overlapping, OC*H*$_2$CH$_2$, 2H), δ 3.10 (m, overlapping, C*H*$_e$, 1H), δ 3.45 (m, overlapping, C*H*$_h$H$_{h'}$, 1H), δ 3.45 (m, overlapping, C*H*$_f$, 1H), δ 4.35 (m, C*H*$_g$, 1H),

References begin on page 98

δ 6.58 (t, NPh-*para*, 1H), δ 6.78 (t, N'Ph-*para*, 1H), δ 7.70 (m, NPh-*meta*, 2H), δ 7.20 (m, overlapping, NPh-*ortho*, 2H), δ 7.20 (m, overlapping, PPh-*para*, 1H), δ 7.39 (m, N'Ph-*meta*, 2H), δ 8.05 (m, AX, PPh-*ortho*, 2H), δ 8.30 (d, N'Ph-*ortho*, 2H). $^{31}P\{^1H\}$ NMR (C_6D_6, 298 K, 202.5 MHz): δ 46.8 (s). $^{13}C\{^1H\}$ NMR (C_7D_8, 298 K, 125.8 MHz) selected data: δ 22.7 (s, C_8), δ 27.7 (s, C_4), δ 27.9 (s, C_3), δ 33.2 (d, C_1, $^2J_{PC}$ = 6.4 Hz), δ 45.0 (d, C_7, $^2J_{PC}$ = 19.2 Hz), δ 46.0 (d, C_5, $^2J_{PC}$ = 2.1 Hz), δ 68.2 (d, C_2, $^2J_{PC}$ = 5.8 Hz), δ 100.5 (s, C_6).

Reaction of complex 4 with NEt_3·HCl

Addition of NEt_3·HCl (0.015 g, 0.109 mmol) to a solution of **4** (0.078 g, 0.108 mol) in toluene (10 mL) resulted in a change in colour from orange to red within two hours. The mixture was filtered to remove insoluble LiCl and the volatile components were removed under vacuum giving a red solid. The ^1H and $^{31}P\{^1H\}$ NMR spectra of the red solid indicate that it is a mixture of the two diastereomers *endo*-**3** and *exo*-**3**.

Reaction of complex 4 with NEt_3·DCl

A similar procedure to that described above for the reaction with NEt_3·HCl was followed: NEt_3·DCl (0.017 g, 0.123 mmol), **4** (0.086 g, 0.119 mmol) and toluene (10 mL). The ^1H and $^{31}P\{^1H\}$ NMR spectra indicate the formation of an equilibrium mixture of *endo*-**3**-d_1 and *exo*-**3**-d_1 in which deuteration at the amino site occurs.

endo- and *exo*-[NPN($SiMe_3$)]Ru(1-3-η^3-5,6-η^2-C_8H_{11}) (*endo*-**6** and *exo*-**6**)

A ten-fold excess of chlorotrimethylsilane (0.292 g, 2.69 mmol) was added to an orange solution of **4** (0.194 g, 0.269 mmol) in toluene (30 mL). Over the period of 48 hours the solution turns red with the formation of a white solid (LiCl). The solvent and other volatiles were removed *in vacuo*. Toluene was added to the remaining solid and the mixture was filtered to remove insoluble by-products. The soluble fraction was dried under vacuum to give a mixture of *endo*-**6**

References begin on page 98

and *exo*-**6** as a red solid material (0.17 g, 88 %). Attempts to separate the two isomers by rinsing with hexanes or pentane proved unsuccessful. Isomer *endo*-**6**: ^{1}H NMR (C_6D_6, 298 K, 500 MHz): δ 0.12 (s, overlapping, SiC*H*$_3$, 3H), δ 0.15 (s, overlapping, terminal N-SiC*H*$_3$), δ 0.18 (s, overlapping, SiC*H*$_3$), δ 0.33 (s, SiC*H*$_3$, 3H), δ 0.46 (s, SiC*H*$_3$, 3H), δ 1.00 to 1.50 (m, overlapping, P-C*H*$_2$), δ 1.47 (m, CH$_c$*H*$_{c'}$, 1H), δ 1.52 (m, C*H*$_f$, 1H), δ 1.85 (m, CH$_d$*H*$_{d'}$, 1H), δ 2.05 (m, CH*H*$_{h'}$, 1H), δ 2.10 (m, C*H*$_c$H$_{c'}$, 1H), δ 2.25 (m, C*H*$_d$H$_{d'}$, 1H), δ 2.77 (m, C*H*$_h$H$_{h'}$, 1H), δ 2.90 (m, C*H*$_g$, 1H), δ 4.00 (m, C*H*$_b$, 1H), δ 4.16 (m, C*H*$_e$, 1H), δ 4.25 (m, C*H*$_a$, 1H), δ 6.80 – 7.45 (m, overlapping, N*Ph*, NH*Ph* and P*Ph*). ^{31}P{^{1}H} NMR (C_7D_8, 298 K, 202.5 MHz): δ 32.9 (s). ^{13}C{^{1}H} NMR (C_7D_8, 298 K, 125.8 MHz) selected peaks: δ 25.5 (s, $C_{8,}$), δ 28.5 (s, C_3), δ 35.0 (s, C_4), δ 35.6 (s, C_7), δ 61.6 (d, C_1, $^2J_{PC}$ = 6.3 Hz), δ 61.8 (s, C_5), δ 70.1 (s, C_6), δ 107.6 (d, C_2, $^2J_{PC}$ = 10.6 Hz). Isomer *exo*-**6**: ^{1}H NMR (C_7D_8, 298 K, 500 MHz): δ 0.12 (s, overlapping, terminal N-SiC*H*$_3$), δ 0.13 (s, overlapping, SiC*H*$_3$, 3H), δ 0.16 (s, overlapping, SiC*H*$_3$), δ 0.57 (s, SiC*H*$_3$, 3H), δ 0.60 (s, SiC*H*$_3$, 3H), δ 1.00 to 1.50 (m, overlapping, P-C*H*$_2$), δ 1.43 (m, overlapping, C*H*$_f$, 1H), δ 1.45 (m, CH$_c$*H*$_{c'}$, 1H), δ 1.75 (m, CH$_d$*H*$_{d'}$, 1H), δ 2.08 (m, C*H*$_c$H$_{c'}$, 1H), δ 2.12 (m, C*H*$_d$H$_{d'}$, 1H), δ 2.20 (m, overlapping, CH$_h$*H*$_{h'}$, 1H), δ 2.95 (m, C*H*$_h$H$_{h'}$, 1H), δ 3.27 (m, C*H*$_g$, 1H), δ 3.60 (m, C*H*$_e$, 1H), δ 3.87 (m, C*H*$_b$, 1H), δ 4.50 (m, C*H*$_a$, 1H), δ 6.80 – 7.45 (m, overlapping, N*Ph*, NH*Ph* and P*Ph*). ^{31}P{^{1}H} NMR (C_7D_8, 298 K, 202.5 MHz): δ 32.3 (s). ^{13}C{^{1}H} NMR (C_7D_8, 298 K, 125.8 MHz) selected peaks: δ 26.5 (s, $C_{8,}$), δ 26.9 (s, C_3), δ 36.2 (s, C_7), δ 36.9 (s, C_4), δ 62.9 (d, C_1, $^2J_{PC}$ = 5.9 Hz), δ 63.7 (s, C_5), δ 69.9 (s, C_6), δ 108.1 (d, C_2, $^2J_{PC}$ = 11.6 Hz).

Reaction of [NPN]Li_2·$(C_4H_8O)_2$ with $RuCl_2(PPh_3)_3$

A colourless solution of [NPN]Li_2·$(C_4H_8O)_2$ (0.412 g, 0.695 mol) in 25 mL of toluene was added to a brown slurry of $RuCl_2(PPh_3)_3$ (0.665 g, 0.695 mol) in 25 mL of toluene. After several hours the solution gradually turns orange with the formation of a light coloured precipitate. The solid was removed by filtration and the solvent was removed under reduced pressure giving an orange coloured solid. ^{1}H and ^{31}P{^{1}H} NMR spectroscopy of the crude solid revealed that numerous products had been produced.

References begin on page 98

[NPNH]Ru(1-3-η^3:5,6-η^2-C_8H_{11})(CO) (7)

In a J-Young valve NMR tube (with a pre-determined volume of 3.17 mL) was added complex **3** (0.049 g, 0.078 mmol), which was dissolved by adding 1.28 mL of toluene-d_8. The contents of the NMR tube were degassed by performing three freeze-pump-thaw cycles and the NMR tube was then back-filled with CO gas (1.89 mL, 0.078 mmol). Within a few seconds of rotating the NMR tube the colour of the solution changed from red to yellow. The NMR data indicated the presence of a single product characterized as [NPNH]Ru(1-3-η^3:5,6-η^2-C_8H_{11})(CO) (**7**). ^{1}H NMR (C_7D_8, 298 K, 500 MHz): δ -0.15, 0.02, 0.47 and 0.56 (s, SiC*H*$_3$, 12H total), δ 0.98 (m, PC*H*$_2$, 1H), δ 1.41 (m, overlapping, PC*H*$_2$, 1H), δ 1.45 (m, overlapping, CH$_d$*H*$_{d'}$, 1H), δ 1.61 (m, C*H*$_d$H$_{d'}$, 1H), δ 1.80 (m, CH$_c$*H*$_{c'}$, 1H), δ 1.89 and 2.14 (m, PC*H*$_2$, 2H), δ 2.29 (m, C*H*$_c$H$_{c'}$, 1H), δ 2.40 (s, N-*H*, 1H), δ 2.62 (m, overlapping, C*H*$_e$, 1H), δ 2.72 (m, overlapping, CH$_h$*H*$_{h'}$, 1H), δ 2.76 (m, overlapping, C*H*$_h$H$_{h'}$, 1H), δ 3.14 (m, C*H*$_g$, 1H), δ 3.23 (m, C*H*$_a$, 1H), δ 3.41 (m, C*H*$_f$, 1H), δ 5.26 (m, C*H*$_b$, 1H), δ 6.21 - 7.36 (m, overlapping, N*Ph*, NH*Ph* and P*Ph*). ^{31}P{^{1}H} NMR (C_7D_8, 298 K, 202.5 MHz): δ 46.0 (s). ^{13}C{^{1}H} NMR (C_7D_8, 298 K, 125.8 MHz) selected peaks: δ 21.3 (s, C_8), δ 27.3 (s, C_4), δ 32.5 (s, C_3), δ 43.9 (s, C_7), δ 53.9 (s, C_5), δ 69.9 (d, C_1, $^2J_{PC}$ = 6.72 Hz), δ 101.0 (s, C_6), δ 105.1 (d, C_2, $^2J_{PC}$ = 7.63 Hz).

{[PhN(H)SiMe$_2$CH$_2$][(C_8H_{11})C(O)N(Ph)SiMe$_2$CH$_2$][Ph]}PRu(CO)$_4$ (8)

A solution of **3** (0.380 g, 0.586 mmol) in 20 mL toluene was added to a glass reaction vessel equipped with a Teflon valve and a ground glass joint. The vessel was evacuated by three freeze-pump-thaw cycles and then one atmosphere of CO gas was added at room temperature. The colour of the solution immediately changed in colour from red to yellow-orange. The vessel was sealed and the contents were stirred for 12 hours. The solvent and excess CO gas were removed under reduced pressure until an orange solid remained. This solid was rinsed with hexanes, collected and dried under vacuum to give complex **8** (0.383 g, 83 %). ^{1}H NMR (C_6D_6, 298 K, 500 MHz): δ 0.0 - 0.6 (s, br, overlapping, SiC*H*$_3$), δ 1.4 - 2.0 (m, overlapping, PC*H*$_2$), δ 2.2 - 4.0 (m, br overlapping, cyclooctadienyl C*H*$_2$), δ 5.2 - 5.8 (m, br, cyclooctadienyl CH$_2$=CH$_2$),

References begin on page 98

δ 6.4 - 8.6 (m, br, overlapping, aromatic-*H*). $^{31}P\{^1H\}$ NMR (C_6D_6, 298 K, 202.5 MHz): δ 20.7 (s, br).

X-ray Crystallographic Analyses of Complexes 1, 2, *endo*-3, 4, 5, 7 and 8

Selected crystallographic data and structure refinement data are provided in Appendix 1.

2.10 References

(1) Noyori, R.; Ohkuma, T. *Angew. Chem. Int. Ed.* **2001**, *40*, 40.

(2) Abdur-Rashid, K.; Lough, A. J.; Morris, R. H. *Organometallics* **2001**, *20*, 1047.

(3) Abdur-Rashid, K.; Lough, A. J.; Morris, R. H. *Organometallics* **2000**, *19*, 2655.

(4) Ohkuma, T.; Ishii, D.; Takeno, H.; Noyori, R. *J. Am. Chem. Soc.* **2000**, *122*, 6510.

(5) Mikami, K.; Korenaga, T.; Terada, M.; Ohkuma, T.; Pham, T.; Noyori, R. *Angew. Chem. Int. Ed.* **1999**, *38*, 495.

(6) Ohkuma, T.; Koizumi, M.; Doucet, H.; Pham, T.; Kozawa, M.; Kunihiko, M.; Katayama, E.; Yokozawa, T.; Ikariya, T.; Noyori, R. *J. Am. Chem. Soc.* **1998**, *120*, 13529.

(7) Doucet, H.; Ohkuma, T.; Murata, K.; Yokozawa, T.; Kozawa, M.; Katayama, E.; England, A. F.; Ikariya, T.; Noyori, R. *Angew. Chem. Int. Ed.* **1998**, *37*, 1703.

(8) Ohkuma, T.; Doucet, H.; Pham, T.; Mikami, K.; Korenaga, T.; Terada, M.; Noyori, R. *J. Am. Chem. Soc.* **1998**, *120*, 1086.

(9) Ohkuma, T.; Ooka, H.; Hashiguchi, S.; Ikariya, T.; Noyori, R. *J. Am. Chem. Soc.* **1995**, *117*, 2675.

References begin on page 98

(10) Ohkuma, T.; Koizumi, M.; Muniz, K.; Hilt, G.; Kabuto, C.; Noyori, R. *J. Am. Chem. Soc.* **2002**, *124*, 6508.

(11) Ohkuma, T.; Ooka, H.; Ikariya, T.; Noyori, R. *J. Am. Chem. Soc.* **1995**, *117*, 10417.

(12) Xiao, D.; Zhang, X. *Angew. Chem. Int. Ed.* **2001**, *40*, 3425.

(13) Kobayashi, S.; Haruro, I. *Chem. Rev.* **1999**, *99*, 1069.

(14) Kainz, S.; Brinkman, A.; Leitner, W.; Pfaltz, A. *J. Am. Chem. Soc.* **1999**, *121*, 6421.

(15) Tararov, V. I.; Kadyrov, R.; Riermeier, T. H.; Holz, J.; Borner, A. *Tetrahedron: Asymmetry* **1999**, *10*, 4009.

(16) Mao, J.; Baker, D. C. *Org. Lett.* **1999**, *1*, 841.

(17) James, B. R. *Catalysis Today* **1997**, *37*, 209.

(18) Sablong, R.; Osborn, J. A. *Tetrahedron Letters* **1996**, *37*, 4937.

(19) Sablong, R.; Osborn, J. A. *Tetrahedron: Asymmetry* **1996**, *7*, 3059.

(20) Sablong, R.; Osborn, J. A.; Faller, J. W. *J. Organomet. Chem.* **1997**, *527*, 65.

(21) Uematsu, N.; Fujii, A.; Hashiguchi, S.; Ikariya, T.; Noyori, R. *J. Am. Chem. Soc.* **1996**, *118*, 4916.

(22) Fogg, D. E.; James, B. R. *Inorganica Chimica Acta* **1994**, *222*, 85.

(23) Willoughby, C. A.; Buchwald, S. L. *J. Am. Chem. Soc.* **1994**, *116*, 11703.

(24) Willoughby, C. A.; Buchwald, S. L. *J. Am. Chem. Soc.* **1994**, *116*, 8952.

References begin on page 98

(25) Willoughby, C. A.; Buchwald, S. L. *J. Am. Chem. Soc.* **1992**, *114*, 7562.

(26) Lensink, C.; de Vries, J. G. *Tetrahedron: Asymmetry* **1992**, *3*, 235.

(27) Buriak, J. M.; Osborn, J. A. *Organometallics* **1996**, *15*, 3161.

(28) Burk, M. J. *J. Am. Chem. Soc.* **1992**, *114*, 6266.

(29) Noyori, R. *Angew. Chem. Int. Ed.* **2002**, *41*, 2008.

(30) Knowles, W. S. *Angew. Chem. Int. Ed.* **2002**, *41*, 1998.

(31) Sharpless, K. B. *Angew. Chem. Int. Ed.* **2002**, *41*, 2024.

(32) Noyori, R.; Yamakawa, M.; Hashiguchi, S. *J. Org. Chem.* **2001**, *66*, 7931.

(33) Abdur-Rashid, K.; Faatz, M.; Lough, A. J.; Morris, R. H. *J. Am. Chem. Soc.* **2001**, *123*, 7473.

(34) Hartmann, R.; Chen, P. *Angew. Chem. Int. Ed.* **2001**, *40*, 3581.

(35) Yamakawa, M.; H., I.; Noyori, R. *J. Am. Chem. Soc.* **2000**, *122*, 1466.

(36) Fryzuk, M. D.; Montgomery, C. D.; Rettig, S. J. *Organometallics* **1991**, *121*, 155.

(37) Fryzuk, M. D.; MacNeil, P. A.; Rettig, S. J. *Organometallics* **1986**, *5*, 2469.

(38) Fryzuk, M. D.; Johnson, S. A.; Patrick, B. O.; Albinati, A.; Mason, S. A.; Koetzle, T. K. *J. Am. Chem. Soc.* **2001**, *123*, 3960.

(39) Fryzuk, M. D.; Love, J. B.; Rettig, S. J. *Chem. Commun.* **1996**, 2783.

References begin on page 98

(40) Giesbrecht, G. R. *Amidophosphine Complexes of Electron Poor Metals*; University of British Columbia: Vancouver, 1998.

(41) Fryzuk, M. D.; Love, J. B.; Rettig, S. J. *Organometallics* **1998**, *17*, 846.

(42) Corkin, J. R. *Hafnium Complexes Stabilized by a Macrocyclic Ligand*; University of British Columbia: Vancouver, 2000.

(43) Leznoff, D. B. *Paramagnetic Organometallic Complexes*; University of British Columbia: Vancouver, 1997.

(44) Johnson, S. A. *Ligand Design and The Synthesis of Reactive Organometallic Complexes of Tantalum for Dinitrogen Activation*; University of British Columbia: Vancouver, 2000.

(45) Kozak, C. M. *Activation of Small Molecules by Low Valent Niobium Complexes Stabilized by a Bis(Amidophosphine) Macrocycle*; University of British Columbia: Vancouver, 2002.

(46) James, B. R.; Markham, L. D.; Wang, D. K. W. *Chem. Commun.* **1974**, 439.

(47) McKinney, R. J.; Knobler, C. B.; Huie, B. T.; Kaesz, H. D. *J. Am. Chem. Soc.* **1977**, *99*, 2988.

(48) Perego, G.; Del Piero, G.; Cesari, M.; Clerici, M. G.; Perrotti, E. *J. Organomet. Chem.* **1973**, *54*, C51.

(49) Cotton, F. A.; Wilkinson, G. *Advanced Inorganic Chemistry: A Comprehensive Text*; 4th ed.; John Wiley and Sons Inc.: New York, 1980, pp 804-805.

(50) Cole-Hamilton, D. J.; Wilkinson, G. *J. Chem. Soc., Dalton Trans.* **1977**, 797.

(51) Fryzuk, M. D.; Montgomery, C. D.; Rettig, S. J. *Organometallics* **1991**, *10*, 467.

References begin on page 98

(52) Hoffman, P. R.; Caulton, K. G. *J. Am. Chem. Soc.* **1975**, *97*, 4221.

(53) La Placa, S. J.; Ibers, J. A. *Inorg. Chem.* **1965**, *4*, 778.

(54) Cotton, F. A.; Wilkinson, G.; Murillo, C. A.; Bochmann, M. *Advanced Inorganic Chemistry: A Comprehensive Text*; 6th Ed.; John Wiley and Sons Inc.: Toronto, 1999, pp 29-30.

(55) Pez, G. P.; Grey, R. A.; Corsi, J. *J. Am. Chem. Soc.* **1981**, *103*, 7528.

(56) Cotton, F. A.; Wilkinson, G. *Advanced Inorganic Chemistry: A Comprehensive Text*; 4th Ed.; John Wiley and Sons Inc.: New York, 1980, pp 1199-1202.

(57) Fryzuk, M. D.; MacNeil, P. A.; Rettig, S. J. *J. Am. Chem. Soc.* **1987**, *109*, 2803.

(58) Joesten, M. D.; Schaad, L. J. *Hydrogen Bonding*; Marcel Dekker, Inc.: New York, 1974.

(59) Ashworth, T. V.; Nolte, M. J.; Reimann, R. H.; Singleton, E. *Chem. Commun.* **1977**, 937.

(60) Ashworth, T. V.; Chalmers, A. A.; Liles, D. C.; Meintjies, E.; Singleton, E. *Organometallics* **1987**, *6*, 1543.

(61) Wiles, J. A.; Lee, C. E.; McDonald, R.; Bergens, S. H. *Organometallics* **1996**, *15*, 3782.

(62) Lappert, M. F.; Power, P. P.; Sanger, A. R.; Srivastava, R. C. *Metal and Metalloid Amides*; John Wiley and Sons Canada Limited: Toronto, 1980.

(63) Fryzuk, M. D.; Montgomery, C. D. *Coord. Chem. Rev.* **1989**, *95*, 1.

(64) Hartwig, J. F.; Andersen, R. A.; Bergman, R. H. *Organometallics* **1991**, *10*, 1875.

(65) Boncella, J. M.; Eve, T. M.; RickMan, B.; Abboud, K. A. *Polyhedron* **1998**, *17*, 725.

References begin on page 98

(66) Jayaprakash, K. N.; Gunnoe, T. B.; Boyle, P. D. *Inorg. Chem.* **2001**, *40*, 6481.

(67) Rachidi, I. E. I.; Eisentstein, O.; Jean, Y. *New. J. Chem.* **1990**, *14*, 671.

(68) Riehl, J. F.; Jean, Y.; Eisenstein, O.; Pelissier, M. *Organometallics* **1992**, *11*, 729.

(69) Johnson, T. J.; Folting, K.; Streib, W. E.; Martin, J. D.; Huffman, J. C.; Jackson, S. A.; Eisenstein, O.; Caulton, K. G. *Inorg. Chem.* **1995**, *34*, 488.

(70) Bickford, C. C.; Johnson, T. J.; Davidson, E. R.; Caulton, K. G. *Inorg. Chem.* **1994**, *33*, 1080.

(71) Fryzuk, M. D.; MacNeil, P. A. *J. Am. Chem. Soc.* **1986**, *108*, 6414.

(72) Poulton, J. T.; Sigalas, M. P.; Folting, K.; Streib, W. E.; Eisenstein, O.; Caulton, K. G. *Inorg. Chem.* **1994**, *33*, 1476.

(73) Caulton, K. G. *New. J. Chem.* **1994**, *18*, 25.

(74) Dewey, M. A.; Stark, G. A.; Gladysz, J. A. *Organometallics* **1996**, *15*, 4798.

(75) Perrin, C. L.; Dwyer, T. J. *Chem. Rev.* **1990**, *90*, 935.

(76) Jeener, J.; Meier, B. H.; Bachmann, P.; Ernst, R. R. *J. Chem. Phys.* **1979**, *71*, 4546.

(77) VanderLende, D. D.; Abboud, K. A.; Boncella, J. M. *Inorg. Chem.* **1995**, *34*, 5319.

(78) Glassman, T. E.; Vale, M. G.; Schrock, R. R. *Organometallics* **1991**, *10*, 4046.

(79) Bennett, M. A.; Bruce, M. I. *Comprehensive Organometallic Chemistry*; 1 ed.; Wilkinson, S., G., Stone, F. G. A. and Abel, E. W., Ed.; Permagon Press: Toronto, 1982; Vol. 4, pp 699.

References begin on page 98

(80) Cobbledick, R. E.; Einstein, F. W. B.; Pomeroy, R. K.; Spetch, E. R. *J. Organomet. Chem.* **1980**, *195*, 77.

(81) Cotton, F. A.; Wilkinson, G.; Murillo, C. A.; Bochmann, M. *Advanced Inorganic Chemistry: A Comprehensive Text*; 6th ed.; John Wiley and Sons Inc.: Toronto, 1999, pp 14-16.

(82) Fryzuk, M. D.; MacNeil, P. A. *Organometallics* **1982**, *1*, 1540.

(83) Fryzuk, M. D.; MacNeil, P. A. *J. Am. Chem. Soc.* **1984**, *106*, 6993.

(84) Albers, M. O.; Ashworth, T. V.; Oosthuizen, E. *Inorg. Synth.* **1989**, *26*, 68.

(85) Hallman, P. S.; Stephenson, T. A.; Wilkinson, G. *Inorg. Synth.* **1970**, *12*, 237.

References begin on page 98

Chapter 3

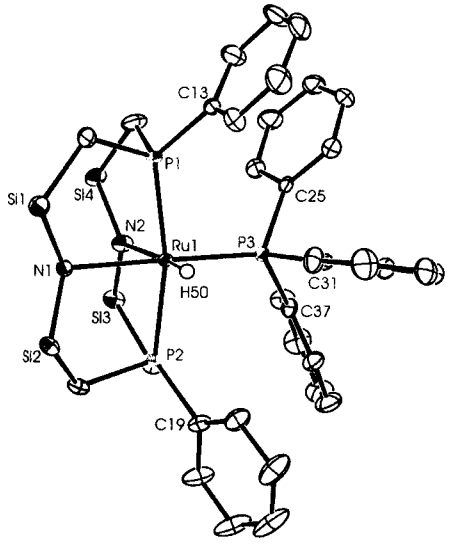

Heterolytic Activation of Dihydrogen (H_2) by Amidophosphine Complexes of Ruthenium(II) and Catalytic Hydrogenation

3.1 Introduction

(i) Catalytic Homogeneous Hydrogenation by Transition Metal Complexes

Homogeneously catalyzed hydrogenation by soluble transition metal complexes is an important process in organometallic chemistry that allows for the reduction of unsaturated organic functionalities.[1-5] One of the earliest documented examples of the homogeneous catalytic activation of H_2 dates back to 1938 when copper (I) salts were employed for the catalytic reduction of substrates such as copper (II) and quinone.[6,7] About a decade later it was observed that the reaction of olefins with carbon monoxide and dihydrogen in the presence of a cobalt carbonyl complex afforded aldehydes (the oxo-process).[8] Perhaps the most significant advance in this field came in 1966 with the discovery of the complex $RhCl(PPh_3)_3$ (Wilkinson's catalyst) that allowed for the rapid and practical catalytic hydrogenation of alkenes and alkynes under mild conditions (equation 3.1).[9] Subsequent to this finding, related complexes that contained phosphine ligands

References begin on page 184

were investigated for their potential for the hydrogenation of unsaturated organic substrates including neutral species (e.g. $RuHCl(PPh_3)_3$) as well as cationic complexes (e.g. $[Rh(diene)(PPh_3)_2]^+$).[2]

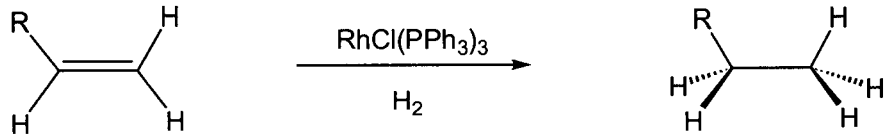

[3.1]

The mechanism for the catalyzed hydrogenation depicted in equation 3.1 and related systems involves intermediate metal hydrides that are transferred to the substrate via insertion and reductive elimination steps.[10,11] Consequently, the formation of metal hydrides from molecular hydrogen is a crucial step in the catalytic process. The two most common modes for the activation of H_2 by transition metals are *homolytic* and *heterolytic* cleavage.[4,12,13]

(ii) The Activation of Dihydrogen (H_2) by Transition Metal Complexes

The nature of the interaction of H_2 with a metal centre is of significance given the importance of the activation of dihydrogen by transition metal complexes in catalytic hydrogenation reactions. A molecule of H_2 can coordinate to a metal centre in a side-on fashion (η^2-H_2) in which the resulting complex contains an intact dihydrogen ligand. Since the discovery of the first transition metal dihydrogen complex, $W(H_2)(CO)_3(P^iPr_3)_2$, in 1984,[14] the chemistry of these compounds has developed considerably and the coordination of dihydrogen has been achieved on both electrophilic and nucleophilic metal centres.[12,15] Interestingly, the chemistry associated with the H_2 ligand in these two types of complexes can differ dramatically. An investigation into the bonding considerations between a metal centre and an H_2 ligand allows for a better understanding of the properties of coordinated H_2 moieties. As shown in Figure 3.1, the M-η^2-H_2 coordination results from a subtle balance between σ donation from H_2 to an empty *d*-orbital of the metal and back-donation from a filled d_π-metal orbital to a σ^*-antibonding orbital of the H_2 ligand.[12,15-18]

References begin on page 184

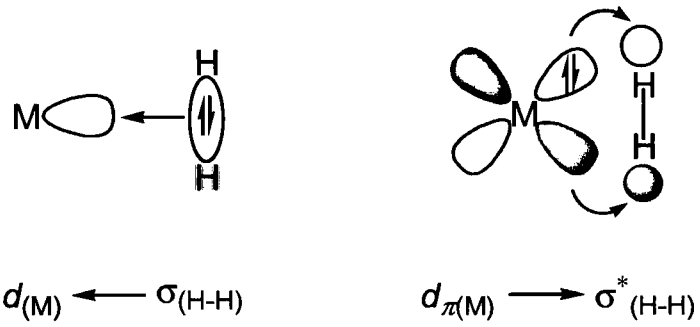

Figure 3.1. The bonding scheme for a transition metal η^2-H_2 complex involving σ-donation from H_2 and π back-bonding from the metal centre.

In complexes that contain nucleophilic metal centres a significant contribution to the bonding is a result of back-donation from the electron-rich metal centre and this leads to a lengthening of the H-H bond while forming a strong metal-H_2 interaction.[12,19] In most cases the H_2 ligand binds very tightly and the resulting complexes are stable with respect to loss of H_2 as well as displacement of the H_2 moiety by neutral donor ligands. Complexes of this type have been referred to as containing an "elongated" dihydrogen ligand.[19-23] They usually exhibit H-H distances (d_{HH}) intermediate between those of dihydrogen complexes ($d_{HH} \leq 1$Å) and distances usually associated with dihydride complexes ($d_{HH} \geq 1.5$ Å).[19] Examples of complexes that have been shown to posses an elongated dihydrogen ligand include $[Cp^*Ru(PPh_2CH_2PPh_2)(H_2)]^+$ (d_{HH} = 1.08 Å)[24] and *trans*-$[Os(H_2)Cl(PPh_2CH_2CH_2PPh_2)_2]^+$ (d_{HH} = 1.22 Å).[25]

Due to the lengthening of the H-H bond and consequent activation of the H_2 molecule in these complexes, they have been said to represent an arrested intermediate state in the very important oxidative addition reaction of H_2.[12,19,22] Homolytic cleavage of H_2 by transition metal complexes involves the incorporation of both atoms of the H_2 molecule onto the metal as hydride ligands. An example of this reactivity is given in equation 3.2, in which the iridium (I) complex $IrCl(CO)(PPh_3)_2$ reacts with H_2 reversibly to give the iridium (III) dihydride $IrCl(CO)(PPh_3)_2(H)_2$.[26] This example illustrates how the transition metal must have accessible higher oxidation states for homolysis to occur as well as the importance of the transition metal to allow for changes in coordination number. In the iridium species the geometry changes from four-coordinate and square-planar to six-coordinate and octahedral upon homolysis of H_2. The

References begin on page 184

oxidative addition reaction displayed in the iridium complex is a critically important process in many homogeneous hydrogenation systems.

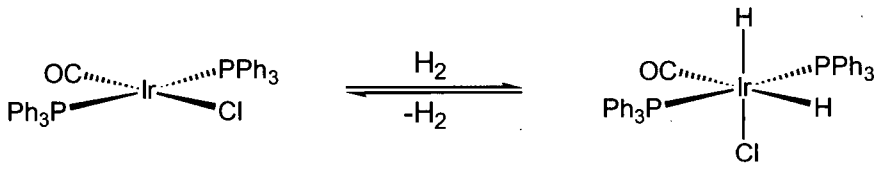

[3.2]

The interaction between H_2 with electrophilic metal complexes involves predominately σ-donation from H_2 and the coordinated dihydrogen ligand can become a Brϕnsted acid.[12,27,28] Such complexes have been shown to promote the activation of dihydrogen towards heterolytic cleavage providing a metal hydride and a proton equivalent.[29-40] For example, the electrophilic monocationic rhenium complex $[Re(CO)_4(PR_3)]^+$ contains π-acceptor ligands that enhance σ-donation from H_2 to the metal at the cost of back-donation, thus enhancing the tendency of H_2 to undergo heterolysis.[41] The acidity of the coordinated H_2 ligand in these types of complexes can vary drastically and this is illustrated by the variety of bases that can be used to effect H_2 cleavage. The complex $[Re(CN^tBu)_3(PCy_3)_2(H_2)]^+$ is weakly acidic and requires strong bases such as alkyl lithium or alkoxides for deprotonation.[42] The species $[CpRu(Me_2PCH_2CH_2Me_2)(H_2)]^+$, on the other hand, requires a mild base such as triethylamine for heterolysis,[43] whereas the highly acidic complexes $[Cp^*Ru(CO)(H_2)]^+$ and $[Os(bpy)(CO)(PPh_3)(H_2)]^{2+}$ have been shown to protonate diethyl ether.[44]

Intramolecular heterolytic splitting of H_2 arises from deprotonation by a basic site on a co-ligand. This process has been suggested as a key step in the protonation of alkyl or alkenyl ligands in hydrogenation reactions[45,46] as well as in transition metal catalyzed H/D exchange reactions.[47,48] Of particular significance to this work is the intramolecular heterolytic cleavage of H_2 by amido donors in ruthenium(II) complexes generating ruthenium hydride and amine ligands. This process can be envisioned as occurring via σ-bond metathesis as is depicted in Figure 3.2.[12] The ability of a coordinated amido ligand in late transition metal complexes to heterolytically cleave H_2 was demonstrated in the Fryzuk group; complexes of iridium,[49] rhodium[49] and ruthenium[50] that contain the amidodiphosphine ligand [PNP] have been shown to cleave H_2 under mild conditions. As was described in chapter 2 the heterolytic activation of H_2 was proposed to be

References begin on page 184

a key step in the catalytic reduction of imine and ketone substrates by coordinatively saturated ruthenium(II) complexes.

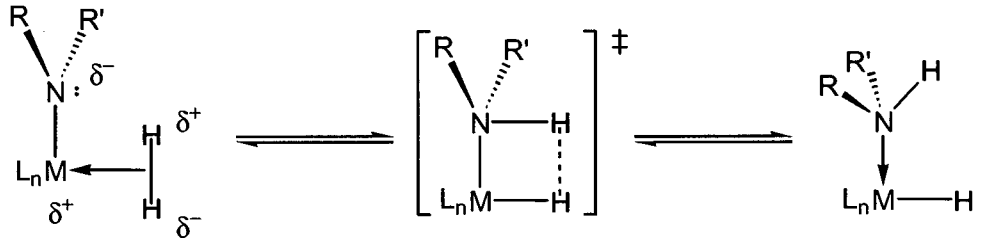

Figure 3.2. Depiction of the intramolecular heterolytic cleavage of H_2 by an amido ligand via σ-bond metathesis.

Recently, the presence of hydrogen bonds between a transition metal hydride and a hydrogen bond donor such as an O-H or N-H group (e.g. M-H···H-N) has been established.[48,51-53] This protonic-to-hydridic interaction has the strength (~5 kcal/mol) and directionality of a conventional hydrogen bond, and consequently can influence structure,[54-57] reactivity and selectivity[58-60] in solution and in the solid-state. Such proton-hydride interactions are believed to be important as intermediates in the base-promoted heterolytic splitting of dihydrogen[61] as well as the reverse reaction, namely, the protonation of metal hydrides to give dihydrogen complexes.[62-64]

3.2 Hydrogenation of $[P_2N_2]Ru(\eta^2:\eta^2\text{-}C_8H_{12})$ (1)

(i) Reaction of $[P_2N_2]Ru(\eta^2:\eta^2\text{-}C_8H_{12})$ (1) with hydrogen gas

Under an atmosphere of hydrogen gas a solution of $[P_2N_2]Ru(\eta^2:\eta^2\text{-}C_8H_{12})$ (**1**) gradually lightens from yellow to colourless. The reaction proceeds slowly and is complete within 3 days to give the ruthenium(II) dihydrogen complex $[P_2NNH]Ru(H_2)H$ (**10**). Monitoring the reaction mixture by ^1H and $^{31}P\{^1H\}$ NMR spectroscopy revealed that an intermediate hydrogenation product, **9**, is initially formed and is converted to **10** over a period of 3 days. This is portrayed in Scheme 3.1. After four hours at room temperature the $^{31}P\{^1H\}$ NMR spectrum shows that the solution contains a mixture of three species. The starting material **1** is the major species present

References begin on page 184

followed by complex **9**; there is only a small amount of the dihydrogen complex **10** present after 4 hours. After 48 hours complex **1** has been consumed and the two ruthenium hydride species **9** and **10** are present in solution in an approximately 1:4 ratio, respectively. Attempts at isolating these two complexes have failed, and consequently, their characterization is based on solution NMR spectroscopy.

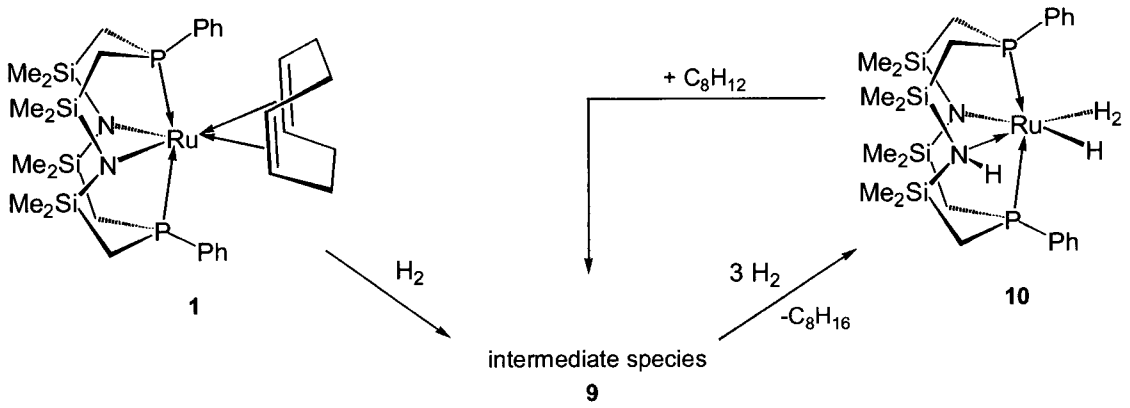

Scheme 3.1

(ii) Spectroscopic identification of the intermediate hydride complex 9

Although the transient hydride complex **9** could not be isolated, various structural characteristics could be gleaned from the spectroscopic data. Prominent in the ^{1}H NMR spectrum of the hydrogenation intermediate is a hydride resonance at δ -9.60 ($^2J_{PH}$ = 25.4 Hz). This signal integrates to one proton per metal centre and is a triplet due to coupling to two equivalent phosphorus-31 nuclei. This is in accordance with the $^{31}P\{^1H\}$ NMR spectrum, which contains a singlet at δ 30.0. Four silyl methyl proton resonances are observed for the macrocycle, however, the ligand methylene protons could not be assigned as they are obscured by other peaks.

The presence of a single hydride ligand in **9** suggests that heterolytic cleavage of H_2 by a ruthenium-amido unit in complex **1** has occurred, thus generating a "[P_2NNH]RuH" fragment. The assignment of the N-*H* resonance arising from the resulting amine ligand could not be made due to overlapping peaks in the ^{1}H NMR spectrum. An amino proton resonance has been identified for complex **10** verifying that heterolysis of H_2 does take place. The heterolytic

References begin on page 184

cleavage of dihydrogen by complex **1** requires that dissociation of a bound olefin moiety of the bidentate cyclooctadiene ligand occurs, thus, creating an open site at the metal centre so that a molecule of H_2 can coordinate. This may be one reason why the reaction of **1** with hydrogen gas proceeds slowly.

A possible structure for the intermediate **9** that is consistent with the spectroscopic data is the monomeric ruthenium hydride depicted in Figure 3.3. This species is believed to contain an η^2-bound cyclooctadiene ligand and represents the direct product of H_2 heterolysis by complex **1**. The pseudo-octahedral coordination geometry in **9** contains a mirror plane bisecting the two phosphine ligands. This accounts for the equivalence of the two phosphorus-31 nuclei as well as the four silyl methyl proton environments that are observed. It is also possible that **9** may exist as a hydride-bridged dimer of formula $\{[P_2NNH]RuH\}_2$. If this complex was present one would expect to observe free cyclooctadiene, cyclooctene or cyclooctane in solution, however, none of these species were evident in the ^1H NMR spectrum during the formation of **9**. The structural characterization of hydrido-olefin ruthenium(II) complexes similar to **9** have been described in the literature.[65-68] In an attempt to provide further support for the proposed identification of the intermediate **9**, the dihydrogen-hydride complex **10** was treated with an excess of cyclooctadiene. As was anticipated, displacement of an equivalent of H_2 in **10** by cyclooctadiene resulted in its conversion to **9** as monitored by ^1H and $^{31}P\{^1H\}$ NMR spectroscopy.

When the same reaction was performed with an excess of cyclooctene the formation of a new high-field resonance at δ -10.8 was noted in the ^1H NMR spectrum. This most likely corresponds to the hydride ligand in a complex similar to **9** only this bearing a coordinated cyclooctene ligand. This same species was noted (albeit in very small quantities) during the conversion of **9** to **10** during later stages when the concentration of hydrogen gas in the NMR tube was diminished.

References begin on page 184

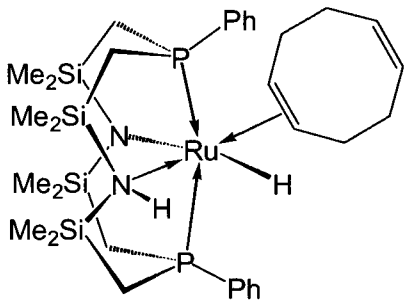

9

Figure 3.3. Proposed structure of the intermediate complex **9**.

(iii) Characterization of complex 10 as a fluxional dihydrogen-hydride complex by variable-temperature NMR spectroscopy and deuterium labelling studies

In the ^{1}H NMR spectrum of complex **10** a triplet is observed at δ -11.44 ($^2J_{PH}$ = 13.8 Hz) that integrates to three protons per metal centre. This feature may be the result of a dihydrogen-hydride complex, [P_2NNH]Ru(H_2)H, however, another candidate that satisfies this condition is a ruthenium (IV) trihydride species, [P_2NNH]Ru(H)$_3$. We favour the formulation of **10** as the Ru(H_2)(H) tautomer since this arrangement is also evident in the structurally related dihydrogen-hydride complexes **A** and **B** that are shown in Figure 3.4.[69] The ^{1}H NMR spectra for complexes **A** and **B** contain a high-field triplet near δ -11.0 ($^2J_{PH}$ = *ca.* 14 Hz) for the three ruthenium-bound hydrogens, and singlets in their ^{31}P{^{1}H} NMR spectra between δ 45 - δ 50. These spectral data are identical to those of **10**. Dihydrogen-hydride complexes of several other late transition metals are also known.[70-77] In order to further classify **10** as a dihydrogen-hydride complex the measurement of the relaxation rate of the hydride ligands and an analysis of the effect of deuterium substitution were undertaken.

References begin on page 184

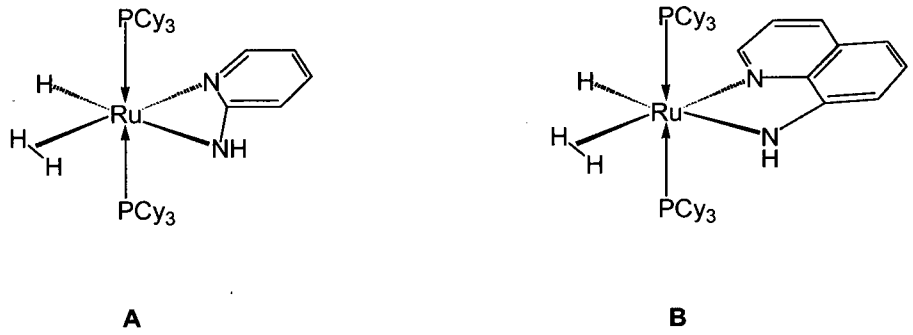

Figure 3.4. Dihydrogen-hydride complexes of ruthenium(II) that are related to complex **10**.[69]

The measurement of the minimum of the longitudinal relaxation time (T_1(min)) for metal-bound hydrogen atoms is one method that has been employed to discriminate between classical hydride (M-H) versus non-classical dihydrogen (M-η^2-H_2) ligands in transition metal complexes.[78-80] The basis for this approach is the assumption that dipole-dipole interactions are almost solely responsible for the relaxation of the NMR signals, and since a dihydrogen ligand has a short H-H distance (compared to a dihydride) it will therefore give rise to a distinctively short T_1(min) relaxation time. In general, the criterion for distinguishing between classical and non-classical hydrides is based on the distinction of whether T_1(min) is shorter than 80 ms ($M(H_2)$) or greater than 150 ms ($M(H)_2$) at 250 MHz. Since T_1(min) values are proportional to the magnetic field strength these limits correspond to 160 ms and 300 ms, respectively at 500 MHz.

Using an inversion-recovery pulse sequence, the relaxation time (T_1) for the metal-bound hydrogen atoms in **10** was determined at a variety of temperatures ranging from 200 to 300 K at 500 MHz. The minimum value of 62 ms observed at 240 K is qualitatively consistent with the presence of a dihydrogen ligand in **10**, supporting its formulation as a dihydrogen-hydride species.

A quantitative method for determining the H-H distance (d_{HH}) from the experimentally determined T_1(min) value has been developed.[80,81] The underlying principle states that if the relaxation of proton A from dipole interaction with nucleus B can be determined, then the A-B distance can be accurately calculated when both A and B are relatively immobile in the molecule.[82] Dihydrogen complexes, however, have the complication that the H_2 ligand can undergo fast internal rotation which can effect dipolar relaxation. In order to address this problem

References begin on page 184

a correction factor of 0.794 is applied to the calculated H-H distance for a rapidly rotating H_2 ligand.[81] The equations that are used to calculate d_{HH} for slow and fast H_2 rotational regimes are:

$$d_{HH}\,(\text{slow rotation}) = 5.81(T_{1(HH)}/\upsilon)^{1/6}\ \text{Å} \qquad [3.3]$$

$$d_{HH}\,(\text{fast rotation}) = 4.61(T_{1(HH)}/\upsilon)^{1/6}\ \text{Å} \qquad [3.4]$$

where υ is the spectrometer frequency in megahertz, and $T_{1(HH)}$ is the minimum T_1 value for the H_2 ligand and is given in units of seconds.

An accurate determination of the H-H bond length requires that the mutual relaxation rate of the hydrogen atoms in the coordinated H_2 ligand (R_{HH}, where $R_{HH} = 1/T_{1(HH)}$) be known explicitly. The rate of dipolar relaxation for a dihydrogen ligand (R_{H2}) is actually the sum of R_{HH} and the relaxation resulting from other dipoles in the molecule (R_{other}):[75,76]

$$R_{H2} = R_{HH} + R_{other} \qquad [3.5]$$

Additionally, in the case of a fluxional polyhydride complex the observed relaxation rate is the population weighted average of all of the hydride sites. Specifically, for a dihydrogen-hydride species the observed relaxation rate is:[75,76]

$$R_{obs} = (2R_{H2} + R_H)/3 \qquad [3.6]$$

where R_H is the relaxation rate of the hydride ligand. In order to extract the desired R_{HH} value, it is necessary to measure the relaxation rate for the hydride ligand in a related monohydride complex. This relaxation rate will be denoted as $R_{obs'}$. The relaxation value $R_{obs'}$ can be used to represent relaxation contributions in the molecule other than those within the H_2 ligand (i.e. $R_{obs'} \sim R_H + R_{other}$).[75,76] In doing so, equations 3.5 and 3.6 can be combined to yield the following formula for the relaxation rate of the coordinated H_2 ligand:

$$R_{HH} = 3(R_{obs} - R_{obs'})/2 \qquad [3.7]$$

References begin on page 184

In order to obtain an accurate determination for the relaxation rate of the dihydrogen ligand in complex **10** a related monohydride complex of the type [P_2NNH]RuH(L) (where L is a neutral donor ligand) was required. The monohydride complex [P_2NNH]RuH(PPh_3) (**13**), that forms from the addition of hydrogen gas to [P_2NNH]Ru($C_6H_4PPh_2$) (**2**) was a suitable candidate. The details concerning the synthesis and characterization of **13** are found in section 3.3 of this chapter. The T_1(min) value for the Ru-*H* hydride in **13** was found to be 370 ms at 260 K, corresponding to a relaxation rate of 2.70 s^{-1}. The relaxation of this hydride, however, is also influenced by the *ortho*-protons of the *cis*-coordinated triphenylphosphine ligand, which come into close contact with the hydride ligand (~ 2 Å as determined by X-ray analysis). By a method previously reported,[80] the relaxation contribution due to the *ortho*-protons is calculated to be approximately 1.03 s^{-1}. Consequently, a relaxation rate of 1.67 s^{-1} ($R_{obs'}$ = 2.70 s^{-1} – 1.03 s^{-1}) can be used as an estimation of the contribution to relaxation of all factors but H-H dipole-dipole relaxation within the dihydrogen ligand in complex **10**. The observed rate of dipolar relaxation in complex **10** is 16.1 s^{-1} (R_{obs} = 1/0.062 s). Substituting these values into equation 3.7 gives a relaxation rate of 21.7 s^{-1} for the hydrogen atoms of the coordinated H_2 ligand. This leads to a calculated H-H distance of approximately 1.2 Å assuming slow rotation of the H_2 ligand or 1.0 Å assuming fast rotation.

Another characterization tool that has been utilized to provide evidence for the existence of a coordinated dihydrogen ligand in a transition metal complex is the measurement of the coupling between hydrogen and deuterium in the HD isotopomer ($^1J_{HD}$).[12,19,21-25,83] The HD resonance in the ^{1}H NMR spectrum becomes a 1:1:1 triplet and is considered to be direct proof of an intact H_2 ligand since classical hydrides do not show appreciable spin-spin coupling because no residual H-D bond is present. The $^1J_{HD}$ measured in HD gas is 43.2 Hz, but in transition metal dihydrogen complexes this value is reduced and has been found to exist in the range of 5 to 35 Hz.[12] Qualitatively, the smaller couplings that are observed for dihydrogen complexes can be rationalized by a lengthening of the H-D bond upon coordination to a metal centre. It has been proposed that when such couplings fall between 5 and 25 Hz an elongated or stretched dihydrogen ligand is present.[13,24] The observation of the inverse relation between H-H distance (d_{HH}) and HD coupling ($^1J_{HD}$) has been quantified and the equation that describes this relationship is given in equation 3.8.[44]

References begin on page 184

$$d_{HH} = 1.44 - 0.0168(^1J_{HD}) \text{ Å} \quad [3.8]$$

For fluxional dihydrogen-polyhydride complexes the use of deuterium labelling is often critical for the establishment of an H_2 ligand and this is achieved by the observation of an exchange-averaged spin-spin coupling ($^{av}J_{HD}$) and/or a perturbation in the chemical shift for the hydride isotopomers.[12,74,75,77,84-88] For a dihydrogen-hydride complex $L_nM(H)(H_2)$ with rapidly exchanging hydrogen atoms an average J_{HD} is normally observed upon partial substitution by deuterium. In order to get an estimate of the H-H distance of the η^2-H_2 ligand within such systems the $^1J_{HD}$ value must be extracted from the experimentally measured $^{av}J_{HD}$. The average HD coupling observed in a species with n hydrogen atoms at the metal is the following for an HD_{n-1} isotopomer:[12,82]

$$^{av}J_{HD} = n^{-1}\Sigma_i\chi_i[\Sigma_j\{^1J_{HD}/(n-1)\}] \quad [3.9]$$

where $i \neq j$. Here, χ_i is the likelihood that the proton occupies site i, and $\Sigma_i\chi_i = 1$. For an HD_2 species, equation 3.9 simplifies to $^1J_{HD} = 3(^{av}J_{HD})$. A potential source of error is neglecting the two-bond H-D couplings ($^2J_{HD}$) between the hydrogen atoms in the hydride and dihydrogen sites. Some classical hydrides, for example, have been shown to exhibit $^2J_{HD}$ couplings as large as 3.8 Hz.[12,82]

Exposure of a solution of **10** to an atmosphere of D_2 gas results in the incorporation of deuterium into the hydride and dihydrogen environments as evidenced by the appearance of new resonances in the hydride region of the ^{1}H NMR spectrum. Representative spectra of the new hydride resonances of the partially deuterated isotopomers acquired with ^{31}P decoupling at 300 K are shown in Figure 3.5. After one hour, resonances due to the Ru-H_3 (**10**) and Ru-H_2D (**10**-d_1) isotopomers are evident with the mono-deuterated species slightly downfield shifted by *ca.* 20 ppb. Although the two resonances are slightly overlapping the H-D coupling of 4.5 ± 0.5 Hz in **10**-d_1 is partially resolved. Upon prolonged exposure to D_2 gas the solution consists almost exclusively of the Ru-HD_2 (**10**-d_2) isotopomer. The chemical shift of **10**-d_2 is downfield shifted with respect to **10** by *ca.* 30 ppb. The broadness of this peak does not allow for the expected quintet to be completely resolved, nevertheless, an H-D coupling of 5.0 ± 0.5 Hz could be measured. This coupling constant represents the exchange-averaged value ($^{av}J_{HD}$) and gives a

References begin on page 184

calculated $^1J_{HD}$ of 15.0 ± 1.5 Hz for the η^2-HD ligand. The magnitude of this coupling is consistent with the presence of an elongated dihydrogen ligand in complex **10** with an estimated H-H distance of 1.2 Å (from equation 3.8). This value coincides well with the H-H distance determined from the NMR relaxation data assuming that the coordinated dihydrogen ligand in complex **10** is modelled as slowly rotating. An elongated H_2 moiety may be expected to have a higher rotational barrier due to an increase in metal back-bonding.[24]

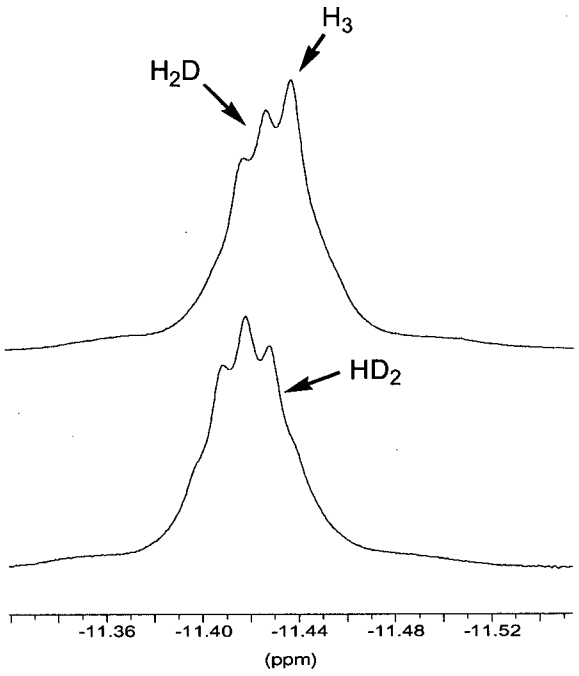

Figure 3.5. High-field region of the $^1H\{^{31}P\}$ NMR spectrum of the isotopomers **10** (H_3), **10**-d_1 (H_2D) and **10**-d_2 (HD_2) (C_7D_8, 500 MHz, 300 K). The upper spectrum was recorded 1 hour after the addition of D_2 gas and the lower spectrum was recorded after 16 hours.

The estimation of the H-H bond length in complex **10** as determined by the T_1 method as well as $^1J_{HD}$ NMR data indicates the presence of a stretched H_2 ligand in **10**. The H-H distance of 1.2 Å is similar to the H-H separations that have been determined in structurally related dihydrogen-hydride complexes of ruthenium(II) (Table 3.1). A trend that is apparent from inspection of the data in Table 3.1 is that the H-H distance increases in going from electron-poor to

References begin on page 184

electron-rich complexes. For instance, the species $[Ru(PCy_3)_2(CO)_2(H_2)H]^+$ (entry 1) contains two π-accepting CO ligands which decreases the delocalization of electron density from the metal (d_π) to the H_2 antibonding orbital (σ^*), thereby limiting the degree of H-H bond lengthening. At the other extreme, the complexes in entries 4 and 5 contain π-donating amide and alkoxide ligands respectively, and the resulting H_2 moieties are elongated. This trend has also been noted for dihydrogen complexes of other transition metals particularly when the π-accepting or π-donating ligands are located *trans* to the H_2 ligand.[89]

Table 3.1. Comparison of H-H distances (d_{HH}) in some related ruthenium(II) dihydrogen-hydride complexes and the method in which they were determined.

Entry	Complex	d_{HH} (Å)	Method	Ref.
1	$[Ru(PCy_3)_2(CO)_2(H_2)H]^+$	~ 0.9	J_{HD}	74
2	$[Ru(PCy_3)_2(bipy)(H_2)H]^+$	~ 1.1	J_{HD}	74
3	$[Ru(P^iPr_3)_2(py\text{-}Ph)(H_2)H]^+$	1.08	T_1(min)	70
4	$Ru(PCy_3)_2(py\text{-}NH)(H_2)H$	~ 1.28	T_1(min)/J_{HD}	69
5	$Ru(PCy_3)_2(py\text{-}O)(H_2)H$	1.30	T_1(min)	69
6	$[P_2NNH]Ru(H_2)H$ (**10**)	~ 1.2	T_1(min)/J_{HD}	this work

(iv) The dynamic behaviour of complex 10 in solution: isotopic perturbation of equilibria and proton-hydride exchange processes via protonic-hydridic bonding interactions

An examination of the temperature dependence on the chemical shift and H-D coupling constants for the various isotopomers of **10** was attempted by performing variable-temperature $^1H\{^{31}P\}$ NMR studies. Unfortunately, broadening of the peaks below 300 K did not allow for a detailed analysis of the H-D couplings. As mentioned above, the deuterated complexes **10**-d_1 and **10**-d_2 experience slight downfield shifts in their hydride resonances with respect to that of **10** ($\Delta\delta_1$ *ca.* 20 ppb and $\Delta\delta_2$ *ca.* 30 ppb at 300 K). Similar isotopic shifts (downfield or upfield) have been observed upon partial substitution of deuterium atoms in the hydride positions of dihydrogen[74-76,84,88] and polyhydride[86,90,91] complexes, and in some instances these isotope shifts have exhibited a dependence on temperature. The effect of temperature on the chemical shift of the H_3 and HD_2 isotopomers of complex **10** is represented graphically in Figure 3.6. In both cases an

References begin on page 184

upfield shift occurs upon warming a toluene-d_8 solution of each of the isotopomers. What is also apparent from Figure 3.6 is that an increase in the separation between the two resonances occurs at lower temperatures; at 215 K, for instance, the hydride signal for the isotopomer **10**-d_2 is shifted *ca.* 90 ppb downfield from **10** as opposed to 30 ppb at 300 K.

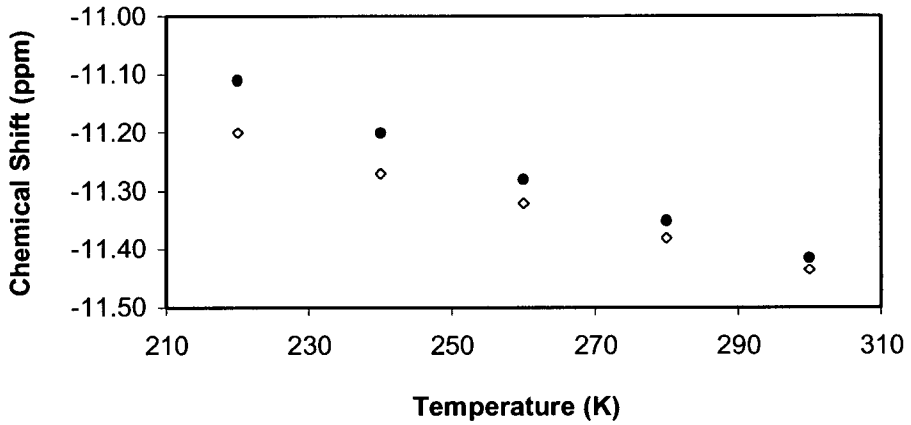

Figure 3.6. Plot of chemical shift of the hydride resonance in **10** (orange diamonds) and **10**-d_2 (green circles) as a function of observation temperature (from 215 to 300 K).

It has been proposed that large isotope shifts for the hydride resonances that may arise for transition metal polyhydride complexes could be attributed to an isotopic perturbation of equilibrium.[92-94] One situation could involve an equilibrium that is established between classical and non-classical tautomers in solution. This behaviour has been used to rationalize the isotope shifts observed in the rhenium polyhydride complex $[Re(H)_4(CO)(PMe_2Ph)_3]^+$[87] as well as in the species $Cp^*Os(CO)_2(H)_2$.[95] In the case of a dihydrogen-hydride structure an equilibrium can be established in which the isotopes may fractionate between the non-equivalent M-H sites (i.e. the hydride or the dihydrogen environments). This behaviour is demonstrated in Figure 3.7 for the partially deuterated derivatives of an $M(H_2)H$ fragment. If the equilibria depicted in Figure 3.7 lie to the left (i.e. deuterium is enriched in the dihydrogen ligand) then a shift in the ^1H NMR spectrum towards the hydride resonance would be observed for the H_2D and HD_2 isotopomers. Without a low-temperature "static" spectrum which clearly identifies the hydride and dihydrogen resonances the direction of the observed shift does not provide information as to which side the

References begin on page 184

equilibria lie. However, measurement of the J_{HD} coupling constants of the H_2D and HD_2 isotopomers can also provide important details about the equilibria. A preference for deuterium to concentrate in the dihydrogen ligand would be evidenced by a $J_{HD}(H_2D) > J_{HD}(HD_2)$; this type of behaviour is exhibited by the complex $[Ru(PMe_3)_4(H_2)H]^+$ (10.9 and 10.2 Hz, respectively).[77] Conversely, when $J_{HD}(HD_2) > J_{HD}(H_2D)$ there is a non-statistical distribution of deuterium between the dihydrogen and the hydride environments, with a preference for deuterium to occupy the hydride site. The complex $[Ru(PCy_3)_2(bipy)(H_2)H]^+$ displays this type of behaviour ($J_{HD}(HD_2)$ = 6.7 Hz and $J_{HD}(H_2D)$ = 5.5 Hz).[74] A true isotopic perturbation effect should show a dependence on temperature due to the Boltzmann equilibrium operating on the isotopic fractionation between the non-equivalent hydride sites.[85]

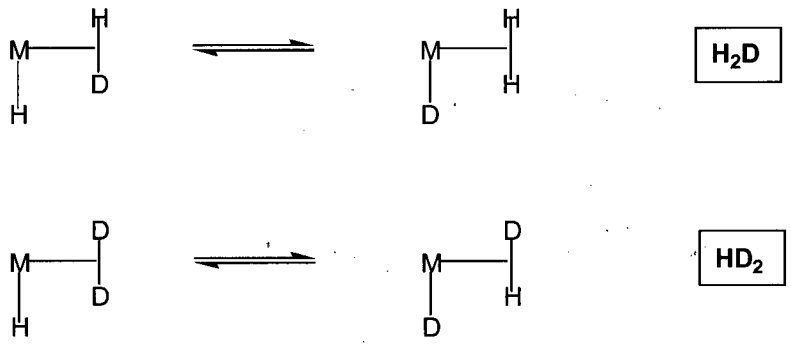

Figure 3.7. Equilibria for partially deuterated complexes of an $M(H_2)(H)$ species.

In complex **10** the isotopic shifts that are evident in the partially deuterated derivatives, and in particular, the temperature dependence on the observed chemical shifts are consistent with the occurrence of an isotopic perturbation of equilibria as shown in Figure 3.7. At 300 K the J_{HD} couplings in the HD_2 and H_2D isotopomers of **10** are the same (within experimental error), and thus a conclusion as to the whether deuterium preferentially resides in either the hydride or the dihydrogen sites can not be made.

The isotopic perturbation of equilibria found in complex **10** requires a dynamic process that exchanges the hydrogen atoms between the hydride and dihydrogen environments. The observation of a single hydride resonance in the ^1H NMR spectrum for these two distinct environments in **10** (from 180 to 300 K) indicates that this rearrangement process is rapid on the

References begin on page 184

NMR time scale. A low temperature limiting spectrum could not be obtained and broadening of the hydride resonance was apparent upon cooling; no coupling to the ^{31}P nucleus could be resolved below 220 K. These features can be attributed to efficient dipole-dipole relaxation at lower temperatures leading to short T_1 and T_2 values.[96] This result exemplifies the limitation of using ^{1}H NMR spectroscopy for probing very rapid dynamic processes, and in particular, for cases in which short H-H separations lead to effective dipolar relaxation.

The facile exchange of hydride and dihydrogen environments that occurs in complex **10** has also been observed in related polyhydride species. The free energy of activation ($\Delta G^{\neq}$) for site exchange in the complex $[(PCy_3)_2RuH(H_2)(bipy)]^+$ has been measured to be approximately 5.5 kcal mol^{-1} (at 120 K).[74] As shown in Figure 3.8, this dynamic process is proposed to take place via a transient trihydrogen species that forms via a *cis*-interaction between the hydride and dihydrogen ligands.[12,74] The *cis*-interaction arises due to an electrostatic attraction (a dipole/induced-dipole interaction) between the negatively charged hydride and a positively charged H-atom of the coordinated H_2 ligand. The M-H bond is especially suited to this interaction because it is highly localized onto the hydride *s*-orbital and is high in energy owing to the elevated electron density on the hydride.[12] The acidity of coordinated H_2 moieties suggests that these ligands are also well suited for this electrostatic interaction.

References begin on page 184

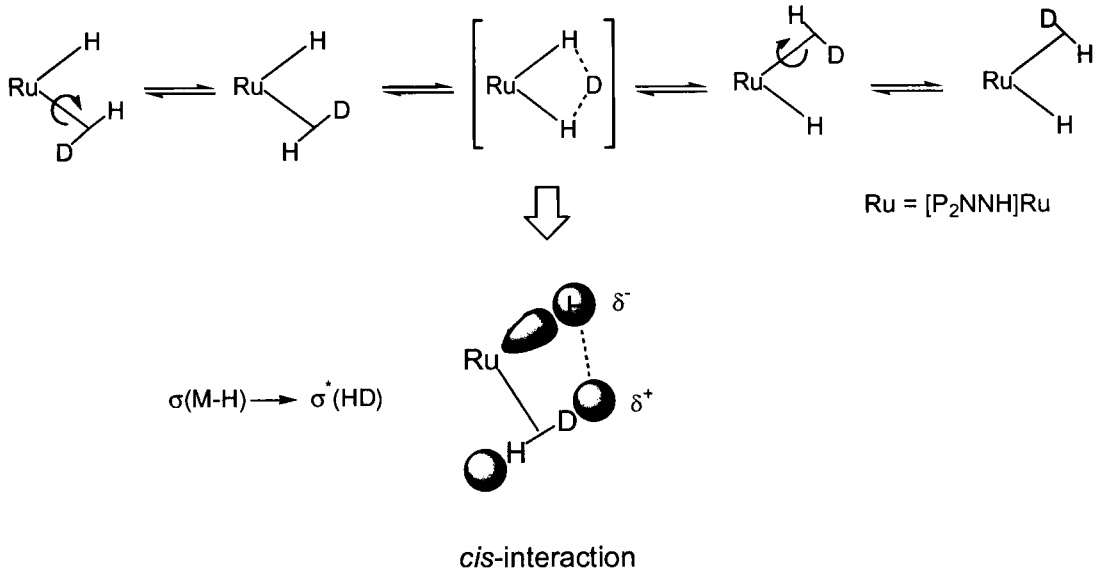

Figure 3.8. Exchange of the ruthenium-bound hydrogen atoms in complex **10** occurring via a transient trihydrogen complex.

Although the *cis*-effect allows for exchange between hydride and dihydrogen environments, complete scrambling of all three H-atoms requires that rotation of the bound H_2 ligand also occurs. In complex **10** the H_2 ligand has been described as slowly rotating with an elongated H-H bond. The observation of a single hydride resonance at all observation temperatures (180 to 300 K), however, indicates that the rotational motion of the H_2 ligand must occur fast enough on the NMR time scale to average the magnetic environments of the Ru-*H* nuclei.

The room-temperature ^{1}H NMR spectrum of complex **10** is representative of a highly symmetrical complex. Two resonances are observed for the silyl methyl protons and two peaks for the methylene protons of the [P_2NNH] ligand backbone along with one resonance for the *ortho*-protons, and one for the *meta*- and *para*-protons of the phosphine phenyl groups. This number of peaks is indicative of a complex that has C_{2v} symmetry. While the above dynamic process can explain the exchange of the ruthenium-bound hydrogen atoms, on its own it does not account for the observed symmetry of complex **10** in solution. Consequently, there must be a second fluxional process that is taking place. Insights into this mechanism were gained when it was noticed that upon exposure of **10** to D_2 gas incorporation of deuterium into the amino proton

References begin on page 184

site of the macrocyclic [P_2NNH] ligand also occurred. This observation suggested that the amino proton was interacting with the hydride ligand in some way that would allow for atom-exchange between these two distinct chemical environments.

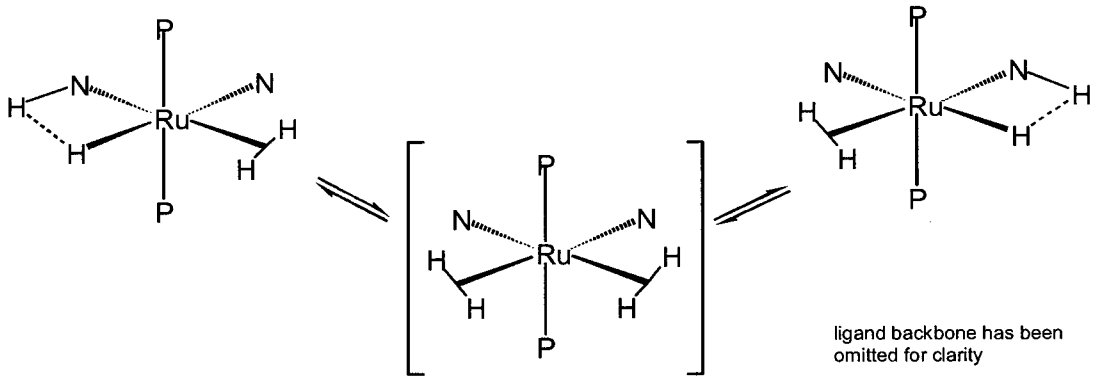

Scheme 3.2.

As illustrated in Scheme 3.2, it is proposed that an electrostatic attraction between the hydride and the amine proton in **10** results in the formation of an intramolecular hydrogen bonding interaction. This unique type of hydrogen bond has recently been established and the presence of this interaction has been shown to influence the structure and reactivity of the resulting complexes.[51,52] For example, proton-hydride bonding is believed to be an important interaction leading to the protonation of metal hydrides to give dihydrogen complexes. We suggest that this occurs in complex **10** to form an (unobserved) intermediate bis-dihydrogen complex. Stable and isolable bis(H_2) complexes of the type "Ru(H_2)(H)$_2$(PR_3)$_2$" are known to exist.[97-100] Heterolysis of one of the coordinated H_2 ligands in the intermediate species by an amido donor regenerates **10**. A related mechanism involving a transient metal-H_2 species has been invoked to rationalize the exchange reactions of hydrogen and deuterium in an iridium hydride dithiol complex.[47] According to this proposal, complex **10** exists as a rapidly equilibrating mixture of two enantiomers. The presence of a proton-hydride bonding interaction in **10** may also explain the temperature dependence of its hydride signal, which shifts from δ -11.44 at 300 K to δ -11.20 at 215 K (see Figure 3.6). The high-field shift that occurs upon warming a solution of **10** is in accordance with a stronger proton-hydride bonding interaction at elevated temperatures.[101] Consistent with this finding is the observation that the amino proton resonance in **10** experiences a

References begin on page 184

downfield shift towards higher temperatures (*ca.* 30 ppb between 240 and 300 K). Similar hydride and proton resonance shifts have been observed in other complexes that are known to contain protonic-hydridic bonding interactions.[54,56]

The electrostatic attraction between the hydride and the amino proton in **10** parallels the electrostatic *cis*-interaction that exists between the hydride and the dihydrogen ligand. The introduction of deuterium into both the N-*H* and Ru-H_3 sites suggests that the energy of each of these competing interactions is similar. Together, these two independent dynamic processes account for the high symmetry of complex **10** in solution as indicated by the ^1H and $^{31}P\{^1H\}$ NMR data.

(v) Proposed mechanisms for the formation of complex 10

In the classical mechanisms of olefin hydrogenation, insertion of an olefin into a metal-hydrogen bond followed by reductive elimination of hydride and alkyl ligands are regarded as the key steps in the catalytic cycle. Recent studies concerning the reactivity of metal hydride complexes with unsaturated substrates, however, have shown that substrate reduction may occur through alternative pathways. For example, olefins could be hydrogenated by alkyl-dihydrogen $[M(R)(H_2)L_n]$[45,102,103] or olefin-dihydrogen complexes $[M(olefin)(H_2)L_n]$.[104,105] In the former case, protonation of the alkyl ligand by the coordinated H_2 moiety occurs whereas in the latter, direct transfer of both H-atoms of the dihydrogen ligand to the olefin takes place.

The conversion of complex **9** to **10** under an atmosphere of hydrogen gas is accompanied by the formation of an equivalent of cyclooctane as a reaction by-product. Two possible mechanisms for this transformation are given in Scheme 3.3; the intermediates shown in brackets are not observed by ^1H and $^{31}P\{^1H\}$ NMR spectroscopy. In pathway **A**, following heterolysis of a molecule of H_2 by the starting material **1** to give **9**, hydride transfer to the bound olefin and coordination of an H_2 ligand occurs. The next step involves hydrogenolysis of the alkyl bound cyclooctene ligand via protonation by the coordinated H_2 ligand. Similar reactivity has been invoked to explain the catalytic activity of $RuHCl(PPh_3)_3$[106] and $[MH(H_2)(P(CH_2CH_2PPh_2)_3]^+$ (M = Fe, Ru)[45] for the hydrogenation of olefins and acetylenes. In this system, a molecule of cyclooctene coordinates to the unsaturated "$[P_2NNH]RuH$" species that forms after the protonation

References begin on page 184

step (structure **B**) and the process is repeated until cyclooctane (C_8H_{16}) has been eliminated. When there is no longer any free olefin present in solution a molecule of dihydrogen coordinates to the ruthenium centre, thus forming complex **10**. It has already been mentioned that when the concentration of H_2 in solution is low, small amounts of the intermediate species **B** are evident in the ^1H NMR spectrum due to competition for coordination at the metal centre between H_2 and cyclooctene.

A recent study reports on the hydrogenation of norbornadiene to norbornene in the complex $RuH(OTf)(NBD)(PPh_3)_2$ (where OTf = triflate and NBD = norbornadiene).[67] Computational details on this system indicated that initial hydride transfer (from Ru-*H*) from the active species $RuH(H_2)(NBD)(PPh_3)_2$ followed by proton transfer from the H_2 ligand was the energetically favourable pathway. This route resembles the proposed pathway **A** in Scheme 3.3. It was also determined that the initial hydride transfer step was the rate-limiting step. This coincides with the experimental finding that complexes **9** and **10** are the only two species to be observed in the ^1H and $^{31}P\{^1H\}$ NMR spectra during the hydrogenation reaction. If pathway **A** is the operative mechanistic route for the conversion of **9** into **10** one reason that hydride insertion may be a slow step is due to its involvement in potential proton-hydride bonding interactions with the amino proton.

In an alternative route (shown as pathway **B** in Scheme 3.3) hydrogenation of the olefin groups of the cyclooctadiene ligand may result from the transfer of both hydrogen atoms of an η^2-bound H_2 moiety. It has been reported that protonation of the olefin-hydride complex $Cp^*Ru(NBD)H$ results in the hydrogenation of the NDB ligand presumably via transfer of protons from a coordinated dihydrogen ligand to the olefin.[73,105] Displacement of the aquo ligand in $[Cp^*Ru(NBD)(H_2O)]^+$ by H_2 shows similar results providing further evidence for olefin hydrogenation directly from a coordinated H_2 ligand. Para-hydrogen induced polarization (PHIP) studies of the photo-catalyzed hydrogenation of the NBD ligand in the complex $Mo(H_2)(CO)(NBD)$ offers direct proof for the transfer of both hydrogen atoms of an η^2-H_2 to the olefin.[104]

Intramolecular protonation of the hydride ligand in **9** by the amino proton could result in the formation of an unobserved dihydrogen species, $[P_2N_2]Ru(\eta^2\text{-}C_8H_{16})(H_2)$ (intermediate **C** in

References begin on page 184

Scheme 3.3). There is evidence for the interaction of the amino proton and ruthenium hydride nuclei in complex **10** leading to a transient bis(H_2) species, and so it is a reasonable assumption that similar behaviour exists in complex **9**. Intramolecular hydrogen transfer from the H_2 ligand to the olefin would result in the generation of a ruthenium (IV) alkyl-hydride complex. Reductive elimination of the hydride and alkyl ligands produces a coordinatively unsaturated ruthenium(II) species to which an equivalent of H_2 and cyclooctene can coordinate, and the process is repeated until cyclooctane (C_8H_{16}) has been eliminated.

At this point a distinction between the two possible mechanistic pathways for the conversion of complex **9** to **10** has not been made and future studies will be required in order to do so. In either case, this system is proposed to involve a coordinated H_2 ligand in key proton transfer steps in addition to classical elementary processes such as hydride insertion and reductive elimination.

References begin on page 184

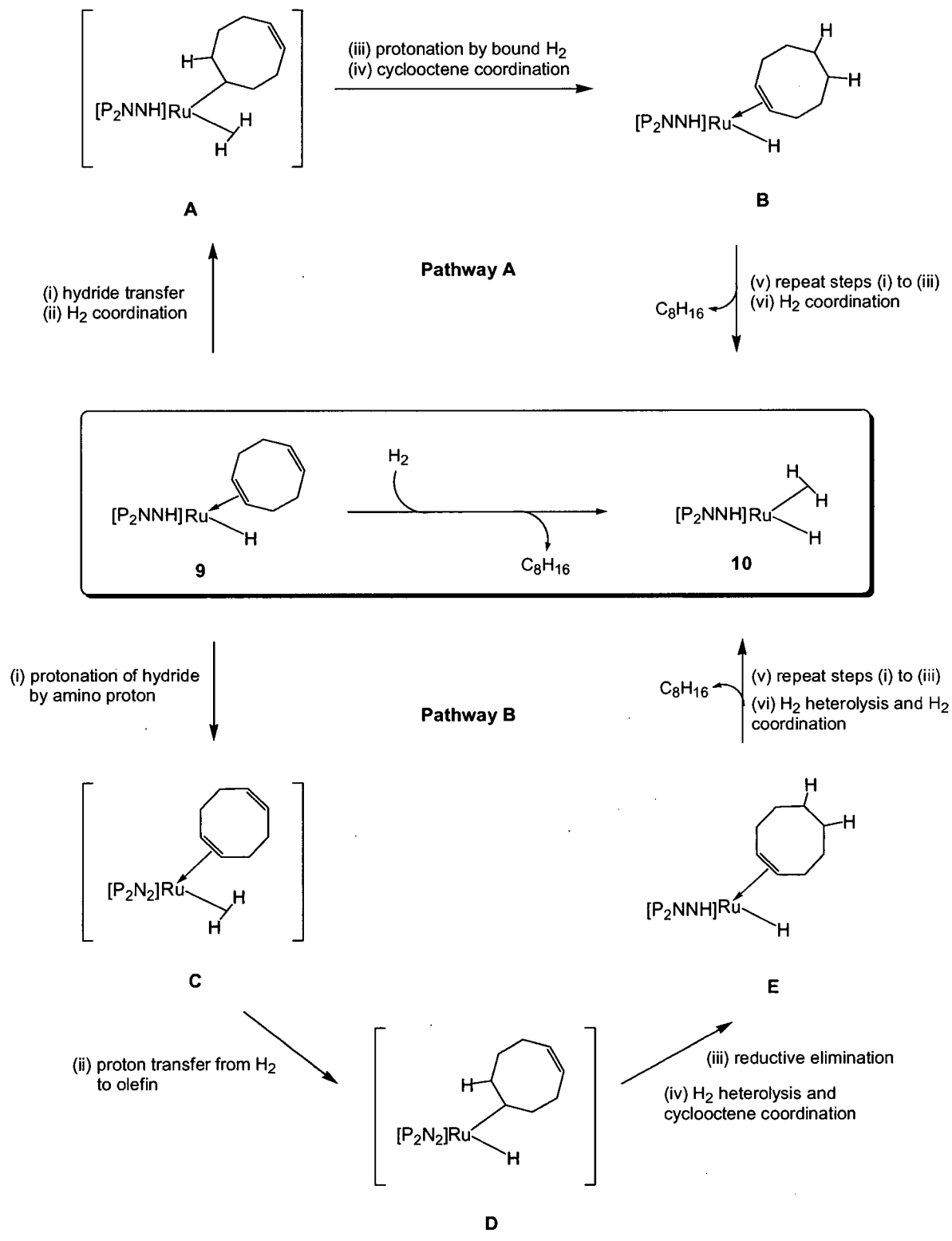

Scheme 3.3

References begin on page 184

3.3 Hydrogenation of $[P_2NNH]Ru(C_6H_4PPh_2)$ (2) to give the mono-hydride complex $[P_2NNH]RuH(PPh_3)$ (11)

(i) Synthesis and characterization of $[P_2NNH]RuH(PPh_3)$ (11)

The complex $[P_2NNH]Ru(C_6H_4PPh_2)$ (**2**) reacts quantitatively with hydrogen gas to form the ruthenium(II) mono-hydride amide species $[P_2NNH]RuH(PPh_3)$ (**11**), as shown in equation 3.10, via hydrogenolysis of the *ortho*-metalated triphenylphosphine ligand in **2**. Complex **11** has been characterized in the solid-state by a single crystal X-ray diffraction study as well as in solution by ^1H and $^{31}P\{^1H\}$ NMR spectroscopy. The molecular structure of **11** is shown in Figure 3.9 and selected bond lengths and angles are highlighted in Table 3.2.

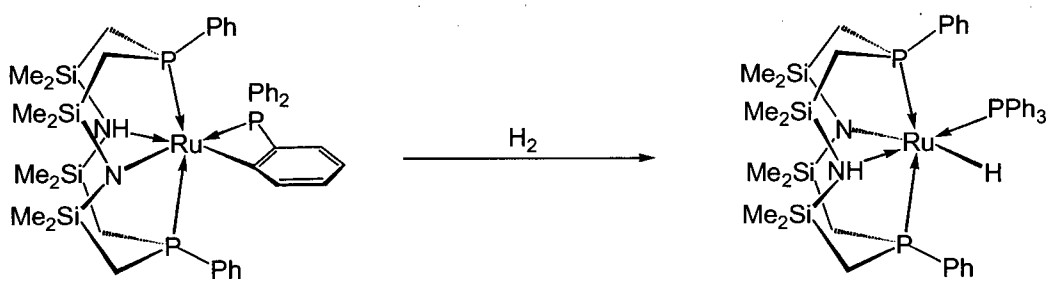

2 **11** **[3.10]**

References begin on page 184

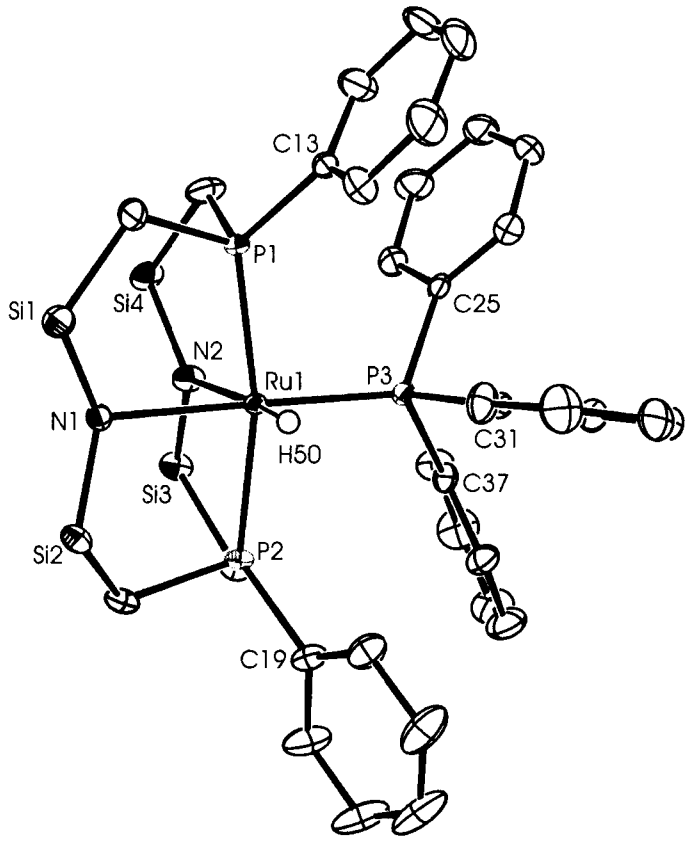

Figure 3.9. ORTEP representation (thermal ellipsoids shown at 50 % probability) of the solid-state molecular structure of $[P_2NNH]RuH(PPh_3)$ (**11**) as determined by X-ray crystallography. The ruthenium hydride H(50) was located and refined isotropically, the amino proton was not located.

Table 3.2. Selected bond lengths and angles in the complex $[P_2NNH]RuH(PPh_3)$ (**11**).

Atom	Atom	Distance (Å)	Atom	Atom	Distance (Å)
Ru(1)	P(1)	2.3189(6)	Ru(1)	N(1)	2.381(2)
Ru(1)	P(2)	2.3302(6)	Ru(1)	N(2)	2.315(2)
Ru(1)	P(3)	2.2434(6)	Ru(1)	H(50)	1.61(2)

References begin on page 184

Atom	Atom	Atom	Angle (°)	Atom	Atom	Atom	Angle (°)
P(1)	Ru(1)	P(2)	166.74(2)	P(3)	Ru(1)	N(2)	101.25(5)
P(1)	Ru(1)	P(3)	94.98(2)	N(1)	Ru(1)	N(2)	85.87(7)
P(2)	Ru(1)	P(3)	95.93(2)	P(1)	Ru(1)	H(50)	92.3(7)
P(1)	Ru(1)	N(1)	84.85(4)	P(2)	Ru(1)	H(50)	95.9(7)
P(1)	Ru(1)	N(2)	86.71(5)	P(3)	Ru(1)	H(50)	86.0(8)
P(2)	Ru(1)	N(1)	85.26(5)	N(1)	Ru(1)	H(50)	86.9(8)
P(2)	Ru(1)	N(2)	83.78(5)	N(2)	Ru(1)	H(50)	172.8(8)
P(3)	Ru(1)	N(1)	172.86(5)				

The geometry of **11** is best described as distorted octahedral with the two phosphine donors of the macrocyclic ligand approximately *trans* disposed (166.74(2) °) occupying the axial positions. A mirror plane of symmetry is contained within the equatorial plane of the molecule which bears the amide, amine, hydride and triphenylphosphine ligands resulting in overall C_s symmetry for complex **11**. The ruthenium-to-phosphorus distances for the [P_2NNH] ligand are elongated with respect to that of the triphenylphosphine ligand, a feature that can be attributed to the strong *trans*-influence of phosphine donors. Although the amino hydrogen atom was not located, the longer Ru(1)-N(1) bond distance of 2.381(2) Å (compared to 2.315(2) Å for Ru(1)-N(2)) indicates that the amine ligand is positioned *cis* to the hydride.

The solution NMR data is consistent with the solid-state molecular structure of complex **11**. The $^{31}P\{^1H\}$ spectrum, for instance, contains a doublet at δ 35.0 corresponding to the two equivalent phosphines of the [P_2NNH] ligand set and a triplet at δ 72.0 for the triphenylphosphine ligand ($^2J_{PP}$ = ~ 40 Hz). The resonance for the triphenylphosphine ligand in **11** is located approximately 80 ppm units downfield from that in complex **2** in accordance with hydrogenolysis of the *ortho*-metalated aryl group.

The C_s symmetry of complex **11** is reflected in its ^1H NMR spectrum which shows four resonances each for the silyl methyl and methylene protons of the macrocyclic ligand. The aryl protons of complex **11** are located between δ 6.8 and δ 7.5, and the amino proton is observed as a singlet at δ 1.7. Unfortunately, neither the ^1H NMR nor X-ray data provide any structural information in regards to the direction in which the amino proton is oriented. Two possibilities exist: it may align towards the amide nitrogen atom (as in **2**) or it may point in the direction of the

References begin on page 184

hydride ligand (as was shown for complex **10**). Reactivity studies with D_2 gas (to be discussed later) help shed some light on this matter. The ruthenium hydride signal in **11** occurs as an overlapping doublet of triplets at δ -15.3; this pattern arises from coupling of the hydride to the two equivalent phosphorus-31 nuclei of the [P_2NNH] ligand ($^2J_{PH}$ = 16.6 Hz) and the phosphorus-31 nucleus of the PPh_3 ligand ($^2J_{PH}$ = 29.2 Hz). The high-field region of the ^{1}H NMR spectrum containing the hydride resonance is shown in Figure 3.10.

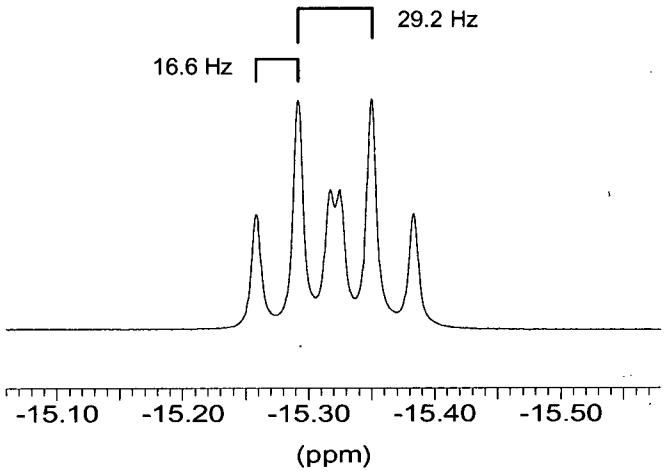

Figure 3.10. Hydride region of the 500 MHz ^{1}H NMR spectrum of [P_2NNH]RuH(PPh_3) (**11**) recorded in benzene-d_6 at 500 MHz and 298 K.

(ii) Reaction of 11 with deuterium gas and evidence for proton-hydride exchange

The reaction of **2** with H_2 gas (1 atmosphere) is complete within a few hours at room temperature; further reactivity was not observed for extended reaction periods or under four atmospheres of H_2 pressure. This finding is not unexpected given the stability of **10** towards the heterolytic activation of H_2. In addition, the related complexes [PNHP]RuCl($C_6H_4PPh_2$) and [PNP]Ru($C_6H_4PPh_2$) were also shown to react with only one equivalent of H_2 per metal centre.[50]

Exposure of **11** to an atmosphere of D_2 gas, however, results in the incorporation of deuterium into the hydride and amino proton sites generating the species **11**-d_2. This result is

References begin on page 184

compatible with the existence of a protonic-hydridic interaction in **11** that leads to the formation of a transient η^2-H_2 complex (**B** and **C** respectively in Scheme 3.4). Exchange of H_2 by D_2 in the intermediate **C** results in the simultaneous incorporation of deuterium into the hydride and proton environments. This mechanism is analogous to that postulated for the incorporation of deuterium into the N-*H* site in complex **10**. Further evidence for this behaviour was provided by the two-dimensional EXSY[107,108] spectrum of complex **11**. A cross-peak between the N-*H* and Ru-*H* sites was observed indicating that these two nuclei are in chemical exchange. Rotation of the H_2 ligand in the intermediate species by 180° allows for this to occur.

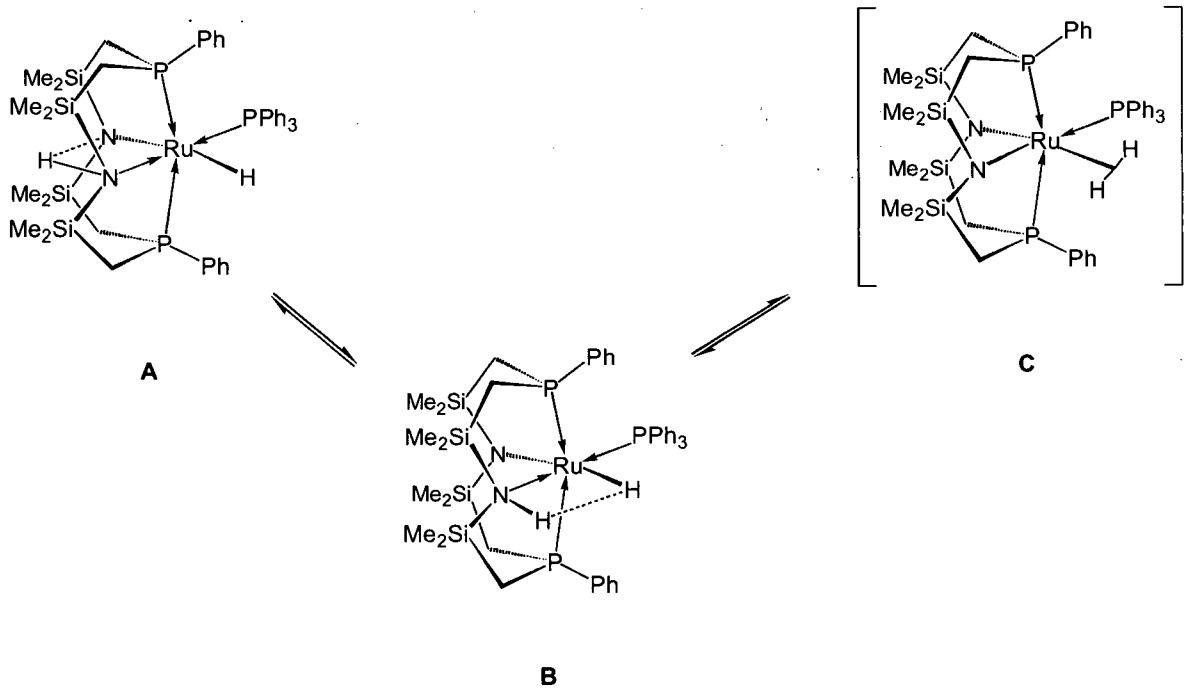

Scheme 3.4

The presence of complex **A** in Scheme 3.4, which contains a hydrogen bond between the amino proton and the amido nitrogen atom, is also possible. If it does exist it must be in equilibrium with **B** as evidenced by the rapid incorporation of deuterium in complex **11**. This implies that the relative strengths of the NH···NRu (in **A**) and NH···HRu (in **B**) interactions would be approximately equal. A related study involves the H/D exchange reactions of the iridium complex $[Ir(H)_2(HNC_5H_4S)_2(PCy_3)_2]BF_4$, which contains two IrNH···HN bonds.[48] It was proposed that H/D exchange in this system proceeds via initial intramolecular proton transfer from NH to

References begin on page 184

IrH to give a dihydrogen tautomer that exchanges readily with D_2 gas. Interestingly, when the reaction of the iridium complex was performed in THF no incorporation of deuterium was observed. In this case, disruption of the proton-hydride interaction in favour of the stronger NH···O hydrogen bond effectively intercepts the exchange process.

3.4 Catalytic Hydrogenation Studies With $[P_2NNH]Ru(H_2)H$ (10) and $[P_2NNH]RuH(PPh_3)$ (11)

As was described in the Introduction section of Chapter 2, one of the goals of this project was to prepare ruthenium(II) complexes that contain *cis*-coordinated hydride and amine ligands via the hydrogenolysis of the ruthenium-amide bonds of precursor complexes bearing the macrocyclic $[P_2N_2]$ ligand. Various coordinatively saturated ruthenium(II) complexes that bear amine and hydride ligands in *cis* positions have been used as effective hydrogenation catalysts for imine substrates operating by the bifunctional mechanism.[109-111] Our intention was to seek further evidence for this unique catalytic process, which does not involve substrate coordination to the metal centre, a condition that is of fundamental importance in most catalytic systems. The synthesis and isolation of the amino-hydride complexes **10** and **11** allowed us to investigate their potential as precursors for the catalytic hydrogenation of imines and to possibly identify the mode of catalysis. For the purpose of this study, benzylidene aniline (PhNCHPh) was utilized as the imine substrate; this substrate has been employed in other systems and therefore a comparison of catalytic activity would be possible. A summary of the catalytic hydrogenation studies performed with complexes **10** and **11** is given in Table 3.3.

Since the bifunctional mechanism involves substrate "recognition" and outer-sphere coordination due to the polar nature of the substrates involved, it was anticipated that the presence of the electrostatic proton-hydride bonding interactions in complexes **10** and **11** may facilitate the transfer of these two atoms directly to the substrate. In performing stoichiometric reactions of **11** with benzylidene aniline, however, no formation of the hydrogenation product benzylphenyl amine was observed, even when solutions of the reaction mixture were heated for extended periods. The lack of reactivity of the imine substrate with **11** may be a result of the stability of **11** with respect to the loss of H_2. Heating solutions of **11** under static vacuum showed no formation of complex **2**,

References begin on page 184

the expected product of H_2 loss. The reduction of benzylidene aniline (stoichiometric or catalytic) with complex **11** under one to four atmospheres of hydrogen gas pressure was also unsuccessful.

The hydrogenation of benzylidene aniline with complex **10** was also attempted. Since complex **11** was unable to transfer its amino proton and hydride to the imine substrate via an outer-sphere interaction it seemed unlikely that this would take place with complex **10**. Transition metal dihydrogen-hydride complexes have been shown to serve as catalyst precursors for alkene and alkyne hydrogenation.[12] The labile nature of the H_2 ligand in these systems provides a site for substrate coordination and the presence of a hydride ligand allows for a viable catalytic pathway. The coordinated H_2 ligand in **10** has been shown to be quite labile. The addition of cyclooctadiene to solutions of **10**, for instance, result in the formation of **9** and displacement of H_2 by triphenylphosphine generates complex **11**. Due to the lability of the dihydrogen ligand in **10** benzylidene aniline could likewise displace this ligand, coordinate to the metal centre, and possibly undergo catalytic hydrogenation either by pathway **A** or **B** in Scheme 3.3. However, even under four atmospheres of hydrogen pressure less than 5 % conversion (as determined by integration of ^{1}H NMR resonances) to benzylphenyl amine resulted when utilizing complex **10** as a precursor.

The catalytic hydrogenation of olefinic substrates (cyclooctadiene, cyclooctene and 1-hexene) was successfully accomplished with complex **10** achieving yields greater than 95 % (see Table 3.3). Complex **11** showed no hydrogenation reactivity towards the same olefin substrates; the triphenylphosphine ligand in **11** is strongly coordinated to the metal centre not allowing for an open site for substrate binding even under catalytic conditions.

References begin on page 184

Table 3.3. Catalytic hydrogenation studies utilizing complexes **10** and **11** as precursors.

		% Conversion	
Entry	Substrate	**10**	**11**
1	Benzylidene aniline	5	0
2	Cyclooctadiene	95	0
3	Cyclooctene	95	0
4	1-hexene	99	0

Reactions were carried out at 25°C and 4 atm H_2 pressure in toluene as the solvent for entry 1; entries 3-4 were done in neat substrate. A catalyst loading of 2 mol % was employed in each case. Conversions were determined after 48 h by ^1H NMR analysis of the crude reaction mixture

3.5 Hydrogenation of *exo*- and *endo*-[NPNH]Ru(1-3:η^3-5,6:η^2-C_8H_{11}) (*exo*-3 and *endo*-3)

(i) Reaction of an equilibrium mixture of *exo*-3 and *endo*-3 with hydrogen gas

When a toluene solution containing an equilibrium mixture of the ruthenium amide complexes *exo*-**3** and *endo*-**3** is exposed to an atmosphere of hydrogen gas, three ruthenium hydride products and cyclooctane (C_8H_{16}) are formed as shown in Scheme 3.5. The $^{31}P\{^1H\}$ NMR spectrum of the crude product mixture when the reaction is performed under four atmospheres of H_2 pressure shows three singlets at δ 47.7, δ 40.2 and δ 32.2 (assigned to **12**, **13** and **14**, respectively) in the approximate ratio of 2:1:1. These ratios vary depending on the hydrogen gas pressure and the solvent employed. For example, under one atmosphere of hydrogen pressure the hydride complex at δ 47.7 still forms as the major species with a product distribution around 5:1:1. In the following sections we outline the conditions that allow for the separation, purification and characterization of each of these three hydride products.

References begin on page 184

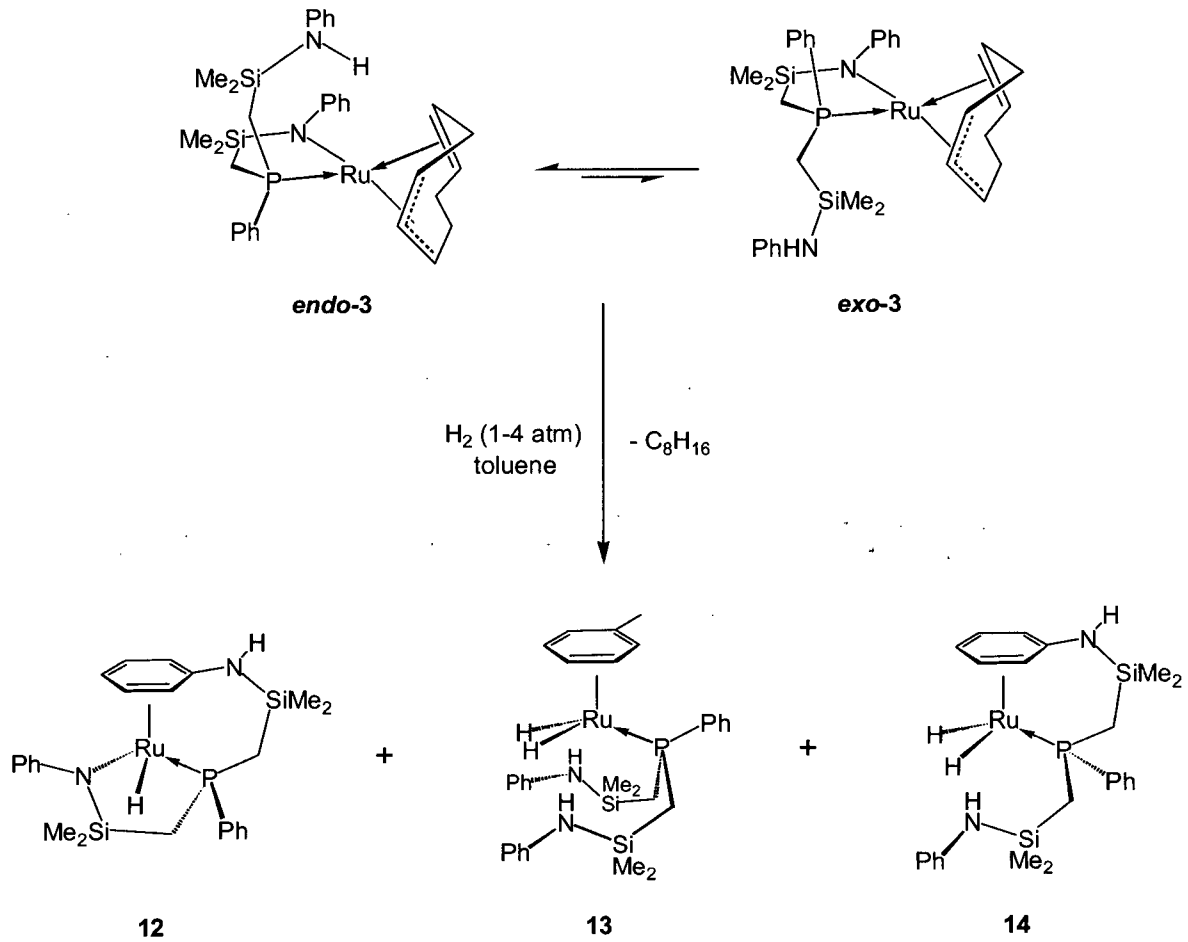

Scheme 3.5

(ii) Isolation and characterization of [NPN(H)(η^6-C_6H_5)]RuH (12)

Addition of hydrogen gas (1 atm) to a solution of *exo*-**3** and *endo*-**3** in toluene results in an immediate change in colour from red to orange. The solution was stirred at room temperature for 30 minutes and the solvent was then removed *in vacuo* until an oily residue remained. Subsequent addition of hexanes caused the deposition of the orange micro-crystalline solid [NPN(H)(η^6-C_6H_5)]RuH (**12**) in approximately 50% yield (Scheme 3.5).

The $^{31}P\{^1H\}$ NMR spectrum of complex **12** consists of a singlet at δ 47.7. The 500 MHz ^1H NMR spectrum contains four peaks for the silyl methyl protons of the [NPN] ligand backbone

References begin on page 184

between δ -0.6 and δ 0.5. The presence of four different silyl methyl resonances is indicative of an unsymmetrical ligand environment about the metal centre. The ligand methylene protons appear as a broad multiplet centered at δ 1.2. The hydride region of the spectrum consists of a doublet due to coupling with the phosphine ligand at δ -7.7 ($^2J_{PH}$ = 47 Hz). A singlet at δ 1.6 has been assigned as the amino proton; deuterium labelling of the N-*H* site can be accomplished by the addition of one equivalent of base (e.g. $LiN(SiMe_3)_2$) to **12** followed by NEt_3·DCl to yield the species [NPN(D)(η^6-C_6H_5)]RuH (**12**-d_1). The most telling feature in the ^{1}H NMR spectrum are the peaks observed in the range δ 3.5 to δ 5.8; these have been assigned as the protons of an η^6–coordinated amino phenyl ring. Integration data, a ^{1}H-^{1}H COSY analysis and proton-proton coupling patterns allowed for the *ortho*-, *meta*- and *para*-positions to be unequivocally identified. The remaining amido-phenyl and phosphine-phenyl signals appear downfield at expected positions between δ 6.6 and δ 7.9.

The solution NMR studies for complex **12** suggest the structure depicted in Scheme 3.5 in which the phenyl ring of the amino side-arm of the [NPNH] ligand has coordinated to the ruthenium centre. Elemental analysis supports this formulation as does the solid-state molecular structure, which has been determined by a single crystal X-ray diffraction study. The structure of **12** is shown in Figure 3.11 and selected bond lengths and angles can be found in Table 3.4. The complex adopts a pseudo-tetrahedral, three legged piano-stool coordination geometry with C_1 symmetry. The ruthenium in complex **12** is a stereogenic centre bound by four different ligands. The NMR data indicate the formation of only one diastereomer. Deviations from an ideal tetrahedral geometry arise due to the constraints of the chelating [NPNH] donor set. The Ru(1)-N(1) bond length of 2.138(2) Å in **12** is similar to the ruthenium-amide bond distance of 2.121(3) Å reported in the related ruthenium(II) arene complex (η^6-C_6Me_6)Ru(Ph)(PMe_3)(NHPh).[112] It is longer, however, than the measured ruthenium-amide distance in *endo*-**3** (2.019(2) Å); this is most likely a consequence of the coordinative and electronic saturation at the metal centre in **12**. The ruthenium-to-carbon distances for the bound amino-phenyl group indicate that it is coordinated in a η^6-fashion.

References begin on page 184

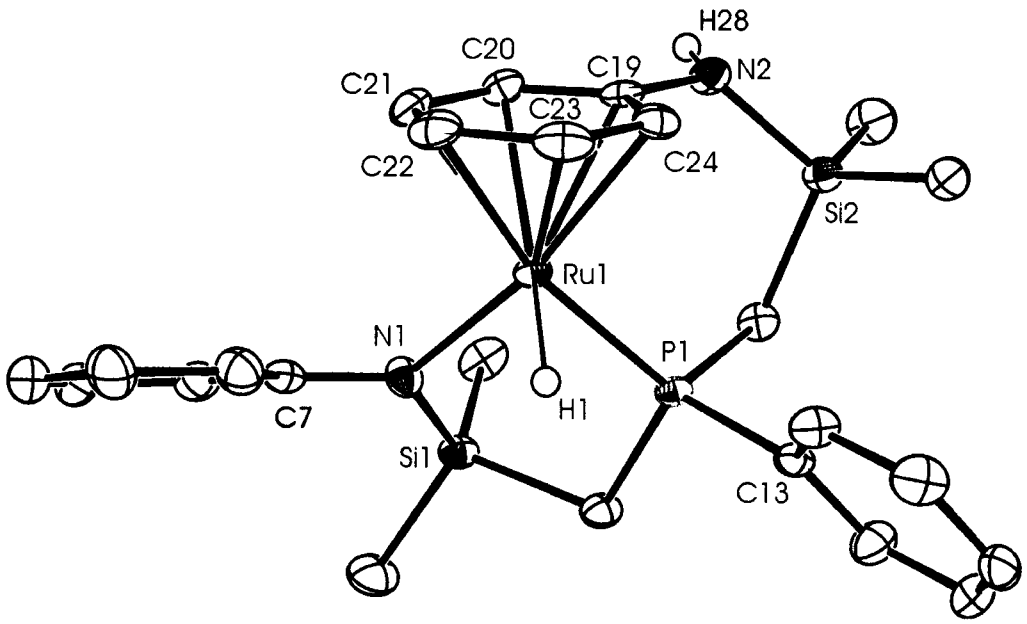

Figure 3.11. An ORTEP representation of the solid-state molecular structure of [NPN(H)(η^6-C_6H_5)]RuH (**12**) as determined by X-ray crystallography with thermal ellipsoids shown at the 50 % probability level. The ruthenium hydride, H(1), and amino proton, H(28), were located and refined isotropically.

Table 3.4. Selected bond lengths and bond angles in the complex [NPN(H)(η^6-C_6H_5)]RuH (**12**).

Atom	Atom	Distance (Å)	Atom	Atom	Distance (Å)
Ru(1)	P(1)	2.708(6)	Ru(1)	H(1)	1.50(3)
Ru(1)	N(1)	2.138(2)	N(2)	H(28)	0.80(3)
Ru(1)	C(19)	2.307(2)	C(19)	C(20)	1.432(3)
Ru(1)	C(20)	2.214(2)	C(19)	C(24)	1.403(4)
Ru(1)	C(21)	2.168(2)	C(20)	C(21)	1.408(4)
Ru(1)	C(22)	2.245(2)	C(21)	C(22)	1.414(4)
Ru(1)	C(23)	2.251(2)	C(22)	C(23)	1.403(4)
Ru(1)	C(24)	2.322(2)	C(23)	C(24)	1.420(4)

Atom	Atom	Atom	Angle (°)	Atom	Atom	Atom	Angle (°)
P(1)	Ru(1)	N(1)	87.97(6)	P(1)	Ru(1)	C_{ring}[a]	131.16
P(1)	Ru(1)	H(1)	75(1)	N(1)	Ru(1)	C_{ring}	128.77
N(1)	Ru(1)	H(1)	86(1)	H(1)	Ru(1)	C_{ring}	129.96

[a] C_{ring} represents the centroid of the coordinated aryl ring

References begin on page 184

(iii) Isolation and characterization of $[NPNH_2]Ru(H)_2(\eta^6\text{-}C_7H_8)$ (13)

The complex $[NPNH_2]Ru(H)_2(C_7H_8)$ (**13**) can be isolated as yellow crystals in approximately 30% yield by the slow evaporation of the hexanes soluble rinsings from the work-up of compound **12**, as described above. In the dihydride complex **13** the amine side-arms of the $[NPNH_2]$ ligand do not coordinate to the metal either via the nitrogen lone pair or through the amino phenyl groups; rather a solvent molecule of toluene coordinates completing the inner coordination sphere of the metal centre. The activation of aromatic solvents seems to be general. When the reaction is performed in C_6D_6 in an NMR tube a peak at δ 31.9 in the $^{31}P\{^1H\}$ NMR spectrum most likely corresponds to a complex similar to **13**, only this bearing an η^6-bound benzene-d_6 molecule.

Single crystals of **13** were obtained and used in an X-ray diffraction study to determine its solid-state molecular structure. This is depicted in Figure 3.12 and a collection of selected bond lengths and angles are listed in Table 3.5. The solid-state structure clearly shows the coordination of a molecule of toluene and the pendant amine arms of the $[NPNH_2]$ ligand set. Similar to complex **12**, the geometry at ruthenium is pseudo-tetrahedral forming a three legged piano-stool structure. In the solid-state complex **13** exhibits C_1 symmetry.

References begin on page 184

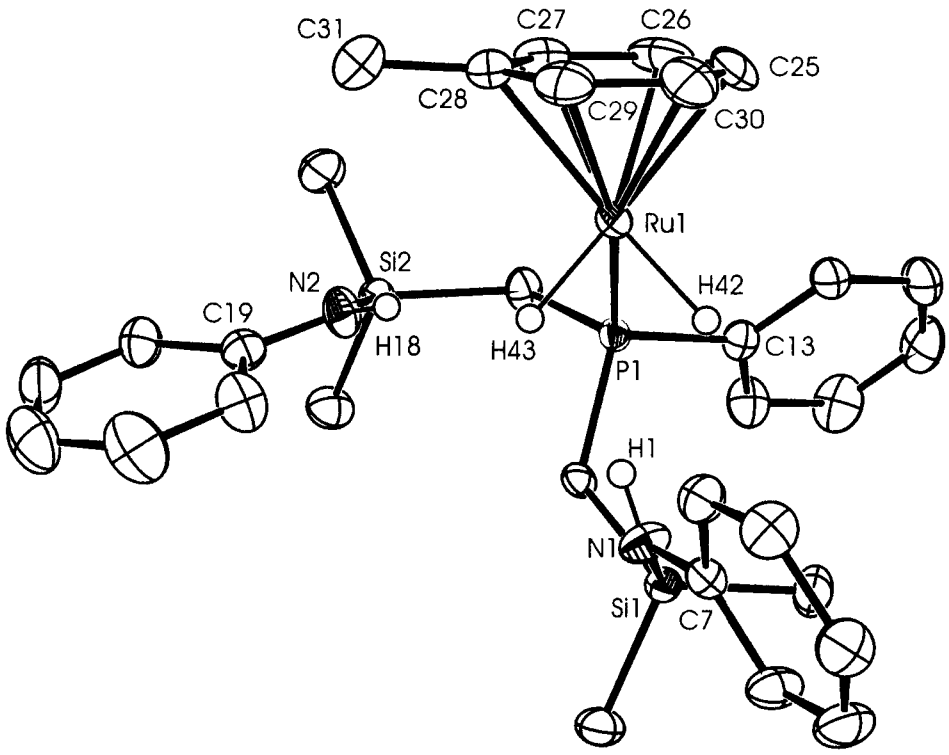

Figure 3.12. The solid-state molecular structure (ORTEP representation, 50 % thermal ellipsoids) of $[NPNH_2]Ru(H)_2(C_7H_8)$ (**13**) as determined by X-ray crystallography. The ruthenium hydrides (H(42) and H(43)) as well as the amino hydrogen atoms (H(1) and H(18)) were all refined isotropically.

Table 3.5. A collection of selected bond lengths and bond angles in the complex $[NPNH_2]Ru(H)_2(C_7H_8)$ (**13**).

Atom	Atom	Distance (Å)	Atom	Atom	Distance (Å)
Ru(1)	P(1)	2.2665(7)	Ru(1)	H(42)	1.61(3)
Ru(1)	C(25)	2.230(3)	Ru(1)	H(43)	1.58(4)
Ru(1)	C(26)	2.248(3)	N(1)	H(1)	0.82(3)
Ru(1)	C(27)	2.268(3)	N(2)	H(18)	0.66(3)
Ru(1)	C(28)	2.287(3)	H(1)	H(42)	2.099
Ru(1)	C(29)	2.243(3)	H(1)	H(43)	2.104
Ru(1)	C(30)	2.226(3)	H(18)	H(43)	2.251

References begin on page 184

Atom	Atom	Atom	Angle (°)	Atom	Atom	Atom	Angle (°)
P(1)	Ru(1)	H(42)	76(1)	H(42)	Ru(1)	C_{ring}	131.44
P(1)	Ru(1)	H(43)	82(1)	H(43)	Ru(1)	C_{ring}	129.24
H(42)	Ru(1)	H(43)	79(2)	Ru(1)	H(42)	H(1)	111.23
P(1)	Ru(1)	C_{ring}[a]	137.47	Ru(1)	H(43)	H(1)	112.23

[a] C_{ring} represents the centroid of the coordinated toluene molecule

An intriguing structural feature evident in the molecular structure of **13** is the approach of the amino protons towards the ruthenium hydrides. In particular, the distance between the amino proton H(1) with hydrides H(42) and H(43) (*ca.* 2.1 Å in each case) can be attributed to an electrostatic attraction resulting in proton-hydride bonding interactions. This can be considered as an intramolecular three-centre hydrogen bond. The similar H···H separations and Ru-H···(NH(1)) angles indicate an equivalent bonding interaction of the proton H(1) with the two hydrides. The species $[ReH_5(PPh_3)_3$·indole] exhibits a similar three-center interaction via the close intermolecular contacts of the indole proton with the two rhenium hydrides.[113] In this complex, however, the proton has a stronger interaction with one of the hydrides over the other as indicated by the shorter proton-hydride distance. The longer intramolecular distance between the amino proton H(18) and the hydride H(43) (2.251 Å) in complex implies a weaker bonding interaction between these nuclei.

The room temperature ^1H and $^{31}P\{^1H\}$ NMR data for complex **13** are diagnostic of an η^6-bound toluene ruthenium dihydride species. In solution, however, **13** displays C_s symmetry implying rapid rotation of the coordinated toluene molecule and unhindered movement of the pendant amine arms of the [$NPNH_2$] ligand. This is evident upon inspection of the ^1H NMR spectrum, which shows only two resonances for the silyl methyl protons at δ 0.0 and δ 0.3. In addition, the two ruthenium hydrides appear as a doublet ($^2J_{PH}$ = 43 Hz) at δ –10.2. A singlet at δ 5.5 that integrates to two protons corresponds to the equivalent amino protons of the dissociated ligand arms. The aromatic protons of the coordinated toluene molecule are upfield shifted between δ 4.8 and δ 5.2 and the toluene methyl protons appear as a singlet at δ 1.9.

Although arene metal dihalide complexes of the type (η^6-arene)$Ru(PR_3)(X)_2$ (where X=halide)[114] are known to exist, to the best of our knowledge there are no reported examples of isolated related species in which X=H. The iridium (III) complex [(η^6-C_6H_6)$Ir(P^iPr_3)H_2$][BF_4] has

References begin on page 184

recently been reported.[115] In this system the coordinated arene moiety is labile and can be replaced with other arene derivatives as well as by weakly coordinating acetone-d_6 ligands. Such complexes have been found to be active catalyst precursors for the hydrogenation of a variety of unsaturated substrates. The bound toluene molecule in **13**, however, does not exhibit the same labile nature. For instance, solutions of **13** in toluene-d_8 or benzene-d_6 show no incorporation of the aromatic NMR solvent; in addition, solutions of **13** in tetrahydrofuran-d_8 indicate no displacement of the coordinated toluene molecule by THF-d_8. The more strongly bound toluene molecule in **13** is also evident by an examination of the upfield shifted aromatic proton resonances. In the iridium complex the proton resonances of the η^6-C_6H_6 ligand are only slightly shifted to δ 6.7. The arene resonances for the toluene molecule in **13**, on the other hand, are found between δ 4.8 and δ 5.2. This upfield shift is a result of a decrease in the deshielding of the aromatic protons indicating that the toluene is strongly coordinated in complex **13**. This feature most likely explains the lack of activity of complex **13** in catalytic hydrogenation studies (to be discussed later).

(iv) Evidence for proton-hydride bonding in the solution structure of complex 13 from measurement of the minimum T_1 values

In an attempt to determine whether or not proton-hydride bonding interactions in **13** are also present in solution, measurement of the T_1(min) relaxation time of the hydride and proton resonances was undertaken. During this study it was noticed that decreasing the temperature of a toluene-d_8 solution of **13** resulted in broadening of both the hydride and proton resonances; below 193 K the doublet for the hydride signal could no longer be resolved. Broadening of the signals at lower temperatures can be attributed to efficient dipolar relaxation between closely spaced Ru-*H* and N-*H* nuclei. This observation suggests that at low temperatures the solution structure of **13** approaches that found in the solid-state with close proton-hydride contacts, however, a C_1 symmetric solution structure was never recognized. The resonance for the amino protons experiences a downfield shift from δ 5.6 at 280 K to δ 6.5 at 200 K providing further evidence for proton-hydride bonding interactions in **13**. Perturbation of the proton resonance is typical for complexes containing these unconventional hydrogen bonds.[56,101] The chemical shift for the hydride resonance in **13** did not display a significant dependence on temperature.

References begin on page 184

Measurement of the minimum relaxation times for the hydride and proton nuclei in complex **13** allowed for an estimation of the average RuH···HN distances in solution. The hydrides were found to have a short T_1(min) time of 0.366 s at 260 K and 500 MHz (Table 3.6). This corresponds to a relaxation rate of 2.73 s^{-1}. When the dipolar relaxation contributions of the *cis* hydrides, separated by 2.03 Å, are accounted for (1.11 s^{-1}), this results in a relaxation rate of 1.62 s^{-1} due to dipole interactions with the amino protons. This corresponds to a calculated H···H distance of about 1.9 Å. In the case of the amino protons the T_1(min) value was determined to be 0.386 s. These protons are close to only two dipolar nuclei: the ^{14}N nucleus and the ruthenium hydrides. In order to obtain an approximation of the relaxation effects due to the ^{14}N nucleus the T_1(min) value of the N-*H* nuclei in the protonated [$NPNH_2$] ligand (**15**) was determined. This was found to be 0.614 s at 240 K (relaxation rate = 1.63 s^{-1}). These results suggest that the hydrides are located approximately 2.0 Å (relaxation rate contribution of 0.96 s^{-1}) from the amino protons.

The relaxation data for the proton and hydride nuclei in complex **13** gave similar RuH···HN distances (~ 2.0 and 1.9 Å, respectively) indicative of weak protonic-hydridic bonding interactions in solution. These estimated distances also correspond well to the proton-hydride separations evident in the solid-state molecular structure of **13**. It is important to point out that since a C_1 symmetric structure was never observed in solution the close proton-hydride contacts correspond to an average of all the hydride and proton environments.

Table 3.6. T_1(min) values measured for the hydride and pendant amino proton nuclei in complexes **12**, **13**, **14** and **15** in toluene-d_8 and 500 MHz.

Complex	T_1(min) (s) Ru-*H*	N-*H*	Temperature (K)
[NPN(H)(η^6-C_6H_5)]RuH (**12**)	0.697	-	250
[$NPNH_2$]Ru($H)_2$(C_7D_8) (**13**)	0.366	0.386	260
[$NPNH_2$(η^6-C_6H_5)]RuH_2 (**14**)	0.334	0.344	246
[$NPNH_2$] (**15**)	-	0.614	240

The ^1H NMR studies (variable temperature and relaxation data) provided evidence for weak proton-hydride bonding interactions in the solution structure of complex **13**. Since this bonding scheme has been proposed to lead to hydrogen/deuterium exchange processes in complexes **10** and **11** we investigated the reactivity of complex **13** with D_2 gas. Exposure of

References begin on page 184

solutions of **13** to an atmosphere of deuterium gas, however, resulted in less than 10 % incorporation into both the N-*H* and Ru-*H* sites after 24 hours. In a related example, the hydride ligand and the proton on the pyridinium ring in the complex $[IrH(\eta^1\text{-}SC_5H_4NH)(\eta^2\text{-}SC_5H_4N)(PPh_3)_2]BF_4$ do not undergo any significant exchange with D_2 even though the presence of an Ir*H*···*H*N interaction has been ascertained.[116]

(v) Isolation and characterization of $[NPNH_2(\eta^6\text{-}C_6H_5)]Ru(H)_2$ (14)

Compound **14** forms when the reaction of **3** with hydrogen gas is performed in toluene as the solvent, however, it is most easily isolated with the use of a non-aromatic solvent such as pentane, which eliminates the formation of **13**. A change in colour from red to orange-brown is observed with the immediate formation of an orange insoluble solid when a slurry of **3** in pentane is exposed to four atmospheres of hydrogen gas. The orange solid was separated by filtration and was identified as the hydride complex **12** (50% isolated yield) by ^1H and $^{31}P\{^1H\}$ NMR spectroscopy. Removal of the solvent from the soluble fraction of the reaction mixture results in the isolation of complex **14** as a brown solid.

The room temperature NMR spectra gave much insight into the structure of **14** (see Scheme 3.5). The phosphine resonance occurs as a singlet at δ 40.2 in the $^{31}P\{^1H\}$ NMR spectrum. An unsymmetrical $[NPNH_2]$ ligand arrangement can be deduced from the four silyl methyl proton resonances ranging from δ -0.5 to δ 0.3 in the ^1H NMR spectrum. Peaks corresponding to a coordinated arene moiety exist between δ 4.7 and δ 5.6; since the reaction was performed in a non-aromatic solvent this is due to coordination of an amino phenyl group of the $[NPNH_2]$ ligand. The *ortho*-, *meta*- and *para*-positions were assigned based on integration as well as ^1H-^1H COSY data. The amino proton adjacent to the bound arene moiety exists as a singlet at δ 1.6 (this is the same location in which the amino proton of **12** is located). The remaining singlet at δ 5.7 consequently corresponds to the amino proton of the dissociated ligand arm, which is in a similar location as the pendant N-*H* protons in **13**. Two doublet of doublets centered at δ –9.9 and δ –10.2 indicates the presence of two inequivalent hydrides. Figure 3.13 illustrates this region of the ^1H NMR spectrum. The magnitude of coupling between the phosphorus nuclei and the two hydrides was measured to be 40 Hz and 43 Hz, while a coupling constant of 6 Hz was measured between the two hydrides. The inequivalency of the ruthenium hydrides is supported by the

References begin on page 184

proposed structure, which has C_1 symmetry. Attempts at obtaining X-ray quality crystals for a solid-state structural analysis of compound **14** resulted in the deposition of an orange crystalline solid that was determined by NMR data to be complex **12**.

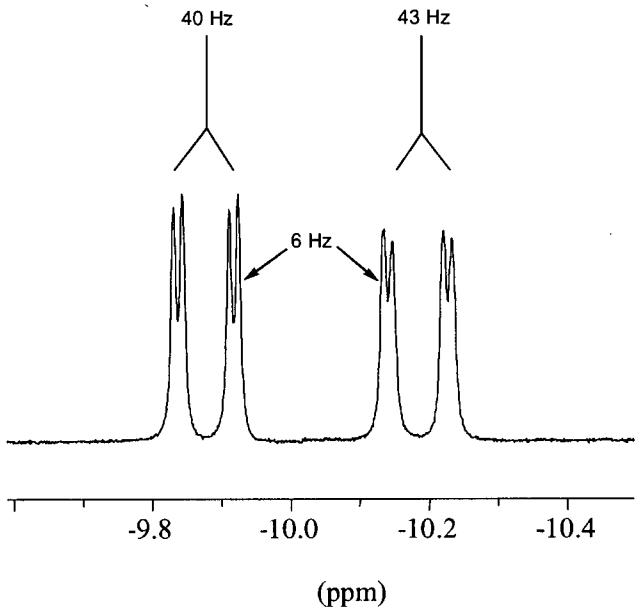

Figure 3.13. High-field region of the 500 MHz ^{1}H NMR spectrum highlighting the hydride resonances of the complex [NPNH$_2$(η^6-C$_6$H$_5$)]Ru(H)$_2$ (**14**) in benzene-d_6.

(vi) Proposed mechanism for the formation of the three ruthenium hydride complexes 12, 13 and 14

The reaction of complex **3** with one atmosphere of hydrogen gas proceeds rapidly at room temperature. Within seconds the initial red-coloured solutions turn orange indicating that the reaction is complete. Because of this, no intermediate species could be identified and this precluded a detailed mechanistic study into the reaction of **3** with H_2. A plausible pathway can be postulated, however, based on various qualitative observations of the reaction products. The key intermediate that allows for a rational explanation for the formation of the three hydride products **12**, **13** and **14** from **3** is a coordinatively unsaturated ruthenium monohydride complex, shown as [NPNH]RuH in Scheme 3.6. Although this species must contain an amide, phosphine and hydride

References begin on page 184

ligand no structural information is implied. One reason for this is because the chirality of the phosphine ligand will be inverted depending on which diastereomer of **3** (*endo* or *exo*) reacts with H_2. The stereochemical outcome of this effect will be addressed later in this section.

The instantaneous reaction of **3** with dihydrogen is most likely a consequence of its coordinative unsaturation. In contrast, the reaction of the six-coordinate complex **1** with hydrogen gas proceeds over a period of several hours. Upon coordination, the H_2 molecule may be cleaved heterolytically transferring a proton equivalent to the π-allyl donor of the cyclooctadienyl ligand, thus affording a ruthenium monohydride cyclooctadiene complex (Scheme 3.6). Since complex **12** is formed during the hydrogenation process and the fact that it contains an intact ruthenium-amide bond and one hydride ligand provides direct proof that initial heterolysis of H_2 does not involve the Ru-N unit of **3**. From this point, hydride transfer followed by hydrogenolysis by another equivalent of H_2 can generate a ruthenium monohydride cyclooctene intermediate; these steps are repeated until cyclooctane (C_8H_{16}) has been eliminated and the unsaturated species "[NPNH]RuH" is formed. This route resembles pathway **A** in Scheme 3.3 for the conversion of **9** into **10**.

References begin on page 184

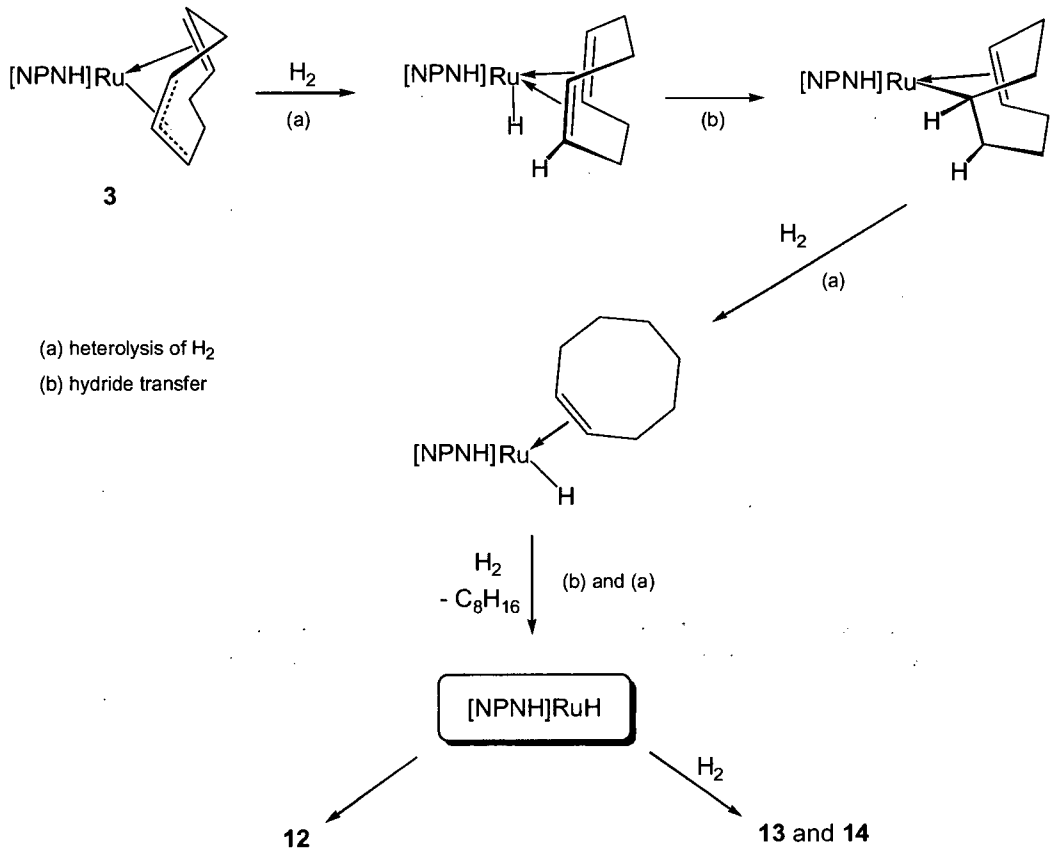

Scheme 3.6

The monohydride complex **12** can form from the "[NPNH]RuH" intermediate simply by coordination of the phenyl group of the pendant amine ligand. It is not unexpected that this donor does not coordinate to the metal centre via the nitrogen lone pair of electrons given the poor Lewis basicity of this group. On the contrary, donation of six-electrons from the aromatic group allows for a stable, 18-electron species to be formed. Coordination of the phenyl group can occur to opposite faces of the metal centre depending on whether the *exo* or *endo* diastereomer of **3** undergoes hydrogenation. This would result in the production of **12** as a mixture of enantiomers. Complex **12** is an intriguing species since it is a chiral metal complex that contains a stereogenic metal centre and a chiral phosphine ligand. The two possible enantiomers that may result are *SR*-**12** and *RS*-**12**, as shown in Figure 3.14. The configurational designations refer to the ruthenium centre and the phosphorus centre, respectively.

References begin on page 184

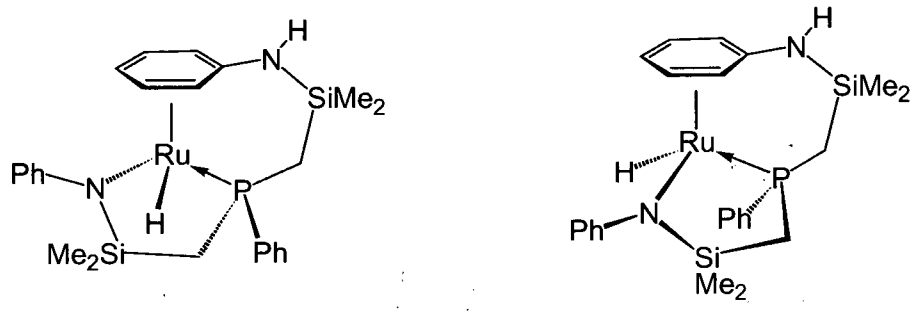

***SR*-12** ***RS*-12**

Figure 3.14. The two possible enantiomers of complex **12** that may form from the hydrogenation of complex **3**. The configurational designations refer to the metal centre and the phosphorus atom, respectively.

Conceptually, complex **14** can be envisioned as forming via the heterolytic cleavage of a molecule of H_2 by the amide ligand in complex **12**. This, however, is not the mechanism by which it is formed as is shown in Scheme 3.7. Exposing compound **12** to hydrogen gas (1-4 atm) for prolonged periods results in the formation of the ruthenium dihydride **14** in very small quantities (< 2%). This implies that once hydrogenation of the cyclooctadienyl ligand occurs in the precursor complex **3**, and prior to coordination of the amino phenyl ring (which results in the formation of **12**), heterolysis of H_2 by the remaining ruthenium amide linkage in "[NPNH]RuH" must occur. This results in a ruthenium dihydride complex with two pendant amine ligands; coordination of the phenyl group of one of these ligands affords complex **14**. The formation of complex **13** would proceed in a similar fashion as **14**, however, instead of coordination of an amino phenyl group, an aromatic solvent molecule coordinates. In this case, both diastereomers of **3** will give rise to a single product (since the phosphine ligand and ruthenium centre are no longer chiral).

We wished to determine if there was preferential coordination of one of the amine ligands in complex **14**. For example, does the pendant amine ligand in **3** coordinate to the metal via its phenyl group, does it remain dissociated, or do both situations take place. It was anticipated that hydrogenation of the amino-deuterated complex **3**-d_1 could allow for a distinction between these possibilities by integration of the ^{1}H NMR signals of the two distinct amino proton environments in complex **14**.

References begin on page 184

For the purpose of this study the reaction was performed at four atmospheres of H_2 pressure (to maximize the formation of **14**) in tetrahydrofuran-d_8 as the solvent (to eliminate the formation of **13**). The N-*H* resonance of the phenyl-bound amine ligand integrated to one proton environment per metal centre suggesting that the pendant (deuterated) side-arm in **3**-d_1 ends up as the dissociated ligand arm in **14**. It was puzzling, therefore, to observe a resonance at δ 5.7 corresponding to the N-*H* proton of the dissociated amine ligand. An accurate integration of this signal was difficult because it was overlapping with proton resonances of the coordinated arene moiety. This finding can be rationalized by a hydrogen/deuterium exchange process that takes place at some point during the hydrogenation of the cyclooctadienyl ligand. As portrayed in Scheme 3.6, the postulated mechanism for this process involves metal-hydride intermediates; it may be possible that the presence of deuteron-hydride bonding interactions in such intermediate species could allow for the exchange to take place. According to this proposal the N-*H* site in complex **12** should also contain a proton rather than a deuteron under identical reaction conditions, and this was indeed found to be the case. Unfortunately, this procedure did not allow for the determination of whether preferential coordination of one of the amine ligands occurs. If both ligands are assumed to have an equal opportunity to coordinate to the metal centre through the phenyl ring then an enantiomeric mixture of complex **14** would be expected.

References begin on page 184

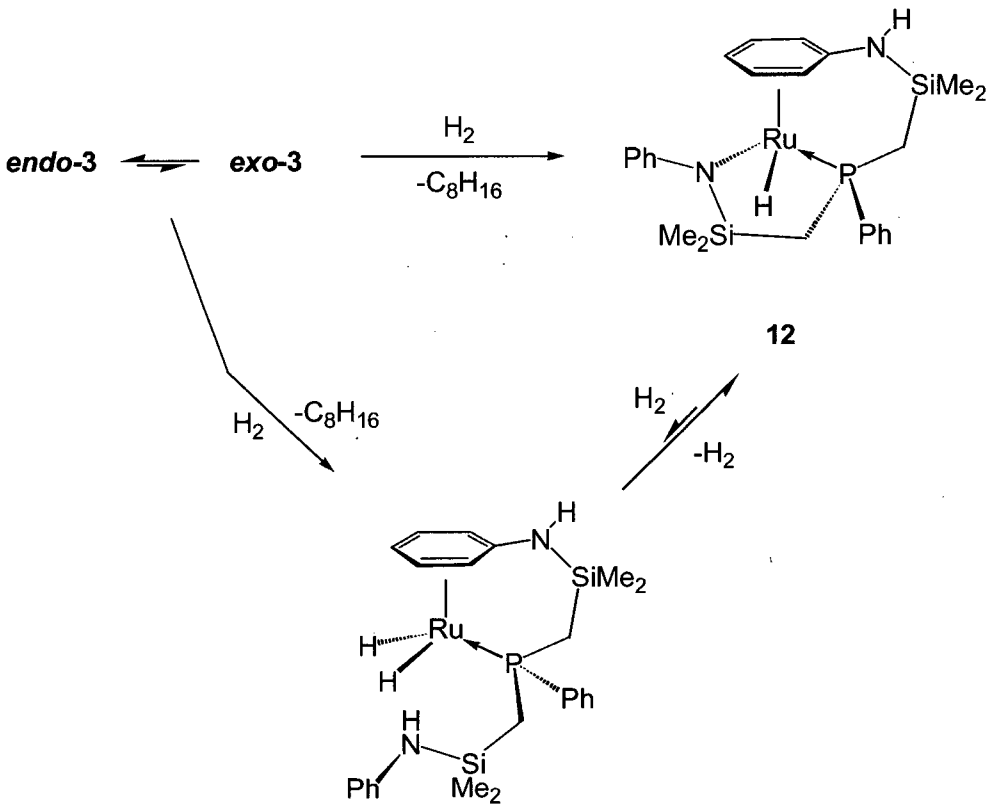

Scheme 3.7

(vii) Loss of H_2 from complex 14 to give complex 12

As shown in Scheme 3.7, solutions of **14** slowly evolved hydrogen gas to generate the mono-hydride, mono-amide species **12**. This explains the isolation of **12** during crystallization attempts of **14**. Similar reactivity has been observed in the complex *trans*-$Ru(H)_2(NH_2CMe_2CMe_2NH_2)$(R-binap) (binap = binapthyl), which slowly loses H_2 in the solid-state or in solution to afford the hydridoamide complex $Ru(H)(NHCMe_2CMe_2NH_2)$(R-binap).[110] The cationic complex $[RuH(dppm)(\eta^5\text{-}C_5H_4(CH_2)_2NMe_2H^+)]BPh_4$ (dppm = diphenylphosphinomethane) containing a pendant protonated amine ligand has also been shown to lose an equivalent of H_2 resulting in the formation of a cationic ruthenium amine species (see Scheme 3.8).[117] Unlike complexes **12** and **14** both of these systems exhibit reversible loss and

References begin on page 184

addition of dihydrogen. This points to the stability of **12** with respect to hydrogenolysis of the ruthenium-amide bond. The mechanism for the loss of H_2 in the above two examples is believed to occur via intramolecular proton-hydride bonding interactions; the loss of dihydrogen then proceeding via an η^2-H_2 intermediate.

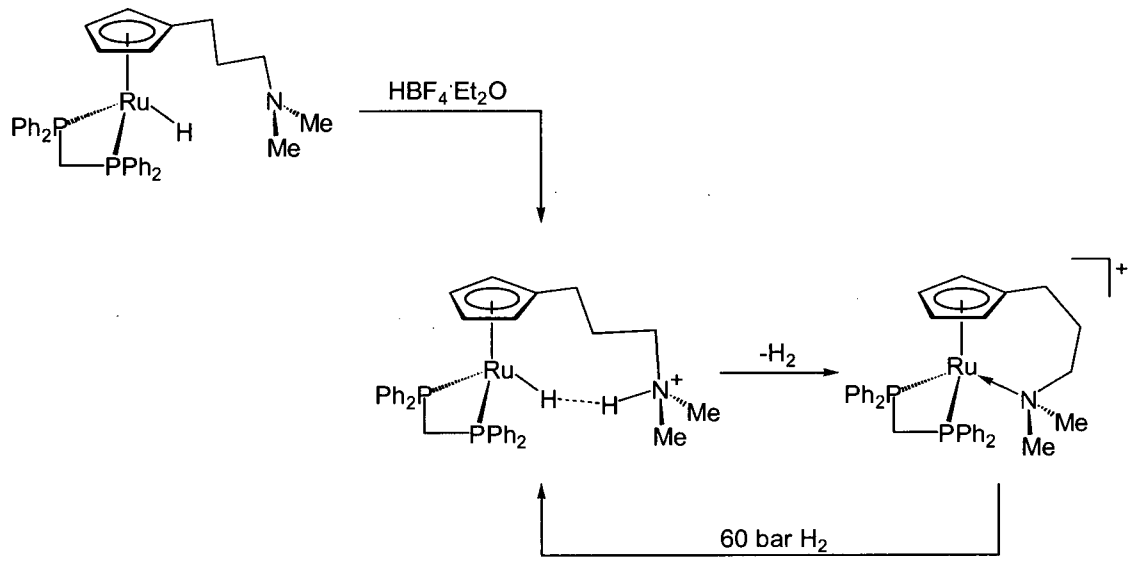

Scheme 3.8

It is possible that a similar pathway is responsible for the loss of H_2 in complex **14** as is shown in Scheme 3.9. Evidence for intramolecular proton-hydride bonding interactions in **14** is given by the short T_1(min) relaxation times for the hydride (0.334 s) and proton (0.344 s) nuclei (see Table 3.6). The inequivalent hydride ligands in **14** had very similar T_1(min) values (within 10 ms) indicating that both come into close contact with the N-*H* proton in solution. The reported value in Table 3.6 is the average T_1(min) value of the two hydride ligands. If the internuclear distance between the two hydride ligands in **14** is assumed to be *ca.* 2.0 Å (based on the fact that the two hydrides in **13** are separated by 2.03 Å) the RuH···HN distance is calculated to be about 1.9 Å. A proton-hydride distance of *ca.* 2.0 Å is calculated based on the relaxation data for the amino protons. The close proton-hydride contacts in **14** could lead to a transient η^2-H_2 species that loses a molecule of dihydrogen, though such an intermediate has not been identified. Interestingly, the isoelectronic complex **13** is stable with respect to loss of H_2 even though there is evidence for proton-hydride bonding in this complex. An alternative route for the conversion of

References begin on page 184

complex **14** into **12** could involve the reductive elimination of H_2 followed by oxidative addition of the N-H bond of the pendant amine ligand. This pathway is also outlined in Scheme 3.9.

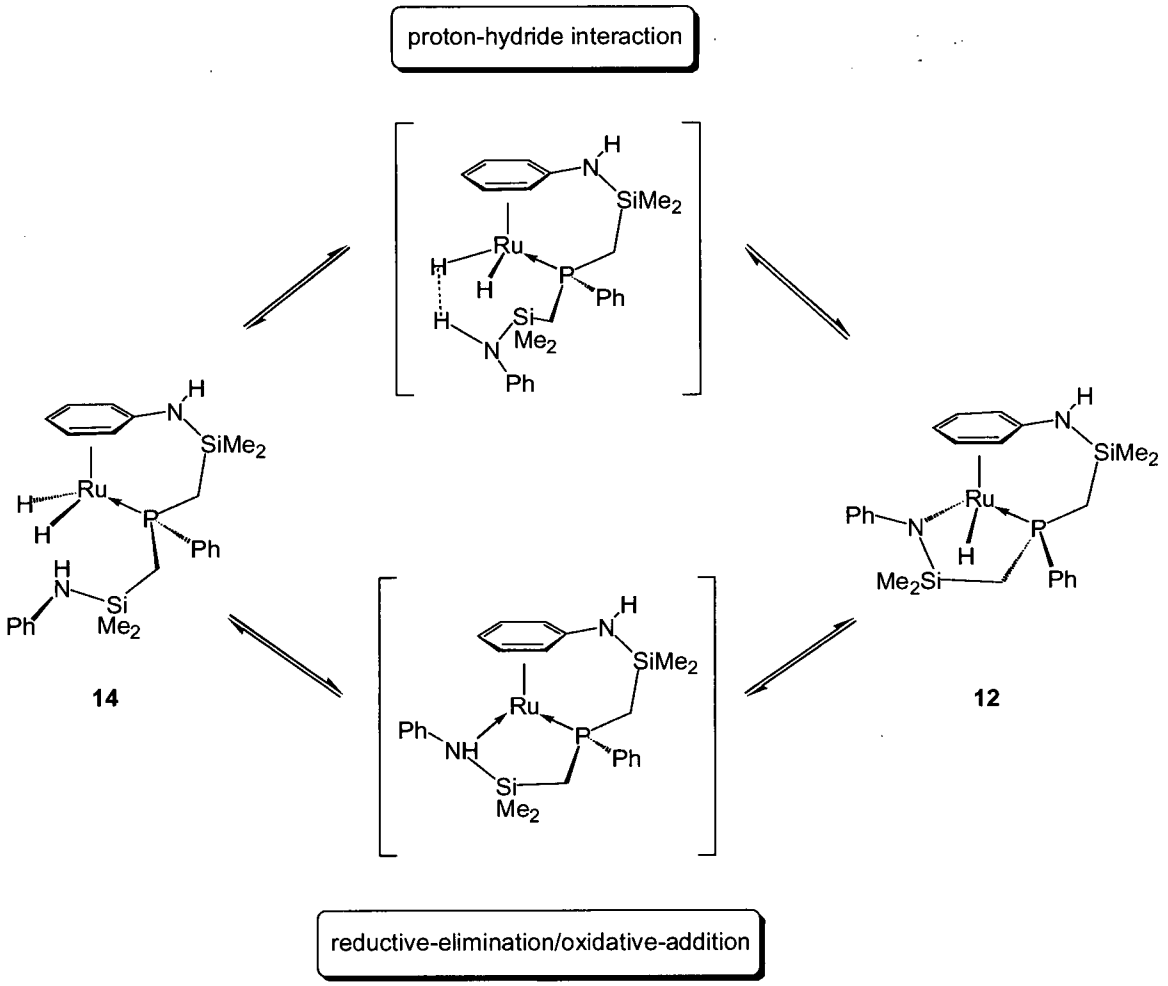

Scheme 3.9

We hypothesized that one way we could identify the method of H_2 loss in complex **14** was to monitor the decomposition of the labelled complex [NPNDH(η^6-C_6H_5)]Ru(H)$_2$ (**14**-d_1), in which the amino proton of the *dissociated* ligand side-arm is specifically deuterated. If the elimination of H_2 in **14**-d_1 proceeds via the reductive elimination mechanism then the resulting complex **12** would be expected to contain a deuterium atom in the hydride position. On the contrary, if H_2 loss occurs via the proton-hydride bonding pathway, then the resulting complex should contain a hydrogen atom at the hydride position. Monitoring the conversion of **14**-d_1 into

References begin on page 184

12 by ^{1}H NMR spectroscopy would allow for a distinction between the two possible decomposition pathways. This hypothesis assumes that no scrambling between hydride and proton environments occurs prior to H_2 loss.

With this strategy in mind we desired a synthetic procedure that would allow for the preferential deuteration at the N-*H* position of the pendant amine ligand without incorporation of deuterium at the hydride positions. Because of this stipulation the synthesis of **14**-d_1 cannot be achieved by the addition of D_2 gas to complex **3** since this would generate a $Ru(D)_2$ fragment with two deuteride ligands. The quantitative and clean formation of **14**-d_1 has proven to be a challenge and at this point we remain unsuccessful in accomplishing this task. Scheme 3.10 highlights one strategy that was devised, namely, replacement of the chloride ligand in the complex [NPNHD(η^6-C_6H_5)]RuHCl (**16**-d_1) by a hydride ligand.

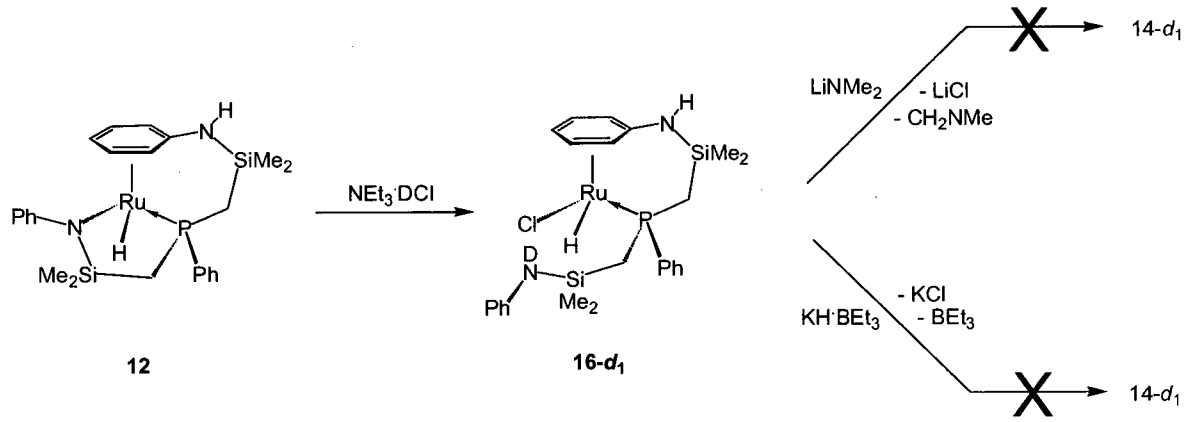

Scheme 3.10

The addition of a stoichiometric amount of NEt_3·DCl to a toluene solution of complex **12** results in the formation of a yellow precipitate over a period of 24 hours. The ^{1}H and $^{31}P\{^1H\}$ NMR spectra of this solid are consistent with the formation of the ruthenium monohydride complex **16**-d_1 shown in Scheme 3.10. The proposed structure of **16**-d_1 is related to the dihydride **14** with a chloride ligand in place of a hydride ligand. Due to its insolubility in aromatic and hydrocarbon solvents NMR characterization of **16**-d_1 was performed in tetrahydrofuran-d_8. The high-field region of the ^{1}H NMR spectrum contains a doublet at δ -8.23 ($^2J_{PH}$ = 52.2 Hz) that integrates to one proton and corresponds to the ruthenium hydride. The N-*H* proton of the η^6-aryl

References begin on page 184

coordinated amine ligand is found at δ 3.75. In comparison, this proton resonance is observed at δ 3.85 in complex **12** and δ 3.51 in complex **14** when the ^{1}H NMR spectra of these species are recorded in THF-d_8. These signals show a significant solvent dependence; in benzene-d_6 this resonance is located at δ 1.6 (for both **12** and **14**). The observation of a downfield shift for this peak may be due to the presence of a hydrogen bond between the amine proton and the oxygen lone pair of a molecule of THF. The presence of four silyl methyl proton resonances and four second-order ABX (X = ^{31}P) multiplets for the inequivalent methylene protons of the [NPNHD] chelating ligand are in accordance with a species that displays C_1 symmetry. Peaks associated with the coordinated amino-aryl protons are found between δ 5.4 to δ 5.9, and the remaining amino-phenyl and phosphine-phenyl resonances are located at expected positions between δ 7.1 to δ 7.9. The N-*H* proton resonance of the pendant amine arm is not observed verifying that deuteration at this site has occurred. In the unlabelled complex (**16**) this resonance is found at δ 5.7. The phosphine ligand gives rise to a singlet at δ 45.6 in the ^{31}P{^{1}H} NMR spectrum.

Having prepared **16**-d_1 the initial attempts at replacing the chloride ligand with a hydride ligand involved the addition of an equimolar amount of potassium triethylborohydride (KH·BEt$_3$). We anticipated that this would result in the formation of **14**-d_1 along with potassium chloride and triethylboron, which could be separated by filtration and evaporation, respectively. Although complex **14**-d_1 did form from this reaction it was only present as a minor species in a mixture of products. Predominant in this product mixture was the monohydride complex **12**. The formation of **12** can be rationalized via deprotonation of the pendant amine ligand in **16**-d_1 by KH·BEt$_3$. This would result in the elimination of HD gas and a potassium-amide ligand which could undergo metathesis with the ruthenium chloride to generate **12** and potassium chloride.

The synthesis of **14**-d_1 was also attempted by the reaction of **16**-d_1 with lithium dimethylamide (LiNMe$_2$). In this situation it was envisioned that metathesis would generate a dimethylamido containing intermediate that could undergo β-hydride elimination to yield **14**-d_1. In performing this reaction three ruthenium hydride products are formed, none of which is complex **14**-d_1. Once again the major species present is complex **12**, which can form by deprotonation of the pendant amine ligand in **16**-d_1 and elimination of deuterium-labelled dimethylamine (DNMe$_2$). The identity of the two other products is not known.

References begin on page 184

(viii) Solution epimerization of complex 16 resulting in the formation of a mixture of diastereomers

The reaction between complex **12** and NEt_3·DCl initially generates a single species as indicated by the NMR data, however, over a period of several hours at room temperature the appearance of a second species is noted. Allowing a THF-d_8 solution to stand for about 24 hours results in an approximately 50:50 ratio of the two species; this ratio does not change when the solutions are left to stand for extended periods. The new complex gives NMR spectral data that are very similar to the original species that is formed. The $^{31}P\{^1H\}$ resonance is found at δ 43.6 slightly shifted from the resonance of the original species suggesting a similar electronic structure at the metal centre for these two compounds. In the ^1H NMR spectrum, a hydride resonance at δ -8.02 is observed as a doublet ($^2J_{PH}$ = 55.8 Hz) due to its coupling with the phosphorus-31 nucleus, and a peak at δ 3.65 has been attributed to the N-*H* proton of an aryl-bound amine ligand. Evidence for the coordination of the amino phenyl group is provided by the presence of upfield shifted resonances between δ 5.2 and δ 6.2. The silyl methyl and methylene environments for this new complex each give rise to four distinct proton resonances indicating an unsymmetrical solution structure.

A summary of the proposed reactivity of a racemic mixture of complex **12** with NEt_3·DCl is given in Scheme 3.11. As can be seen, this reaction results in the formation of two complexes, namely *RR*-**16**-d_1 and *SS*-**16**-d_1; since these are enantiomers only one species is initially observed in the ^1H NMR spectrum. The absolute configurations represent the chirality displayed at the ruthenium and phosphorus centres, respectively. Inspection of the structure of these two complexes shows that they are chiral-at-metal complexes that also contain chiral phosphine ligands. Complexes of this type are known to undergo configurational processes; racemization can occur when the metal is the only stereocentre or epimerization when there are additional stereocentres.[118] During prolonged periods in solution it is possible that epimerization at the metal centre occurs resulting in the formation of two new complexes *SR*-**16**-d_1 and *RS*-**16**-d_1. These two new species are enantiomers of one another, and therefore, are indistinguishable by NMR spectroscopy. These new species are, however, diastereomers of their respective equilibrium partners (i.e. *RR*- and *SR*-**16**-d_1 and *SS*- and *RS*-**16**-d_1 are diastereomeric pairs), and this results in the observation of a second species in solution over several hours. Efforts towards obtaining

References begin on page 184

single crystals for a solid-state molecular structure determination of these isomers by X-ray crystallography are currently underway.

As is shown in Scheme 3.11, epimerization at the ruthenium centre in *RR*-**16**-d_1 can generate the isomer *SR*-**16**-d_1. The mechanism for this transformation can proceed by dissociation of the phosphine ligand to yield a trigonal planar ruthenium complex. The presence of the π-donating chloride ligand can assist in the stabilization of this intermediate.[119] Phosphine dissociation is known to play a key role in the racemization or epimerization of other chiral-at-metal complexes.[118,120] Rotation about the bound amino phenyl ring and re-coordination of the phosphine donor acts to invert the chirality at the metal centre.

Precedent for this type of behaviour can be found in the literature and it has been used to rationalize configurational equilibria processes in structurally related complexes. Of utmost relevance to this work is the epimerization that occurs between the pair of diastereomers of the ruthenium amide complex (η^6-C_6Me_6)-Ru[$C_6H_4N(Ph)(CHCH_3)$](PMe_3).[121] Similar activity is observed for a diastereomeric mixture of (η^5-C_5H_5)Re(NO)(PPh_3)(NHCHPhMe).[118] In both of these cases, phosphine dissociation leads to a three-coordinate planar species; coordination of the phosphine ligand to either of the diastereotopic faces of the intermediate generates the observed mixture of isomers. The only difference for the epimerization of complex **16**-d_1 is that the phosphine donor is part of a chelating ligand, and as such requires rotation of the bound phenyl group to allow for phosphine attack at the opposite face. Three-coordinate ruthenium(II) species exhibiting nearly planar geometries have been characterized in the solid-state in complexes of the type (η^5-C_5Me_5)Ru(PR_3)(X) (where R = $CH(CH_3)_2$ and X = Cl or R = C_6H_{11} and X = $OSiPh_3$).[122,123] These findings suggest that isomerization via a planar intermediate as depicted in Scheme 3.11 is a plausible pathway.

References begin on page 184

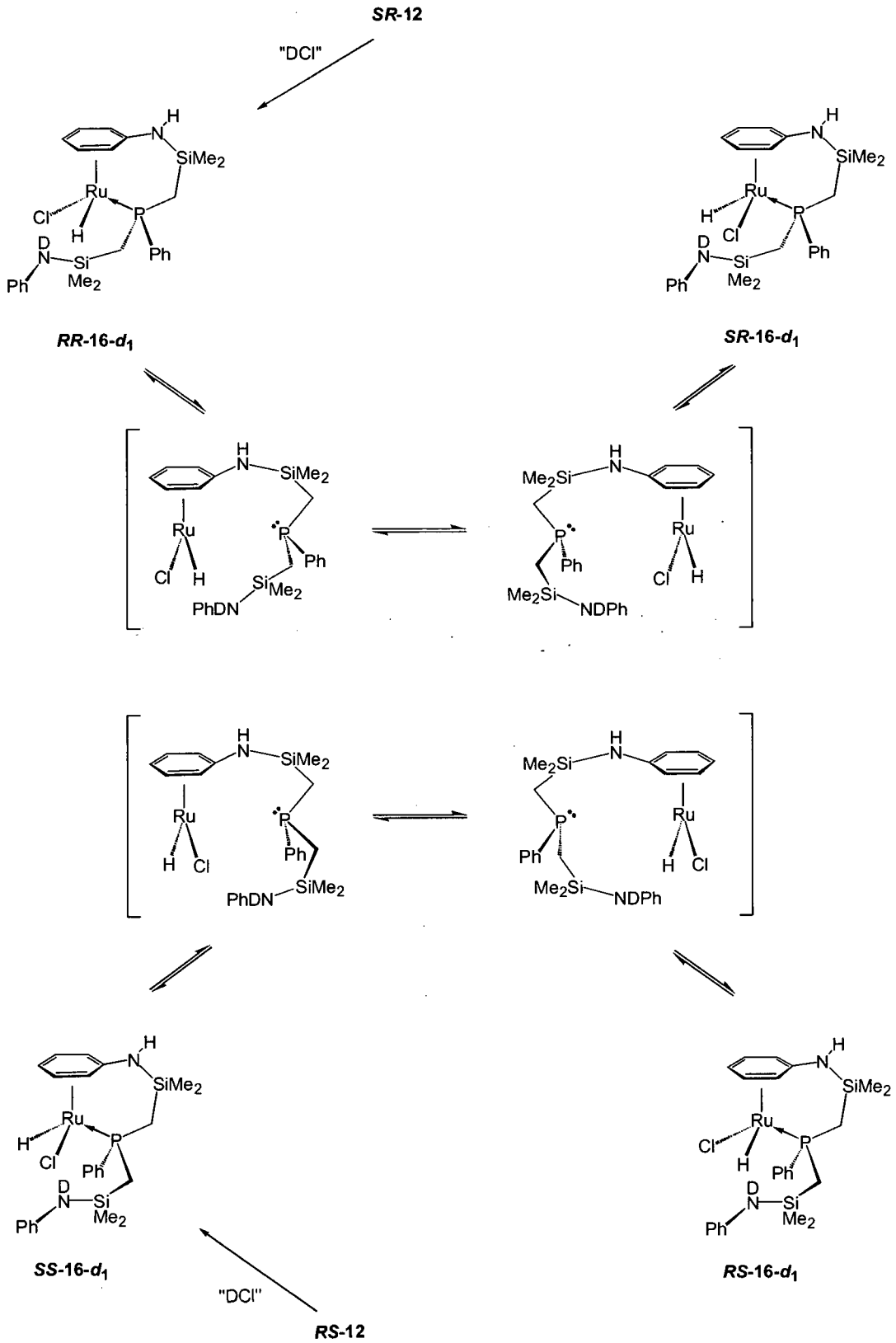

Scheme 3.11

References begin on page 184

(ix) Catalytic hydrogenation studies with complexes 3, 12, 13 and 14, and speculations into mechanistic details

Exposure of an equimolar solution of complex **3** and benzylidene aniline to an atmosphere of hydrogen gas at room temperature results in the quantitative formation of benzylphenyl amine within 12 hours. The mild conditions that were employed in order to achieve reduction of the imine substrate were promising and prompted an investigation into the catalytic potential utilizing complex **3** as a catalyst precursor. In doing so, complex **3** was found to effectively catalyze this hydrogenation reaction, as shown in equation 3.11. Optimal results were attained with a substrate-to-catalyst loading of 50:1 utilizing toluene as the solvent and four atmospheres of hydrogen gas pressure. Conversion to the amine product (99% as determined by integration of ^{1}H NMR signals) occurs within 48 hours.

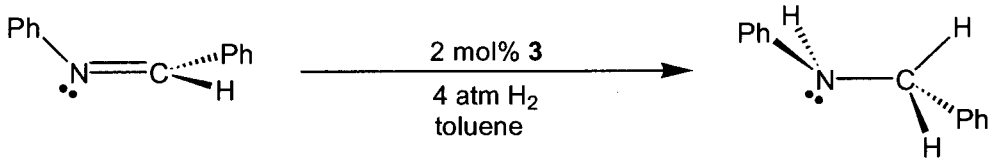

[3.11]

The results of this study were encouraging and we next set out to obtain details about the catalytic mechanism for this process. Compared to other systems that are believed to operate via the bifunctional hydrogenation method the reduction of benzylidene aniline utilizing complex **3** as a precursor proceeds quite slowly. For example, this same substrate was shown to undergo complete conversion in less than four hours utilizing $RuH_2(PPh_3)_2$(R,R-cydn) and a substrate-to-catalyst ratio of 500:1![111] These differences would seem to imply that the concerted transfer of hydride and proton nuclei to the imine substrate is probably not the operative mechanism in our system. In order to obtain more information about the mode of catalysis, as well as possibly identifying what the active species could be, each of the three ruthenium hydride products was individually tested as a possible catalyst precursor. A summary of the catalytic studies performed is outlined in Table 3.7.

References begin on page 184

Table 3.7. A summary of the catalytic studies performed for the hydrogenation of imine and alkene substrates using complexes **3**, **12**, **13** and **14** as precursors.

Entry	Precursor	Substrate	% conversion[a]
1	**3**	Benzylidene aniline	99
2	**12**	Benzylidene aniline	0
3	**13**	Benzylidene aniline	0
4	**14**	Benzylidene aniline	0
5	**3**	1-hexene	99
6	**3**	cyclooctene	99

Reactions were carried out at 25°C and 4 atm H_2 pressure with a substrate/catalyst loading of 50:1. The imine substrate was dissolved in toluene whereas the olefins were neat samples. [b] *Determined by ^1H NMR analysis of crude reaction mixture after 48 h.*

Although the catalytic conversion of benzylidene aniline to benzylphenyl amine is possible utilizing complex **3** (entry 1), the possibility of compounds **12**, **13** or **14** partaking in the catalytic process can be dismissed as each of these was found to be inactive towards imine hydrogenation (entries 2-4). This is not surprising considering the coordinatively saturated nature of these species with tightly bound arene moieties. The inability of the amine arms to coordinate to the metal centre through the nitrogen lone pair of electrons negates the ability to form ruthenium(II) species containing *cis*-coordinated amine and hydride ligands, and therefore, capable of effecting catalysis via the bifunctional mechanism. The ease at which the hydride complexes **12**, **13** and **14** form renders this a poor catalyst system for hydrogenation processes. In essence, this catalyst system can be said to possess "suicidal" characteristics with the three ruthenium hydride species representing catalytic "dead-ends". The formation of stable rhodium (I) arene complexes has also been shown to have inhibitory effects on rhodium catalyzed asymmetric hydrogenations.[124]

The observation that the arene-coordinated ruthenium hydride complexes were inactive towards hydrogenation whereas the starting material **3** did serve as a hydrogenation precursor, suggested that the active species was most likely an unsaturated ruthenium complex. Support for the involvement of a coordinatively unsaturated species as the active complex was given by the addition of an excess of P^iPr_3 to the reaction mixture, which lead to an inhibition of catalysis. The addition of benzylidene aniline directly to complex **3** also showed no reactivity providing further support for the presence of an unsaturated active species. In the proposed mechanism for the

References begin on page 184

hydrogenolysis of the cyclooctadienyl ligand in **3** (Scheme 3.6) such an unsaturated intermediate "[NPNH]RuH" is suggested as the key species that allows for the formation of complexes **12**, **13** and **14**. It is also possible that this intermediate is the catalytically active species present in solution. Alternatively, a coordinatively unsaturated ruthenium dihydride could also be the active species. In either case, coordination of the imine substrate to the ruthenium centre followed by hydride migration may initiate the hydrogenation process, which could then proceed in a similar fashion as that depicted in Scheme 3.6. The proposed catalytic mechanism involving substrate coordination to the metal centre suggested that olefins could also undergo catalytic hydrogenation. Indeed, both 1-hexene and cyclooctene were successfully reduced under similar hydrogenation conditions (entries 5 and 6).

At this point the ideas that are presented are speculative and are intended merely to provide some rudimentary insight into this system. Recent literature reports do lend support to the possibility that a mono-hydride intermediate such as "[NPNH]RuH" could play a key role in the catalytic hydrogenation process. Highly active and well-defined mono-cationic ruthenium hydrogenation catalysts of the type [Ru(bisphosphine)(H)(solvent)$_3$]BF_4 (solvent = acetone, MeOH, EtOH)[125-127] possess some similarities with the proposed active species "[NPNH]RuH" in our system. As shown in equation 3.12, hydrogenation of the cyclooctatriene ligand in **A** generates the active catalyst species **B**, which contains a chelating bisphosphine ligand and a hydride ligand; the inner coordination sphere is filled by labile solvent molecules. Displacement of a solvent molecule by a substrate molecule can initiate the catalytic process. In a similar manner, hydrogenolysis of the cyclooctadienyl ligand in **3** can generate the monohydride intermediate "[NPNH]RuH" (highlighted in Scheme 3.6) bearing a chelating amido-phosphine ligand and a hydride ligand. The presence of the amido donor in the chelating set allows for a neutral complex to be formed. Coordination of a substrate molecule to a vacant site at the ruthenium centre can initiate the hydrogenation process as in the cationic complexes.

References begin on page 184

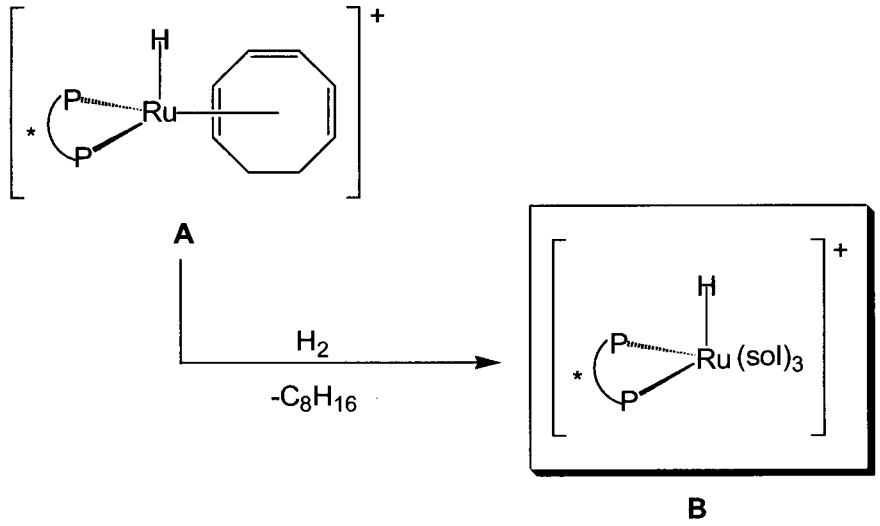

[3.12]

One of the difficulties concerning the hydrogenation of polar substrates such as imines is that coordination to the metal centre through the nitrogen lone pair of electrons results in η^1-binding, thus forming a σ-complex; this contrasts with the side-on (η^2) bonding mode of olefins, which generates π-complexes.[128,129] The side-on binding of a substrate is usually considered an essential requirement within a catalytic hydrogenation cycle since this results in effective orbital overlap with the metal centre and allows for effective hydride transfer. In the case of η^1-binding by an imine substrate the delivery of the hydride ligand from the metal centre to the imine carbon atom is difficult due to the positioning of this atom away from the metal centre; η^2-bonding can alleviate this apparent geometric restraint. In the bifunctional mechanism the requisite interaction between the M-H bond and the π-face of a polar substrate is achieved through a ligand-assisted, outer-sphere electrostatic interaction (see Scheme 2.1).[130]

Having no definitive indication as to the structure of the catalytically active species in our system (besides evidence that it is an unsaturated complex) we can only speculate as to mechanistic possibilities and intermediates within a catalytic cycle. The fact that imine hydrogenation is possible, however, suggests that a side-on bound imine substrate may likely be present at some point. Assuming that a ruthenium monohydride complex of the type "[NPNH]RuH" is the active species the amine ligand may play a role in facilitating η^2-bonding of the imine substrate; this is portrayed in Figure 3.15. An inner-sphere hydrogen-bonding interaction between the amino proton and the imine nitrogen atom can stabilize π-complexation of

References begin on page 184

the imine substrate. A similar interaction has been proposed between a coordinated molecule of methanol (the solvent) and the imine substrate in a rhodium (I) system containing chelating diphosphine ligands.[128] In this example, the use of methanol as a co-solvent was found to be essential for effective conversion and this was rationalized in terms of it facilitating a change from η^1- to η^2-binding of the imine. A "two-point" cooperative binding of ketones by a metal and by a neighbouring pendant NH group in an iridium complex has also recently been published.[131]

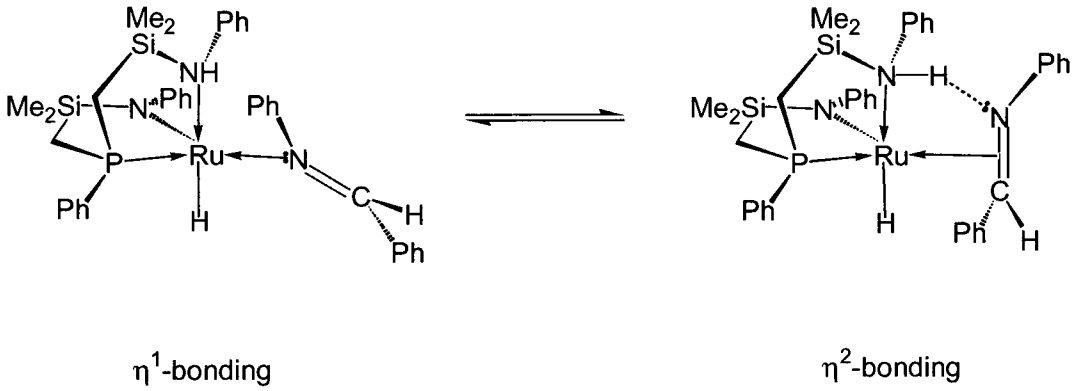

Figure 3.15. Possible role of the amine ligand in facilitating η^2-bonding of the imine substrate.

A mandatory condition for the amine-assisted interaction of the Ru-H bond with the π-face of the imine is that the amine ligand itself must coordinate to the metal centre. We have already seen examples which show that the "$SiMe_2N(H)Ph$" amine donor is not a good Lewis base; in Chapter 4 we see that H_2 displaces this donor group. If the amine ligand exhibits labile behaviour during the hydrogenation reaction then this would act to shift the equilibrium in favour of the η^1-bonding mode of the imine. This could potentially be one reason for the longer reaction times required to achieve complete conversion in our system. It is interesting that although the dihydrogen-hydride complex **10** does contain a coordinated amine ligand and a potential site for substrate coordination it exhibits no catalytic activity towards imine hydrogenation. The reason for this may be a consequence of the *trans* disposition between the amine ligand and the open coordination site, therefore, not allowing the amine ligand to aid in the side-on binding of the imine substrate.

References begin on page 184

3.6 Synthesis of a new [NPN] ligand with variation at the amide positions and its application to ruthenium(II)

(i) The need for ligand variation

In the proceeding discussion concerning the hydrogenation of complex **3** and catalytic hydrogenation studies with **3** serving as a precursor, it is apparent that the presence of phenyl substituents at the amide positions plays a significant role in the resulting reactivity. Our intended goal was to prepare ruthenium(II) complexes containing *cis*-coordinated amine and hydride ligands and to test the ability of these species to hydrogenate imines, possibly via the bifunctional mechanism. The intrinsic drawbacks of the chelating ligand system employed (with poor amine basicity and arene coordination), however, hampered such an investigation. These inadequacies initiated an examination into modification of the amide groups. In the following section a discussion concerning our initial efforts into the preparation of a new [NPN] ligand and its reaction with $[RuCl_2(cod)]_x$ will be presented.

One of the advantages of the tridentate [NPN] donor set is the potential for substituent variation, not only at the amide positions, but for the phosphine ligand as well.[132,133] This can be accomplished by changing the amines or phosphines initially used in the synthesis of the [NPN] ligands. For example, utilizing cyclohexylphosphine in lieu of phenylphosphine in the ligand preparation generates a more Lewis basic, cyclohexyl-substituted phosphine donor in the chelating ligand array. In this way, modification of the steric and electronic properties of the ligand set, and by extension the resulting metal complexes can be achieved.

In an attempt to eliminate the deficiencies within complex **3** with respect to its hydrogenation reactivity, the replacement of the phenyl groups at the amide positions of the [NPN] ligand with alkyl substituents was pursued. Our initial variation involved a methyl substituent. We anticipated that the smaller size and electron-donating ability of this group would aid in coordination of the amine donor through the nitrogen lone pair.

References begin on page 184

(ii) Synthesis and characterization of $[PhP(CH_2SiMe_2NMe)_2]Li_2{\cdot}C_4H_8O_2$ ($^{Me}[NPN]Li_2{\cdot}C_4H_8O_2$) (17) and its reaction with $[RuCl_2(cod)]_x$

The new mixed-donor, tridentate ligand $^{Me}[NPN]Li_2{\cdot}C_4H_8O_2$ (**17**) (where $^{Me}[NPN]$ = $PhP(CH_2SiMe_2NMe)_2$) can be prepared in an analogous fashion as the all phenyl-substituted derivative. The synthetic procedure employed is outlined in Scheme 3.12. The silylated methyl amine, $ClCH_2SiMe_2NHMe$, is formed from the reaction of MeNHLi with $ClCH_2SiMe_2Cl$. The dropwise addition of four equivalents of $^{n}BuLi$ to an ether solution containing a mixture of two equivalents of $ClCH_2SiMe_2NHMe$ and one equivalent of $PhPH_2$ gave the expected dilithiated precursor, $^{Me}[NPN]Li_2$ (**18**). The room-temperature ^{1}H NMR spectrum of the resulting solid (in C_6D_6) consisted of resonances that could be attributed to silyl methyl, methylene, amido methyl and phosphine phenyl proton environments in accordance with the formation of **18**. All of these resonances were observed as broad peaks indicative of fluxional solution behaviour for this species. The $^{31}P\{^{1}H\}$NMR spectrum of this solid (C_6D_6) was also composed of a broad singlet located at δ -38.0. The ligand precursor **18** was isolated as a foamy yellow solid and it readily dissolved in hexanes, which made purification troublesome. The addition of a slight excess of 1,4-dioxane ($C_4H_8O_2$) to a solution of **18** in hexanes resulted in the deposition of **17** as a white, micro-crystalline solid in about 70 % yield.

References begin on page 184

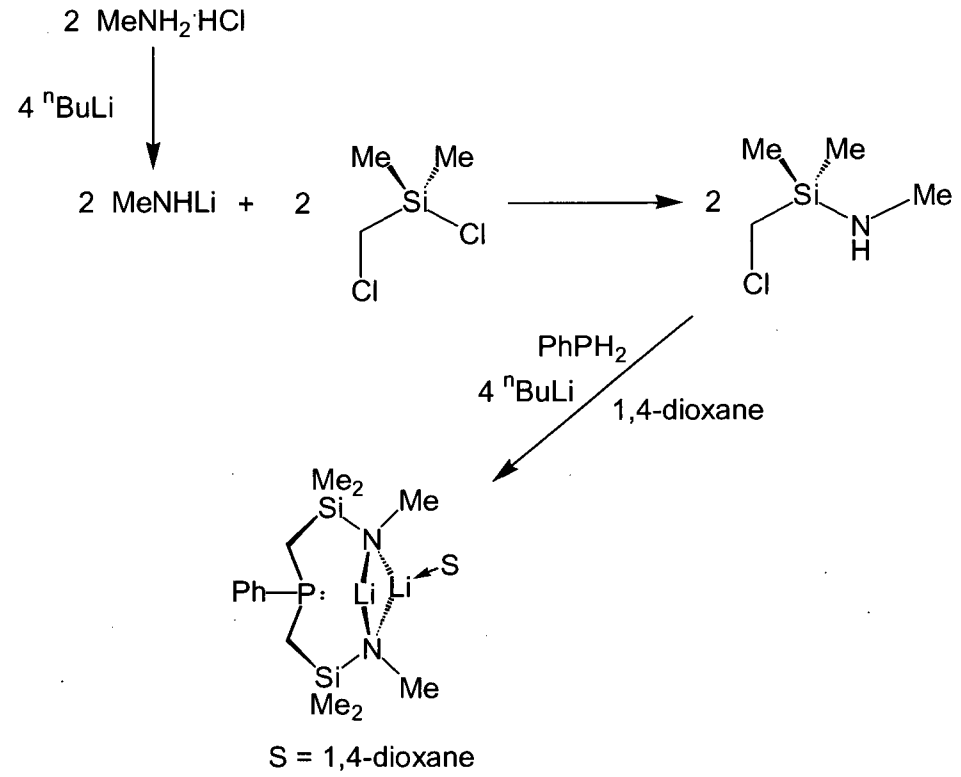

17

Scheme 3.12

The room temperature ^{1}H NMR spectrum of ^{Me}[NPN]Li_2·$C_4H_8O_2$ (**17**) is composed of well resolved peaks and is diagnostic for a mono-dioxane adduct; elemental analysis also supports this ligand composition. The silyl methyl protons appear as two closely spaced singlets near δ 0.1 and the methylene protons of the backbone are observed as a second-order multiplet centered at δ 0.8. A singlet at δ 2.8 corresponds to the six equivalent methyl amide protons. The resonance for the coordinated dioxane molecule is found at δ 3.6 and three multiplets in the range δ 7.1 to δ 7.5 are due to the *ortho*-, *meta*- and *para*-protons of the phenyl group attached to the phosphine donor. The ^{1}H NMR data suggest a symmetrical solution structure for **17** not unlike other [NPN] variants. This would imply that the dioxane molecule undergoes reversible coordination with both lithium centres.

The ^{31}P{^{1}H} NMR spectrum for **17** consists of a singlet at δ -37.5. This is in contrast with the phosphine resonance in the all phenyl [NPN] ligand, which is observed as a quartet due to

References begin on page 184

coupling of the ^{31}P nucleus to a ^{7}Li nucleus (I = 3/2, 92.6 % abundance). This implies that the phosphine donor in **17** does not coordinate to the lithium cations; the $^{7}Li\{^{1}H\}$ spectrum of **17** also consists of a singlet. The lack of phosphine coordination is most likely due to the more basic nature of the amido donors bearing methyl groups as opposed to phenyl groups. This would render the lithium centres in **17** less Lewis acidic. The presence of only one equivalent of dioxane may also be a result of this.

The reaction of $^{Me}[NPN]Li_2{\cdot}C_4H_8O_2$ (**17**) with the ruthenium(II) starting material $[RuCl_2(cod)]_x$ was carried out in an identical fashion as with the phenyl-substituted [NPN] ligand. This resulted in the isolation of an orange solid whose ^{1}H and $^{31}P\{^{1}H\}$ NMR spectra suggested it was a paramagnetic compound. The ^{1}H NMR spectrum, for instance, consisted of very broad and shifted peaks, none of which could be attributed to the specific proton environments of the ^{Me}[NPN] or cyclooctadienyl ligands. The same orange solid was produced when the reaction was performed in THF as the solvent in lieu of toluene. At this point the structure of the isolated compound is unknown, although attempts at obtaining single crystals for an X-ray diffraction study are ongoing. What is certain, however, is that the methyl amido analogue of complex **3** has not been produced. It is possible that β-hydride elimination from the methyl group of a coordinated amide donor occurs,[134-136] leading to the formation of the isolated orange solid. The use of tertiary butyl groups at the amide position would exclude this potential decomposition pathway. Unfortunately, the synthesis of an [NPN] ligand with these bulky amide donors was unsuccessful. The reaction of the diamidophosphine ligand **17** with other ruthenium(II) starting materials has not been investigated.

3.7 Summary and Conclusions

This chapter deals with the reactivity of the amidophosphine complexes $[P_2N_2]Ru(\eta^2{:}\eta^2\text{-}C_8H_{12})$ (**1**), $[P_2NNH]Ru(C_6H_4PPh_2)$ (**2**) and $[NPNH]Ru(1\text{-}3{:}\eta^3\text{-}5,6{:}\eta^2\text{-}C_8H_{11})$ (**3**) with hydrogen gas, including a discussion of the catalytic hydrogenation of imine and alkene substrates utilizing these species as catalyst precursors. The coordinatively saturated complex **1** reacts with hydrogen gas to produce the ruthenium dihydrogen-hydride species $[P_2NNH]Ru(H_2)H$ (**10**). The heterolytic cleavage of a molecule of H_2 generates the ruthenium amine and hydride moieties. The

References begin on page 184

classification of **10** as a dihydrogen-hydride complex as opposed to a ruthenium (IV) trihydride structure was based on the measurement of the short T_1(min) value of 62 ms for the hydride nuclei and the observation of an $^{av}J_{HD}$ coupling of about 5 Hz in the partially deuterated isotopomers. Both the NMR relaxation and the HD coupling data provided an estimated H-H distance of *ca.* 1.2 Å for the coordinated H_2 ligand in **10**. This species undergoes two fluxional processes in solution. In one case, the hydride and dihydrogen environments are readily exchanged. This is proposed to occur through an intermediate trihydrogen species that forms from the electrostatic *cis*-interaction between these nuclei. The second process involves an exchange of the amino proton and hydride sites via a protonic-hydridic bonding interaction. Complex **10** was found to be a precursor for the catalytic hydrogenation of olefins but not for imines. Displacement of the H_2 ligand by a substrate molecule most likely initiates the catalytic process.

Complex **2** reacts with hydrogen gas to generate the ruthenium(II) monohydride complex [P_2NNH]RuH(PPh_3) (**11**) via hydrogenolysis of the *ortho*-metalated triphenylphosphine ligand in **2**. Alternatively, complex **11** can be formed by the addition of triphenylphosphine to **10** by displacement of the H_2 ligand. This compound has been characterized in the solid-state by X-ray diffraction and in solution by ^{1}H and ^{31}P{^{1}H} NMR spectroscopy. In both instances a C_s symmetric structure is evident. Under an atmosphere of deuterium gas, complex **11** was observed to incorporate deuterium at the hydride and amino proton sites. This has been rationalized by the displacement of H_2 in a transient intermediate that forms due to proton-hydride bonding interactions in **11**. In accordance with this proposal, a cross-peak in the two-dimensional EXSY spectrum was observed between the hydride and amino proton environments indicating that these two nuclei are in chemical exchange. Complex **11** was unable to catalyze the hydrogenation of alkene or imine substrates even under four atmospheres of H_2 pressure. The triphenylphosphine ligand in **11** is strongly coordinated to the metal centre not allowing for an open site for substrate binding.

The reaction of the mono-amide complex **3** with hydrogen gas results in the formation of three ruthenium hydride species: [NPN(H)(η^6-C_6H_5)]RuH (**12**), [$NPNH_2$]Ru(H)$_2$(C_7H_8) (**13**) and [$NPNH_2$(η^6-C_6H_5)]RuH_2 (**14**). Complex **12** forms via hydrogenolysis of the cyclooctadienyl ligand in **3** followed by coordination of the amino phenyl ring of the [NPNH] ligand side arm. Compounds **13** and **14** undergo further conversion of the ruthenium amide bond into a ruthenium

References begin on page 184

hydride and amine side arm resulting from the heterolytic cleavage of H_2. Compounds **12** and **13** have been characterized in solution and in the solid state. The X-ray determined molecular structure of **13** shows close hydride and amino proton contacts of about 2 Å; these interactions are maintained in solution as determined from measurement of the T_1(min) relaxation times of these nuclei. Complex **14** was characterized in solution by ^1H and $^{31}P\{^1H\}$ NMR spectroscopy. Evidence for the presence of proton-hydride bonding in **14** was given from the relaxation data; it is believed that this interaction gives rise to an (unobserved) H_2 complex which evolves an equivalent of dihydrogen to give **12**. The coordination of arene substituents, either amino-phenyl or aromatic solvent molecules (toluene or benzene) generates coordinatively saturated species that are inactive for the hydrogenation of imine or olefin substrates. Complex **3**, however, is a precursor for the catalytic hydrogenation of these substrates. We are currently investigating new systems in which the substituents at the amide position of the [NPN] ligand have been modified to electron donating, alkyl groups in an attempt to promote coordination of the resulting amine arms to the metal centre via the nitrogen lone pair. This may lead to the formation of ruthenium systems with *cis*-coordinated hydride and amine moieties, capable of performing catalytic hydrogenation operating by the bifunctional mechanism.

3.8 Future Work

(i) Catalytic ionic hydrogenation utilizing [NPN(H)(η^6-C_6H_5)]RuH (12) as a precursor

Ionic hydrogenation involves the addition of a hydride and a proton across an unsaturated organic moiety.[10,137] The ability of transition metal complexes to accomplish this task stoichiometrically has been known for some time. A mixture of an organometallic hydride such as $CpMoH(CO)_3$ and a strong acid such as CF_3SO_3H is capable of reducing sterically hindered olefins to alkanes via protonation to carbocations followed by hydride transfer from the metal hydride.[138] The reduction of aldehydes and ketones using mixtures of $CpW(H)(CO)_3$ and CF_3SO_3H has also been reported.[139] A more recent study reports on the *catalytic* ionic hydrogenation of methyl aryl pyrrolidinium cations by a piano-stool ruthenium hydride complex as shown in equation 3.13.[10]

References begin on page 184

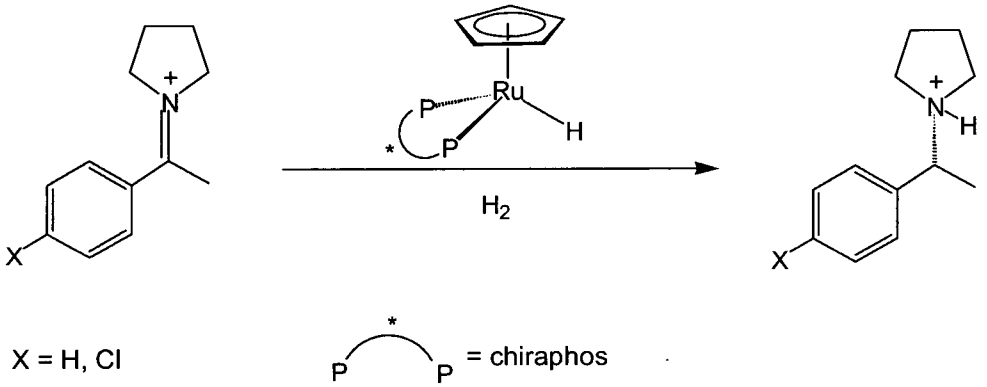

[3.13]

The proposed catalytic cycle for the ionic hydrogenation mechanism is shown in Scheme 3.13. The first step involves hydride transfer to the iminium cation to generate a cationic metal fragment (M^+) which then reacts with an equivalent of H_2. This (unobserved) intermediate then transfers a proton equivalent to generate the ammonium product and the active monohydride complex. The use of chiral chelating phosphine ligands allows for the asymmetric reduction of prochiral immonium substrates, however, the obtained enantiomeric excesses show some room for improvement (typically ~ 30 to 60 % e.e.).

It would be interesting to test the ability of the complex [NPN(H)(η^6-C_6H_5)]RuH (**12**) in ionic hydrogenation processes. Similar to the cyclopentadienyl ruthenium complex discussed above it is a mono-hydride species with a piano-stool structure. A significant difference, however, is the presence of the π-donating amido ligand in **12**, which could enhance its activity. The rate-determining step in the hydrogenation mechanism shown in Scheme 3.13 is the initial hydride transfer step, and this is most likely due to the formation of a cationic unsaturated intermediate. Such an intermediate could be stabilized electronically by delocalization of the amido lone pair of electrons leading to an increase in the catalytic activity. It would also be fascinating to perform asymmetric hydrogenations with **12**. Complex **12** is a chiral-at-metal complex that also contains a chiral phosphine donor. This is in contrast to the reported ruthenium complex, which contains a chiral chelating bisphosphine ligand where the chirality is located in the ligand backbone. One problem that could arise is the fact that complex **12** could potentially exist as a racemic mixture (Figure 3.14).

References begin on page 184

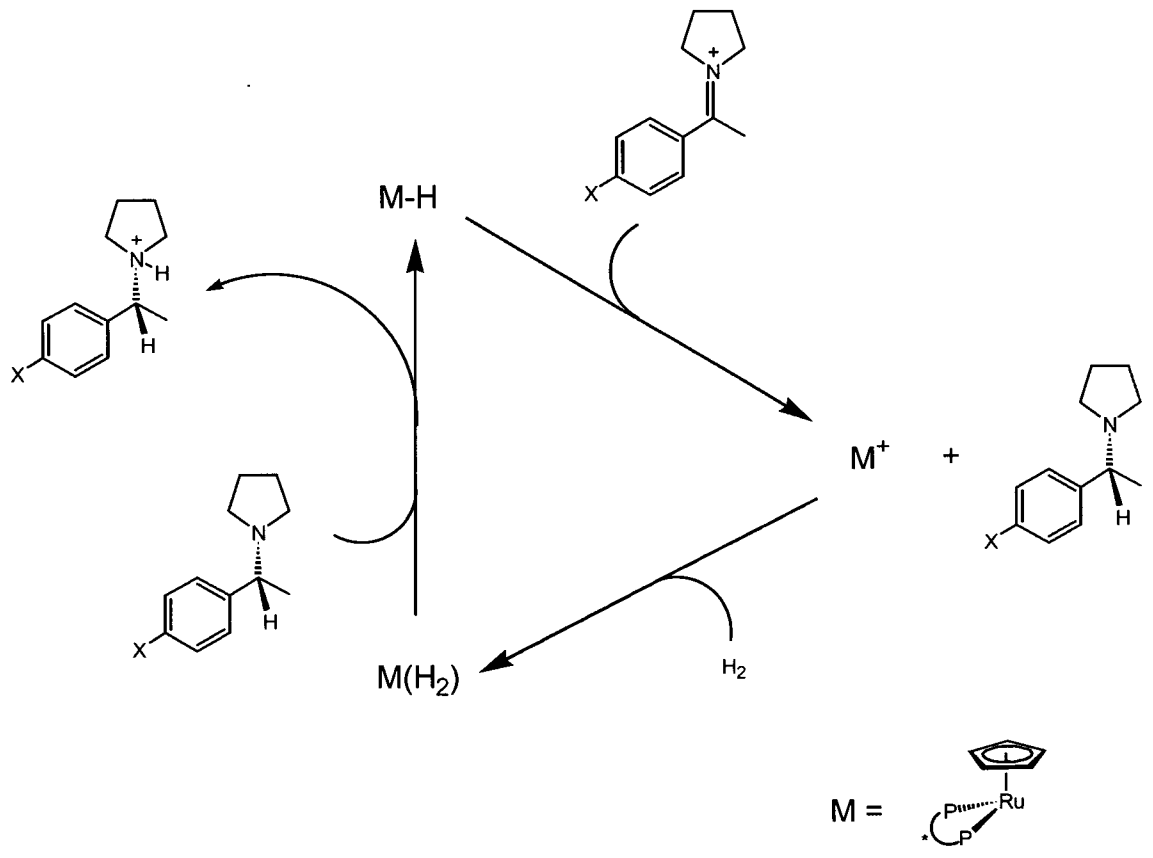

Scheme 3.13

(ii) Another strategy towards the synthesis of amino-deuterated complexes of 14

In section 3.5 (vii) of this chapter we discuss the loss of H_2 from complex **14** to give **12**. One possible mechanism for the evolution of H_2 is through proton-hydride bonding interactions leading to the formation of a transient H_2 complex; T_1 data indicate that there is a close contact between the hydride and proton sites in **14** of about 2.0 Å. An alternate route could involve the reductive elimination of H_2 from the metal centre followed by the oxidative addition of the N-H bond of the amine ligand. A distinction between these two pathways could be achieved by monitoring the decomposition of the amino deuterated complex **14**-d_1, however, our synthetic efforts have not allowed for a clean and quantitative formation of this species. One of the complications that we encountered in our initial attempts was deprotonation of the amino proton(s)

References begin on page 184

in addition to a metathetical exchange of chloride and hydride ligands in reactions of complex **16**-d_1 with KH·BEt_3 or $LiNMe_2$. These observations suggested to us another procedure that could possibly allow for the incorporation of deuterium at both of the amino proton sites to give **14**-d_2. This is illustrated in Scheme 3.14.

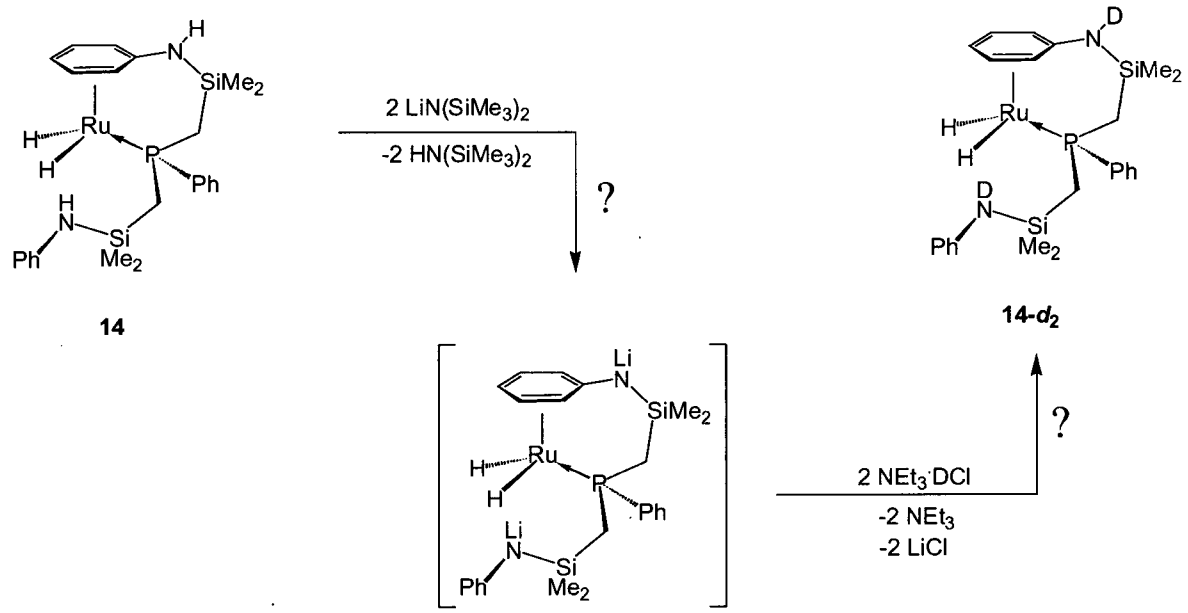

Scheme 3.14

The addition of two equivalents of base (e.g. $LiN(SiMe_3)_2$) to complex **14** followed by two equivalents of deuterium chloride may allow for the incorporation of deuterium into the two N-H sites. Labelling of the amino hydrogen by deuterium in complex **12** was accomplished by employing this reactivity, as was the amino hydrogen atom in complex **3**. Monitoring the decomposition of **14**-d_2 by ^1H NMR spectroscopy would allow for a discrimination between the two possible modes of H_2 loss from **14**.

(iii) Reaction of ^{Me}[NPN]Li_2·$C_4H_8O_2$ (17) with early transition metals

The reaction of the diamidophosphine ligand ^{Me}[NPN]Li_2·$C_4H_8O_2$ (**17**) with the ruthenium(II) starting material $[RuCl_2(cod)]_x$ produced an orange solid that gave rise to very broad and shifted peaks in the ^1H NMR spectrum, characteristic of a paramagnetic species. It was

References begin on page 184

obvious that the anticipated product ^{Me}[NPNH]Ru(1-3:η^3-5,6:η^2-C_8H_{11}), analogous to **3**, did not form. It is possible that the presence of the hydrogen atoms of the methyl-substituted amide donor permitted other reaction pathways via β-hydride elimination; this is a common decomposition route for late transition metal amide complexes. Although **17** is not tailored for late transition metals it may be well-suited for the stabilization of early transition metals.

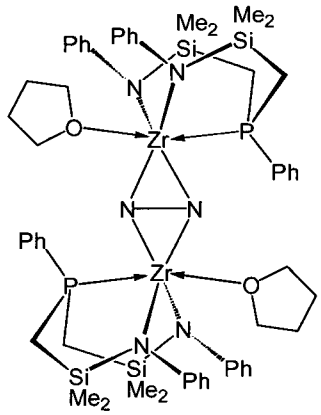

{[NPN]ZrTHF}$_2$(μ-N_2)

A

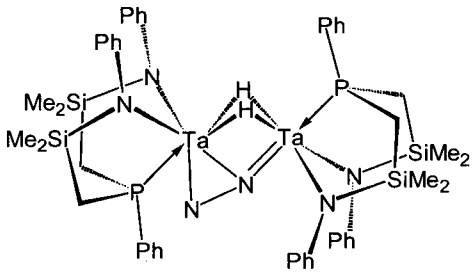

{[NPN]Ta}$_2$(μ-N_2)(μ-H)$_2$

B

Figure 3.16. Examples of [NPN]Zr and [NPN]Ta dinitrogen complexes.

The coordination and functionalization of dinitrogen by early transition metal complexes stabilized by the [P_2N_2] and [NPN] ligand sets is a major area of research in our lab. Highly activated N_2 moieties (as measured by the elongation of the N-N bond upon coordination), reaction with H_2 to form N-H bonds, as well as stoichiometric N-C, N-B and N-Si bond forming reactions have all been achieved with these types of complexes.[133,140,141] Representative examples of dinitrogen complexes of zirconium and tantalum stabilized by the [NPN] ligand are shown in Figure 3.16. Modification of the electronic and steric properties of the metal complexes could be expected to influence the reactivity of the coordinated N_2 ligand within these complexes. The methyl substituted [NPN] ligand **17** offers increased Lewis basicity as compared to the phenyl derivative. As such, one may anticipate an increased activation of coordinated N_2 moieties in complexes bearing this ligand, which could translate into an expansion of the already observed reactivity of this inert molecule.

References begin on page 184

With these ideas in mind, the coordination of **17** to zirconium (IV) was undertaken. As shown in equation 3.14, the reaction of **17** with $ZrCl_4{\cdot}(C_4H_8O)_2$ yields the diamidophosphine complex ^{Me}[NPN]$ZrCl_2(C_4H_8O_2)$ (**19**) in quantitative yield as a white solid. The reaction proceeds cleanly as evidenced by the singlet observed at δ -6.3 in the $^{31}P\{^1H\}$ NMR spectrum for the crude reaction mixture. The ^1H NMR spectrum indicates a symmetrical coordination geometry about the zirconium centre. Only one resonance for the methyl amide protons is present and two peaks for the silyl methyl proton environments. The methylene proton resonances consist of a multiplet at δ 1.22 and the phosphine phenyl protons are located between δ 7.10 and δ 7.76. A singlet at δ 3.30 that integrates to eight protons implies the presence of one equivalent of coordinated 1,4-dioxane per metal centre. The only structure consistent with the observed ^1H NMR data is that shown in equation 3.14, with the chloride and amide ligands occupying the equatorial plane of a six-coordinate octahedral species, and the phosphine and dioxane ligands at the axial positions. A mirror plane of symmetry bisecting the chloride and amide donors exists resulting in a C_s symmetric complex.

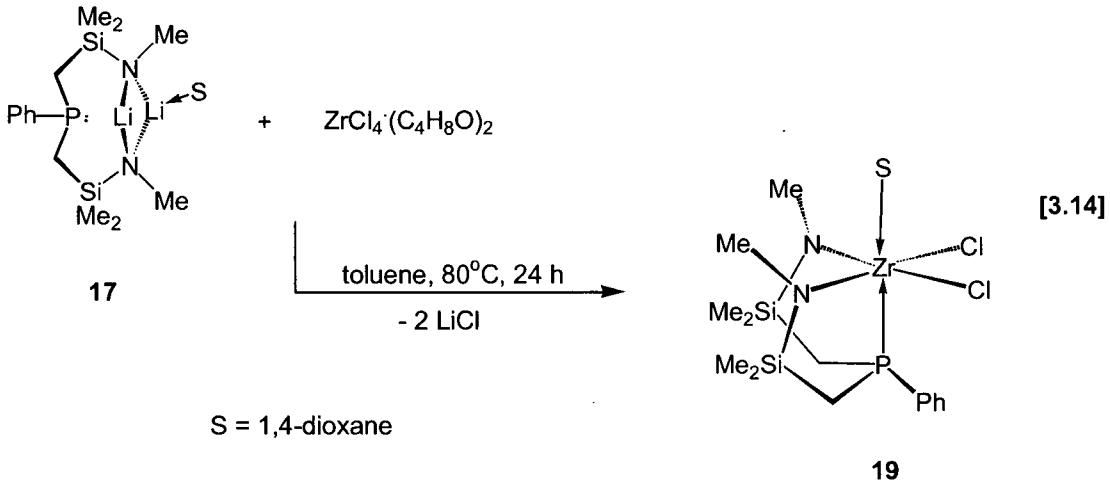

[3.14]

So far, the reduction of **19** under an atmosphere of N_2 to form a dinitrogen complex has not been attempted. It will be exciting to see if an N_2 complex can be prepared, and if so, even more exciting to investigate the reactivity of the N_2 ligand! The coordination of **17** to other metals including tantalum and niobium has not been examined at this point but would also be worthwhile pursuing in the future.

References begin on page 184

3.9 Experimental

(i) General Procedures

Unless otherwise stated, general procedures were performed according to Section 2.9 (i). ^{1}H NMR T_1 relaxation measurements were performed on a Bruker AMX 500 MHz spectrometer using a standard inversion-recovery pulse sequence (180°-τ-90°). The T_1 values were obtained using the non linear three-parameter fitting routine in the Bruker XWINNMR program with an estimated error of ± 10 % in each T_1 value. The temperature was regulated using a Bruker VT 1000 unit. Toluene-d_8 was used as the NMR solvent for these studies. The T_1 data including plots of T_1 versus Temperature for each complex are provided in Appendix 2.

(ii) Materials

Complexes **1**, **2** and **3** were prepared as described in Chapter 2. Hydrogen gas (purchased from Praxair) and deuterium gas (Cambridge Isotope Laboratories) were employed without further purification. Cyclooctadiene, cyclooctene, 1-hexene, 1,4-dioxane and $ClMe_2SiCH_2Cl$ were purchased from Aldrich and all were distilled prior to use. Benzylidene aniline was purchased from Fisher Chemicals and was recrystallized from hot ethanol and dried under vacuum overnight prior to use. ^{n}BuLi (Acros Organics), $LiNMe_2$, $KH{\cdot}BEt_3$ and $HNMe_2{\cdot}HCl$ (Aldrich) were used as received. Phenylphosphine[142] and $ZrCl_4(C_4H_8O)_2$[143] were prepared according to reported literature procedures.

(iii) Synthesis and Reactivity of Complexes

[P_2NNH]RuH(η^2-C_8H_{12}) (9) and [P_2NNH]Ru(H_2)H (10)

A yellow solution of [P_2N_2]Ru(η^2:η^2-C_8H_{12}) (**1**) (0.052 g, 0.070 mmol) in ~ 1.0 mL of toluene-d_8 in a J-Young valve NMR tube was degassed by performing three freeze-pump-thaw cycles. The solution was warmed to room temperature and then exposed to an atmosphere of hydrogen gas. After four hours, an intermediate species is observed. The suggested composition based on ^{1}H and ^{31}P{^{1}H} NMR data is [P_2NNH]RuH(η^2-C_8H_{11}) (**9**). ^{1}H NMR (C_7D_8, 298 K, 500

References begin on page 184

MHz): δ -9.60 (t, $^2J_{PH}$ = 25.4 Hz, Ru-*H*, 1H), δ -0.51, -0.12 (s, SiC*H*$_3$, 12H total), δ 0.63 (s, overlapping, SiC*H*$_3$, 12H total), δ 1.4 – 3.6 (m, overlapping, N-*H*, PC*H*$_2$ and C_8H_{16}), δ 7.0 – 8.2 (m, overlapping, PC$_6$*H*$_5$). $^{31}P\{^1H\}$ NMR (C_7D_8, 298 K, 202.5 MHz): δ 30.0 (s). Stirring the reaction mixture for 48 hours results in the formation of the complex [P_2NNH]Ru(H_2)H (**10**). ^1H NMR (C_7D_8, 298 K, 500 MHz): δ -11.44 (t, $^2J_{PH}$ = 13.8 Hz, Ru-*H*, 3H), δ 0.36 (s, overlapping, SiC*H*$_3$, 24H total), δ 1.42 (m, PC*H*$_2$, 8H total), δ 2.18 (s, N-*H*, 1H), δ 7.62 – 8.02 (m, PC$_6$*H*$_5$, 10H). $^{31}P\{^1H\}$ NMR (C_7D_8, 298 K, 202.5 MHz): δ 35.5 (s). T_1(min) for Ru-*H*$_3$ = 62 ms at 240 K in toluene-d_8.

Reaction of [P_2NNH]Ru(H_2)H (10) with D_2

An NMR tube containing [P_2NNH]Ru(H_2)H (**10**) (*ca.* 0.049 mmol) in toluene-d_8 (~ 1.0 mL) was degassed by three freeze-pump-thaw cycles. The solution was thawed under an atmosphere of D_2 gas. After one hour the sealed NMR tube was transferred into an NMR probe. The ^1H NMR spectrum of the hydride signal had changed from a triplet to a complicated multiplet due to coupling to the ^{31}P and ^2H nuclei. $^1H\{^{31}P\}$ NMR, hydride region (C_7D_8, 298 K, 500 MHz): δ -11.44 (s, overlapping, Ru-*H*$_3$), δ -11.43 (t (br), $^2J_{HD}$ = 4.5 Hz, overlapping, Ru-*H*$_2$D). After 16 hours under an atmosphere of D_2 gas a new multiplet for the hydride signal was observed in the ^1H NMR spectrum. $^1H\{^{31}P\}$ NMR, hydride region (C_7D_8, 298 K, 500 MHz): δ -11.42 (m (br), $^2J_{HD}$ = 5.0 Hz, Ru-*H*D$_2$). Temperature dependence of the hydride resonances (Ru-*H*$_3$ and Ru-*H*D$_2$ isotopomers, respectively): 298 K (δ -11.44, -11.42), 280 K (δ -11.38, -11.35), 260 K (δ -11.32, -11.28), 240 K (δ -11.27, -11.20), 220 K (δ -11.20, -11.11).

Reaction of [P_2NNH]Ru(H_2)H (10) with cyclooctadiene

In an NMR tube containing a solution of **10** (*ca.* 0.064 mmol) in toluene-d_8 (~ 1.0 mL) was added a slight excess of cyclooctadiene (0.008 g, 0.074 mmol). The ^1H and $^{31}P\{^1H\}$ NMR spectra of the reaction mixture indicated the formation of complex **9**.

References begin on page 184

Reaction of [P_2NNH]Ru(H_2)H (10) with PPh_3

In an NMR tube containing a solution of **10** (*ca.* 0.072 mmol) in toluene-d_8 (~ 1.0 mL) was added a slight excess of triphenylphosphine (0.021 g, 0.080 mmol). The ^{1}H and ^{31}P{^{1}H} NMR spectra of the reaction mixture indicated the formation of complex **11**.

[P_2NNH]RuH(PPh_3) (11)

A solution of [P_2NNH]Ru($C_6H_4PPh_2$) (**2**) (0.124 g, 0.138 mmol) in 25 mL toluene was added to a glass reaction vessel equipped with a Teflon valve and a ground glass joint. The vessel was evacuated by three freeze-pump-thaw cycles and one atmosphere of hydrogen gas was added at room temperature. The vessel was sealed and the solution was stirred for two hours. The solvent and excess H_2 gas were then removed under vacuum. The addition of hexanes caused the deposition of [P_2NNH]RuH(PPh_3) (**11**) as an orange solid (0.109 g, 88 %). Crystals suitable for an X-ray diffraction study were grown by the slow evaporation of a saturated toluene solution. ^{1}H NMR (C_6D_6, 298 K, 500 MHz): δ -15.32 (dt (AM_2X), overlapping, $^2J_{[P2N2]H}$ = 16.6 Hz, $^2J_{[PPh3]H}$ = 29.2 Hz, Ru-*H*, 1H), δ 0.12, 0.48, 0.50 and 0.77 (s, SiCH_3, 24H total), δ 0.92, 1.18, 1.30 and 1.48 (m, PCH_2, 8H total), δ 1.73 (s, N-*H*, 1H), δ 6.82 (m, overlapping, PPh-*meta* and *para*, 6H), δ 7.51 (dd, PPh-*ortho*, 4H). ^{31}P{^{1}H} NMR (C_6D_6, 298 K, 202.5 MHz): δ 35.0 (d, $^2J_{PP}$ = 38 Hz, [P_2NNH], 2P), δ 72.0 (t, $^2J_{PP}$ = 38 Hz, PPh_3, 1P). T_1(min) for Ru-*H* = 0.370 s at 260 K in toluene-d_8.

[P_2NND]RuD(PPh_3) (11-d_2)

In a J-Young valve NMR tube [P_2NNH]RuH(PPh_3) (**11**) (0.026 g, 0.029 mmol) was dissolved in benzene-d_6 (~ 1.0 mL). The tube was degassed by two freeze-pump-thaw cycles and warmed to room temperature. An atmosphere of D_2 gas was added to the tube that was then sealed. After four hours the ^{1}H NMR spectrum was recorded, and it showed resonances identical to those for **11** (above) except that the N-*H* and Ru-*H* signals were no longer present. Integration reveals > 95 % incorporation of deuterium into these sites after this time period.

References begin on page 184

[NPN(H)(η^6-C_6H_5)]RuH (12)

A solution of **3** (0.96g, 1.49 mmol) in toluene (25 mL) was degassed by performing three freeze-pump-thaw cycles. Upon warming to room temperature an atmosphere of H_2 gas was added to the system resulting in a change in colour from red to orange. The contents were stirred for 30 minutes and then the solvent and excess H_2 were removed under vacuum until an oily residue remained. The addition of hexanes (25 mL) caused an orange crystalline solid to precipitate from solution. The solid was collected on a frit, rinsed with hexanes and dried under vacuum (0.42 g, 53 %). X-ray quality crystals were obtained by the slow evaporation of a saturated toluene solution of **12**. ^{1}H NMR (C_6D_6, 298 K, 500 MHz): δ -7.7 (d, $^2J_{PH}$ = 47 Hz, Ru-*H*, 1H), δ -0.6, 0.0, 0.3 and 0.5 (s, SiCH_3, 12H total), δ 1.2 (m, PCH_2, 4H), δ 1.6 (s, coordinated N*H*Ph, 1H), δ 3.5 (d, coordinated NHPh *o-H*, 1H), δ 4.8 (m, coordinated NHPh *m-H*, 1H), δ 5.0 (m, coordinated NHPh *o-H*, *p-H*, 2H), δ 5.8 (m, coordinated NHPh *m-H*, 1H), δ 6.6 (m, NPh *p-H*, 1H), δ 7.1-7.3 (overlapping m, NPh *o-H*, *m-H* and PPh *m-H, p-H*, 7H), δ 7.9 (dd, PPh *o-H*, 2H). The amino proton showed a shifted resonance in THF-d_8. ^{1}H NMR (C_4D_8O, 298 K, 500 MHz): δ 3.9 (s, coordinated NPh-*H*, 1H). ^{31}P{^{1}H} NMR (C_6D_6, 298 K, 202.5 MHz): δ 47.7 (s). T_1(min) for Ru-*H* = 0.697 s at 250 K in toluene-d_8. Anal. Calcd. for $C_{24}H_{33}N_2PRuSi_2$: C, 53.60; H, 6.19; N, 5.21. Found: C, 54.00; H, 6.38; N, 5.26.

[NPN(D)(η^6-C_6H_5)]RuH (12-d_1)

To a solution of **12** (0.048 g, 0.009 mmol) in toluene (2 mL) was added $LiN(SiMe_3)_2$ (0.016 g, 0.009 mmol). The mixture was stirred at room temperature for one hour at which time solid NEt_3·DCl (0.014 g, 0.009 mmol) was added to the reaction mixture. After stirring for one hour the mixture was filtered and the volatiles were removed under vacuum. The ^{1}H and ^{31}P{^{1}H} NMR data of the resultant orange solid (**12**-d_1) is identical to that of **12**, except that the N-*H* signal at δ 1.6 is no longer observed (0.045 g, 94 %).

References begin on page 184

[NPNH$_2$]Ru(H)$_2$(C$_7$H$_8$) (13)

Complex **13** is synthesized in an identical fashion as **12**. It is isolated as a yellow crystalline solid by the slow evaporation of the hexanes soluble rinsings of the product mixture (0.30 g, 32 %). X-ray quality crystals are obtained in this manner as well. ^{1}H NMR (C_6D_6, 298 K, 500 MHz): δ -10.2 (d, $^2J_{PH}$ = 43 Hz, Ru-*H*, 2H), δ 0.0 and 0.3 (s, SiC*H*$_3$, 12H total), δ 1.6 (m, PC*H*$_2$, 4H), δ 1.9 (s, coordinated toluene, PhC*H*$_3$, 3H), δ 4.8 (m, coordinated toluene, Ph *p-H*, 1H), δ 5.1 (d, coordinated toluene, Ph *o-H*, 2H), δ 5.2 (m, coordinated toluene, Ph *m-H*, 2H), δ 5.5 (s, N-*H*, 2H), δ 6.8 – 7.3 (m, NPh *o-,m-,p-H*, PPh *m-,p-H*, 13H), δ 7.9 (dd, PPh *o-H*, 2H). ^{31}P{^{1}H} (C_6D_6, 298 K, 202.5 MHz): δ 32.2 (s). T_1(min) for Ru-*H* = 0.366 s and N-*H* = 0.386 s at 260 K in toluene-d_8. Anal. Calcd. for $C_{31}H_{43}N_2PRuSi_2$: C, 58.92; H, 6.86; N, 4.43. Found: C, 58.64; H, 6.77; N, 4.63.

[NPNH$_2$(η^6-C$_6$H$_5$)]RuH$_2$ (14)

Method 1: A slurry of **3** (1.19 g, 1.84 mmol) in pentane (150 mL) was degassed by three free-pump-thaw cycles and stirred under 4 atm of H_2 for 6 hours. The initial red mixture turned brown with the formation of an orange solid. After removal of H_2 *in vacuo* the orange solid was isolated by filtration and washed with pentane (2 x 15 mL). The orange solid was identified as complex **12** by ^{1}H and ^{31}P{^{1}H} NMR spectroscopy. The dark brown filtrate was reduced in volume under vacuum (~ 10 mL) allowing complex **14** to be precipitated as a brown solid over a period of 2 hours (0.31 g, 31 %). **Method 2:** In lieu of pentane, THF may also be employed as the solvent. In this case, no precipitation of an orange solid occurs. Removal of the solvent and excess H_2 under vacuum generated a brown solid. The ^{1}H and ^{31}P{^{1}H} NMR spectra indicated a 50:50 mixture of complexes **12** and **14**. Attempts to separate the two species by rinsing with pentane were not successful. Isolation of **12** and **14** was more successful by employing method 1. ^{1}H NMR (C_6D_6, 298 K, 500 MHz): δ -10.2 (dd, $^2J_{PH}$ = 43 Hz, $^2J_{HH}$ = 6 Hz, Ru-*H*$_a$, 1H), δ -9.9 (dd, $^2J_{PH}$ = 40 Hz, $^2J_{HH}$ = 6 Hz, Ru-*H*$_b$, 1H), δ -0.5, -0.1, 0.0 and 0.3 (s, SiC*H*$_3$, 12H total), δ 0.85 – 1.75 (m, PC*H*$_2$, 4H), δ 1.6 (s, coordinated N*H*Ph, 1H), δ 4.6 (d, coordinated NHPh *o-H*, 1H), δ 4.8 (d, coordinated NHPh *o-H*, 1H), δ 4.9 (m, coordinated NHPh *p-H*, 1H), δ 5.4 (m, coordinated NHPh *m-H*, 1H), δ 5.6 (m, coordinated NHPh *m-H*, 1H), δ 5.7 (s, N*H*Ph, 1H), δ 6.6 – 7.2 (m, NHPh *o-*,

References begin on page 184

m-, p-H and PPh *m-, p-H*, 8H), δ 7.9 (dd, PPh *o-H*, 2H). The proton of the aryl-coordinated amine ligand displayed a shifted resonance in THF-d_8. ^{1}H NMR (C_4D_8O, 298 K, 500 MHz): δ 3.5 (s, coordinated NPh-*H*, 1H). $^{31}P\{^1H\}$ (C_6D_6, 298 K, 202.5 MHz): δ 40.2 (s). T_1(min) for Ru-*H* = 0.334 s and N-*H* = 0.344 s at 246 K in toluene-d_8. Attempts at obtaining single crystals for an X-ray diffraction study by the slow evaporation of a saturated hexanes solution resulted in the deposition of **12**.

Four atmosphere hydrogenation of [NPND]Ru(1-3:η^3-5,6:η^2-C_8H_{11}) (3-d_1)

[NPND]Ru(1-3:η^3-5,6:η^2-C_8H_{11}) (**3**-d_1) (0.058 g, 0.090 mmol) was dissolved in ~ 1.0 mL of THF-d_8 and transferred to a thick-walled glass vessel fitted with a Teflon valve and a ground glass joint. The vessel was evacuated with three freeze-pump-thaw cycles, cooled in a liquid N_2 bath and then one atmosphere of H_2 gas was added. The flask was sealed and thawed, and the mixture was stirred at room temperature for 30 minutes. The excess H_2 gas was removed under vacuum and the contents were placed in an NMR tube. The ^{1}H NMR spectrum showed the clean formation of a 50:50 mixture of complexes **12** and **14** in which all of the amino proton sites contained a hydrogen atom.

H_2 loss in [NPNH_2(η^6-C_6H_5)]RuH_2 (14) to give [NPN(H)(η^6-C_6H_5)]RuH (12)

In an NMR tube a solution of **14** dissolved in C_6D_6 was left to stand for 1 week in the glove box. At this time, the ^{1}H and $^{31}P\{^1H\}$ NMR data indicated the presence of complex **12**.

[NPNH_2] (15)

Toluene (25 mL) was added to a mixture of [NPN]Li_2·(C_4H_8O)$_2$ (0.50 g, 0.84 mmol) and NEt_3·HCl (0.26 g, 1.89 mmol) contained in a glass reaction vessel equipped with a Teflon valve and a ground glass joint. The vessel was sealed and heated at 80°C for two days. The solvent and other volatiles were removed under vacuum until a white solid remained. This solid was extracted

References begin on page 184

with hexanes (25 mL) and filtered. The hexanes was removed *in vacuo* leaving [$NPNH_2$] as a viscous, colourless oil (0.34 g, 92 %). ^{1}H NMR (C_6D_6, 298 K, 200 MHz): δ 0.01 and 0.18 (s, $SiCH_3$, 12H total), δ 1.12 (m, PCH_2, 4H), δ 2.88 (s, N-*H*, 2H), δ 6.98 - δ 7.58 (m, overlapping, PC_6H_5, 10H total). $^{31}P\{^1H\}$ NMR (C_6D_6, 298 K, 81 MHz): δ -41.8 (s). T_1(min) for N-*H* = 0.614 s at 240 K in toluene-d_8.

[$NPNH_2(\eta^6\text{-}C_6H_5)$]RuHCl (16) (*RR/SS* enantiomers)

A slurry of **12** (0.075 g, 0.14 mmol) and NEt_3·HCl (0.020 g, 0.14 mmol) in 15 mL of toluene contained in a sealed thick-walled glass vessel equipped with a Teflon valve and a stir bar was heated at 80°C for 24 hours. During this time the colour of the solution changed from orange to yellow and an insoluble yellow precipitate formed. Hexanes (10 mL) was added to the reaction mixture at room temperature ensure complete precipitation and the yellow solid was collected of a frit. It was then washed with hexanes and dried under vacuum to yield [$NPNH_2(\eta^6\text{-}C_6H_5)$]RuHCl (**16**) (0.078 g, 98 %). ^{1}H NMR (C_4D_8O, 298 K, 500 MHz): δ -8.23 (d, $^2J_{PH}$ = 52.2 Hz, Ru-*H*, 1H), δ -0.48, -0.26, 0.08 and 0.40 (s, $SiCH_3$, 12H total), δ 1.35, 1.68, 1.95 and 2.33 (m, ABX, PCH_2, 4H total), δ 3.75 (s, coordinated NPh-*H*, 1H), δ 5.41 (m, coordinated NHPh *m*-*H*, 1H), δ 5.60 (m, overlapping, coordinated NHPh *o*- and *p*-*H*, 3H total), δ 5.92 (m, coordinated NHPh *m*-*H*, 1H), δ 5.72 (s, pendant NPh-*H*, 1H), δ 7.10 – 7.84 (m, P*Ph* and pendant NH*Ph*, 10H total). $^{31}P\{^1H\}$ NMR (C_4D_8O, 298 K, 202.5 MHz): δ 45.6 (s).

[$NPNH_2(\eta^6\text{-}C_6H_5)$]RuHCl (16) (*SR/RS* enantiomers)

Leaving a solution of **16** (*RR/SS*) in THF-d_8 at room temperature over a period of 24 hours gives rise to a second species of **16** (*SR/RS*). The two complexes are present in approximately 1:1 ratio as determined by integration analysis. ^{1}H NMR (C_4D_8O, 298 K, 500 MHz): δ -8.02 (d, $^2J_{PH}$ = 55.8 Hz, Ru-*H*, 1H), δ -0.25, -0.23, 0.25 and 0.48 (s, $SiCH_3$, 12H total), δ 1.05, 1.30, 1.82 and 1.90 (m, overlapping, PCH_2, 4H total), δ 3.65 (s, coordinated NPh-*H*, 1H), δ 5.20 (m, coordinated NHPh *m*-*H*, 1H), δ 5.58 (m, overlapping, coordinated NHPh *o*-*H*), δ 5.70 (m, coordinated NHPh

References begin on page 184

p-H, 1H), δ 5.72 (s, pendant NPh-*H*, 1H), δ 5.82 (d, coordinated NHPh *o-H*), δ 6.18 (m, coordinated NHPh *m-H*, 1H), δ 6.63 – 8.60 (m, overlapping, P*Ph* and pendant NH*Ph*). $^{31}P\{^{1}H\}$ NMR (C_4D_8O, 298 K, 202.5 MHz): δ 43.6 (s).

[NPNHD(η^6-C_6H_5)]RuHCl (16-d_1)

The mono-deuterated complex **16**-d_1 was prepared in a manner identical to that used for **16** employing NEt_3·DCl in lieu of NEt_3·HCl. Amounts used: **12** (0.098 g, 0.18 mmol), NEt_3·DCl (0.025 g, 0.18 mmol). Yield: 0.099 g, 94 %. The ^{1}H NMR spectrum was identical to that for **16**, except for the peak at δ 5.7, which was no longer observed.

Reaction of [NPNHD(η^6-C_6H_5)]RuHCl (16-d_1) with KH·BEt_3

At room temperature solid KH·BEt_3 (0.012 g, 0.087 mmol) was added to a yellow solution of [NPNHD(η^6-C_6H_5)]RuHCl (**16**-d_1) (0.048 g, 0.084 mmol) in THF-d_8 (~ 1.0 mL). After stirring the reaction mixture for one hour the colour changed to orange. At this time the ^{1}H and $^{31}P\{^{1}H\}$ NMR spectra were recorded and these indicated a mixture of products including complexes **12** and **14**.

Reaction of [NPNHD(η^6-C_6H_5)]RuHCl (16-d_1) with $LiNMe_2$

A colourless solution of $LiNMe_2$ (0.005 g, 0.098 mmol) in THF-d_8 (~ 0.5 mL) was added to a yellow solution of [NPNHD(η^6-C_6H_5)]RuHCl (**16**-d_1) (0.054 g, 0.094 mmol) in THF-d_8 (~ 0.5 mL). After one hour the ^{1}H and $^{31}P\{^{1}H\}$ NMR spectra were recorded and these indicated a mixture of products including complex **12**.

References begin on page 184

^{Me}[NPN]Li_2·$C_4H_8O_2$ (17)

A solution of 1.6 M ^{n}BuLi in hexanes (50 0 mL, 0.080 mol) was added dropwise to a stirred slurry of $MeNH_2$·HCl (2.70 g, 0.040 mol) in 100 mL ether at 0°C. The mixture was then warmed to room temperature and stirred for one hour. Upon cooling to 0°C $ClCH_2SiMe_2Cl$ (5.2 mL, 0.0400 mol) was added dropwise via syringe and the resulting mixture was stirred for one hour at room temperature. After cooling to 0°C once again, $PhPH_2$ (2.20 g, 0.020 mol) was added via syringe followed by the dropwise addition of ^{n}BuLi (50.0 mL, 0.080 mol). The mixture was stirred at room temperature for 18 hours and the solvents were then removed under vacuum generating a foamy yellow solid. This solid was extracted with toluene (30 mL) and filtered through Celite to remove LiCl. Removal of the toluene *in vacuo* gives a yellow solid. The addition of a minimal amount of hexanes to dissolve the yellow solid and then 1,4-dioxane (3.88 g, 0.044 mol) causes ^{Me}[NPN]Li_2·$C_4H_8O_2$ (**17**) to precipitate from solution as a white, micro-crystalline solid (4.62 g, 56 %). ^{1}H NMR (C_6D_6, 298 K, 500 MHz): δ 0.1 (s, overlapping, SiCH_3, 12H), δ 0.8 (m, PCH_2, 4H), δ 2.8 (s, NCH_3, 6H), δ 3.6 (s, $C_4H_8O_2$, 8H), δ 7.1 (m, PPh *p-H*, 1H), δ 7.3 (m, PPh *m-H*, 2H), δ 7.5 (m, PPh *o-H*, 2H). ^{31}P{^{1}H}NMR (C_6D_6, 298 K, 202.5 MHz): δ -37.5 (s). ^{7}Li{^{1}H}NMR (C_6D_6, 298 K): δ 2.0 (s). Anal. Calcd. for $C_{18}H_{35}Li_2N_2O_2PSi_2$: C, 52.41; H, 8.55; N, 6.79. Found: C, 52.70; H, 8.42; N, 7.00.

Reaction of ^{Me}[NPN]Li_2·$C_4H_8O_2$ (17) with $[RuCl_2(cod)]_x$

Toluene (30 mL) was added to a mixture of **17** (0.56 g, 1.36 mmol) and $[RuCl_2(cod)]_x$ (0.38 g, 1.36 mmol) and the mixture was stirred for two days at room temperature. During this time the solution turned orange-brown. The mixture was filtered through Celite and the solvent removed under reduced pressure leaving an oily solid. The addition of hexanes caused the deposition of an orange solid. This was collected on a frit, washed with hexanes and dried under vacuum. The ^{1}H NMR spectrum consisted of very broad peaks indicative of a paramagnetic complex.

References begin on page 184

^{Me}[NPN]$ZrCl_2(C_4H_8O_2)$ (19)

Toluene (30 mL) was added to a mixture of **17** (0.210 g, 0.509 mmol) and $ZrCl_4$·2THF (0.192 g, 0.509 mmol) in a glass vessel equipped with a ground glass joint and a Teflon valve. The solid slurry was heated at 80°C for 18 hours. At room temperature the mixture was filtered through Celite. The toluene was removed under vacuum leaving an oily residue. Addition of hexanes causes the precipitation of ^{Me}[NPN]$ZrCl_2(C_4H_8O_2)$ (**19**) as a white, powdered solid (0.194 g, 67 %). ^{1}H NMR (C_6D_6, 298 K, 200 MHz): δ 0.01 and 0.02 (s, SiCH_3, 12H total), δ 1.22 (m, PCH_2, 4H), δ 3.30 (s, $C_4H_8O_2$, 8H), δ 3.36 (s, NCH_3, 6H), δ 7.10 (m, PPh *m*- and *p*-*H*, 3H), δ 7.76 (m, PPh *o*-*H*, 2H). ^{31}P{^{1}H} NMR (C_6D_6, 298 K, 81 MHz): δ -6.3 (s).

General procedure for catalytic hydrogenation studies

Benzylidene aniline. A typical procedure is as follows: In a thick-walled glass vessel fitted with a Teflon valve and a ground glass joint was added benzylidene aniline (0.100 g, 0.54 mmol) and ~ 2 % (mole %) of the catalyst precursor: **3** (7.0 mg), **11** (9.7 mg), **12** (5.8 mg), **13** (6.9 mg) or **14** (5.9 mg). Approximately 10 mL of toluene was added to dissolve the solids. Degassing was accomplished by three consecutive freeze-pump-thaw cycles, and one atmosphere of H_2 gas was added at –196°C (the flask was immersed in a liquid N_2 bath). The vessel was then sealed, warmed to room temperature and the contents stirred for 48 hours. The solvent and excess H_2 were removed in vacuo until a solid remained. Approximately 1 mL of C_6D_6 was added to dissolve the solid residue and the ^{1}H NMR spectrum was obtained. Conversions were determined by integration of substrate and product peaks. For complex **10**: complex **10** was first prepared by the reaction of **1** (8.1 mg) with hydrogen gas in an NMR tube. The contents of the NMR tube were then transferred to a thick-walled flask (as above) containing benzylidene aniline dissolved in toluene. The procedure was then continued as discussed above.

Olefin substrates. Procedures were performed in a manner identical to that employed for benzylidene aniline except that the reactions were in neat substrate. After 48 hours an aliquot of the reaction mixture was examined via ^{1}H NMR with a few drops of C_6D_6.

References begin on page 184

X-ray Crystallographic Analyses of Complexes 11, 12 and 13

Selected crystallographic data and structure refinement data are provided in Appendix 1.

3.10 References

(1) Ohkuma, T.; Kitamura, M.; Noyori, R. *Asymmetric Hydrogenation*; 2nd ed.; Ojima, I., Ed.; Wiley-VCH, Inc.: Toronto, 2000, pp 1.

(2) Cotton, F. A.; Wilkinson, G.; Murillo, C. A.; Bochmann, M. *Advanced Inorganic Chemistry: A Comprehensive Text*; 6th ed.; John Wiley and Sons, Inc.: Toronto, 1999, pp 1229-1242.

(3) Halpern, J. *J. Organomet. Chem.* **1980**, *200*, 133.

(4) Harmon, R. E.; Gupta, S. K.; Brown, D. J. *Chem. Rev.* **1973**, *73*, 21.

(5) James, B. R. *Homogeneous Hydrogenation*; Wiley: New York, 1973.

(6) Calvin, M. *Trans. Faraday Soc.* **1938**, *34*, 1181.

(7) Calvin, M. *J. Am. Chem. Soc.* **1939**, *61*, 2230.

(8) Roelen, O. *Angew. Chem.* **1948**, *60*, 62.

(9) Osborn, J. A.; Jardine, F. H.; Young, J. F.; Wilkinson, G. *J. Chem. Soc. A.* **1966**, 1711.

(10) Magee, M. P.; Norton, J. R. *J. Am. Chem. Soc.* **2001**, *123*, 1778.

(11) Collman, J. P.; Hegedus, L. S. *Principles and Applications of Organotransition Metal Chemistry*; University Science Books: Mill Valley, 1980, pp 316-402.

References begin on page 184

(12) Kubas, G. J. *Metal Dihydrogen and Sigma-bond Complexes. Structure, Theory and Reactivity*; Fackler, J. P. J., Ed.; Kluwer Academic/Plenum Publishers: New York, 2001.

(13) Jessop, P. G.; Morris, R. H. *Coord. Chem. Rev.* **1992**, *121*, 155.

(14) Kubas, G. J.; Ryan, R. R.; Swanson, B. I.; Vergamin, P. J.; Wasserman, H. J. *J. Am. Chem. Soc.* **1984**, *106*, 451.

(15) Heinekey, D. M.; Oldham, J., W. J. *Chem. Rev.* **1993**, *93*, 913.

(16) Morris, R. H.; Schlaf, M. *Inorg. Chem.* **1994**, *33*, 1725.

(17) Kubas, G. J. *Acc. Chem. Res.* **1988**, *21*, 120.

(18) Morris, R. H.; Earl, K. A.; Luck, R. L.; Lazarowych, N. J.; Sella, A. *Inorg. Chem.* **1987**, *26*, 2674.

(19) Law, J. K.; Mellows, H.; Heinekey, D. M. *J. Am. Chem. Soc.* **2002**, *124*, 1024.

(20) Esteruelas, M. A.; Garcia-Yebra, C.; Olivan, M.; Onate, E.; Tajada, M. A. *Organometallics* **2002**, *21*, 1311.

(21) Law, J. K.; Mellows, H.; Heinekey, D. M. *J. Am. Chem. Soc.* **2001**, *123*, 2085.

(22) Earl, K. A.; Jia, G.; Maltby, P. A.; Morris, R. H. *J. Am. Chem. Soc.* **1991**, *113*, 3027.

(23) Chin, R. M.; Barrera, J.; Dubois, R. H.; Helberg, L. E.; Sabat, M.; Bartucz, T. Y.; Lough, A. J.; Morris, R. H.; Harman, W. D. *Inorg. Chem.* **1997**, *36*, 3553.

(24) Klooster, W. T.; Koetzle, T. F.; Jia, G.; Fong, T. P.; Morris, R. H.; Albinati, A. *J. Am. Chem. Soc.* **1994**, *116*, 7677.

References begin on page 184

(25) Maltby, P. A.; Schlaf, M.; Steinbeck, M.; Lough, A. J.; Morris, R. H.; Klooster, W. T.; Koetzle, T. F.; Srivastava, R. C. *J. Am. Chem. Soc.* **1996**, *118*, 5396.

(26) Vaska, L.; DiLuzio, J. W. *J. Am. Chem. Soc.* **1962**, *84*, 679.

(27) Cappellani, E. P.; Drouin, S. D.; Jia, G.; Maltby, P. A.; Morris, R. H.; Schweitzer, C. T. *J. Am. Chem. Soc.* **1994**, *116*, 3375.

(28) Jia, G.; Morris, R. H. *J. Am. Chem. Soc.* **1991**, *113*, 875.

(29) Rocchini, E.; Mezzetti, A.; Ruegger, H.; Burckhardt, U.; Gramlich, V.; Del Zotto, A.; Martinuzzi, P.; Rigo, P. *Inorg. Chem.* **1997**, *36*, 711.

(30) Nishibayashi, Y.; Takei, I.; Hidai, M. *Angew. Chem. Int. Ed.* **1999**, *38*, 3047.

(31) Majumdar, K. K.; Nanishankar, H. V.; Jagirdar, B. R. *Eur. J. Inorg. Chem.* **2001**, 1847.

(32) Fong, T. P.; Forde, C. E.; Lough, A. J.; Morris, R. H.; Rigo, P.; Rocchini, E.; Stephan, T. *J. Chem. Soc., Dalton Trans.* **1999**, 4475.

(33) Schlaf, M.; Lough, A. J.; Maltby, P. A.; Morris, R. H. *Organometallics* **1996**, *15*, 2270.

(34) Ng, S. M.; Fang, Y. Q.; Lau, C. P.; Wong, W. T.; Jia, G. *Organometallics* **1998**, *17*, 2052.

(35) Jia, G.; Morris, R. H.; Schweitzer, C. T. *Inorg. Chem.* **1991**, *30*, 594.

(36) Chin, B.; Lough, A. J.; Morris, R. H.; Schweitzer, C. T.; D'Agostino, C. *Inorg. Chem.* **1994**, *33*, 6278.

(37) Landau, S. E.; Morris, R. H.; Lough, A. J. *Inorg. Chem.* **1999**, *38*, 6060.

References begin on page 184

(38) Bianchini, C.; Marchi, A.; Marvelli, L.; Peruzzini, M.; Romerosa, A.; Rossi, R.; Vacca, A. *Organometallics* **1995**, *14*, 3203.

(39) Jia, G.; Lee, H. M.; Williams, I. D.; Lau, C. P.; Chem, Y. *Organometallics* **1997**, *16*, 3941.

(40) Chinn, M. S.; Heinekey, D. M.; Payne, N. G.; Sofield, C. D. *Organometallics* **1989**, *8*, 1824.

(41) Huhmann-Vincent, J.; Scott, B. L.; Kubas, G. J. *J. Am. Chem. Soc.* **1998**, *120*, 6808.

(42) Heinekey, D. M.; Voges, M. H.; Barnhart, D. M. *J. Am. Chem. Soc.* **1996**, *118*, 10792.

(43) Chinn, M. S.; Heinekey, D. M. *J. Am. Chem. Soc.* **1990**, *112*, 5166.

(44) Heinekey, D. M.; Luther, T. A. *Inorg. Chem.* **1996**, *35*, 4396.

(45) Bianchini, C.; Meli, A.; Peruzzini, M.; Frediani, P.; Bohanna, C.; Esteruelas, M. A.; Oro, L. A. *Organometallics* **1992**, *11*, 138.

(46) Liu, S. H.; Lo, S. T.; Wen, T. B.; Zhou, Z. Y.; Lau, C. P.; Jia, G. *Organometallics* **2001**, *20*, 667.

(47) Jessop, P. G.; Morris, R. H. *Inorg. Chem.* **1993**, *32*, 2236.

(48) Lough, A. J.; Park, S.; Ramachandran, R.; Morris, R. H. *J. Am. Chem. Soc.* **1994**, *116*, 8356.

(49) Fryzuk, M. D.; MacNeil, P. A.; Rettig, S. J. *J. Am. Chem. Soc.* **1987**, *109*, 2803.

(50) Fryzuk, M. D.; Montgomery, C. D.; Rettig, S. J. *Organometallics* **1991**, *10*, 467.

(51) Custelcean, R.; Jackson, J. E. *Chem. Rev.* **2001**, *101*, 1963.

References begin on page 184

(52) Crabtree, R. H.; Siegbahn, P. E. M.; Eisenstein, O.; Rheingold, A. L.; Koetzle, T., F. *Acc. Chem. Res.* **1996**, *29*, 348.

(53) Lee, J., J. C.; Peris, E.; Rheingold, A. L.; Crabtree, R. H. *J. Am. Chem. Soc.* **1994**, *116*, 11014.

(54) Gusev, D. G.; Lough, A. J.; Morris, R. H. *J. Am. Chem. Soc.* **1998**, *120*, 13138.

(55) Abdur-Rashid, K.; Gusev, D. G.; Landau, S. E.; Lough, A. J.; Morris, R. H. *J. Am. Chem. Soc.* **1998**, *120*, 11826.

(56) Abdur-Rashid, K.; Gusev, D. G.; Lough, A. J.; Morris, R. H. *Organometallics* **2000**, *19*, 834.

(57) Landau, S. E.; Groh, K. E.; Lough, A. J.; Morris, R. H. *Inorg. Chem.* **2002**, *41*, 2995.

(58) Chu, H. S.; Lau, C. P.; Wong, K. Y.; Wong, W. T. *Organometallics* **1998**, *17*, 2768.

(59) Xu, W.; Lough, A. J.; Morris, R. H. *Inorg. Chem.* **1996**, *35*, 1549.

(60) Yao, W.; Crabtree, R. H. *Inorg. Chem.* **1996**, *35*, 3007.

(61) Schlaf, M.; Lough, A. J.; Morris, R. H. *Organometallics* **1996**, *15*, 4423.

(62) Grundemann, S.; Ulrich, S.; Limbach, H. H.; Golubev, N. S.; Denisov, G. S.; Epstein, L. M.; Sabo-Etienne, S.; Chaudret, B. *Inorg. Chem.* **1999**, *38*, 2550.

(63) Ayllon, J. A.; Sayers, S. F.; Sabo-Etienne, S.; Donnadieu, B.; Chaudret, B. *Organometallics* **1999**, *18*, 3981.

(64) Ayllon, J. A.; Gervaux, C.; Sabo-Etienne, S.; Chaudret, B. *Organometallics* **1997**, *16*, 2000.

References begin on page 184

(65) Bennett, M. A.; Bruce, M. I.; Matheson, T. W. *Comprehensive Organometallic Chemistry*; Wilkinson, S. G., Stone, F. G. A. and Abel, E. W., Ed.; Permagon Press: Toronto, 1982; Vol. 4, pp 741-742.

(66) Liu, S. H.; Yang, S. Y.; Lo, S. T.; Xu, Z.; Ng, W. S.; Wen, T. B.; Zhou, Z. Y.; Lin, Z.; Lau, C. P.; Jia, G. *Organometallics* **2001**, *20*, 4161.

(67) Lo, S. T.; Xu, Z.; Wen, T. B.; Ng, W. S.; Liu, S. H.; Zhou, Z. Y.; Lin, Z.; Lau, C. P.; Jia, G. *Organometallics* **2000**, *19*, 4523.

(68) Jalon, F. A.; Otero, A.; Rodriguez, A.; Perez-Manrique, M. *J. Organomet. Chem.* **1996**, *508*, 69.

(69) Guari, Y.; Sabo-Etienne, S.; Chaudret, B. *Organometallics* **1996**, *15*, 3471.

(70) Guari, Y.; Sabo-Etienne, S.; Chaudret, B. *J. Am. Chem. Soc.* **1998**, *120*, 4228.

(71) Guari, Y.; Ayllon, J. A.; Sabo-Etienne, S.; Chaudret, B.; Hessen, B. *Inorg. Chem.* **1998**, *37*, 640.

(72) Bautista, M.; Earl, K. A.; Morris, R. H.; Sella, A. *J. Am. Chem. Soc.* **1987**, *109*, 3780.

(73) Jia, G.; Lau, C. P. *Coord. Chem. Rev.* **1999**, *190-192*, 83.

(74) Heinekey, D. M.; Mellows, H.; Pratum, T. *J. Am. Chem. Soc.* **2000**, *122*, 6498.

(75) Taw, F. L.; Mellows, H.; White, P. S.; Hollander, F. J.; Bergman, R. G.; Brookhart, M.; Heinekey, D. M. *J. Am. Chem. Soc.* **2002**, *124*, 5100.

(76) Oldham Jr., W. J.; Hinkle, A. S.; Heinekey, D. M. *J. Am. Chem. Soc.* **1997**, *119*, 11028.

References begin on page 184

(77) Gusev, D. G.; Hubener, R.; Burger, P.; Orama, O.; Berke, H. *J. Am. Chem. Soc.* **1997**, *119*, 3716.

(78) Hamilton, D. G.; Crabtree, R. H. *J. Am. Chem. Soc.* **1988**, *110*, 4126.

(79) Luo, X. L.; Crabtree, R. H. *Inorg. Chem.* **1990**, *29*, 2788.

(80) Desrosiers, P. J.; Cai, L.; Lin, Z.; Richards, R.; Halpern, J. *J. Am. Chem. Soc.* **1991**, *113*, 4173.

(81) Bautista, M. T.; Earl, K. A.; Maltby, P. A.; Morris, R. H.; Schweitzer, C. T.; Sella, A. *J. Am. Chem. Soc.* **1988**, *110*, 7031.

(82) Gusev, D. G.; Kuhlman, R. L.; Renkema, K. B.; Eisenstein, O.; Caulton, K. *Inorg. Chem.* **1996**, *35*, 6775.

(83) Luther, T. A.; Heinekey, D. M. *Inorg. Chem.* **1998**, *37*, 127.

(84) Heinekey, D. M.; Oldham Jr., W. J. *J. Am. Chem. Soc.* **1994**, *116*, 3137.

(85) Hamilton, D. G.; Luo, X. L.; Crabtree, R. H. *Inorg. Chem.* **1989**, *28*, 3198.

(86) Paneque, M.; Poveda, M. L.; Taboada, S. *J. Am. Chem. Soc.* **1994**, *116*, 4519.

(87) Luo, X. L.; Crabtree, R. H. *J. Am. Chem. Soc.* **1990**, *112*, 6912.

(88) Bampos, N.; Field, L. D. *Inorg. Chem.* **1990**, *29*, 587.

(89) King, W. A.; Scott, B. L.; Eckert, J.; Kubas, G. J. *Inorg. Chem.* **1999**, *38*, 1069.

(90) Gutierrez-Puebla, E.; Monge, A.; Paneque, M.; Poveda, M. L.; Taboada, S.; Trujillo, M.; Carmona, E. *J. Am. Chem. Soc.* **1999**, *121*, 346.

References begin on page 184

(91) Heinekey, D. M.; Hinkle, A. S.; Close, J. D. *J. Am. Chem. Soc.* **1996**, *118*, 5353.

(92) Saunders, M.; Jaffe, M. H.; Vogel, P. *J. Am. Chem. Soc.* **1971**, *93*, 2558.

(93) Saunders, M.; Kates, M. R. *J. Am. Chem. Soc.* **1977**, *99*, 8071.

(94) Saunders, M.; Telkowski, L.; Kates, M. R. *J. Am. Chem. Soc.* **1977**, *99*, 8070.

(95) Bullock, R. M.; Song, J. S.; Szalda, D. J. *Organometallics* **1996**, *15*, 2504.

(96) Yao, W.; Faller, J. W.; Crabtree, R. H. *Inorg. Chim. Acta* **1997**, *259*, 71.

(97) Abdur-Rashid, K.; Gusev, D. G.; Lough, A. J.; Morris, R. H. *Organometallics* **2000**, *19*, 1652.

(98) Sabo-Etienne, S.; Chaudret, B. *Coord. Chem. Rev.* **1998**, *178-180*, 381.

(99) Rodriguez, V.; Sabo-Etienne, S.; Chaudret, B.; Thoburn, J.; Ulrich, S.; Limbach, H. H.; Eckert, J.; Barthelat, J. C.; Hussein, K.; Marsden, C. J. *Inorg. Chem.* **1998**, *37*, 3475.

(100) Borowski, A. F.; Sabo-Etienne, S.; Christ, M. L.; Donnadieu, B.; Chaudret, B. *Organometallics* **1996**, *15*, 1427.

(101) Shubina, E. S.; Belkova, N. V.; Krylov, A. N.; Vorontsov, E. V.; Epstein, L. M.; Gusev, D. G.; Niedermann, M.; Berke, H. *J. Am. Chem. Soc.* **1996**, *118*, 1105.

(102) Esteruelas, M. A.; Oro, L. A.; Valero, C. *Organometallics* **1992**, *11*, 3362.

(103) Esteruelas, M. A.; Oro, L. A. *Chem. Rev.* **1998**, *98*, 577.

References begin on page 184

(104) Jackson, S. A.; Hodges, P. M.; Poliakoff, M.; Turner, J. J.; Grevels, F. W. *J. Am. Chem. Soc.* **1990**, *112*, 1221.

(105) Jia, G.; Ng, W. S.; Lau, C. P. *Organometallics* **1998**, *17*, 4538.

(106) Crabtree, R. H. *The Organometallic Chemistry of the Transition Metals*; 2nd ed.; John Wiley and Sons: New York, 1994, pp 221.

(107) Perrin, C. L.; Dwyer, T. J. *Chem. Rev.* **1990**, *90*, 935.

(108) Jeener, J.; Meier, B. H.; Bachmann, P.; Ernst, R. R. *J. Chem. Phys.* **1979**, *71*, 4546.

(109) Abdur-Rashid, K.; Lough, A. J.; Morris, R. H. *Organometallics* **2001**, *20*, 1047.

(110) Abdur-Rashid, K.; Faatz, M.; Lough, A. J.; Morris, R. H. *J. Am. Chem. Soc.* **2001**, *123*, 7473.

(111) Abdur-Rashid, K.; Lough, A. J.; Morris, R. H. *Organometallics* **2000**, *19*, 2655-2657.

(112) Boncella, J. M.; Eve, T. M.; RickMan, B.; Abboud, K. A. *Polyhedron* **1998**, *17*, 725.

(113) Patel, B. P.; Wessel, J.; Yao, W.; Lee, J., J. C.; Peris, E.; Koetzle, T. F.; Yap, G. P. A.; Fortin, J. B.; Ricci, J. S.; Sini, G.; Albinati, A.; Eisenstein, O.; Rheingold, A. L.; Crabtree, R. H. *New J. Chem.* **1997**, *21*, 413.

(114) Simal, F.; Jan, D.; Demonceau, A.; Noels, A. F. *Tetrahedron Lett.* **1999**, *40*, 1653.

(115) Torres, F.; Sola, E.; Martin, M.; Ochs, C.; Picazo, G.; Lopez, J. A.; Lahoz, F. J.; Oro, L. A. *Organometallics* **2001**, *20*, 2716.

(116) Park, S.; Lough, A. J.; Morris, R. H. *Inorg. Chem.* **1996**, *35*, 3001.

References begin on page 184

(117) Chu, H. S.; Lau, C. P.; Wong, K. Y. *Organometallics* **1998**, *17*, 2768.

(118) Dewey, M. A.; Stark, G. A.; Gladysz, J. A. *Organometallics* **1996**, *15*, 4798.

(119) Bryndza, H. E.; Domaille, P. J.; Paciello, R. A.; Bercaw, J. E. *Organometallics* **1989**, *8*, 379.

(120) Brunner, H. *Adv. Organomet. Chem.* **1980**, *18*, 152.

(121) Martin, G. C.; Boncella, J. M.; Wucherer, E. J. *Organometallics* **1991**, *10*, 2804.

(122) Bickford, C. C.; Johnson, T. J.; Davidson, E. R.; Caulton, K. G. *Inorg. Chem.* **1994**, *33*, 1080.

(123) Johnson, T. J.; Folting, K.; Streib, W. E.; Martin, J. D.; Huffman, J. C.; Jackson, S. A.; Eisenstein, O.; Caulton, K. G. *Inorg. Chem.* **1995**, *34*, 488.

(124) Heller, D.; Drexler, H.; Spannenberg, A.; Heller, B.; You, J.; Baumann, W. *Angew. Chem. Int. Ed.* **2002**, *41*, 777.

(125) Wiles, J. A.; Bergens, S. H. *Angew. Chem. Int. Ed.* **2001**, *40*, 914.

(126) Dobbs, D. A.; Vanhessche, K. P. M.; Brazi, E.; Rautenstrauch, V.; Lenoir, J. Y.; Genet, J. P.; Wiles, J.; Bergens, S. H. *Angew. Chem. Int. Ed.* **2000**, *39*, 1992.

(127) Rossen, K. *Angew. Chem. Int. Ed.* **2001**, *40*, 4611.

(128) James, B. R. *Catalysis Today* **1997**, *37*, 209.

(129) Fryzuk, M. D.; Piers, W. E. *Organometallics* **1990**, *9*, 986.

References begin on page 184

(130) Noyori, R.; Ohkuma, T. *Angew. Chem. Int. Ed.* **2001**, *40*, 40.

(131) Gruet, K.; Crabtree, R. H.; Lee, D. H.; Liable-Sands, L.; Rheingold, A. L. *Organometallics* **2000**, *19*, 2228.

(132) Fryzuk, M. D.; Johnson, S. A.; Rettig, S. J. *J. Am. Chem. Soc.* **1998**, *120*, 11024.

(133) Fryzuk, M. D.; Johnson, S. A.; Patrick, B. O.; Albinati, A.; Mason, S. A.; Koetzle, T. K. *J. Am. Chem. Soc.* **2001**, *123*, 3960.

(134) Fryzuk, M. D.; Montgomery, C. D. *Coord. Chem. Rev.* **1989**, *95*, 1.

(135) Hartwig, J. F. *J. Am. Chem. Soc.* **1996**, *118*, 7010.

(136) Cetinkaya, B.; Lappert, M. F.; Torroni, S. *Chem. Commun.* **1979**, 599.

(137) Bullock, R. M.; Voges, M. H. *J. Am. Chem. Soc.* **2000**, *122*, 12594.

(138) Bullock, R. M.; Rappoli, B. J. *J. Chem. Soc., Chem. Commun.* **1989**, 1447.

(139) Song, J. S.; Szalda, D. J.; Bullock, R. M.; Lawrie, C. J. C.; Rodkin, M. A.; Norton, J. R. *Angew. Chem. Int. Ed. Engl.* **1992**, *31*, 1233.

(140) Johnson, S. A. *Ligand Design and The Synthesis of Reactive Organometallic Complexes of Tantalum for Dinitrogen Activation*; University of British Columbia: Vancouver, 2000.

(141) Fryzuk, M. D.; Love, J. B.; Rettig, S. J.; Young, V. G. *Science* **1997**, *275*, 1445.

(142) Baudler, M.; Zarkdas, A. *Chem. Ber.* **1965**, *104*, 1034.

References begin on page 184

(143) Manzer, L. E. *Inorganic Synthesis* **1982**, *21*, 135.

References begin on page 184

Chapter 4

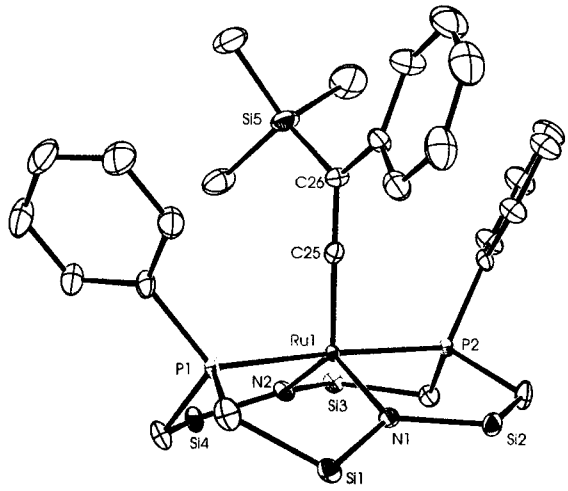

Reaction of the Amidophosphine Ligands [NPN] and [P_2N_2] with Ruthenium(II) Alkylidene and Vinylidene Complexes

4.1 Introduction

Transition metal catalyzed olefin metathesis is an important method for the formation of carbon-carbon bonds.[1,2] Some of the diverse applications of olefin metathesis include the formation of heterocycles by ring-closing metathesis (RCM),[1,3-9] the synthesis of polymers by ring-opening metathesis polymerization (ROMP),[1,3,4,10-12] and the preparation of new substituted acyclic olefins by cross metathesis.[1,4,13-15] During the last decade the development of well-defined ruthenium(II) alkylidene complexes has allowed for tremendous progress to be made in this area.[13,14,16-25] The ruthenium benzylidene complex $(PCy_3)_2Cl_2Ru(CHPh)$ (**A** in Figure 4.1) is one example of these complexes that have been utilized for the olefin metathesis reaction.[13] Complex **A**, commonly referred to as Grubbs' catalyst, is five-coordinate and exhibits a distorted square pyramidal geometry with the

References begin on page 237

mutually *trans* phosphine and chloride ligands in the plane of the molecule, and the benzylidene unit at the vertex of the pyramid. Both experimental and theoretical studies implicate phosphine dissociation generating a 14-electron mono-phosphine benzylidene species as the initial step in the catalytic process. Substrate coordination to the vacant site allows for olefin metathesis to proceed via a metallocyclobutane intermediate. This mechanism is depicted in Figure 4.1.[26-29] Other ruthenium "alkylidene-type" complexes have also found success in olefin metathesis processes. Among these include vinylidene (M=C=C)[30-33] and allenylidene (M=C=C=C)[32,34-41] complexes of ruthenium(II). The ease of synthesis compared to that of the Grubbs' catalyst is an attractive feature of the vinylidene and allenylidene metal complexes.

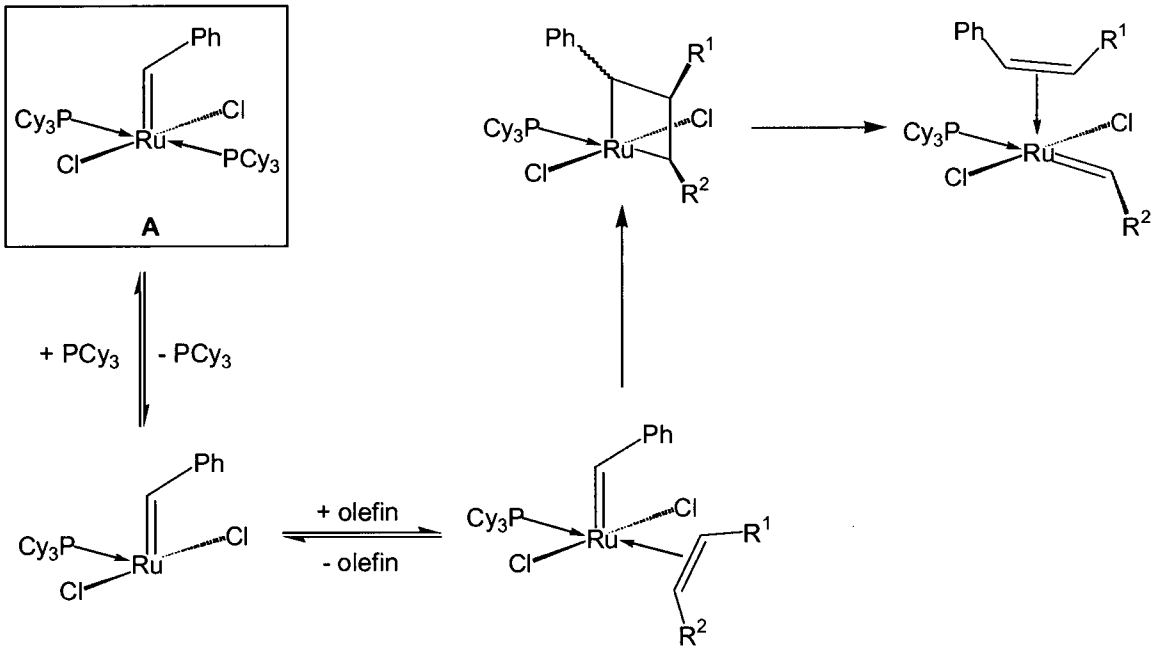

Figure 4.1. The mechanism for olefin metathesis utilizing the Grubbs' catalyst (**A**). A cross metathesis reaction is shown.

The presence of a labile phosphine donor and the two chloride ligands in the benzylidene complex **A** suggested that it may be a suitable precursor for the coordination of the [P_2N_2] and [NPN] ligands. This chapter discusses our attempts at isolating ruthenium(II)

References begin on page 237

alkylidene complexes containing the [NPN] and [P_2N_2] ligand sets and utilizing these species in olefin metathesis processes. Our initial investigations involved the Grubbs' catalyst $(PCy_3)_2Cl_2Ru(CHPh)$ as a starting material, however, due to difficulties that we encountered in the coordination of the [NPN] and [P_2N_2] ligands with this complex we examined related vinylidene precursors, $(P^iPr_3)_2Cl_2Ru(CCRPh)$ (R = H or $SiMe_3$).

4.2 Reaction of $[NPN]Li_2{\cdot}(C_4H_8O)_2$ and $[P_2N_2]Li_2{\cdot}(C_4H_8O_2)$ with $(PCy_3)_2Cl_2Ru(CHPh)$

The reaction of the [NPN] and [P_2N_2] ligands with the alkylidene complex $(PCy_3)_2Cl_2Ru(CHPh)$ did not give clean formation of the expected substitution products [NPN]$(PCy_3)Ru(CHPh)$ or [P_2N_2]Ru(CHPh); rather, a mixture of products resulted as indicated by the ^1H and $^{31}P\{^1H\}$ NMR data. Variation in the solvent employed or the reaction temperature had no significant effect on the outcome of the reactions. It is possible that the bulky and basic PCy_3 ligands may not allow for facile substitution to take place, and consequently other avenues for reaction may be more likely. A potential competitive side-reaction could be the deprotonation of the alkylidene proton to give a ruthenium carbyne (Ru≡CPh) complex. A ruthenium carbyne complex has been suggested as a probable intermediate in the hydrogen-deuterium exchange reactions of the starting material $(PCy_3)_2Cl_2Ru(CHPh)$.[42] Several cationic ruthenium carbyne-hydride species have recently been isolated from ruthenium vinylidene complexes.[43,44]

In contrast, metathetical and substitution reactions have been successfully employed with the Grubbs' complex $(PCy_3)_2Cl_2Ru(CHPh)$. For example, its reaction with an excess of KO^tBu generates the four coordinate species $(PCy_3)(^tBuO)_2Ru(CHPh)$,[45] and the addition of KTp (where Tp = tris(pyrazolyl)borate) allows for the preparation of the neutral six-coordinate complex $Tp(PCy_3)(Cl)Ru(CHPh)$ containing the chelating Tp ligand.[46] The substitution reactions of Grubbs' complex with bidentate Schiff-base ligands incorporating substituted phenoxy donors was performed after converting the ligands to the corresponding

References begin on page 237

thallium salts, as shown in Scheme 4.1.[47] Among the various salts tested the thallium salts proved to be the most effective, however, the efficiency of the substitution reactions varied depending on the bulk of the substituents on the ligands. For example, while ligands bearing a methyl group at the 6-position of the phenoxy fragment readily underwent substitution, the reaction of ligands bearing the bulkier tertiary butyl substituent at the same position gave poor conversion under similar substitution conditions.

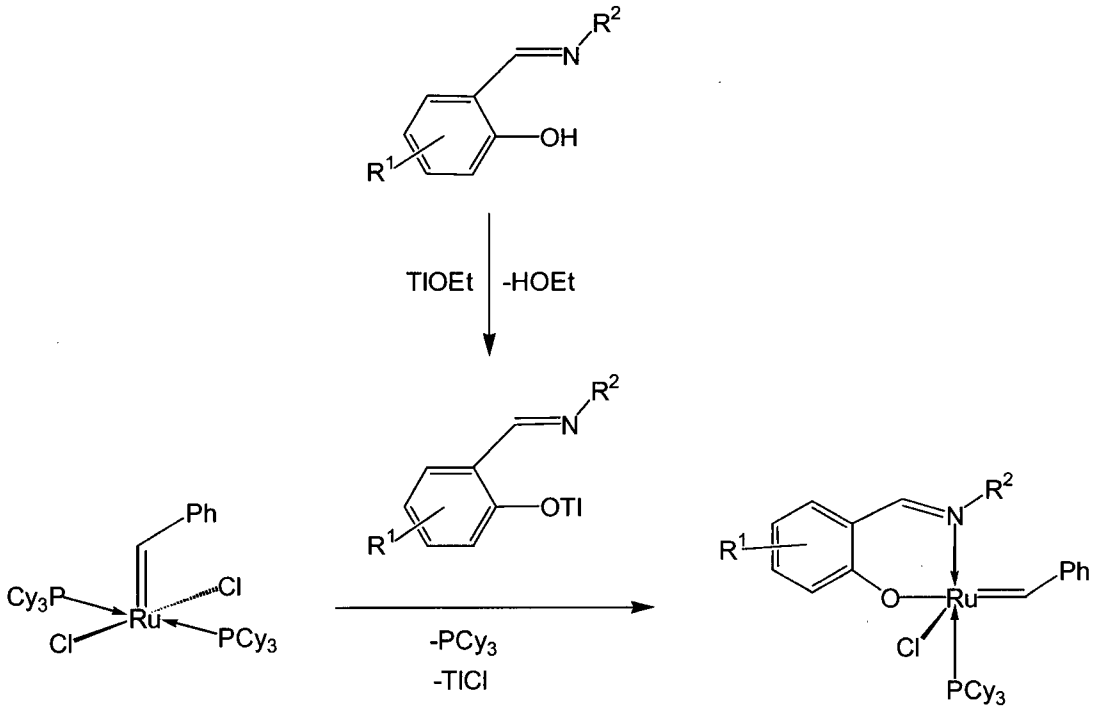

Scheme 4.1

These studies show that subtle differences in the electronic and steric properties of the ligands can influence the outcome of the substitution reactions. The successful incorporation of the [NPN] and [P_2N_2] ligands onto $(PCy_3)_2Cl_2Ru(CHPh)$ may be possible by employing other salts of these ligands, such as potassium or thallium. This will be addressed in the Future Work section of this chapter (section 4.9).

References begin on page 237

4.3 Synthesis and Characterization of [NPNH](P^iPr_3)Ru(CCPh) (20)

(i) Reaction of [NPN]Li_2·$(C_4H_8O)_2$ with (P^iPr_3)$_2Cl_2$Ru(CCHPh)

Initial investigations into the reaction of the [NPN] ligand with the vinylidene complex (P^iPr_3)$_2Cl_2$Ru(CCHPh) utilized tetrahydrofuran as the solvent. An immediate change in colour from purple to dark brown takes place at room temperature. The $^{31}P\{^1H\}$ NMR spectrum of the crude product mixture shows the presence of two products and triisopropylphosphine. The same results are obtained when the reaction is performed at -78 °C and then warmed to room temperature. The major species (*ca.* 60 %) contains two doublets in the $^{31}P\{^1H\}$ NMR spectrum at δ 45.9 and δ 80.5 ($^2J_{PP}$ = 48 Hz), and the minor species contains two doublets at δ 57.1 and δ 76.4 ($^2J_{PP}$ = 41 Hz). These similar spectral features suggest that the two products may be structurally related. The doublet coupling pattern arises due to the presence of a coordinated P^iPr_3 ligand and a coordinated [NPN] ligand, and the small phosphorus-31 coupling constants indicate a *cis* arrangement between the phosphine donors in both complexes. The ^1H NMR spectrum shows resonances that are commonly observed for metal complexes containing the [NPN] ligand set. The inequivalent silyl methyl and aromatic proton resonances suggest that both species posses low symmetry in solution. In the ruthenium precursor, the β-hydrogen atom of the vinylidene moiety is observed as a well-resolved triplet at δ 4.6 due to coupling with the two equivalent P^iPr_3 ligands. If the substitution product [NPN](P^iPr_3)Ru(CCHPh) was produced this resonance may be expected to appear as a higher-order multiplet arising from coupling with the two different phosphine ligands. Although no such resonance is apparent in the ^1H NMR spectrum of the crude product mixture, two singlets are observed at δ 4.9 (minor species) and δ 5.1 (major species) suggesting that a vinylidene moiety may not be present in the products of this reaction. This implies that displacement of the two chloride ligands and one equivalent of P^iPr_3 by the chelating [NPN] donor to yield the anticipated complex [NPN](P^iPr_3)Ru(CCHPh) did not occur. The β-hydrogen atom of the vinylidene unit is known to be acidic,[48-50] and it is therefore possible that deprotonation by one of the amido

References begin on page 237

donors of the [NPN] ligand set has occurred. Attempts at separating the two products of this reaction were unsuccessful due to the similar solubilities of these species in hydrocarbon solvents, and consequently, further structural elucidation was not possible.

Given the success utilizing toluene as the solvent for the reactions of the [NPN] ligand with the starting material $[RuCl_2(cod)]_x$ the above reaction was also attempted in toluene. The initial purple coloured solution gradually lightens to a violet colour within 30 minutes at room temperature; after two hours the solution is dark brown, similar to what is observed when the reaction is performed in THF. The ^1H and $^{31}P\{^1H\}$ NMR data of the crude product show the formation of a single species (**20**) and free P^iPr_3. Interestingly, this new species exhibits spectra identical to those of the minor product when the reaction was performed in THF. Purification of this complex was accomplished by the slow evaporation of a hexanes solution, which results in the deposition of purple block crystals. The isolated yield of **20** is low, however, due to the high solubility of this species in hexanes.

(ii) Solid-state and solution characterization of [NPNH](P^iPr_3)Ru(CCPh) (20)

The solid-state infra-red spectrum (KBr pellet) of a sample of powdered crystals of complex **20** shows significant differences than that of the precursor vinylidene complex. For example, the vinylidene (C=C) band occurs at 1600 cm^{-1} in $(P^iPr_3)_2Cl_2Ru(CCHPh)$,[51] however, no such peak is evident in the IR spectrum of **20**. Rather a peak at 2050 cm^{-1} is observed consistent with the presence of a carbon-to-carbon triple bond (C≡C). In comparison, the spectrum of the complex $[Ru(C{\equiv}CPh)(PPh_3)_2(\eta^5\text{-}C_5Me_5)]$ contains ν(C≡C) at 2066 cm^{-1}.[48] In addition, a peak at 3194 cm^{-1} is indicative of an N-H stretching mode. Based on the IR data we propose the formulation of complex **20** as [NPNH](P^iPr_3)Ru(CCPh), in which proton transfer from the vinylidene moiety to one of the amido donors generates an [NPNH] chelating array and a σ-alkynyl ligand (equation 4.1). Elemental analysis supports this formulation.

References begin on page 237

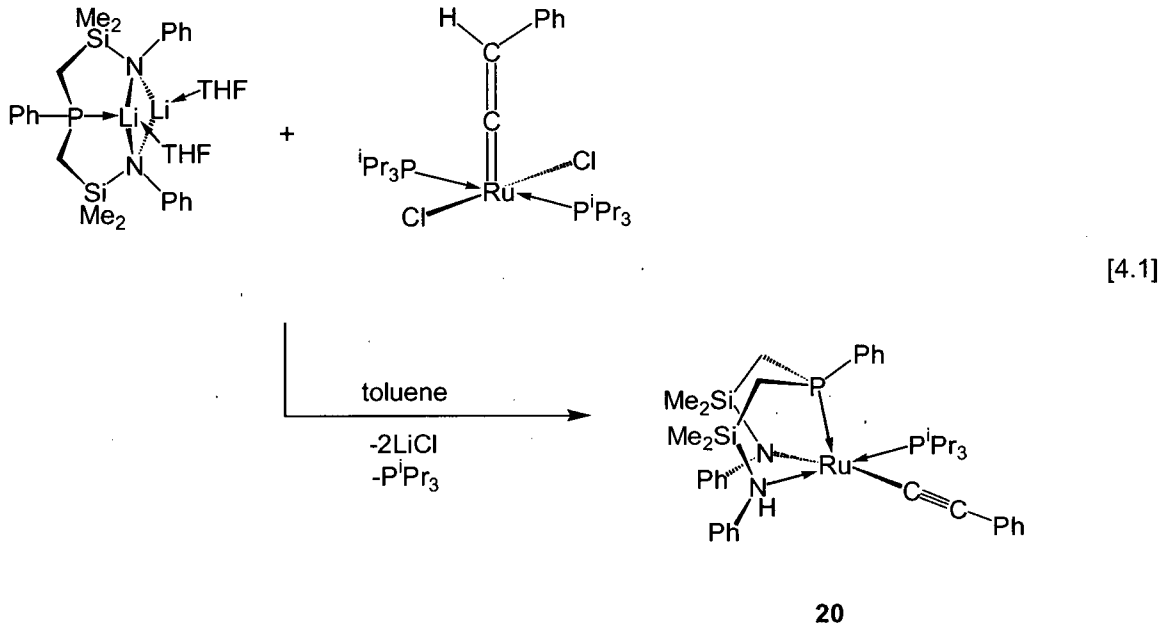

[4.1]

20

The structure of **20** was verified by a single crystal X-ray diffraction study. The solid-state molecular structure is shown in Figure 4.2 and selected bond lengths and angles are listed in Table 4.1. As seen from the ORTEP drawing, complex **20** has a distorted square pyramidal structure with the phosphine donor of the chelating [NPNH] ligand set at the apical position. The Ru-P distance for this ligand is significantly shorter than that to the P^iPr_3 ligand (2.1901(6) Å vs. 2.3131(6) Å). The shorter bond distance is most likely a consequence of the vacant site located *trans* to the chelating phosphine donor. The solid-state molecular structure confirms the presence of a terminal alkynyl ligand in complex **20** as indicated by the short carbon-carbon bond length (1.222(3) Å) and the linearity of the Ru(1)-C(34)-C(35) and C(34)-C(35)-C(36) bonds (*ca.* 177° and 174°, respectively). The amino proton H(58) was located confirming that proton transfer from the vinylidene moiety has occurred.

The ruthenium-amide distance in **20** (2.189(2) Å) is longer than that observed in complex **3** (2.019(2) Å). Although both complexes are five-coordinate ruthenium(II) species, **20** is square pyramidal whereas **3** adopts a distorted trigonal bipyramidal geometry (or Y-shape). As was discussed in chapter 2, the presence of a single π-donating ligand in d^6 ML_5

References begin on page 237

complexes usually favours a distorted trigonal bipyramidal structure since this allows for multiple bonding between the empty metal *d*-orbital (d_{xy}) and the lone pair of the π-donor.[52,53] This manifests as a shortening of the M-X bond. In the case of a square pyramidal geometry such a π-interaction is not possible because all of the symmetry adapted *d*-orbitals are filled.[52,53] In complex **20** there is an intramolecular hydrogen bonding interaction between the amido nitrogen lone pair and the proton of the *cis* coordinated amine donor. The N(2)···H(58) separation of 2.367 Å is well within the van der Waals contact distance of 2.7 Å between nitrogen and hydrogen nuclei.[54] Since the amide lone pair partakes in this interaction it is not available for π-bonding with the metal centre and this may be the reason that a distorted trigonal bipyramidal geometry is not observed. Alternatively, a square planar structure may allow for minimized steric interactions. As can be seen in Figure 4.2, the phenyl groups of the amido and amino donors are oriented towards the open face of the molecule. In a Y-shaped structure either the alkynyl ligand or the P^iPr_3 ligand would be located adjacent to these phenyl substituents, thus, increasing the steric interactions between these groups. As seen in the ORTEP drawing, the [NPNH] phenyl groups as well as the P^iPr_3 methyl groups can shield the vacant site at the metal centre.

References begin on page 237

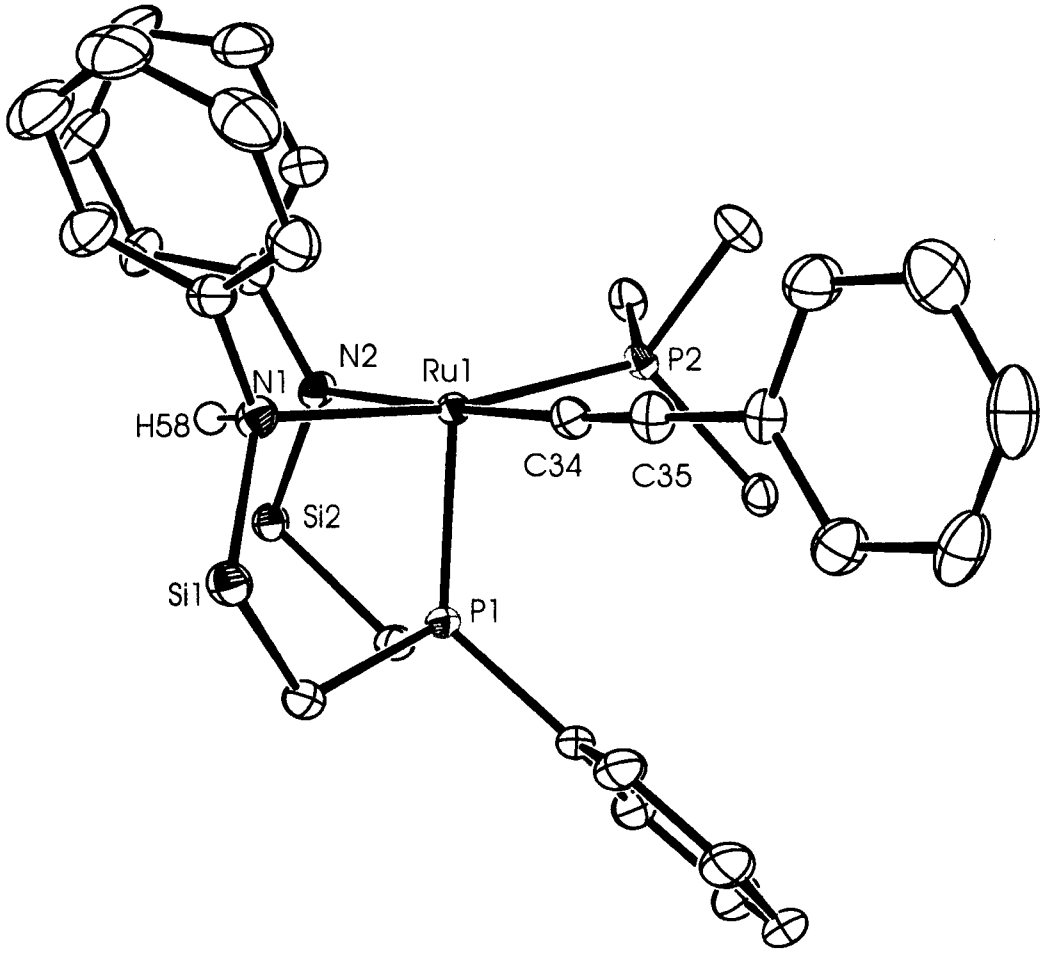

Figure 4.2. ORTEP representation (50% thermal ellipsoids) of the solid-state molecular structure of [NPNH](P^iPr_3)Ru(CCPh) (**20**) as determined by X-ray diffraction. The silyl methyl groups of the [NPNH] ligand and the isopropyl methyl groups of the P^iPr_3 ligand have been omitted for clarity. The amino proton H(58) was located.

Table 4.1. Selected bond lengths and bond angles in [NPNH](P^iPr_3)Ru(CCPh) (**20**).

Atom	Atom	Distance (Å)	Atom	Atom	Distance (Å)
Ru(1)	P(1)	2.1901(6)	Ru(1)	C(34)	2.003(2)
Ru(1)	P(2)	2.3131(6)	C(34)	C(35)	1.222(3)
Ru(1)	N(1)	2.259(2)	N(1)	H(58)	0.842
Ru(1)	N(2)	2.189(2)	N(2)	H(58)	2.367

References begin on page 237

Atom	Atom	Atom	Angle (°)	Atom	Atom	Atom	Angle (°)
N(1)	Ru(1)	N(2)	80.59(7)	P(1)	Ru(1)	N(1)	89.78(5)
N(1)	Ru(1)	C(34)	93.33(8)	P(1)	Ru(1)	N(2)	87.24(5)
N(1)	Ru(1)	P(2)	169.79(5)	P(1)	Ru(1)	C(34)	95.80(6)
N(2)	Ru(1)	P(2)	99.97(5)	Ru(1)	C(34)	C(35)	176.5(2)
N(2)	Ru(1)	C(34)	173.22(8)	C(34)	C(35)	C(36)	174.4(2)
P(2)	Ru(1)	C(34)	85.48(6)	Ru(1)	N(1)	H(58)	94(2)
P(1)	Ru(1)	P(2)	100.44(2)	N(1)	H(58)	N(2)	119.67

Complex **20** has also been characterized in solution by ^{1}H and ^{31}P{^{1}H} NMR spectroscopy. The ^{1}H NMR spectrum indicates the presence of a single, non-fluxional species; furthermore, the number of peaks that are observed reveals that the complex possesses low symmetry. This is consistent with the solid-state structure, which shows that complex **20** exhibits C_1 symmetry, and contains a chiral metal centre as well as chiral amine, amide and phosphine ligands. For example, four silyl methyl proton resonances and four methylene resonances of the tridentate ligand backbone are observed. A multiplet at δ 2.10 that integrates to three protons has been assigned as the methine hydrogen atoms of the P^{i}Pr$_3$ ligand and the two diastereotopic methyl groups of the P^{i}Pr$_3$ ligand are observed at δ 0.92 and δ 1.08. The presence of a single peak for the methine hydrogen atoms and two peaks for the methyl groups of the P^{i}Pr$_3$ ligand indicate that there is free rotation about the ruthenium-phosphorus bond, but hindered rotation about the phosphorus-carbon bonds within this ligand. The amino proton appears as a singlet at δ 4.95 and the aromatic protons in complex **20** are dispersed between δ 5.75 and δ 8.08. In the ^{31}P{^{1}H} NMR spectrum, the P^{i}Pr$_3$ ligand exists as a doublet at δ 57.0 and the phosphorus signal for the phosphine donor of the [NPNH] ligand occurs as a doublet at δ 76.5. These assignments were made by performing selective ^{1}H{^{31}P} decoupling experiments. The magnitude of coupling between these two sites ($^2J_{PP}$ = 41 Hz) implies a *cis* orientation between the phosphine ligands consistent with that observed in the solid state.

References begin on page 237

(iii) Speculations into the identity of the second species that forms in THF

It is interesting that a simple modification in the synthetic procedure (i.e. changing the solvent from THF to toluene) would have such a drastic effect on the outcome of this reaction. The formation of a single species (**20**) when the reaction is performed in toluene as opposed to two products in THF is not easy to rationalize; it is also intriguing that complex **20** forms as the sole product in toluene but would form as the minor species in THF. The characterization of **20** allows for speculations regarding the identity of the second species that forms in THF. The similar ^{1}H and $^{31}P\{^{1}H\}$ NMR data of these two compounds suggests that they are structurally related. It has already been mentioned that **20** is a chiral complex, and it is therefore likely that the unknown species is a diastereomer of **20**. Two examples are shown in Figure 4.3. Isomer **A** exhibits a distorted trigonal bipyramidal geometry with the $P^{i}Pr_3$ ligand in the plane of the molecule; this is a necessary condition given the small coupling (48 Hz) between the two phosphine donors. We have already suggested that such a structure would be unfavourable for steric reasons. Furthermore, there is no electronic stabilization since the amido donor is not located opposite the acute angle in the trigonal plane allowing for π overlap with the metal d_{xy} orbital.[52,53] Similar to complex **20**, isomer **B** also possesses a square pyramidal structure, however, the alkynyl and amine ligands are now located *trans* to one another as are the amido and $P^{i}Pr_3$ ligands. Isomer **B** could be envisioned as forming via transfer of the amino proton to the amido nitrogen atom in complex **20**. We have already established that proton transfer is a common occurrence in other [P_2NNH] and [NPNH] complexes of ruthenium. In fact, this proposal resembles the mechanism portrayed in Scheme 2.7 for the formation of complex **2**. In that circumstance the thermodynamic product also contained *trans* phosphine and amido donors as well as amine and σ-bound carbon ligands. If complex **20** is the kinetic product of this reaction it may be possible that proton transfer to yield the thermodynamic product (**B**) may not proceed in toluene but may be mediated in more polar solvents such as THF. For these reasons we favour isomer **B** as the second species that forms in THF although isomer **A** cannot be ruled out definitively.

References begin on page 237

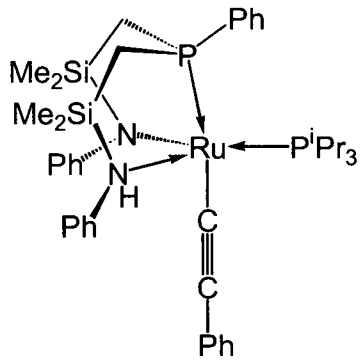

A

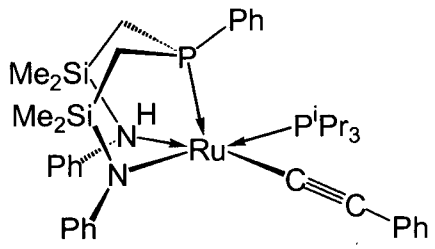

B

Figure 4.3. Two possible diastereomers of complex **20**. Isomer **A** is distorted trigonal bipyramidal (Y-shape) and isomer **B** is square pyramidal.

4.4 Reaction of [NPNH](P^iPr_3)Ru(CCPh) (20) with H_2

Since the reaction between the [NPN] ligand and the vinylidene precursor (P^iPr_3)$_2$$Cl_2$Ru(CCHPh) did not yield a product containing a Ru=C double bond, olefin metathesis reactivity could not be investigated. The presence of a ruthenium-amido linkage, however, prompted us to investigate the ability of complex **20** to heterolytically activate H_2. Upon exposure of a solution of **20** to an atmosphere of hydrogen gas an immediate change in colour from violet to orange takes place. The ^{1}H NMR spectrum shows the formation of a single, symmetrical ruthenium polyhydride complex. The [NPNH] ligand gives rise to two resonances for the silyl methyl protons and two sets of multiplets for the methylene protons. There is a single peak for the *ortho* protons of the phosphine phenyl group. A broad peak at δ 3.98 that integrates to two proton environments has been assigned as equivalent N-H protons. The presence of two amino protons implies that heterolysis of a molecule of H_2 has occurred. The methyl groups of the P^iPr_3 ligand are also equivalent and occur as a multiplet at δ 0.98. The hydride region of the ^{1}H NMR spectrum consists of a single resonance that appears as an overlapping set of doublets and integrates to six proton equivalents. The ^{1}H

References begin on page 237

NMR spectrum also shows the presence of ethyl benzene, a hydrogenation by-product from this reaction. The $^{31}P\{^1H\}$ NMR spectrum contains two doublets at δ 25.0 and δ 86.0 with a large coupling of 225 Hz indicating a *trans* arrangement of the two phosphine ligands within the complex. A portion of the $^{31}P\{^1H\}$ NMR spectrum that contains these resonances is shown in Figure 4.4.

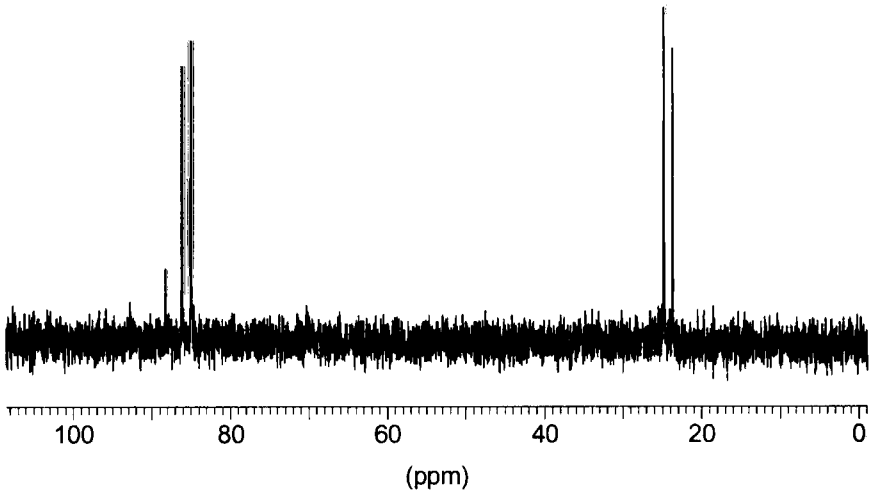

Figure 4.4. The $^{31}P\{^1H\}$ NMR spectrum for the reaction of **20** with H_2. The magnitude of coupling for the two doublets is 225 Hz.

The integration of six protons for the hydride signal in this new complex suggested the existence of one or more coordinated dihydrogen ligands. Since only one resonance is observed these η^2-bound moieties must be in fast exchange with any classical hydride ligands that may also be present. The two most likely candidates that satisfy these conditions are the ruthenium (IV) species $[NPNH_2](P^iPr_3)Ru(\eta^2\text{-}H_2)(H)_4$, and a ruthenium(II) bis dihydrogen complex, $[NPNH_2](P^iPr_3)Ru(\eta^2\text{-}H_2)_2(H)_2$. A survey of the literature indicates that although bis dihydrogen complexes are not that common there are several examples of structurally characterized late transition metal complexes containing two intact dihydrogen

References begin on page 237

moieties; some representative examples of octahedral ruthenium(II) bis dihydrogen complexes are shown in Figure 4.5.[55,56]

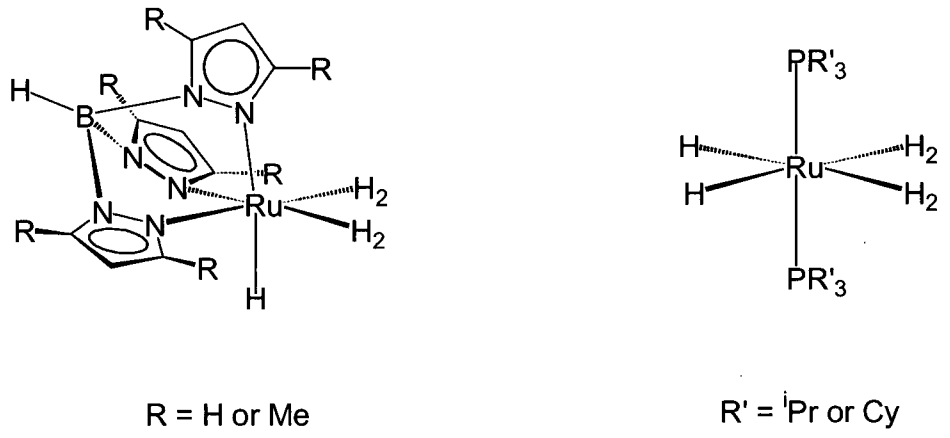

Figure 4.5. Some examples of octahedral ruthenium(II) bis dihydrogen complexes.

Based on the many similarities that are observed in the solution NMR data for this new species with known bis dihydrogen complexes we propose that the reaction of complex **20** with H_2 generates $[NPNH_2](P^iPr_3)Ru(\eta^2\text{-}H_2)_2(H)_2$ (**21**), as illustrated in equation 4.2. The *trans* disposed phosphine ligands are in accordance with known complexes, and is verified by the large phosphorus-phosphorus scalar coupling (225 Hz). The observation of a single "hydride" resonance is a common feature in these types of complexes and indicates that the dihydrogen and hydride ligands undergo facile exchange within the equatorial plane of the molecule. The mechanism for this dynamic process can occur via the formation of a transient trihydrogen complex in a similar fashion to that depicted in Figure 3.8 for the exchange of hydride and dihydrogen environments in complex **10**. This fluxional process, in addition to free rotation of the two phosphine ligands about the Ru-P bonds accounts for the high symmetry for complex **21** that is observed in solution. Low temperature spectra of complex **21** in toluene-d_8 (as low as 180 K) show no significant deviations from its room temperature spectrum indicating that the dynamic behaviour of **21** is maintained at low temperatures. As shown in equation 4.2, a "static" complex **21** contains a mirror plane of

References begin on page 237

symmetry lying in the P-Ru-P plane bisecting the H-Ru-H angle, and therefore possesses C_s symmetry.

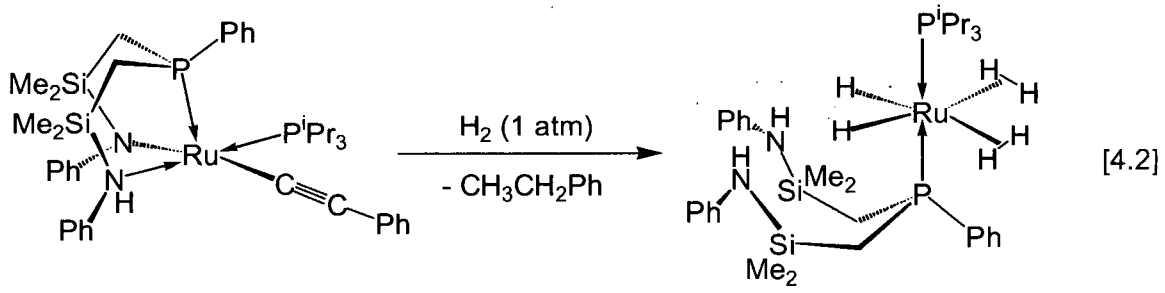

20 **21** [4.2]

To confirm the presence of a dihydrogen ligand within complex **21** the minimum of the longitudinal relaxation time (T_1(min)) for the metal-bound hydrogen atoms was measured.[57-59] Using an inversion-recovery pulse sequence this value was determined to be 51 ms at 220 K and 500 MHz in toluene-d_8, consistent with the presence of at least one coordinated H_2 ligand in **21**. This value corresponds well with the T_1(min) values that have been measured in related bis dihydrogen complexes;[55,56] some examples are highlighted in Table 4.2. Also listed in Table 4.2 are the chemical shift, multiplicity and phosphorus coupling constants of the "hydride" ligands as well as the chemical shift of the phosphine ligands. The most significant difference between complex **21** and the other bis H_2 complexes is the coupling pattern that is observed for the hydride resonance. In the P^iPr_3 and PCy_3 complexes for instance, a triplet pattern arises due to coupling with the two equivalent phosphine ligands. In the case of **21** the two phosphine ligands are different, and consequently an overlapping pair of doublets is observed. By performing selective $^1H\{^{31}P\}$ decoupling experiments the magnitude of coupling to each of the phosphine ligands was determined. The phosphine donor of the [NPNH] ligand gives rise to a 7.6 Hz coupling, and the P^iPr_3 ligand couples to the Ru-H ligands with a magnitude of 6.7 Hz.

References begin on page 237

Table 4.2. A comparison of hydride chemical shift (δ_H), multiplicity (m), $^2J_{PH}$ and T_1(min) values for the hydride ligands as well as phosphine chemical shifts (δ_P) in complex **21** and related bis dihydrogen complexes.

Complex	δ_H (ppm)	m	$^2J_{PH}$ (Hz)	T_1(min) (ms)	δ_P (ppm)
21	-7.60	d	6.7, 7.6	51[a]	86.0, 25.0
$(P^iPr_3)_2Ru(H_6)$	-8.31	t	8.0	45[b]	88.4
$(PCy_3)_2Ru(H_6)$	-7.90	t	7.0	28[c]	76.5

[a] 220 K, 500 MHz, toluene-d_8
[b] 193 K, 300 MHz, toluene-d_8 (Ref. 56)
[c] 203 K, 250 MHz, toluene-d_8 (Ref. 55)

In general, complexes of the type $(PR_3)_2Ru(\eta^2\text{-}H_2)_2(H)_2$ are unstable particularly with respect to loss of H_2 (except for R = Cy).[56,60] Loss of H_2 from these types of species normally results in the formation of mixed-valent dimeric species of general formula $Ru_2H_6(PR_3)_4$. At room temperature, solutions of complex **21** under a dihydrogen atmosphere are unstable and slowly decompose to yield a new species. After four days complex **21** is still the major product in solution, however, a new triplet in the hydride region of the ^1H NMR spectrum is now apparent; this is accompanied by the appearance of a singlet in the $^{31}P\{^1H\}$ NMR spectrum near δ 88.0. The spectral features of the decomposition product match the reported literature data for the complex $(P^iPr_3)_2Ru(H_2)_2(H)_2$; after two weeks the complex $(P^iPr_3)_2Ru(\eta^2\text{-}H_2)_2(H)_2$ is the only NMR active species present. The mechanism for this conversion is not known. The fate of the $[NPNH_2]$ ligand is also uncertain as no other decomposition products were evident in the ^1H and $^{31}P\{^1H\}$ NMR spectra. Exposure of solutions of complex **21** to an atmosphere of dinitrogen also resulted in its decomposition as noted by a change in colour from orange to brown. The complex $(P^iPr_3)_2Ru(\eta^2\text{-}H_2)_2(H)_2$ is reported to react with N_2 to generate a thermally stable dinitrogen-bridged complex $\{(P^iPr_3)_2Ru(H)_2(N_2)\}_2(\mu\text{-}N_2)$.[56,60] We are currently investigating the reactivity of complex **21** with D_2 gas in order to provide further evidence for the classification of **21** as a bis dihydrogen dihydride species.

References begin on page 237

4.5 Reaction of $[P_2N_2]Li_2{\cdot}(C_4H_8O_2)$ with $(P^iPr_3)_2Cl_2Ru(CCHPh)$

The reaction of the $[P_2N_2]$ ligand with the ruthenium vinylidene complex $(P^iPr_3)_2Cl_2Ru(CCHPh)$ yields two products. The $^{31}P\{^1H\}$ NMR spectrum of the crude reaction mixture contains a singlet at δ 25.6 indicating the formation of a highly symmetrical species. Also present is a doublet and a triplet that integrate in the ratio 2:1 respectively, suggesting the presence of a ruthenium complex bearing the $[P_2N_2]$ ligand as well as one equivalent of P^iPr_3. A singlet observed at δ 19.4 in the $^{31}P\{^1H\}$ NMR spectrum corresponds to free P^iPr_3. The two complexes could be partially separated by rinsing the crude mixture with hexanes. We propose that the two products formed in this reaction are the vinylidene complex $[P_2N_2]Ru(CCHPh)$ (**22**), and the terminal alkynyl species $[P_2NNH](P^iPr_3)Ru(CCPh)$ (**23**) as shown in equation 4.3.

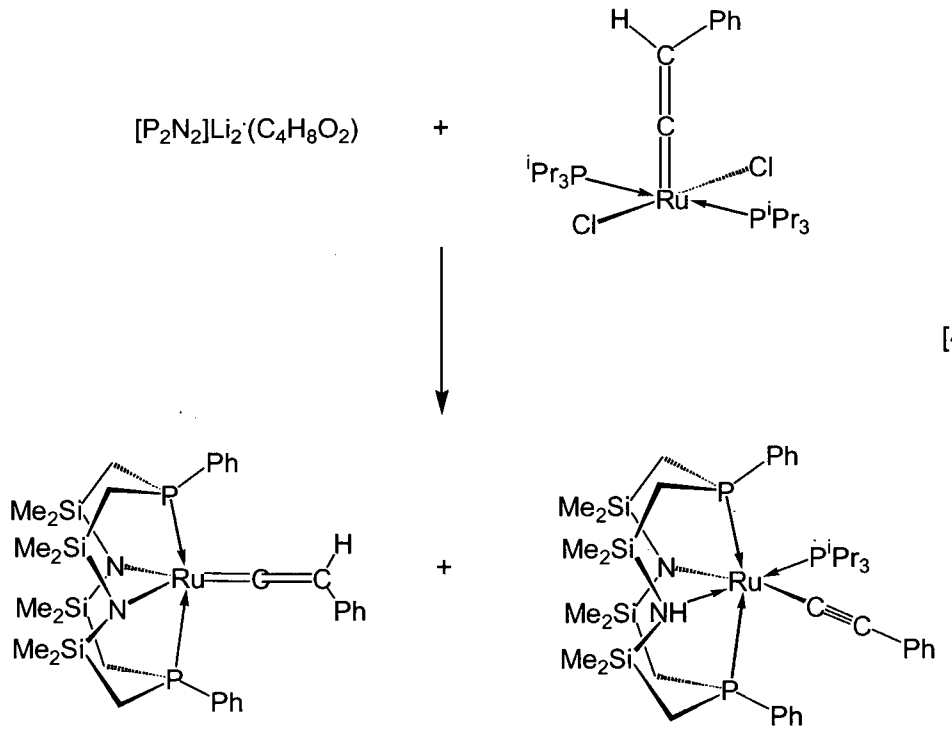

[4.3]

40%

22

60%

23

References begin on page 237

Complex **22** forms via the replacement of the two chlorides and two phosphine donors in the starting material by the [P_2N_2] ligand. The most telling feature in the ^{1}H NMR spectrum of complex **22** is the triplet located at δ 4.85. This observed pattern arises from coupling with the two equivalent phosphine donors of the [P_2N_2] ligand ($^4J_{PH}$ = 4.2 Hz). This resonance is similar to that observed for the vinylidene hydrogen atom in the starting material, which occurs as a triplet at δ 4.71 with a magnitude of coupling to the phosphorus nuclei of 3.6 Hz. The [P_2N_2] ligand gives rise to two silyl methyl proton resonances indicative of a complex with high symmetry; this is consistent with the singlet that is observed in the ^{31}P{^{1}H} NMR spectrum. The equivalency of the phosphine donors in complex **22** requires that a mirror plane of symmetry exists within the trigonal plane of the molecule. This can arise if the proton and phenyl groups of the vinylidene moiety also lie within this plane. The observation of two silyl methyl signals, however, also requires that a mirror plane exists along the P-Ru-P axis. This may occur if the proton and phenyl groups of the vinylidene moiety are aligned perpendicular to the trigonal plane. Therefore, the NMR data suggest that the vinylidene ligand in **22** is fluxional and that facile rotation of this moiety about the Ru=C=C axis occurs. This behaviour is also apparent in many five-coordinate vinylidene complexes of the type $(PR_3)_2(X)(Cl)M(CCHR)$ (e.g. M = Ru or Os and X = H or Cl).[61] Rotational isomers have been detected at low temperatures for the species $(P^iPr_3)_2(H)(Cl)Os(CCHPh)$[62] whereas evidence for the co-existence of two isomers in the complex $(P^iPr_3)_2(H)(Cl)Ru(CCHPh)$ could not be obtained.[63] Theoretical studies on the model complex $(PH_3)_2Cl_2Ru(CCH_2)$ indicate a barrier to vinylidene rotation of 7.3 kcal mol^{-1}.[61] Low temperature NMR studies on complex **22** have not been attempted.

Complex **23** can be envisioned as forming in a similar manner as complex **20**, namely, via transfer of the vinylidene hydrogen atom to one of the amido donors of the [P_2N_2] macrocycle resulting in the formation of an amine and a terminal alkynyl ligand. In fact, complex **23** may be considered as a coordinatively saturated analogue of **20** in which one of the [P_2N_2] phosphine donors has capped the open face to generate an octahedral structure. The small coupling of 33 Hz for the resonances in the ^{31}P{^{1}H} NMR spectrum implies a *cis* arrangement between the P^iPr_3 and [P_2NNH] phosphine donors. The ^{1}H NMR spectrum contains four singlets for the silyl methyl protons of the [P_2NNH] ligand as well as

References begin on page 237

four multiplets for the methylene protons within the ligand backbone. The methyl groups of the P^iPr_3 ligand occur as a broad multiplet at δ 0.94; the methine protons are located as a multiplet at δ 1.66. A singlet at δ 2.12 that integrates to one proton has been assigned as the amino proton in complex **23**. The aromatic protons exist at normal positions between δ 7.0 and δ 8.2. The presence of a mirror plane of symmetry contained within the equatorial plane accounts for the observation of four silyl methyl groups and the equivalent phosphine donors of the [P_2NNH] set.

Due to the formation of a mixture of complexes **22** and **23** in the reaction of the [P_2N_2] ligand with $(P^iPr_3)_2Cl_2Ru(CCHPh)$ and the need for separation and purification, further reactivity involving complexes **22** and **23** was not pursued. The drawback of the precursor complex $(P^iPr_3)_2Cl_2Ru(CCHPh)$ in its reaction with the [NPN] and [P_2N_2] ligands is that deprotonation of the acidic vinylidene proton allows for an alternate reaction pathway other than direct halide metathesis and phosphine displacement. In an attempt to circumvent this problem we desired a ruthenium vinylidene starting material that was disubstituted at the terminal position. A recent literature report discusses the convenient synthesis of β-silylvinylidene ruthenium complexes of the general formula $(PR_3)_2Cl_2Ru\{CC(SiMe_3)Ph\}$ (where R = Cy or ^{i}Pr).[64] The following sections detail the reactions of the [NPN] and [P_2N_2] ligands with the P^iPr_3 derivative. This complex was chosen since it allows for a direct comparison with the parent vinylidene complex.

4.6 Reaction of $[NPN]Li_2{\cdot}(C_4H_8O)_2$ and $[P_2N_2]Li_2{\cdot}(C_4H_8O_2)$ with $(P^iPr_3)_2Cl_2Ru\{CC(SiMe_3)Ph\}$

(i) Synthesis and characterization of $[P_2N_2]Ru\{CC(SiMe_3)Ph\}$ (24)

The mixed-donor [P_2N_2] ligand reacts cleanly with the vinylidene precursor $(P^iPr_3)_2Cl_2Ru\{CC(SiMe_3)Ph\}$ to give the anticipated product $[P_2N_2]Ru\{CC(SiMe_3)Ph\}$ (**24**) in quantitative yield, as shown in equation 4.4. Toluene solutions containing the two starting

References begin on page 237

materials change in colour from purple to orange over a period of two hours. The insoluble LiCl by-product is easily removed by filtration. Complex **24** can be isolated as large block crystals by the slow evaporation of a saturated pentane solution.

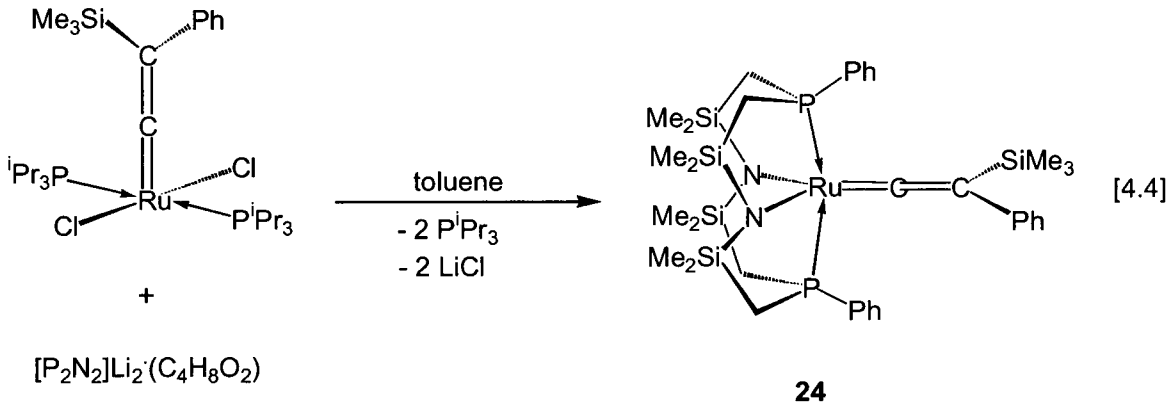

[4.4]

The $^{31}P\{^1H\}$ NMR spectrum of complex **24** contains a singlet at δ 26.5 for the phosphine donors of the macrocycle; this is located close to the phosphorus-31 signal in the structurally related species **22** (δ 25.6). In the ^1H NMR spectrum a singlet is observed for the silyl methyl protons of the vinylidene moiety indicating free rotation of this group, while the [P_2N_2] ligand gives rise to four silyl methyl resonances. The equivalency of the phosphine donors in complex **24** coupled with the observation of four distinct [P_2N_2] silyl methyl groups suggests that it possesses C_s symmetry with a mirror plane containing the two amido donors and the vinylidene fragment. This is only possible if the silyl and phenyl substituents of the vinylidene moiety lie in this plane and do not rotate about the Ru=C=C axis. This is in contrast to complex **22** in which the vinylidene ligand does undergo fast rotation. The larger size of a trimethylsily group versus a hydrogen atom most likely accounts for this difference. An unfavourable interaction of the bulky $SiMe_3$ group with the phenyl substituents of the [P_2N_2] phosphine donors may keep the vinylidene ligand in this observed orientation. The [P_2N_2] methylene protons appear as overlapping multiplets between δ 1.25 and δ 1.65, and the aromatic protons are located between δ 7.02 and δ 7.58.

The structure of complex **24** was confirmed by a single crystal X-ray diffraction study. The solid-state molecular structure of **24** is shown in Figure 4.6 with selected bond

References begin on page 237

lengths and angles collected in Table 4.3. The X-ray structure shows a ruthenium centre surrounded by the [P_2N_2] macrocycle and a vinylidene ligand. The Ru(1)-C(25)-C(26) angle is almost linear (178.5(2)°) and the C(25) to C(26) distance of 1.332(4) Å is consistent with a carbon-carbon double bond. The trimethylsilyl and phenyl groups of the vinylidene moiety are aligned with the amido donors of the [P_2N_2] ligand as predicted from the solution NMR data. It is apparent from the solid-state structure that this arrangement minimizes interactions with the phenyl groups of the [P_2N_2] framework. The Ru(1)-C(25) distance of 1.781(2) Å in **24** is longer than that observed in the related five-coordinate ($P^iPr_3)_2Cl_2Ru(CCHPh)$ (1.750(4) Å) and ($PCy_3)_2Cl_2Ru(CCHPh)$ (1.761(2) Å) complexes,[64] but is shorter than those of the coordinatively saturated vinylidene ruthenium species $[Cp(PPh_3)_2Ru\{CC(Me)Ph\}]^+I^-$ (1.863(10) Å),[65] and $Tp(PPh_3)ClRu(CCHPh)$ (1.801(4) Å).[66] This trend most likely reflects the arrangement of the vinylidene ligand within the complexes with or without a ligand located in the *trans* position. The ruthenium amide distances in **24** (*ca.* 2.07 Å) are shorter than those observed in the six-coordinate complexes **1** (*ca.* 2.22 Å) and **2** (*ca.* 2.26 Å). These data reflect the tighter binding of a ligand that is expected for an electron deficient complex. Both complexes **1** and **2** are 18-electron species, whereas complex **24** has a 16-electron valence count.

References begin on page 237

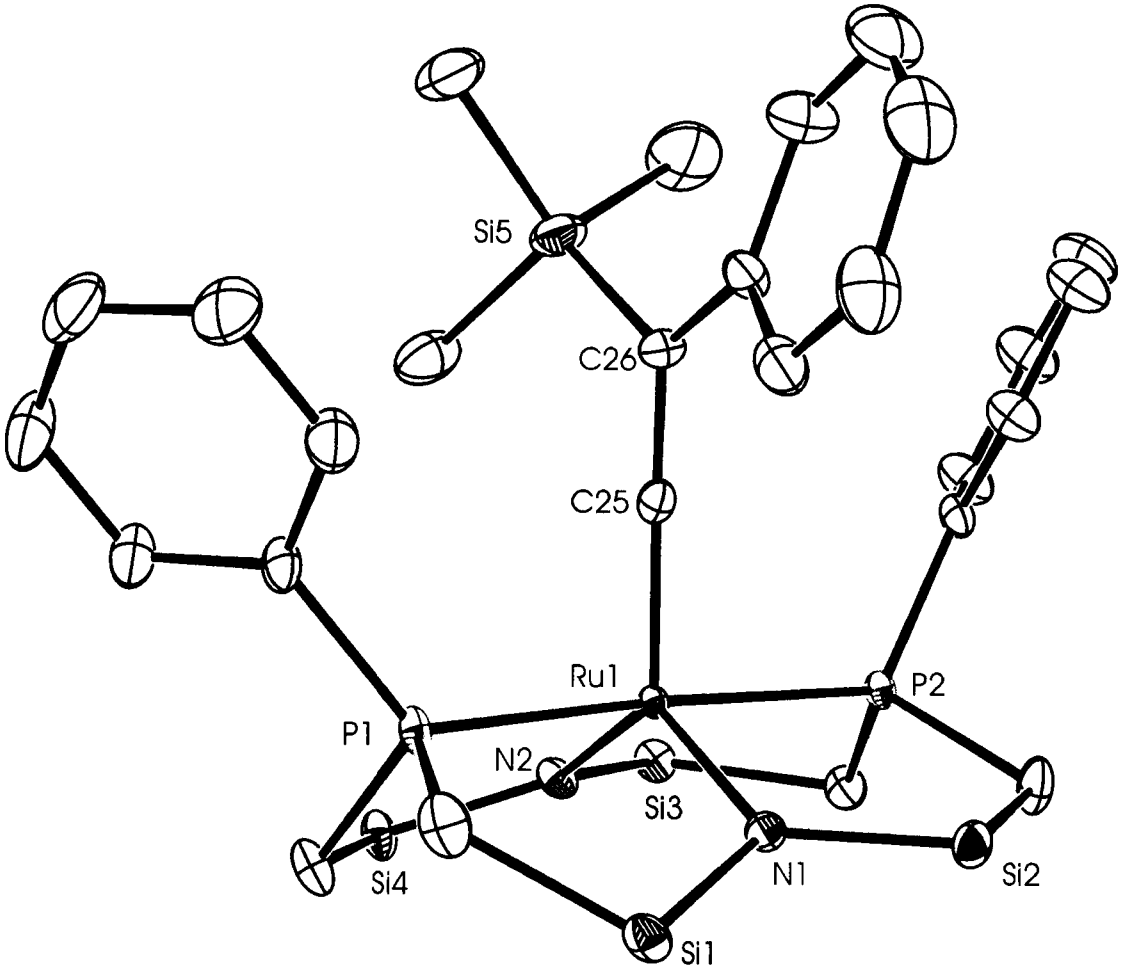

Figure 4.6. ORTEP representation (50% thermal ellipsoids) of the solid-state molecular structure of [P_2N_2]Ru{CC($SiMe_3$)Ph} (**24**) as determined by X-ray diffraction. The silyl methyl groups of the [P_2N_2] ligand have been omitted for clarity.

Table 4.3. Selected bond lengths and bond angles in [P_2N_2]Ru{CC($SiMe_3$)Ph} (**24**).

Atom	Atom	Distance (Å)	Atom	Atom	Distance (Å)
Ru(1)	P(1)	2.3394(6)	Ru(1)	N(2)	2.075(2)
Ru(1)	P(2)	2.3419(6)	Ru(1)	C(25)	1.781(2)
Ru(1)	N(1)	2.066(2)	C(25)	C(26)	1.332(4)

References begin on page 237

Atom	Atom	Atom	Angle (°)	Atom	Atom	Atom	Angle (°)
P(1)	Ru(1)	P(2)	176.58(2)	P(1)	Ru(1)	N(1)	89.83(6)
P(1)	Ru(1)	N(2)	88.97(6)	P(1)	Ru(1)	C(25)	91.54(8)
P(2)	Ru(1)	N(1)	88.54(6)	P(2)	Ru(1)	N(2)	89.70(6)
P(2)	Ru(1)	C(25)	91.87(8)	N(1)	Ru(1)	N(2)	128.65(8)
N(1)	Ru(1)	C(25)	112.16(9)	N(2)	Ru(1)	C(25)	119.18(9)
Ru(1)	C(25)	C(26)	178.5(2)	Si(5)	C(26)	C(25)	117.0(2)

Although the structure of **24** more closely resembles a trigonal bipyramid with the phosphine donors of the [P_2N_2] ligand at the apical positions, and the amido donors and the vinylidene ligand lying in the equatorial plane of the molecule, its geometry may be better described as a highly distorted square pyramid. To support this claim a brief discussion concerning the structure and bonding in related vinylidene complexes is in order. Five-coordinate vinylidene complexes formulated as $L_2(H)(Cl)Ru(CCHR)$ (where L is a phosphine) have been synthesized and these complexes adopt a distorted trigonal bipyramidal geometry with the phosphine donors occupying the apical positions and the Cl, H and vinylidene ligands in the plane of the molecule.[61,63,67] Furthermore, the angles within the equatorial plane are inequivalent giving rise to a Y-shape structure with the Cl donor located at the foot of the Y (i.e. opposite the acute angle). This type of distortion is typical of d^6 ML_5 complexes that contain a π-donating ligand since this allows for effective overlap of the lone pair of the π-donor with the vacant metal d_{xy} orbital.[52,53] This concept has been previously addressed in chapter 2 (see Figure 2.10). Unlike these complexes, however, the species $L_2(H)(Cl)Ru(CCHR)$ also contains a π-acceptor ligand, which usually favours a square pyramidal geometry. Theoretical calculations performed on the model complex $(PH_3)_2(H)(Cl)Ru(CCH_2)$ have shown that the preference for a distorted trigonal bipyramidal geometry (or Y-structure) originates from a neutral vinylidene being a strong π-acceptor in the $C_\beta H_2$ plane and a weak π-donor orthogonal to this plane.[63,67] As depicted in Figure 4.7, two stabilizing interactions occur when the $C_\beta H_2$ vinylidene moiety lies in the Cl-Ru-H plane. The phosphine ligands, which would project in and out of the page have been omitted for clarity. The first interaction involves the formation of a Ru-Cl π-bond that is characteristic of all Y-shaped d^6 ML_5 fragments (**A** in Figure 4.7), and the second involves

References begin on page 237

back-donation from the filled x^2-y^2 metal orbital to the vacant p-orbital on C_α of the vinylidene (**B**). In fact destabilization of the x^2-y^2 orbital by its interaction with the Cl p_x orbital permits for greater overlap between the metal x^2-y^2 and the empty p-orbital of the vinylidene enhancing this π-interaction.[63]

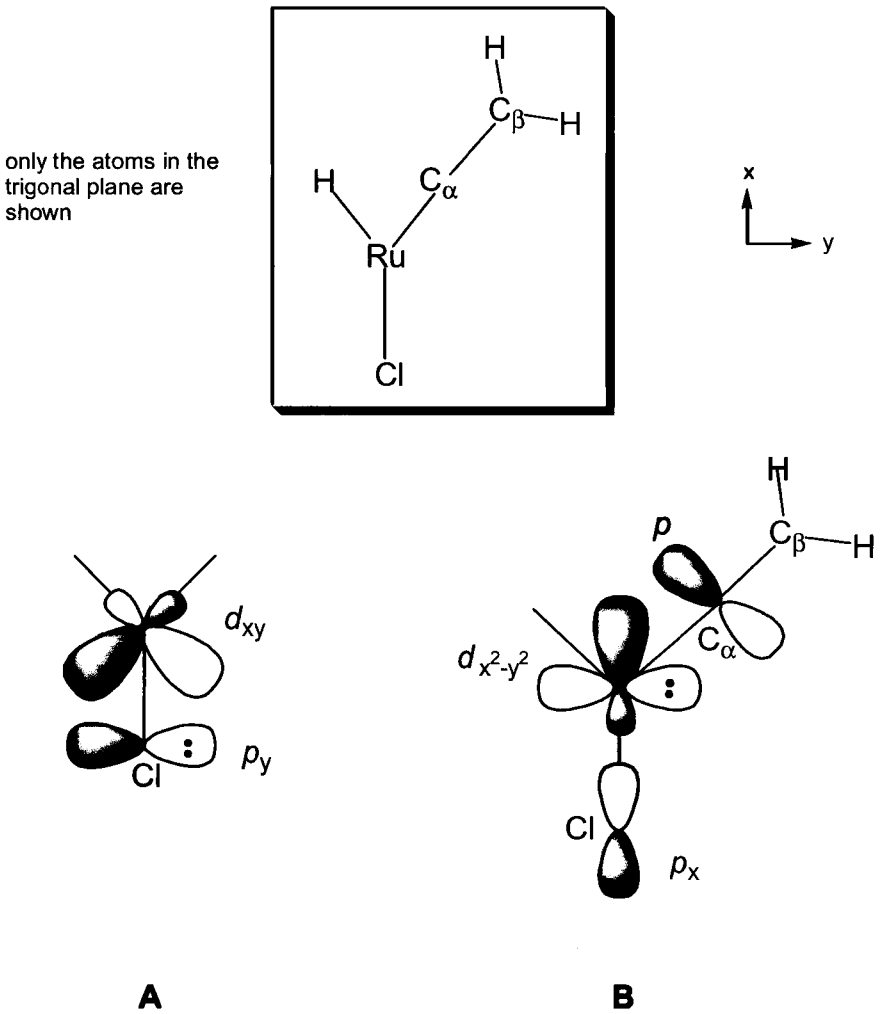

Figure 4.7. An illustration of the two stabilizing bonding interactions in five-coordinate vinylidene complexes of the type $L_2(H)(Cl)Ru(CCHR)$, which adapt distorted trigonal bipyramidal (or Y-shaped) structures. In **A** π-donation from the Cl lone pair (p_y) to the empty metal xy orbital occurs. In **B** back-donation from the filled metal x^2-y^2 orbital to the vacant p-orbital on C_α of the vinylidene occurs. This can only take place if the $C_\beta H_2$ group lies in the xy plane.

References begin on page 237

Changing the hydride ligand (a strong σ-donor) to a chloride ligand (a σ and a π-donor) generating complexes of the type $L_2Cl_2Ru(CCHR)$ (L is a phosphine) also results in a change in the coordination geometry at the metal. Theoretical calculations on the model system $(PH_3)_2Cl_2Ru(CCH_2)$ show that these complexes adopt a distorted square pyramidal structure with the vinylidene ligand at the apical position.[61] The terminal $C_\beta H_2$ fragment is aligned in the Cl-Ru-Cl plane. This arrangement allows for back donation from the filled metal d_{xy} orbital to the empty *p*-orbital on C_α of the vinylidene ligand. The Cl-Ru-Cl angle is less than 180° and is a result of using the in-plane *d*-orbital (d_{xy}) for metal-vinylidene π-bonding. By bending away from the vinylidene ligand the two chloride ligands destabilize the d_{xy} orbital, thus enhancing its interaction with the vacant *p*-orbital on C_α and strengthening the π-interaction.[61] The vinylidene-metal-chloride angles are found to be equal and this is probably due to the two chloride ligands competing equally for bonding with the metal centre. These findings are supported by experimental data. The complex $(P^iPr_3)_2Cl_2Ru(CCHPh)$,[64] for instance, contains the two phosphine and two chloride donors in a square plane and the vinylidene ligand at the apical site. The chloride atoms are actually slightly pinched back giving a Cl-Ru-Cl angle close to 160° as are the two phosphine ligands, which are skewed at an angle of about 170°. The phenyl and hydrogen substituents of the vinylidene ligand lie in the Cl-Ru-Cl plane.

Complex **24** is closely related to the $L_2Cl_2Ru(CCHR)$ vinylidene complexes in that both species contain two π-donating ligands. For this reason, one may expect that **24** would also adopt a distorted square pyramidal geometry. Inspection of the bond angles about the metal centre in complex **24** indicate that no Y-shape is present; in fact, widening of the N(1)-Ru(1)-N(2) angle above 120° is consistent with a distortion towards a square pyramidal structure. In the case of complex **24**, however, this distortion is limited by the macrocyclic nature of the [P_2N_2] ligand. Opening of the amide bite-angle in **24** results in a nearly linear arrangement of the two phosphine donors (176.58(2)°), and as a consequence, the phenyl substituents of the phosphine donors come into closer contact with the trimethylsilyl and phenyl groups of the vinylidene ligand. Minimizing these interactions may also play a role in the widening of the amide bite-angle (and therefore approaching a square pyramidal

References begin on page 237

geometry) in complex **24**. A structural feature that complex **24** shares with the precursor complex $(P^iPr_3)_2Cl_2Ru(CCHPh)$ is that the vinylidene ligand resides in the apical position and that the terminal substituents lie in the same plane as the π-donating ligands.

A qualitative representation of the bonding scheme of the vinylidene ligand in complex **24** is given in Figure 4.8. This scheme has been adapted from Figure 2.10, which describes the effects on the relative energies of the metal valence x^2-y^2 and *xy* *d*-orbitals as a d^6 ML_5 complex distorts towards a square pyramidal geometry. The vinylidene ligand can coordinate to the metal through σ-donation of its filled sp_y orbital (on C_α) to the vacant x^2-y^2 orbital on the metal. An empty p_x orbital is available for π-bonding with the filled *xy* orbital on the metal; this synergistic bonding mode assists in the stabilization of the vinylidene fragment. The remaining p_z orbital on C_α is involved in a π-bond with C_β of the vinylidene moiety. This terminal position contains a sp^2-hydridized carbon atom involving the *s*, p_x and p_y orbitals. Based on this simplified bonding model the phenyl and trimethylsilyl substituents of the vinylidene ligand will be located in the *xy* plane along with the amido donors of the [P_2N_2] ligand (for a ground-state structure). This arrangement is also observed experimentally as is shown in the solid-state molecular structure of **24**.

References begin on page 237

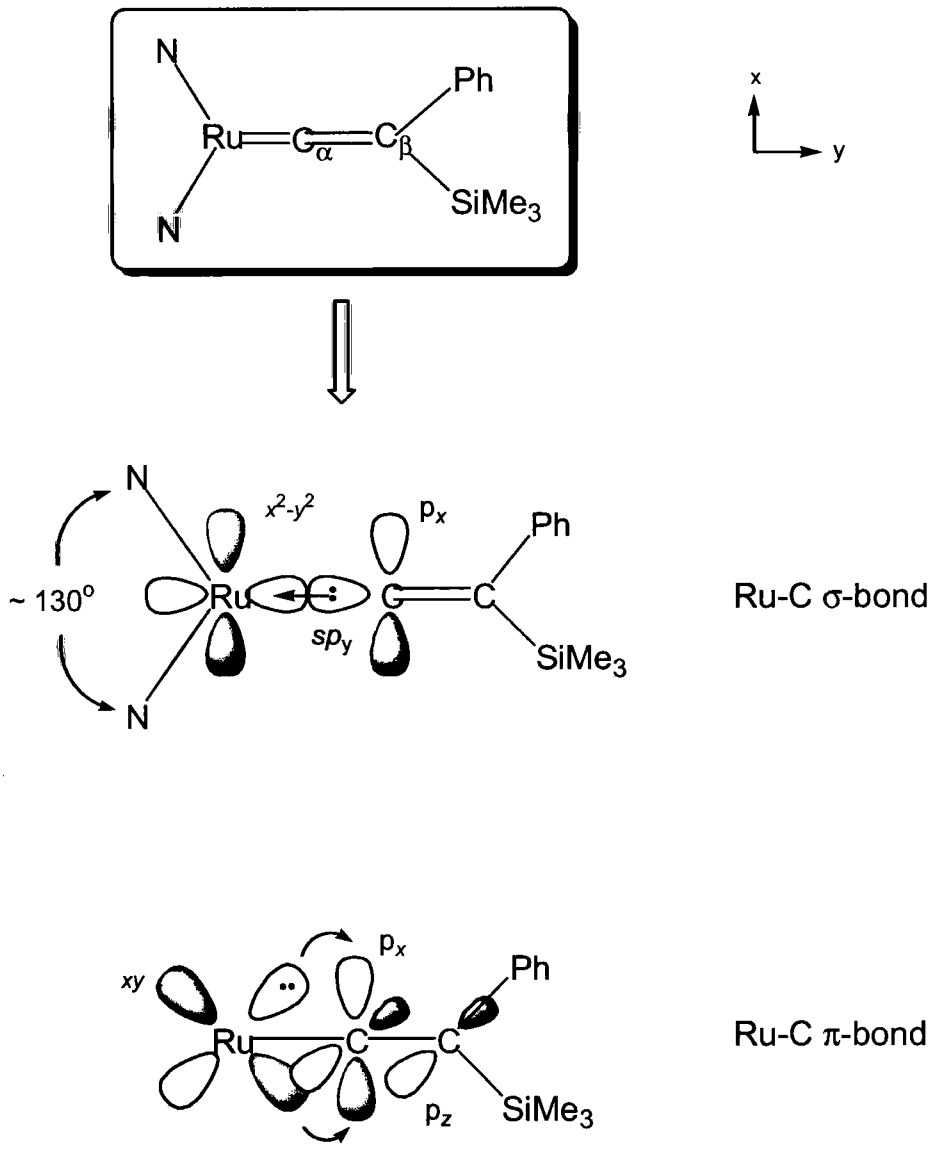

Figure 4.8. A qualitative representation of the bonding scheme for the vinylidene ligand in complex **24**.

(ii) Attempted synthesis of [NPN](P^iPr_3)Ru{CC($SiMe_3$)Ph}

Although coordination of the [P_2N_2] ligand to the vinylidene complex (P^iPr_3)$_2Cl_2$Ru(CCHPh) was possible, the analogous substitution reaction employing the [NPN] ligand proved unsuccessful. The ^1H and $^{31}P\{^1H\}$ NMR spectra indicated the

References begin on page 237

formation of a mixture of unidentified products. It is unclear why this reaction has failed and attempts are being made to optimize the reaction conditions to favour the formation of the substitution product [NPN](P^iPr_3)Ru{CC($SiMe_3$)Ph}. A difference in reactivity between the [P_2N_2] and [NPN] ligands was also observed in their reactions with $RuCl_2(PPh_3)_2$; whereas the reaction with the [NPN] ligand gave a mixture of products the reaction with the [P_2N_2] ligand yields the complex [P_2NNH]Ru($C_6H_4PPh_2$) (**2**).

4.7 Reactivity studies of [P_2N_2]Ru{CC($SiMe_3$)Ph} (24)

(i) Reaction of 24 with olefin substrates

Five-coordinate vinylidene ruthenium dichlorides of the type $L_2Cl_2Ru\{CCH(R)\}$ (L = P^iPr_3 or PCy_3 and R = ^{t}Bu or Ph) serve as good catalyst precursors for the ring-opening metathesis polymerization (ROMP) of norbornene.[31] Related complexes such as LClRu(CCHPh) (L = Tp or Cp) that incorporate the tris(pyrazolylborate) (Tp) and cyclopentadienyl (Cp) ligands also exhibit catalytic activity in this polymerization process.[30] The ROMP of norbornene and ruthenium vinylidene complexes that catalyze this reaction are shown in Figure 4.9. Although efficiency of the vinylidene complexes is much lower than that of the Grubbs' alkylidene complexes, the polymerization rate is sufficient for practical use and the resulting polymers have high molecular weights with polydispersity equivalent to the alkylidene systems.

References begin on page 237

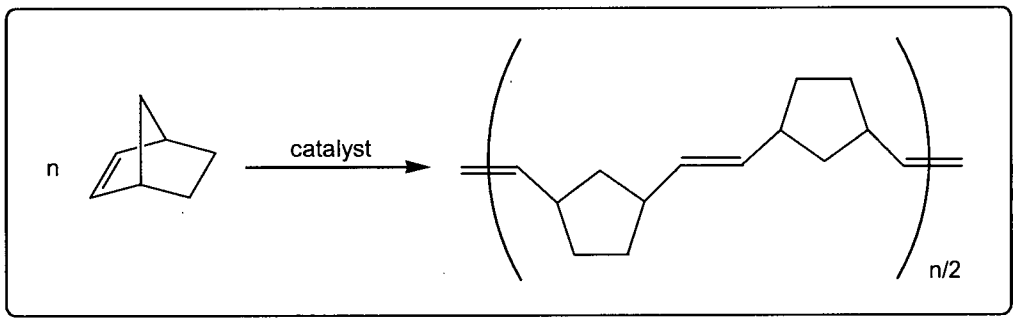

example catalysts:

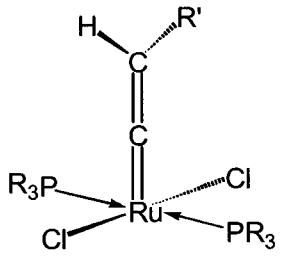

R = ^{i}Pr or Cy
R' = Ph or ^{t}Bu

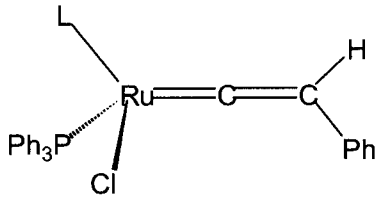

L = Cp, Cp* or Tp

Figure 4.9. The ring-opening metathesis polymerization of norbornene (highlighted) and vinylidene complexes that are used as catalyst precursors.[30,31]

Given the success of other ruthenium vinylidene complexes for the ROMP of norbornene, complex **24** was tested for its catalytic potential in this process. Unfortunately, **24** showed no activity even at elevated temperatures. Stoichiometric reactions with norbornene and styrene were also unsuccessful. Structurally, the [P_2N_2] vinylidene complex **24** more closely resembles the five-coordinate species $L_2Cl_2Ru\{CCH(R)\}$; the major difference is that **24** does not contain monodentate phosphine and chloride ligands but a chelating array of phosphine and amide ligands. This difference would be expected to have a significant consequence on the reactivity of complex **24**. The catalytic mechanism for square planar $L_2Cl_2Ru\{CCH(R)\}$complexes can be related to that of the Grubbs' catalyst with phosphine dissociation as the initial step (Figure 4.1). Due to the macrocyclic nature of the

References begin on page 237

[P_2N_2] ligand, phosphine dissociation to generate a vacant site *cis* to the vinylidene ligand is an unlikely occurrence, and most likely accounts for the observed lack of reactivity of complex **24**. Since the amido donors in complex **24** do not lie *trans* to one another but are pinched back at an angle of about 130° we envisioned that a substrate molecule could approach the metal centre along one of the amide-ruthenium-vinylidene (N-Ru-C) angles. Another factor that may contribute to the lack of reactivity of complex **24** is the steric bulk of the disubstituted vinylidene ligand, which can effectively shield the metal centre.

(ii) Reaction of 24 with H_2

Although complex **24** was stable with respect to the addition of olefin substrates it was observed to react readily with hydrogen gas. The addition of H_2 (1 atmosphere) to solutions of **24** resulted in a lightening in the colour of the solution from orange to yellow within an hour to yield the ruthenium hydride complex [P_2NNH]Ru(H){CC($SiMe_3$)Ph} (**25**) (Scheme 4.2). The $^{31}P\{^1H\}$ NMR spectrum of **25** consists of a singlet at δ 25.6 indicating that there are equivalent phosphine environments within the complex. The hydride resonance occurs as a triplet at δ -8.55 with a magnitude of coupling to the phosphorus-31 nuclei of 17.8 Hz. This signal integrates to one hydrogen environment per metal centre, and is therefore consistent with the heterolytic cleavage of a molecule of H_2 across the ruthenium-amide bond in **24**. The amino proton is located at δ 1.80. The trimethylsilyl group of the vinylidene ligand gives rise to a singlet and four silyl methyl resonances are observed for the [P_2NNH] ligand. This number of peaks is diagnostic of a mirror plane of symmetry that bisects the two phosphine donors of the macrocycle. Exposure of solutions of complex **25** (or **24**) to four atmospheres of H_2 pressure resulted in the formation of the previously characterized dihydrogen-hydride complex [P_2NNH]Ru(H_2)H (**10**).

References begin on page 237

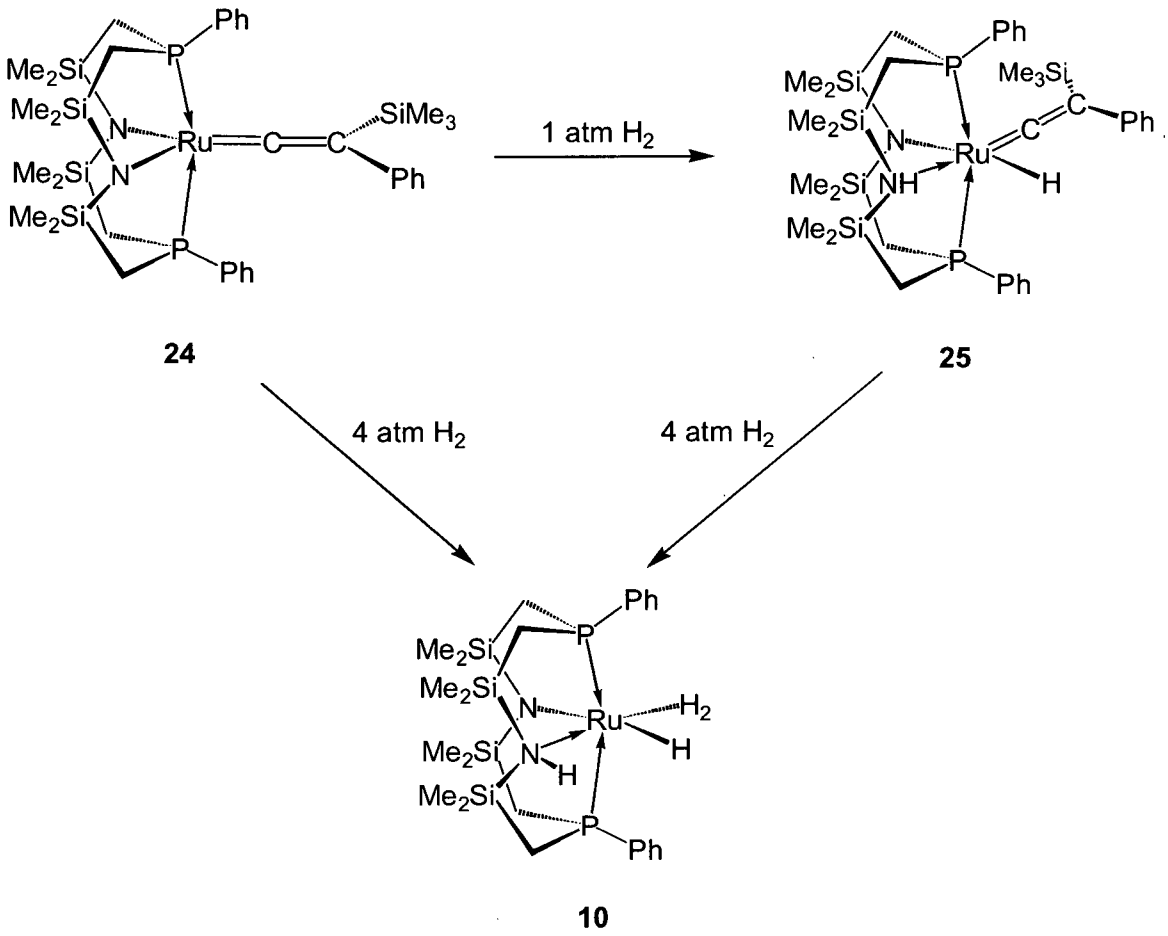

Scheme 4.2

4.8 Summary and Conclusions

This chapter discusses our attempts at preparing alkylidene and vinylidene complexes of ruthenium that incorporate the [NPN] and [P_2N_2] ligands. Our initial studies involved substitution of the chloride and phosphine donors in the Grubbs' complex $(PCy_3)_2Cl_2Ru(CHPh)$, however, a mixture of products resulted in these reactions.

Our investigations turned to ruthenium vinylidene complexes as starting materials due to their ease of preparation. The reaction of the [NPN] ligand with $(P^iPr_3)_2Cl_2Ru(CCHPh)$

References begin on page 237

generates the terminal alkynyl complex [NPNH](P^iPr_3)Ru(CCPh) (**20**), which forms via deprotonation of the vinylidene moiety by one of the basic amido donors of the [NPN] ligand. Complex **20** has been characterized in the solid-state by X-ray diffraction, infra-red spectroscopy and elemental analysis, and in solution by ^1H, $^{31}P\{^1H\}$ and $^{13}C\{^1H\}$ NMR spectroscopy. Exposure of complex **20** to an atmosphere of hydrogen gas results in the formation of the bis dihydrogen complex [$NPNH_2$](P^iPr_3)Ru(η^2-H_2)$_2$(H_2) (**21**). At room temperature solutions of **21** slowly decompose to yield the known bis dihydrogen complex (P^iPr_3)$_2$Ru(η^2-H_2)$_2$(H_2). The reaction of the [P_2N_2] ligand with (P^iPr_3)$_2$$Cl_2$Ru(CCHPh) gives a mixture of two products, the vinylidene complex [P_2N_2]Ru(CCHPh) (**22**) and the terminal alkynyl species [P_2NNH](P^iPr_3)Ru(CCPh) (**23**).

In order to eliminate deprotonation of the vinylidene ligand the disubstituted precursor (P^iPr_3)$_2$$Cl_2$Ru{CC($SiMe_3$)Ph} was utilized. Substitution of the chloride and phosphine ligands was successfully accomplished by the addition of [P_2N_2]Li_2·($C_4H_8O_2$) forming [P_2N_2]Ru{CC($SiMe_3$)Ph} (**24**). Complex **24** was characterized in the solid-state by X-ray diffraction. The solution structure of complex **24**, as determined by ^1H, $^{31}P\{^1H\}$ and $^{13}C\{^1H\}$ NMR spectroscopy is consistent with that found in the solid-state. Unfortunately, **24** demonstrated no reactivity with olefin substrates such as norbornene and styrene. It does react, however, with hydrogen gas. The ruthenium mono-hydride complex [P_2NNH]Ru(H){CC($SiMe_3$)Ph} (**25**) forms under one atmosphere of H_2, whereas the dihydrogen-hydride complex [P_2NNH]Ru(H_2)H (**10**) forms when higher pressures of H_2 gas are employed. The reaction of the [NPN] ligand with (P^iPr_3)$_2$$Cl_2$Ru{CC($SiMe_3$)Ph} gave a mixture of unidentified products.

References begin on page 237

4.9 Future Work

(i) Synthesis of [NPN](MgBr)$_2$·(C_4H_8O) (26)

In section 4.2 of this chapter we discussed the attempted incorporation of the [NPN] and [P_2N_2] ligands onto the benzylidene complex (PCy_3)$_2Cl_2$Ru(CHPh) via substitution of the chloride and phosphine ligands. The exchange of halide ligands on late transition metal complexes by anionic donors via salt metathesis is often dependent on the choice of cation and solvent system employed. For example, the incorporation of phenoxy-substituted Schiff base ligands onto (PCy_3)$_2Cl_2$Ru(CHPh) was most effective when the thallium salts of the corresponding ligands were utilized (Scheme 4.1).[47] One potential side-reaction that may occur where salt metathesis reactions are used to attach ancillary ligands to a late transition metal is metal reduction, in particular when lithium reagents are employed.[68] This suggested to us that modification of the cationic counter ions of the [NPN] and [P_2N_2] ligands may alter the reactivity of these mixed-donor chelating sets with ruthenium(II) alkylidene and vinylidene complexes as well as other ruthenium(II) precursors. Scheme 4.3 portrays two possible strategies for the preparation of other [NPN] ligand precursors, namely, [NPN]M_2 (where M is a univalent metal) and [NPN]M (where M is a divalent metal). As shown in pathway **A**, transmetalation may proceed by the addition of metal halide to the [NPN]Li_2·(C_4H_8O)$_2$ ligand with loss of lithium chloride. Alternatively, an [NPN]M_2 ligand can be envisioned as forming via deprotonation of the amino protons in the neutral ligand [$NPNH_2$] (**15**) (**B** in Scheme 4.3).

References begin on page 237

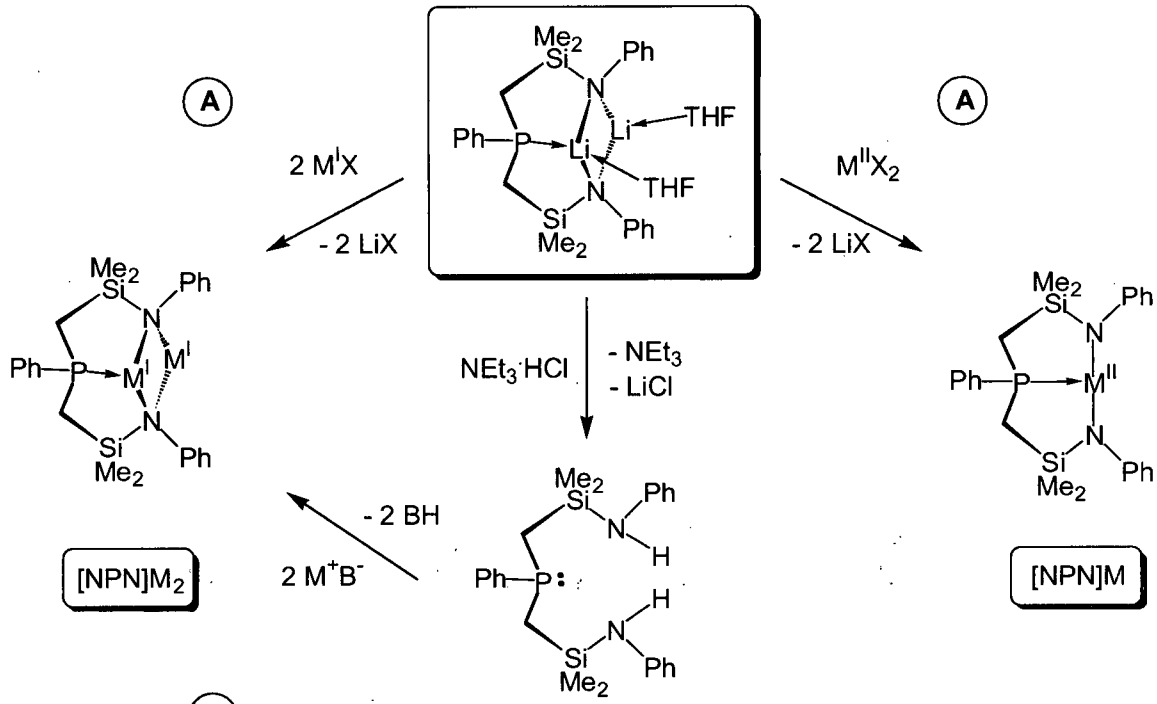

Scheme 4.3

Grignard reagents are less reducing than their corresponding lithium reagents; therefore, by analogy, magnesium salts of amides should be less reducing than lithium amides. The tetrahydrofuran adduct of the magnesium salt [P_2N_2]Mg·(C_4H_8O) has previously been prepared from the reaction of [P_2N_2]Li_2·($C_4H_8O_2$) with an excess of $MgBr_2$·(OEt_2) using tetrahydrofuran as the solvent.[69] In an attempt to prepare the related magnesium precursor of the [NPN] ligand an excess of $MgBr_2$·(OEt_2) was reacted with [NPN]Li_2·(C_4H_8O)$_2$ in tetrahydrofuran. As shown in equation 4.5, this reaction does not yield the anticipated "[NPN]Mg" salt. Instead the tetrahydrofuran adduct [NPN](MgBr)$_2$·(C_4H_8O) (**26**) forms containing two {MgBr}$^+$ monocations. This example further illustrates the difference in reactivity between the [P_2N_2] and [NPN] ligands that has been noted throughout this thesis. The stoichiometric reaction of [NPN]Li_2·(C_4H_8O)$_2$ with $MgBr_2$·(OEt_2) presumably would afford an "[NPN]Mg" salt analogous to the [P_2N_2] ligand, however, this reaction has yet to be attempted.

References begin on page 237

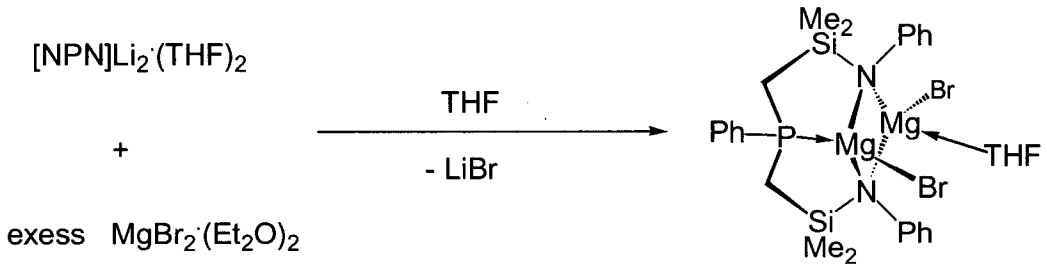

[4.5]

26

The solid-state molecular structure of complex **26** as determined from X-ray crystallography is shown in Figure 4.10, and selected bond lengths and angles are listed in Table 4.4. Complex **26** contains a four-membered $N_2\{MgBr\}_2$ core, which is similar to the N_2Li_2 core observed in the solid-state structure of the dilithium salt of the [NPN] ligand. One of the magnesium atoms is coordinated to the phosphine donor and the other is coordinated to a molecule of tetrahydrofuran; both magnesium centres are four-coordinate. Both amide-to-magnesium distances are similar at approximately 2.12 Å. The $N_2\{MgBr\}_2$ core is quite symmetrical with N-Mg-N angles of about 92° and Mg-N-Mg angles close to 87°. The $^{31}P\{^1H\}$ NMR spectrum of complex **26** clearly demonstrates that the lithium cations have been replaced by magnesium; the ^{31}P resonance is observed as a singlet at δ -47.0. In contrast, a quartet is observed at δ -37.7 ($^1J_{PLi}$ = 38 Hz) in the $^{31}P\{^1H\}$ NMR spectrum of $[NPN]Li_2\cdot(C_4H_8O)_2$. The ^1H NMR spectrum of the ligand framework is comprised of two silyl methyl resonances, two methylene resonances, and one set of *ortho*, *meta* and *para* phenyl proton resonances each for the phosphine and amido phenyl groups. This number of peaks is consistent with a mirror plane of symmetry within complex **26**.

References begin on page 237

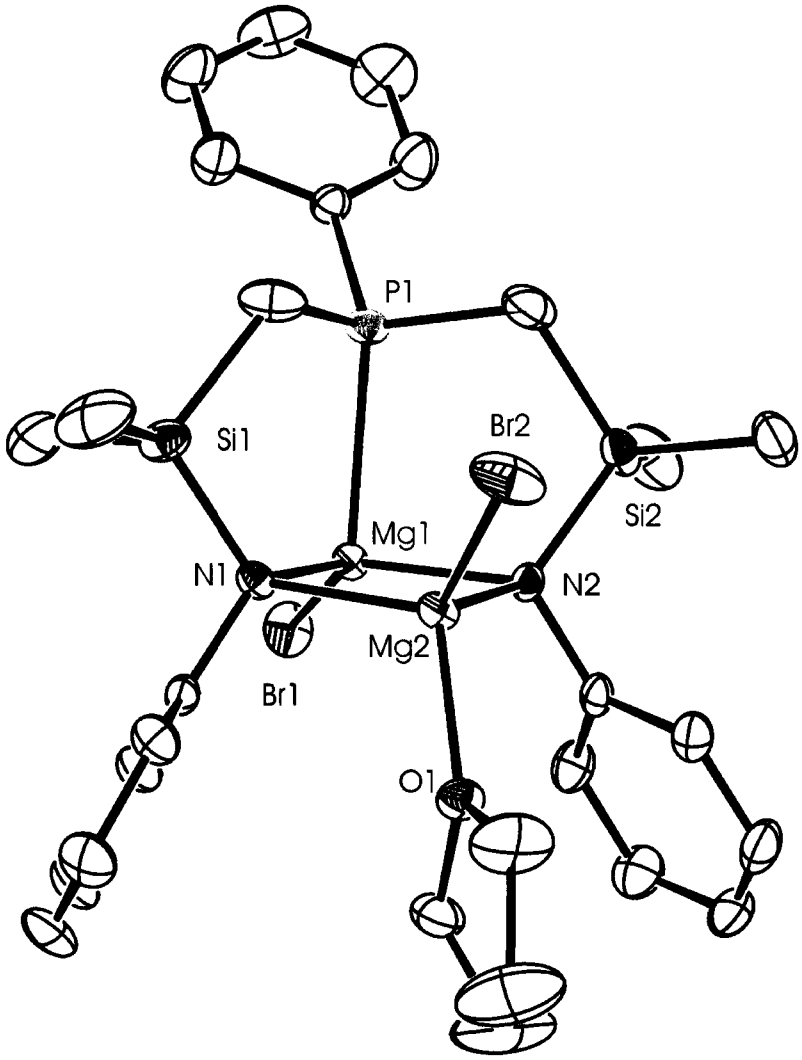

Figure 4.10. ORTEP representation (50% thermal ellipsoids) of the solid-state molecular structure of [NPN](MgBr)$_2$·(C_4H_8O) (**26**) as determined by X-ray diffraction.

Table 4.4. Selected bond lengths and bond angles in [NPN](MgBr)$_2$·(C_4H_8O) (**26**).

Atom	Atom	Distance (Å)	Atom	Atom	Distance (Å)
P(1)	Mg(1)	2.573(1)	N(2)	Mg(2)	2.120(2)
N(1)	Mg(1)	2.127(2)	O(1)	Mg(2)	2.024(2)
N(1)	Mg(2)	2.116(2)	Mg(1)	Br(1)	2.424(9)
N(2)	Mg(1)	2.122(2)	Mg(2)	Br(2)	2.418(1)

References begin on page 237

Atom	Atom	Atom	Angle (°)	Atom	Atom	Atom	Angle (°)
N(1)	Mg(1)	N(2)	92.34(9)	O(1)	Mg(2)	Br(2)	102.12(6)
P(1)	Mg(1)	Br(1)	118.11(4)	O(1)	Mg(2)	N(1)	111.86(9)
P(1)	Mg(1)	N(1)	89.73(7)	O(1)	Mg(2)	N(2)	111.85(9)
P(1)	Mg(1)	N(2)	88.66(7)	N(1)	Mg(2)	Br(2)	119.23(7)
N(2)	Mg(1)	Br(1)	127.67(8)	Mg(1)	N(1)	Mg(2)	87.40(9)
N(1)	Mg(2)	N(2)	92.73(9)	Mg(1)	N(2)	Mg(2)	87.42(8)

The reaction of the ligand precursor **26** with ruthenium(II) starting materials including the benzylidene complex $(PCy_3)_2Cl_2Ru(CHPh)$ have not yet been attempted. The preparation of other salts of the [NPN] ligand including potassium and thallium may also be possible via the methods outlined in Scheme 4.3.

4.10 Experimental

(i) General Procedures

Unless otherwise stated, general procedures were performed according to Section 2.9 (i). ^{1}H NMR T_1 relaxation measurements were performed on a Bruker AMX 500 MHz spectrometer using a standard inversion-recovery pulse sequence (180°-τ-90°). The T_1 values were obtained using the non linear three-parameter fitting routine in the Bruker XWINNMR program with an estimated error of ± 10 % in each T_1 value. The temperature was regulated using a Bruker VT 1000 unit. Toluene-d_8 was used as the NMR solvent.

(ii) Materials

Hydrogen gas (Praxair) and deuterium gas (Cambridge Isotope Laboratories) were employed without further purification. Norbornene was recrystallized prior to use and

References begin on page 237

styrene was used as received. The complexes $(P^iPr_3)_2Cl_2Ru(CCHPh)$[64] and $(P^iPr_3)_2Cl_2Ru\{CC(SiMe_3)Ph\}$[64] were prepared according to published literature procedures.

(iii) Synthesis and Reactivity of Complexes

[NPNH](P^iPr_3)Ru(CCPh) (20)

A solution of toluene (25 mL) cooled to -78 °C was added dropwise to an intimate mixture of $[NPN]Li_2{\cdot}(C_4H_8O)_2$ (0.996 g, 1.680 mmol) and $(P^iPr_3)_2Cl_2Ru(CCHPh)$ (1.000 g, 1.680 mmol) also maintained at –78 °C, and the resulting purple slurry was stirred for 10 minutes. The mixture was warmed to room temperature and stirred for a further 30 minutes. During this time the colour lightened to yield an intense violet coloured solution. The contents were once again chilled to –78 °C and then cannula transferred to a Schlenk frit containing a layer of Celite in order to remove insoluble by-products. The solvent was evaporated from the filtrate under reduced pressure until an oily residue remained. The solid was dissolved in a minimal amount of hexanes and the solution allowed to slowly evaporate in the glove-box to give purple block crystals of [NPNH](P^iPr_3)Ru(CCPh) (**20**) (0.483 g, 36 %) and a brown coloured filtrate. The crystals were washed with hexanes and the rinsings were combined with the original filtrate. X-ray quality crystals were obtained in this manner. A further crop of crystals can sometimes be obtained by the slow evaporation of the hexanes soluble fraction. The total isolated yields typically range from 40 to 50 %. ^{1}H NMR (C_6D_6, 298 K, 500 MHz): δ -0.06, 0.54 and 0.70 (s, SiCH_3, 9H total), δ 0.90 (s, overlapping, SiCH_3, 3H), δ 0.92 (m, overlapping, PCHCH_3, 9H), δ 1.08 (m, PCHCH_3, 9H), δ 1.23, 1.35 and 1.65 (m, PCH_2, 8H total), δ 2.10 (m, PCHCH_3, 3H), δ 4.95 (s, NH, 1H), δ 5.75 to 8.08 (m, overlapping, aromatic-H). ^{31}P{^{1}H} NMR (C_6D_6, 298 K, 202.5 MHz): δ 57.0 (d, $^2J_{PP}$ = 41.2 Hz, P^iPr_3) and δ 76.5 (d, $^2J_{PP}$ = 41.2 Hz, [NPNH]). Infra-red (KBr): ν(C≡C) at 2050 cm^{-1} and ν(N-H) at 3194 cm^{-1}. Anal. Calcd. for $C_{41}H_{58}N_2P_2RuSi_2$: C, 61.70; H, 7.32; N, 3.51. Found: C, 62.10; H, 7.48; N, 3.58.

References begin on page 237

[$NPNH_2$](P^iPr_3)Ru(η^2-H_2)$_2$(H_2) (21)

A J-Young NMR tube containing a solution of [NPNH](P^iPr_3)Ru(CCPh) (**20**) (0.042 g, 0.053 mmol) dissolved in benzene-d_6 (~ 1.0 mL) was degassed by performing two freeze-pump-thaw cycles and then warmed to room temperature. An atmosphere of H_2 gas was added to the NMR tube, which was then flame-sealed. Mixing the contents of the NMR tube resulted in an immediate change in colour from violet to orange yielding the complex [$NPNH_2$](P^iPr_3)Ru(η^2-H_2)$_2$(H_2) (**21**) as the only NMR active ruthenium species. Solutions of **21** gradually lighten to give the known bis dihydrogen complex (P^iPr_3)$_2$Ru(H_2)$_2$(H_2). The solution NMR data for complex **21**: ^{1}H NMR (C_6D_6, 298 K, 500 MHz): δ -7.60 (dd (AB), $^2J_{PH}$ = 7.6 Hz [N*P*NH], $^2J_{PH}$ = 6.7 Hz P^iPr_3, Ru-*H*, 6H), δ -0.08 and 0.00 (s, SiCH_3, 12H total), δ 0.98 (m, overlapping, PCHCH_3, 9H), δ 1.00 and 1.58 (m, overlapping, PCH_2, 8H total), δ 1.56 (m, overlapping, PC*H*CH_3, 3H), δ 3.98 (s, N-*H*, 2H), δ 6.52 to 7.81 (m, overlapping, aromatic-*H*, 15H total). ^{31}P{^{1}H} NMR (C_6D_6, 298 K, 202.5 MHz): δ 25.0 (d, $^2J_{PP}$ = 225 Hz, [N*P*NH]) and δ 86.0 (d, $^2J_{PP}$ = 225 Hz, P^iPr_3). T_1(min) for Ru-H_6 = 51 ms at 220 K in toluene-d_8.

[P_2N_2]Ru(CCHPh) (22) and [P_2NNH](P^iPr_3)Ru(CCPh) (23)

Toluene (25 mL) was added to a mixture of [P_2N_2]Li_2·($C_4H_8O_2$) (0.530 g, 0.835 mmol) and (P^iPr_3)$_2$$Cl_2$Ru(CCHPh) (0.496 g, 0.834 mmol) in a Schlenk flask and the contents were stirred at room temperature for two hours. The toluene was removed under reduced pressure leaving an oily residue. The addition of a minimal amount of hexanes to this residue allowed for the separation of a dark precipitate from a dark-brown coloured filtrate. The soluble fraction was removed via pipette, and the precipitate was further rinsed with hexanes until the washings were light brown in colour. The precipitate was dried under vacuum to give [P_2NNH](P^iPr_3)Ru(CCPh) (**23**) as a brown solid in approximately 95 % purity as determined by ^{1}H and ^{31}P{^{1}H} NMR spectroscopy. Complex **22** and P^iPr_3 were also present as minor impurities. Removal of the hexanes (*in vacuo*) from the soluble

References begin on page 237

fraction gave a dark-brown oily solid, which the ^{1}H and ^{31}P{^{1}H} NMR data showed to be [P_2N_2]Ru(CCHPh) (**22**) (*ca.* 60 % purity). Also present were complex **23**, P^{i}Pr$_3$ as well as other unidentified impurities. The solution NMR data for complex **22**: ^{1}H NMR (C_6D_6, 298 K, 500 MHz): δ 0.25 and 0.38 (s, SiC*H*$_3$, 24H total), δ 0.92 to 1.35 (m, overlapping, PC*H*$_2$, 8H total), δ 4.85 (t, $^4J_{PH}$ = 4.2 Hz, RuCC*H*Ph, 1H), δ 6.95 to 8.10 (m, overlapping, aromatic-*H*). ^{31}P{^{1}H} NMR (C_6D_6, 298 K, 202.5 MHz): δ 25.6 (s, [*P*$_2$N$_2$]). The solution NMR data for complex **23**: ^{1}H NMR (C_6D_6, 298 K, 500 MHz): δ 0.20, 0.42, 0.56 and 0.75 (s, SiC*H*$_3$, 24H total), δ 0.94 (m, br, PCHC*H*$_3$, 9H), δ 1.34 and 1.49 (m, PC*H*$_2$, 4H total), δ 1.66 (m, PC*H*CH$_3$, 3H), δ 1.93 and 2.08 (m, PC*H*$_2$, 4H total), δ 2.12 (s, N-*H*, 1H), δ 7.02 to 8.18 (m, overlapping, aromatic-*H*). ^{31}P{^{1}H} NMR (C_6D_6, 298 K, 202.5 MHz): δ 20.6 (d, $^2J_{PP}$ = 33 Hz, [*P*$_2$N$_2$], 2P), δ 59.3 (t, $^2J_{PP}$ = 33 Hz, *P*^{i}Pr$_3$, 1P).

[P_2N_2]Ru{CC(SiMe$_3$)Ph} (24)

At room temperature toluene (15 mL) was added to an intimate mixture of [P_2N_2]Li$_2$·($C_4H_8O_2$) (0.138 g, 0.217 mmol) and (P^{i}Pr$_3$)$_2$Cl$_2$Ru{CC(SiMe$_3$)Ph} (0.145 g, 0.217 mmol). Over the course of two hours the colour of the solution changed from purple to orange with the formation of a precipitate. In the glove-box the mixture was filtered and the toluene was removed under reduced pressure. A minimal amount of pentane solution was added to re-dissolve the solid. The slow evaporation of the pentane solution resulted in the deposition of [P_2N_2]Ru{CC(SiMe$_3$)Ph} (**24**) as large block crystals. Yield: (0.163 g, 93 %). Single crystals for an X-ray diffraction study were obtained from the saturated pentane solution. ^{1}H NMR (C_6D_6, 298 K, 500 MHz): δ 0.22 (s, CCSC*H*$_3$, 9H), δ 0.20, 0.25, 0.36 and 0.44 (s, SiC*H*$_3$, 24H total), δ 1.25 to 1.65 (m, overlapping, PC*H*$_2$, 8H), δ 7.02 to 7.58 (m, overlapping, aromatic-*H*). ^{31}P{^{1}H} NMR (C_6D_6, 298 K, 202.5 MHz): δ 26.5 (s, [*P*$_2$N$_2$]). Anal. Calcd. for $C_{35}H_{56}N_2P_2RuSi_5$: C, 52.01; H, 6.98; N, 3.47. Found: C, 52.09; H, 7.22; N, 3.66.

References begin on page 237

Reaction of [P_2N_2]Ru{CC(SiMe$_3$)Ph} (24) with styrene and norbornene

In an NMR tube complex **24** (0.036 g, 0.045 mmol) and an excess of styrene (0.014 g, 0.134 mmol) were dissolved in ~ 1 mL of toluene-d_8. The contents were mixed and stirred at room-temperature. After 24 hours no change in the reaction mixture was evident upon inspection of the ^{1}H and ^{31}P{^{1}H} NMR spectroscopy. The sample was heated to 80°C for a further 24 hours but NMR spectroscopy showed that no reaction had taken place. A similar procedure was employed for the reaction of **24** with norbornene.

[P_2NNH]Ru(H){CC(SiMe$_3$)Ph} (25)

In a J-Young valve NMR tube, complex **24** (0.044 g, 0.054 mmol) was dissolved in ~ 1 mL of benzene-d_6. The sample was degassed by performing three freeze-pump-thaw cycles, warmed to room temperature, and then one atmosphere of hydrogen gas was vented into the NMR tube. The tube was sealed and the contents were stirred for an hour. The ^{1}H and ^{31}P{^{1}H} NMR spectrum showed the quantitative formation of **25** with complex **10** present in less than 2 % yield. ^{1}H NMR (C_6D_6, 298 K, 500 MHz): δ -8.55 (t, $^2J_{PH}$ = 17.8 Hz, Ru-*H*, 1H), δ 0.00 (s, CCSCH_3, 9H), δ 0.10, 0.26, 0.28 and 0.64 (s, SiCH_3, 24H total), δ 1.28, 1.47, 1.52 and 1.78 (m, P-CH_2, 8H total), δ 1.80 (s, overlapping, N-*H*, 1H), δ 6.90 to 7.62 (m, overlapping, aromatic-*H*). ^{31}P{^{1}H} NMR (C_6D_6, 298 K, 202.5 MHz): δ 25.6 (s, [P_2N_2]). Complex **10** is exclusively formed when the reaction is performed at four atmospheres of hydrogen pressure as indicated by the ^{1}H and ^{31}P{^{1}H} NMR data.

[NPN](MgBr)$_2$·(C_4H_8O) (26)

To an intimate mixture of [NPN]Li$_2$·(C_4H_8O)$_2$ (0.65 g, 1.09 mmol) and an excess of MgBr$_2$·(OEt$_2$)$_2$ (1.00 g, 3.01 mmol) at –78°C was added 20 mL of tetrahydrofuran. The solution was warmed to room temperature and stirred for one hour, after which the solvent

References begin on page 237

was removed under vacuum. The remaining solid was extracted into toluene and filtered. The filtrate was evaporated to dryness, leaving a white powder that was rinsed with hexanes and dried under vacuum to afford [NPN](MgBr)$_2$·(C_4H_8O) (**26**) in 90 % yield. Single crystals suitable for an X-ray diffraction study were grown from the slow evaporation of a saturated toluene solution. ^{1}H NMR (C_6D_6, 298 K, 500 MHz): δ 0.05 and 0.52 (s, SiCH_3, 12H total), δ 0.64 (m, THF-OCH$_2$CH_2, 4H), δ 1.12 and 1.97 (m, P-CH_2, 4H total), δ 2.58 (m, THF-OCH_2CH$_2$, 4H), δ 6.63 to 7.78 (m, N-phenyl and P-phenyl, 15H total). ^{31}P{^{1}H} NMR (C_6D_6, 298 K, 202.5 MHz): δ -47.0 (s).

X-ray Crystallographic Analyses of Complexes 20, 24 and 26

Selected crystallographic and solution refinement data are provided in Appendix 1.

4.11 References

(1) Grubbs, R. H.; Chang, S. *Tetrahedron* **1998**, *54*, 4413.

(2) Buchmeiser, M. R. *Chem. Rev.* **2000**, *100*, 1565.

(3) Bielawski, C. W.; Louie, J.; Grubbs, R. H. *J. Am. Chem. Soc.* **2000**, *122*, 12872.

(4) Dias, E. L.; Grubbs, R. H. *Organometallics* **1998**, *17*, 2758.

(5) Jafarpour, L.; Heck, M. P.; Baylon, C.; Lee, H. M.; Mioskowski, C.; Nolan, S. P. *Organometallics* **2002**, *21*, 671.

(6) Yoa, Q. *Angew. Chem. Int. Ed.* **2000**, *39*, 3896.

References begin on page 237

(7) Kingsbury, J. S.; Harrity, J. P. A.; Bonitatebus, J., P. J.; Hoveyda, A. H. *J. Am. Chem. Soc.* **1999**, *121*, 791.

(8) Ackermann, L.; Furstner, A.; Weskamp, T.; Kohl, F. J.; Herrmann, W. A. *Tetrahedron Lett.* **1999**, *40*, 4787.

(9) Scholl, M.; Trnka, T. M.; Morgan, J. P.; Grubbs, R. H. *Tetrahedron Lett.* **1999**, *40*, 2247.

(10) Amoroso, D.; Fogg, D. E. *Macromolecules* **2000**, *33*, 2815.

(11) Hansen, S. M.; Volland, M. A. O.; Rominger, F.; Eisentrager, F.; Hofmann, P. *Angew. Chem. Int. Ed.* **1999**, *38*, 1273.

(12) Huang, J.; Schanz, H. J.; Stevens, E. D.; Nolan, S. P. *Organometallics* **1999**, *18*, 5375.

(13) Schwab, P.; Grubbs, R. H.; Ziller, J. W. *J. Am. Chem. Soc.* **1996**, *118*, 100.

(14) Wu, Z.; Nguyen, S. T.; Grubbs, R. H.; Ziller, J. W. *J. Am. Chem. Soc.* **1995**, *117*, 5503.

(15) Pietraszuk, C.; Marciniec, B.; Fischer, H. *Organometallics* **2000**, *19*, 913.

(16) Wilhelm, T. E.; Belderrain, T. R.; Brown, S. N.; Grubbs, R. H. *Organometallics* **1997**, *16*, 3867.

(17) Gandelman, M.; Rybtchinski, B.; Ashkenazi, N.; Gauvin, R. M.; Milstein, D. *J. Am. Chem. Soc.* **2001**, *123*, 5372.

(18) Olivan, M.; Caulton, K. G. *Inorg. Chem.* **1999**, *38*, 566.

References begin on page 237

(19) Caolter III, J. N.; Spivak, G. J.; Gerard, H.; Clot, E.; Davidson, E. R.; Eisenstein, O.; Caulton, K. G. *J. Am. Chem. Soc.* **1998**, *120*, 9388.

(20) Kingsbury, J. S.; Garber, S. B.; Giftos, J. M.; Gray, B. L.; Okamoto, M. M.; Farrer, R. A.; Fourkas, J. T.; Hoveyda, A. H. *Angew. Chem. Int. Ed.* **2001**, *40*, 4251.

(21) Belderrain, T. R.; Grubbs, R. H. *Organometallics* **1997**, *16*, 4001.

(22) Furstner, A.; Thiel, O. R.; Lehmann, C. W. *Organometallics* **2002**, *21*, 331.

(23) Jafarpour, L.; Nolan, S. P. *Organometallics* **2000**, *19*, 2055.

(24) Trnka, T. M.; Morgan, J. P.; Sanford, M. S.; Wilhelm, T. E.; Scholl, M.; Choi, T. L.; Ding, S.; Day, M. W.; Grubbs, R. H. *J. Am. Chem. Soc.* **2003**, *125*, 2546.

(25) Jafarpour, L.; Hiller, A. C.; Nolan, S. P. *Organometallics* **2002**, *21*, 442.

(26) Dias, E. L.; Nguyen, S. T.; Grubbs, R. H. *J. Am. Chem. Soc.* **1997**, *119*, 3887.

(27) Aagaard, O. M.; Meier, R. J.; Buda, F. *J. Am. Chem. Soc.* **1998**, *120*, 7174.

(28) Sanford, M. S.; Ulman, M.; Grubbs, R. H. *J. Am. Chem. Soc.* **2001**, *123*, 749.

(29) Sanford, M. S.; Love, J. A.; Grubbs, R. H. *J. Am. Chem. Soc.* **2001**, *123*, 6543.

(30) Katayama, H.; Yoshida, T.; Ozawa, F. *J. Organomet. Chem.* **1998**, *562*, 203.

(31) Bruneau, C.; Dixneuf, P. H. *Acc. Chem. Res.* **1999**, *32*, 311.

(32) Saoud, M.; Romerosa, A.; Peruzzini, M. *Organometallics* **2000**, *19*, 4005.

References begin on page 237

(33) Del Rio, I.; Van Koten, G. *Tetrahedron Lett.* **1999**, *40*, 1401.

(34) Picquet, M.; Bruneau, C.; Dixneuf, P. H. *Chem. Commun.* **1998**, 2249.

(35) Furstner, A.; Picquet, M.; Bruneau, C.; Dixneuf, P. H. *Chem. Commun.* **1998**, 1315.

(36) Furstner, A.; Ackermann, L. *Chem. Commun.* **1999**, 95.

(37) Furstner, A.; Hill, A. F.; Liebl, M.; Wilton-Ely, J. D. E. T. *Chem. Commun.* **1999**, 601.

(38) Harlow, K. J.; Hill, A. F.; Wilton-Ely, J. D. E. T. *J. Chem. Soc., Dalton Trans.* **1999**, 285.

(39) Jafarpour, L.; Huang, J.; Stevens, E. D.; Nolan, S. P. *Organometallics* **1999**, *18*, 3760.

(40) Jafarpour, L.; Schanz, H. J.; Stevens, E. D.; Nolan, S. P. *Organometallics* **1999**, *18*, 5416.

(41) Schanz, H. J.; Jafarpour, L.; Stevens, E. D.; Nolan, S. P. *Organometallics* **1999**, *18*, 5187.

(42) Lynn, D. M.; Grubbs, R. H. *J. Am. Chem. Soc.* **2001**, *123*, 3187.

(43) Stuer, W.; Wolf, J.; Werner, H.; Schwab, P.; Schulz, M. *Angew. Chem. Int. Ed.* **1998**, *37*, 3421.

(44) Gonzalez-Herrero, P.; Weberndorfer, B.; Ilg, K.; Wolf, J.; Werner, H. *Angew. Chem. Int. Ed.* **2000**, *39*, 3266.

References begin on page 237

(45) Sanford, M. S.; Henling, L. M.; Day, M. W.; Grubbs, R. H. *Angew. Chem. Int. Ed.* **2000**, *39*, 3451.

(46) Sanford, M. S.; Henling, L. M.; Grubbs, R. H. *Organometallics* **1998**, *17*, 5384.

(47) Chang, S.; Jones II, L.; Wang, C.; Henling, L. M.; Grubbs, R. H. *Organometallics* **1998**, *17*, 3460.

(48) Bruce, M. I.; Hall, B. C.; Zaitseva, N. N.; Skelton, B. W.; White, A. H. *J. Chem. Soc., Dalton Trans.* **1998**, 1793.

(49) Touchard, D.; Haquette, P.; Daridor, A.; Romero, A.; Dixneuf, P. H. *Organometallics* **1998**, *17*, 3844.

(50) Kawata, Y.; Sato, M. *Organometallics* **1997**, *16*, 1093.

(51) Grunwald, C.; Gevert, O.; Wolf, J.; Gonzalez-Herrero, P.; Werner, H. *Organometallics* **1996**, *15*, 1960.

(52) Rachidi, I. E. I.; Eisentstein, O.; Jean, Y. *New. J. Chem.* **1990**, *14*, 671.

(53) Riehl, J. F.; Jean, Y.; Eisenstein, O.; Pelissier, M. *Organometallics* **1992**, *11*, 729.

(54) Joesten, M. D.; Schaad, L. J. *Hydrogen Bonding*; Marcel Dekker, Inc.: New York, 1974.

(55) Sabo-Etienne, S.; Chaudret, B. *Coord. Chem. Rev.* **1998**, *178-180*, 381.

(56) Abdur-Rashid, K.; Gusev, D. G.; Lough, A. J.; Morris, R. H. *Organometallics* **2000**, *19*, 1652.

References begin on page 237

(57) Hamilton, D. G.; Crabtree, R. H. *J. Am. Chem. Soc.* **1988**, *110*, 4126.

(58) Luo, X. L.; Crabtree, R. H. *Inorg. Chem.* **1990**, *29*, 2788.

(59) Desrosiers, P. J.; Cai, L.; Lin, Z.; Richards, R.; Halpern, J. *J. Am. Chem. Soc.* **1991**, *113*, 4173.

(60) Arligule, T.; Chaudret, B.; Morris, R. H.; Sella, A. *Inorg. Chem.* **1988**, *27*, 598.

(61) Yang, S. H.; Wen, T. B.; Jia, G.; Lin, Z. *Organometallics* **2000**, *19*, 5477.

(62) Bourgault, M.; Castillo, A.; Esteruelas, M. A.; Onate, E.; Ruiz, N. *Organometallics* **1997**, *16*, 636.

(63) Olivan, M.; Clot, E.; Eisenstein, O.; Caulton, K. G. *Organometallics* **1998**, *17*, 897.

(64) Katayama, H.; Ozawa, F. *Organometallics* **1998**, *17*, 5190.

(65) Bruce, M. I.; Humphrey, M. G.; Snow, M. R.; Tiekink, E. R. T. *J. Organomet. Chem.* **1986**, *314*, 213.

(66) Slugovc, C.; Mereiter, K.; Zobetz, E.; Schmid, R.; Kirchner, K. *Organometallics* **1996**, *15*, 5275.

(67) Olivan, M.; Eisenstein, O.; Caulton, K. G. *Organometallics* **1997**, *16*, 2227.

(68) Fryzuk, M. D.; Montgomery, C. D. *Coord. Chem. Rev.* **1989**, *95*, 1.

References begin on page 237

(69) Johnson, S. A. *Ligand Design and The Synthesis of Reactive Organometallic Complexes of Tantalum for Dinitrogen Activation*; University of British Columbia: Vancouver, 2000.

References begin on page 237

Appendix 1

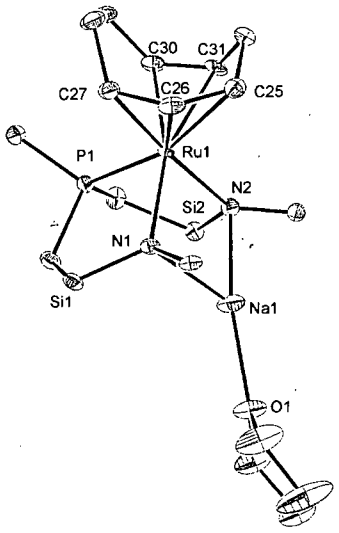

X-ray Crystal Structure Data

In all cases, suitable crystals were selected and mounted on a glass fiber using Paratone-N oil and freezing to -100 °C (complex **1** was cooled to -85 °C and complex **4** was cooled to -75 °C). All measurements were made on a Rigaku/ADSC CCD area detector with graphite monochromated Mo-Kα radiation. Data were collected and processed using the d*TREK program.[1] The data were corrected for Lorentz and polarization effects. All of the structures were solved by direct methods[2] and expanded using Fourier techniques.[3] The non-hydrogen atoms were refined anisotropically. All Ru-*H* and N-*H* hydrogen atoms were refined isotropically, the rest were included in fixed positions. Neutral atom scattering factors were taken from the *International Tables for X-ray Crystallography*.[4] All calculations were performed using the teXsan crystallographic software package.[5] ORTEP drawings of complexes **1**, **2**, ***endo*-3**, **4**, **7**, **8**, **11**, **12**, **13**, **20**, **24** and **26** are given throughout the thesis along with tables of selected bond lengths and bond angles; an ORTEP drawing of complex **5** is shown in Figure A1. Crystallographic and structure refinement data for all complexes are given in Tables A1 – A4. All of the structures presented in this thesis have been solved by Dr. Brian O. Patrick of the X-ray Crystallography department at the University of British Columbia.

Additional information can be obtained from the UBC X-ray lab. A list of the reference names for each of the complexes is given below.

Complex	UBC X-ray Reference Name
1	mf472
2	mf498
***endo*-3**	mf428
4	mf437
5	mf482
7	mf495
8	mf466
11	mf502
12	mf451
13	mf456
20	mf411
24	mf490
26	mf477

References

(1) d*TREK *Area Detector Software. Version 4.13. Molecular Structure Corporation* **1996-1998.**

(2) Altomare, A.; Burla, M. C.; Cammalli, G.; Cascarano, M.; Giacovazzo, C.; Guagliardi, A.; Moliterni, A. G. G.; Polidori, G.; Spagna, A. *J. Appl. Cryst.* **1999**, *32*, 115-119.

(3) Beurskens, P. T.; Admiraal, G.; Beurskens, G.; Bosman, W. P.; de Gelder, R.; Israel, R.; Smits, J. M. M. *DIRDIF94, Technical Report of the Crystallography Laboratory, University of Nijmegen, The Netherlands* **1994.**

(4) Cromer, D. T.; Waber, J. T. *International Tables for X-ray Crystallography* **1974**, *Vol. IV, The Kynoch Press, Birmingham, England*, Table 2.2 A.

(5) teXsan *Crystal Structure Analysis Package, Molecular Structure Corporation* **1992.**

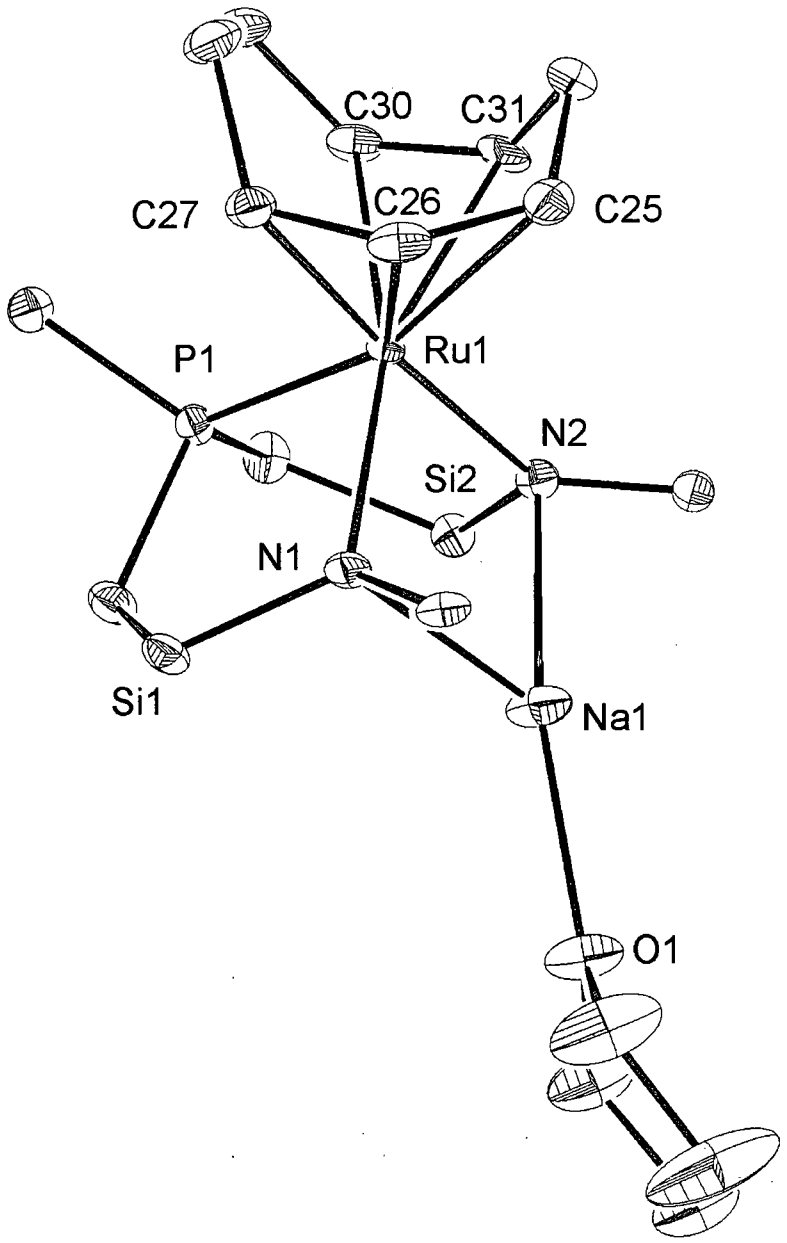

Figure A1. ORTEP representation (50 % thermal ellipsoids) of the solid-state molecular structure of {[NPN]Ru(1-3-η^3:5,6-η^2-C_8H_{11})}{Na•THF} (**5**) as determined by X-ray diffraction. The [NPN] silyl methyl groups have been omitted for clarity and only the *ipso* carbon atoms of the amido and phosphine phenyl rings are shown.

Table A1. Crystallographic Data and Structure Refinement Data for complexes $[P_2N_2]Ru(\eta^2:\eta^2\text{-}C_8H_{12})$ (**1**), $[P_2NNH]Ru(C_6H_4PPh_2)$ (**2**), *endo*-$[NPNH]Ru(1\text{-}3\text{-}\eta^3\text{:}5,6\text{-}\eta^2\text{-}C_8H_{11})$ (*endo*-**3**) and $\{[NPN]Ru(1\text{-}3\text{-}\eta^3\text{:}5,6\text{-}\eta^2\text{-}C_8H_{11})\}\{Li\bullet THF\}$ (**4**).

	1	**2**	***endo*-3**	**4**
Formula	$C_{32}H_{56}N_2P_2Si_4.C_6H_{14}Ru$	$2[C_{42}H_{57}N_2P_3Si_4Ru].C_5H_{12}$	$C_{32}H_{43}N_2PRuSi_2$	$C_{36}H_{50}N_2PSi_2LiORu.C_7H_8$
Fw	830.34	1864.67	643.92	814.10
Colour, Habit	yellow, platelet	yellow, chip	red, prism	red, block
Crystal size, mm	0.50 x 0.20 x 0.05	0.25 x 0.25 x 0.10	0.25 x 0.15 x 0.10	0.40 x 0.30 x 0.10
Crystal system	monoclinic	orthorhombic	trigonal	orthorhombic
Space group	P2/n (#13)	Pbca (#61)	R3 (#148)	$P2_12_12_1$ (#19)
a, Å	11.113(1)	20.3845(8)	42.2752(7)	9.0674(3)
b, Å	10.854(1)	21.7255(8)		19.9274(5)
c, Å	17.994(2)	43.150(2)	9.0004(3)	23.055(1)
α, deg				
β, deg	96.944(3)			
γ, deg				
V, Å^3	2154.6(3)	19109(1)	13930.4(4)	4165.8(2)
Z	2	8	18	4
T, °C	-85 ± 1	-100 ± 1	-100 ± 1	-75 ± 1
ρ_{calc}, g/cm^3	1.280	1.296	1.382	1.298
F_{000}	884.00	7824.00	6048.00	1712.00
μ(MoKα), cm^{-1}	5.77	5.61	6.60	5.07
correction factors	0.6695 – 1.0000	0.7109 – 1.0000	0.7589 – 1.0000	0.7804 – 1.0000
$2\theta_{max}$, deg	55.8	50.0	55.8	55.8
total no. of reflns	20052	151583	36357	31090
no. of unique reflns	4799	16723	6957	9060
R_{int}	0.046	0.112	0.060	0.047
no. observations (I > nσ(I))	3680 (n=2)	13461 (n=2)	4940 (n=3)	7849 (n=3)
no. of variables	218	1006	391	480
R (F^2, all data)	0.047	0.083	0.050	0.046
R_w (F^2, all data)	0.095	0.158	0.076	0.069
R (F, I > nσ(I))	0.035 (n=2)	0.064 (n=2)	0.028 (n=3)	0.026 (n=3)
R_w (F, I > nσ(I))	0.091 (n=2)	0.148 (n=2)	0.035 (n=3)	0.032 (n=3)
Gof	1.00	1.10	0.88	0.94

Rigaku/ADSC CCD diffractometer, $R = \Sigma||F_o^2| - |F_c||/\Sigma|F_o|$; $R_w = [\Sigma(F_o^2 - F_c^2)^2/\Sigma\omega(F_o^2)^2]^{1/2}$.

Table A2. Crystallographic Data and Structure Refinement Data for complexes {[NPN]Ru(1-3-η^3:5,6-η^2-C_8H_{11})}{Na•THF} (**5**), [NPNH]Ru(1-3-η^3:5,6-η^2-C_8H_{11})(CO) (**7**), {[PhN(H)Si-Me_2CH_2][(C_8H_{11})C(O)N(Ph)SiMe_2CH_2][Ph]}PRu(CO)$_4$ (**8**) and [P_2NNH]RuH(PPh_3) (**11**).

	5	**7**	**8**	**11**
Formula	$C_{36}H_{50}N_2NaPSi_2RuO.C_7H_8$	$C_{33}H_{43}N_2OPSi_2Ru$	$C_{37}H_{38}N_2O_5Si_2PRu$	$C_{49}H_{66}N_2P_3RuSi_4$
Fw	814.15	671.93	778.93	989.41
Colour, Habit	orange, chip	yellow, block	orange, block	orange, irregular
Crystal size, mm	0.25 x 0.25 x 0.10	0.35 x 0.10 x 0.10	0.25 x 0.25 x 0.13	0.40 x 0.30 x 0.10
Crystal system	triclinic	monoclinic	orthorhombic	monoclinic
Space group	$P\bar{1}$ (#2)	$P2_1/n$ (#14)	Pbca (#61)	$P2_1/n$ (#14)
a, Å	10.2121(4)	9.1968(4)	16.0035(5)	10.3948(4)
b, Å	10.3162(3)	14.4543(5)	18.5094(8)	15.0228(5)
c, Å	22.133(1)	23.979(1)	26.638(2)	32.490(1)
α, deg	87.707(7)			
β, deg	79.077(6)	96.731(2)		98.418(2)
γ, deg	64.334(4)			
V, Å^3	2061.3(2)	3165.6(2)	7890.6(5)	5019.0(3)
Z	2	4	8	4
T, °C	-100 ± 1	-100 ± 1	-100 ± 1	-100 ± 1
ρ_{calc}, g/cm^3	1.312	1.410	1.311	1.309
F_{000}	856.00	1400.00	3208.00	2076.00
μ(MoKα), cm^{-1}	5.20	6.51	5.39	5.38
correction factors	0.8093 – 1.0000	0.8278 – 1.0000	0.8230 – 1.0000	0.7056 – 1.0000
$2\theta_{max}$, deg	55.7	55.8	55.7	55.7
total no. of reflns	18786	29377	63160	44199
no. of unique reflns	8409	7258	9419	11386
R_{int}	0.032	0.047	0.075	0.054
no. observations (I > nσ(I))	7131 (n=3)	5079 (n=3)	5240 (n=2)	7511 (n=3)
no. of variables	480	385	461	536
R (F^2, all data)	0.052	0.046	0.075	0.053
R_w (F^2, all data)	0.082	0.066	0.085	0.075
R (F, I > nσ(I))	0.029 (n=3)	0.026 (n=3)	0.035 (n=2)	0.031 (n=3)
R_w (F, I > nσ(I))	0.037 (n=3)	0.030 (n=3)	0.074 (n=2)	0.034 (n=3)
Gof	1.48	0.91	0.78	0.97

Rigaku/ADSC CCD diffractometer, $R = \Sigma||F_o^2| - |F_c||/\Sigma|F_o|$; $R_w = [\Sigma(F_o^2 - F_c^2)^2/\Sigma\omega(F_o^2)^2]^{1/2}$.

Table A3. Crystallographic Data and Structure Refinement Data for complexes [NPN(H)(η^6-C_6H_5)]RuH (**12**), [$NPNH_2$]Ru(H)$_2$(η^6-C_7H_8) (**13**), [NPNH](P^iPr_3)Ru(CCPh) (**20**) and [P_2N_2]Ru{CC($SiMe_3$)Ph} (**24**).

	12	**13**	**20**	**24**
Formula	$C_{24}H_{33}N_2Si_2PRu$	$C_{31}H_{43}N_2PRuSi_2$	$C_{41}H_{58}N_2P_2RuSi_2$	$C_{35}H_{56}N_2P_2Si_5Ru$
Fw	537.75	631.91	798.11	808.29
Colour, Habit	orange, platelet	yellow, block	brown, platelet	red, chip
Crystal size, mm	0.35 x 0.15 x 0.04	0.50 x 0.50 x 0.20	0.40 x 0.40 x 0.05	0.35 x 0.35 x 0.15
Crystal system	monoclinic	triclinic	monoclinic	triclinic
Space group	$P2_1/a$ (#14)	$P\bar{1}$ (#2)	$P2_1/c$ (#14)	$P\bar{1}$ (#2)
a, Å	10.2540(4)	10.2259(4)	14.8185(4)	10.3088(1)
b, Å	22.2088(8)	11.0654(7)	14.7405(3)	10.6551(2)
c, Å	11.0383(4)	15.8325(9)	20.1233(4)	20.5014(6)
α, deg		89.778(3)		83.512(7)
β, deg	101.362(3)	76.184(2)	108.932(2)	81.490(7)
γ, deg		65.090(2)		66.922(5)
V, Å^3	2464.5(1)	1568.3(1)	4157.8(2)	2045.1(1)
Z	4	2	4	2
T, °C	-100 ± 1	-100 ± 1	-100 ± 1	-100 ± 1
ρ_{calc}, g/cm^3	1.449	1.338	1.275	1.312
F_{000}	1112.00	660.00	1680.00	848.00
μ(MoKα), cm^{-1}	8.13	6.49	5.41	6.34
correction factors	0.6936 – 1.0000	0.7021 – 1.0000	0.7673 – 1.0000	0.8153 – 1.0000
$2\theta_{max}$, deg	57.4	55.8	55.8	55.7
total no. of reflns	20492	14121	34448	18902
no. of unique reflns	6064	6272	9095	8404
R_{int}	0.050	0.036	0.051	0.035
no. observations (I > nσ(I))	4216 (n=3)	5184 (n=3)	6567 (n=3)	6847 (n=3)
no. of variables	299	350	437	406
R (F^2, all data)	0.048	0.054	0.053	0.052
R_w (F^2, all data)	0.073	0.094	0.083	0.081
R (F, I > nσ(I))	0.027 (n=3)	0.032 (n=3)	0.029 (n=3)	0.030 (n=3)
R_w (F, I > nσ(I))	0.032 (n=3)	0.044 (n=3)	0.037 (n=3)	0.039 (n=3)
Gof	0.85	1.38	1.08	1.35

Rigaku/ADSC CCD diffractometer, $R = \Sigma||F_o^2| - |F_c||/\Sigma|F_o|$; $R_w = [\Sigma(F_o^2 - F_c^2)^2/\Sigma\omega(F_o^2)^2]^{1/2}$.

Table A4. Crystallographic Data and Structure Refinement Data for complex [NPN](MgBr)$_2$•(C_4H_8O) (**26**).

	26
Formula	$C_{28}H_{39}N_2OSi_2P$ Mg_2Br_2
Fw	715.19
Colour, Habit	clear, chip
Crystal size, mm	0.50 x 0.20 x 0.20
Crystal system	orthorhombic
Space group	Pbca (#61)
A, Å	17.7617(6)
B, Å	16.3058(8)
C, Å	23.452(1)
α, deg	
β, deg	
γ, deg	
V, Å^3	6792.1(9)
Z	8
T, °C	-100 ± 1
ρ_{calc}, g/cm^3	1.399
F_{000}	2928.00
μ(MoKα), cm^{-1}	25.72
Correction factors	0.7812 – 1.0000
$2\theta_{max}$, deg	55.8
Total no. of reflns	59874
No. of unique reflns	8702
R_{int}	0.094
No. observations (I > nσ(I))	3792 (n=3)
No. of variables	343
R (F^2, all data)	0.060
R_w (F^2, all data)	0.077
R (F, I > nσ(I))	0.026 (n=3)
R_w (F, I > nσ(I))	0.029 (n=3)
Gof	0.63

Rigaku/ADSC CCD diffractometer, $R = \Sigma||F_o^2| - |F_c||/\Sigma|F_o|$; $R_w = [\Sigma(F_o^2 - F_c^2)^2/\Sigma\omega(F_o^2)^2]^{1/2}$.

Appendix 2

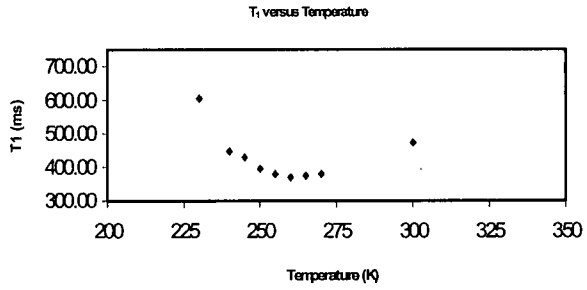

^{1}H NMR Longitudinal Relaxation (T_1) Measurements

^{1}H NMR T_1 relaxation measurements were performed on a Bruker AMX 500 MHz spectrometer using a standard inversion-recovery pulse sequence (180°-τ-90°). The T_1 values were obtained using the non linear three-parameter fitting routine in the Bruker XWINNMR program with an estimated error of ± 10 % in each T_1 value. The temperature was regulated using a Bruker VT 1000 unit. Toluene-d_8 was used as the NMR solvent for these studies.

Table A5. Temperature and T_1 values for the ruthenium hydrides in $[P_2NNH]Ru(H_2)H$ (**10**).

Temperature (K)	T_1 (ms) Ru-*H*
300	108
280	82
260	74
245	65
240	62
235	68
230	75
220	94

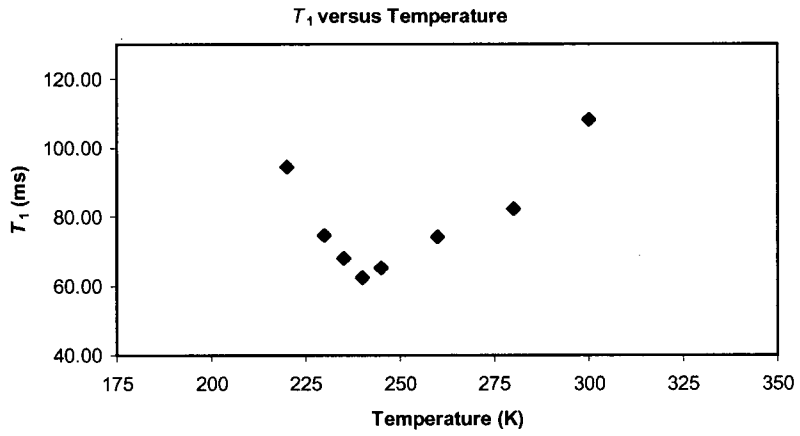

Figure A2. Plot of T_1 versus Temperature for the ruthenium hydrides in $[P_2NNH]Ru(H_2)H$ (**10**).

Table A6. Temperature and T_1 values for the ruthenium hydride in $[P_2NNH]RuH(PPh_3)$ (**11**)

Temperature (K)	T_1 (ms) Ru-*H*
300	475
270	379
265	375
260	370
255	379
250	396
245	429
240	446
230	606

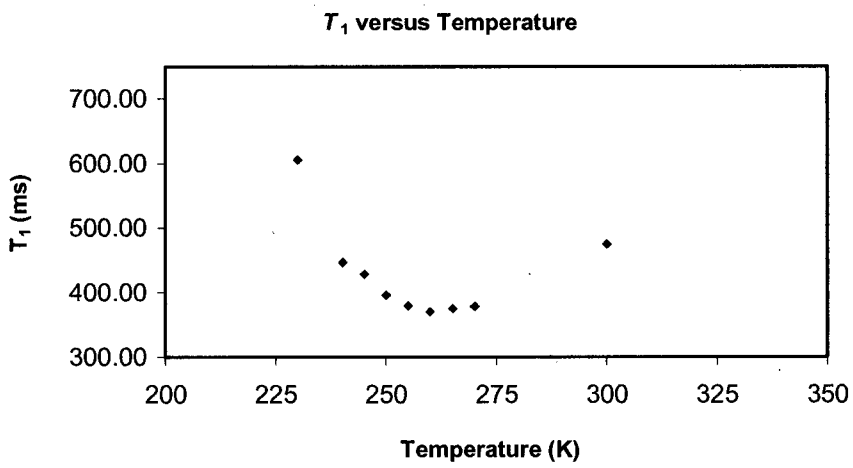

Figure A3. Plot of T_1 versus Temperature for the ruthenium hydride in $[P_2NNH]RuH(PPh_3)$ (**11**).

Table A7. Temperature and T_1 values for the ruthenium hydride in [NPN(H)(η^6-C_6H_5)]RuH (**12**).

Temperature (K)	T_1 (ms) Ru-*H*
298	1198
275	902
255	724
250	697
246	699
240	715
230	802

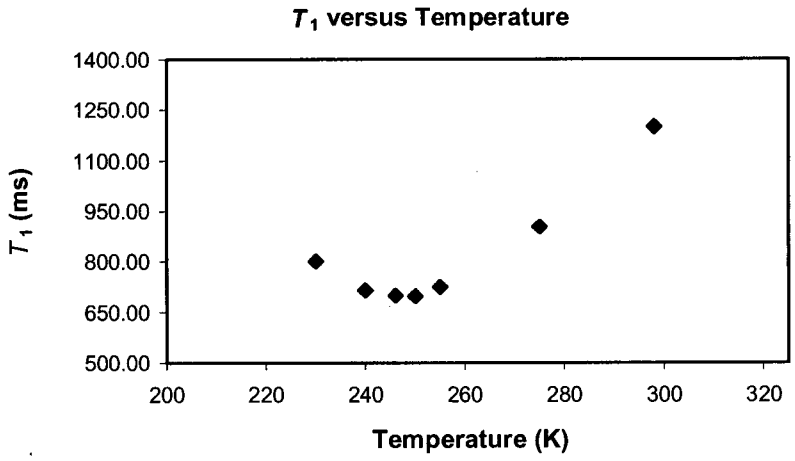

Figure A4. Plot of T_1 versus Temperature for the ruthenium hydride in the complex [NPN(H)(η^6-C_6H_5)]RuH (**12**).

Table A8. Temperature and T_1 values for the ruthenium hydride and amino proton in the complex $[NPNH_2]Ru(H)_2(\eta^6\text{-}C_7D_8)$ (**13**).

	T_1 (ms)	
Temperature (K)	**Ru-*H***	**N-*H***
300	469	632
270	381	421
265	372	398
260	366	386
255	382	395
250	414	415
240	499	479

(a)

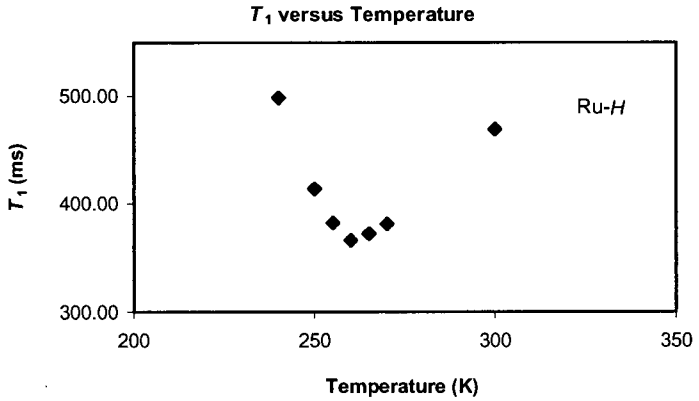

(b)

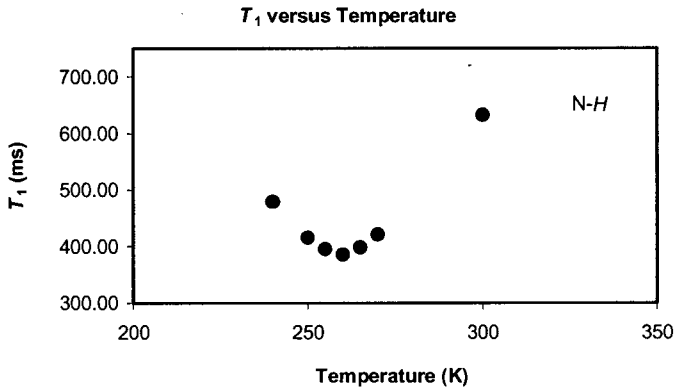

Figure A5. Plot of T_1 versus Temperature for (a) the ruthenium hydrides and (b) the amino protons in the complex $[NPNH_2]Ru(H)_2(\eta^6\text{-}C_7D_8)$ (**13**).

Table A9. Temperature and T_1 values for the ruthenium hydrides and amino proton in the complex $[NPNH_2(\eta^6\text{-}C_6H_5)]RuH_2$ (**14**).

	T_1 (ms)	
Temperature (K)	**Ru-*H***	**N-*H***
298	651	741
275	458	504
255	368	357
250	351	350
246	334	344
240	358	352
230	464	425

(a)

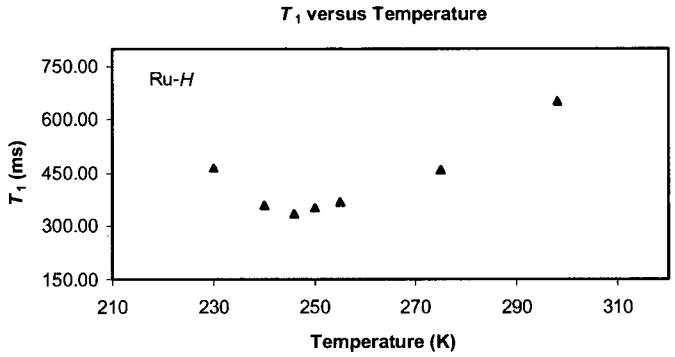

(b)

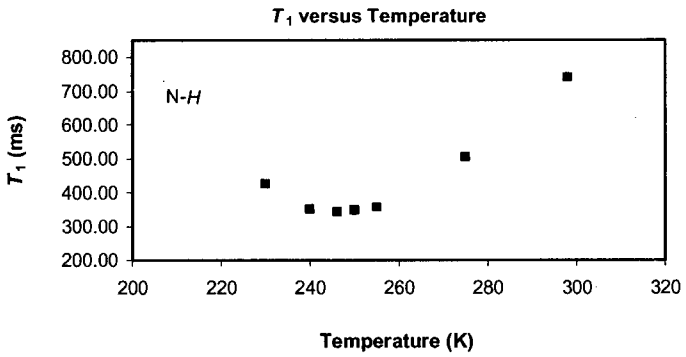

Figure A6. Plot of T_1 versus Temperature for (a) the ruthenium hydrides and (b) the amino proton in the complex $[NPNH_2(\eta^6\text{-}C_6H_5)]RuH_2$ (**14**).

Table A10. Temperature and T_1 values for the amino protons in the complex [$NPNH_2$] (**15**).

Temperature (K)	T_1 (ms) N-*H*
300	1327
280	1058
260	798
245	666
240	614
235	690
230	732

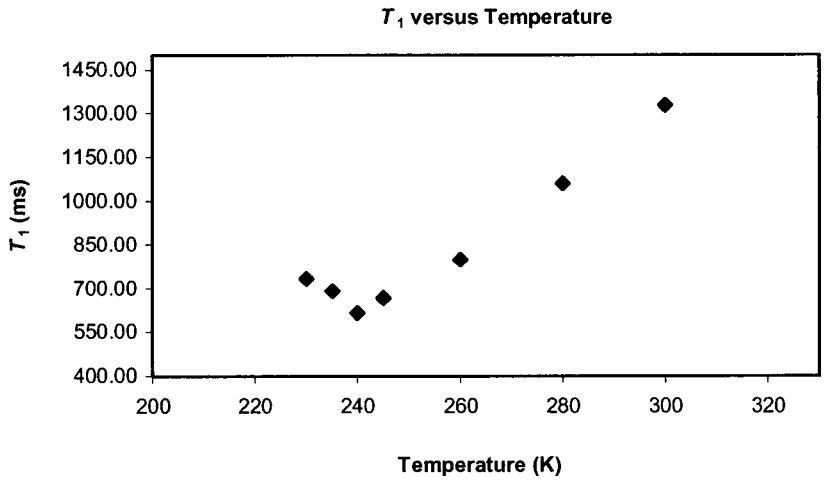

Figure A7. Plot of T_1 versus Temperature for the amino protons in the complex [$NPNH_2$] (**15**).

Appendix 3

Estimation of Rate Constants for Kinetic Analyses

Rate constants were estimated from line width analysis of the variable-temperature NMR data using the following equations:

Slow rate of exchange: $k = 2\pi\delta'\nu$

Intermediate rate of exchange: $k = 2^{½}\pi(\Delta\nu_o^2 - \Delta\nu^2)^{½}$

Coalescence: $k = 2^{½}\pi\Delta\nu_o$

Fast rate of exchange: $k = (4\pi\Delta\nu_o^2)/(\delta'\nu)$

where, $\delta'\nu$ is the broadening at half-height (Hz), $\Delta\nu_o$ is the peak separation in the absence of exchange (Hz), and $\Delta\nu$ is the peak separation during exchange (Hz). An estimated error of ± 5% was applied to each calculated rate constant.

Estimated rate constants for the fluxionality of the $[P_2N_2]$ ligand in the complex $[P_2N_2]Ru(\eta^2:\eta^2\text{-}C_8H_{12})$ (10).

Temperature = 243 ± 1 K (fast exchange)

$\Delta\nu_o$ = 194.8 Hz; $\delta'\nu$ = 89.89 Hz; k = 5304 ± 265 s^{-1}

Temperature = 234 ± 1 K (coalescence)

$\Delta\nu_o$ = 194.8 Hz; k = 865 ± 43 s^{-1}

Temperature = 230 ± 1 K (intermediate rate of exchange)

$\Delta\nu_o$ = 194.8 Hz; $\Delta\nu$ = 148.5 Hz; k = 560 ± 28 s^{-1}

Temperature = 227 ± 1 K (intermediate rate of exchange)

$\Delta\nu_o$ = 194.8 Hz; $\Delta\nu$ = 168.8 Hz; k = 433 ± 22 s^{-1}

Temperature = 219 ± 1 K (slow rate of exchange)

$\delta'\nu$ = 10.44 Hz; k = 66 ± 3 s^{-1}

Temperature = 212 ± 1 K (slow rate of exchange)

$\delta'\nu$ = 2.82 Hz; k = 18 ± 1 s^{-1}

Estimated rate constants for the inter-conversion of diastereomers *exo*-3 and *endo*-3.

Temperature = 285 ± 1 K (slow rate of exchange)

$\delta'\nu = 4.69$ Hz; $k = 30 \pm 2$ s^{-1}

Temperature = 293 ± 1 K (slow rate of exchange)

$\delta'\nu = 9.71$ Hz; $k = 61 \pm 3$ s^{-1}

Temperature = 308 ± 1 K (intermediate rate of exchange)

$\Delta\nu_o = 145.8$ Hz; $\Delta\nu = 128.3$ Hz; $k = 308 \pm 15$ s^{-1}

Temperature = 320 ± 1 K (coalescence)

$\Delta\nu_o = 145.8$ Hz; $k = 648 \pm 32$ s^{-1}